Cytoskeletal morphogenesis in *Trypanosoma brucei*

Amy Neville Sinclair Roth
B.S./B.A. University of Kansas, 2014

A dissertation submitted in partial fulfillment of the requirement of the Degree of Doctor of Philosophy in the Division of Biology and Medicine at Brown University.

Providence, Rhode Island
February 2021

This dissertation by Amy Neville Sinclair Roth is accepted in its present form by the Molecular Biology, Cell Biology, and Biochemistry Graduate Program and the Department of Molecular Biology, Cell Biology, and Biochemistry as satisfying the dissertation requirement for the degree of Doctor of Philosophy.

Date: _____ _____

Christopher L. de Graffenried, Advisor

Recommended to the Graduate Council

Date: _____ _____

Mark A. Johnson, Reader

Date: _____ _____

Richard J. Bennett, Reader

Date: _____ _____

Nicolas L. Fawzi, Reader

Date: _____ _____

Luke M. Rice, Reader

Approved by the Graduate Council

Date: _____ _____

Andrew Campbell, Ph.D.

Dean of the Graduate School

To my Grandfather, Irving S. Johnson, Ph.D.

Curriculum Vitae
Amy Neville Sinclair Roth

I. Education

Brown University — Providence, RI
Ph.D. Molecular Biology, Cell Biology, and Biochemistry (MCB) — 2020 (Expected)

University of Kansas — Lawrence, KS
B.S. Microbiology — 2014
B.A. Slavic Languages and Literature: Russian Language

II. Research Experience

Brown University — Providence, RI
Graduate Student — 2014-Present
Advisor: Christopher L. de Graffenried, Ph.D.

University of Kansas — Lawrence, KS
Undergraduate Researcher — 2012-2014
Advisor: P. Scott Hefty, Ph.D.

University of Kansas — Lawrence, KS
Undergraduate Researcher — 2011-2014
Advisor: Kathy Suprenant, Ph.D.

III. Funding

NIH NIAID NRSA Predoctoral Fellowship F31 AI143163 — 2018-Present
Brown MCBGP Training Grant NIH T32GM007601 — 2015-2017
Oliver Cromwell Gorton Arnold Biological Graduate Fellowship — 2015

IV. Publications

1. **Amy N. Sinclair**, Christine T. Huynh, Thomas E. Sladewski, Jenna L. Zuromski, Amanda E. Ruiz, and Christopher L. de Graffenried. *The* Trypanosoma brucei *subpellicular microtubule array is organized into subdomains defined by functionally discrete microtubule associated proteins.* Under review, PLoS Pathogens, 2020.

2. Christiane Brugger, Margaret Suhanovsky, Cheng Zhang, David Kim, **Amy N. Sinclair**, Dmitry Lyumkis, Alexandra M. Deaconescu. *Molecular Determinants for dsDNA Translocation by the Transcription-Repair Coupling and Evolvability Factor Mfd.* Nature Communications. 11(3740), 2020.

3. **Amy N. Sinclair** and Christopher L. de Graffenried. *More than microtubules: the structure and function of the subpellicular array in trypanosomatids.* Trends in Parasitology*.* 35(10):760-777, 2019.*
   *Selected as the best *Trends in Parasitology* review of 2019.

4. Nicholas A. Hilton, Thomas E. Sladewski, Jenna A. Perry, Zemplen Pataki, **Amy N. Sinclair-Davis**, Richard S. Muniz, Holly L. Tran, Jenna I. Wurster, Jiwon Seo, Christopher L. de Graffenried. *Mapping the TOEFAZ1 interactome identifies key regulators of* Trypanosoma brucei *cytokinesis*. Molecular Microbiology*.* 109(3):306-326, 2018.

5. Jenna A. Perry, **Amy N. Sinclair-Davis**, Michael R. McAllaster, Christopher L. de Graffenried. *TbSmee1 regulates hook complex morphology and the rate of flagellar pocket uptake in* Trypanosoma brucei. Molecular Microbiology*.* 107(3):344-362, 2018.

6. **Amy N. Sinclair-Davis**, Michael R. McAllaster, Christopher L. de Graffenried. *A functional analysis of TOEFAZ1 uncovers protein domains essential for cytokinesis in* Trypanosoma brucei. Journal of Cell Science. 130(22):3918-3932, 2017.

7. Michael R. McAllaster, **Amy N. Sinclair-Davis**, Nicholas Hilton, Christopher L. de Graffenried. *A unified approach towards* Trypanosoma brucei *functional genomics using Gibson assembly. Molecular & Biochemical Parasitology.* 16:30108-16, 2016.

8. Michael L. Barta, Scott Lovell, **Amy N. Sinclair**, Kevin P. Battaile, P. Scott Hefty. Chlamydia trachomatis *CT771 (nudH) is an asymmetric Ap_4A hydrolase. Biochemistry*. 53(1):214-224, 2014.

V. Presentations & Invited Talks

The role of microtubule organizing proteins in *Trypanosoma brucei* morphogenesis. British Society for Parasitology Meeting. Talk.	Granada, Spain 2020
The role of microtubule organizing proteins in *Trypanosoma brucei* morphogenesis. Boston Area Parasitology Society. Talk.	Boston, MA 2019
The cell architecture of *Trypanosoma brucei* is adapted for survival in the mammalian host. BIOL 1550: Biology of Emerging Microbial Diseases, Brown University. Lecture.	Providence, RI 2018 & 2019

PAVE1 maintains the microtubules of the subpellicular array in *Trypanosoma brucei* to generate its polarized shape.
Kinetoplastid Molecular and Cellular Biology Meeting. Poster.
Wood's Hole, MA
2019

PAVE1 links the plasma membrane to the subpellicular microtubule array in *Trypanosoma brucei* to generate its polarized shape.
Plant & Microbial Cytoskeleton GRC. Poster.
Andover, NH
2018

Functional analysis of TOEFAZ1 uncovers protein domains essential for cytokinesis in *Trypanosoma brucei.*
British Society for Parasitology Meeting. Poster.
Ceske Budejovice, Czech Republic
2016

VI. Honors & Awards

Sigma Xi Scientific Research Honor Society	2020
Brown MCBGP Retreat Art in Science Award	2019
Brown MCBGP Retreat Poster Prize	2016
Phi Beta Kappa	2014
Dobro Slovo National Slavic Honor Society	2013
University of Kansas Global Scholar	2011
National Society of Collegiate Scholars	2010
University of Kansas Mount Oread Scholar	2009

VII. Teaching & Mentorship Experience

Undergraduate and Graduate Student Mentor
de Graffenried Laboratory, Brown University

•*Christine T. Huynh,* Undergraduate Student	2017-Present
•*Jenna L. Zuromski,* Graduate Rotation Student	2018
•*Amanda E. Ruiz,* Graduate Rotation Student	2018
•*Meghan Wimmer,* Undergraduate Student	2017
•*Anastasia Murthy,* Graduate Rotation Student	2017
•*Jenna I. Wurster,* Graduate Rotation Student	2016
•*Garvin Dodard,* Graduate Rotation Student	2016

MCB Graduate Program Tutor, Brown University — 2016 & 2018
BIOL 2030: Foundations in the Advanced Study of Life Sciences

Teaching Assistant, Brown University — 2016
BIOL 2010: Quantitative Approaches to Biology

Teaching Assistant, University of Kansas — 2013 & 2014
BIOL 416: Cell Structure and Function

VIII. Professional Service

MCB Graduate Program Student Representative — 2016-2017
Brown University

Graduate Womxn in Science and Engineering Coordinator — 2015-2017
Brown University

Young Scholars Conference Planning Committee — 2015-2017
Brown University

IX. Professional Certifications & Memberships

Brown University Sheridan Teaching Center, Reflective Teaching Certification — 2019

British Society for Parasitology Member — 2016

Preface and Acknowledgements

A Ph.D. is not completed in a vacuum. I, and my work, are the products of innumerable people, interactions, discussions, and experiences accumulated in my life before graduate school and during the last six-and-a-half years.

To my Grandfather—you encouraged me since I was a young girl to be curious. I wish you were here to see where that curiosity led.

To my family—you cheered me on no matter what I decided to try. Piano, violin, debate, dance, history, Russian, science—it didn't matter, as long as I was happy.

To my husband, Nate—you helped me overcome the darkest days of my life and made me a stronger person. Your endless encouragement is my greatest comfort.

To the members of the CLD/AJ lab—science is hard: countless days of failure punctuated by bright bursts of success. You made working a joy, even on the bad days.

To my mentee, Christine—Xtine, you have shaped how I approach teaching and thinking. It has been an absolute delight to see you come into your own the last 3.5 years as the successful young scientist you are, and I cannot wait to see where life takes you.

To Geoff Williams—you were my surrogate advisor at Brown. The first time we met, I almost broke the sapphire on the TEM and cried in your office. You never held it against me, and taught me to just keep trying, again and again, until I got it right. You helped me see the art and beauty in microscopy and science.

And finally, to Chris—who I am today is in large part due to you. You never once doubted my abilities, and knew I could do things even before I did. You pushed me to reach higher and try harder with every setback, to balance my expectations and think independently, and to be unapologetically myself. Grad school has been a wild ride, and I consider myself lucky to have learned from you.

Table of Contents

List of Tables and Figures

Chapter 1: Introduction

Chapter 2: Functional analysis of TOEFAZ1 uncovers protein domains essential for cytokinesis in *Trypanosoma brucei*

Chapter 3: The *Trypanosoma brucei* subpellicular microtubule array is organized into functionally discrete subdomains defined by microtubule associated proteins

Chapter 1:

Introduction

Modified from its original publication as *More than microtubules: The structure and function of the subpellicular array in trypanosomatids*.

Trends in Parasitology, October 2019. Volume 35, Issue 10, pages 760-777.

Trypanosomatid parasites are etiological agents of major neglected tropical diseases

Neglected tropical diseases affect over one billion individuals across the globe and disproportionately afflict the world's poorest and most marginalized populations (Fitzpatrick et al., 2017). Leishmaniasis, Chagas disease, and African trypanosomiasis, caused by the related human-infectious trypanosomatid parasites *Leishmania spp., Trypanosoma cruzi,* and *Trypanosoma brucei*, respectively, account for over 20 million cases yearly and cost billions of dollars in lost economic productivity annually (Fitzpatrick et al., 2017; Varikuti et al., 2018). The effect of these diseases amount to over 5 million disability-adjusted life years (DALYs) lost and over 80,000 deaths a year (Torres-Guerrero et al., 2017; World Health Organization, 2013). Leishmaniasis, Chagas disease, and African trypanosomiasis have limited treatment options that are expensive and require intensive administration (Barrett and Croft, 2012; Bern and Montgomery, 2009; Fèvre et al., 2008; Fitzpatrick et al., 2017). In the event that these diseases are not fatal, they often disable, disfigure, and impair the cognitive abilities of those who contract them (Fitzpatrick et al., 2017). The socio-economic burden of these neglected tropical diseases trap low-income households in a cycle of poverty, as costs associated with treatment can amount to more than 20% of annual household incomes and can deprive households of breadwinners (Fitzpatrick et al., 2017).

Leishmania, T. cruzi, and *T. brucei* are kinetoplastids, a class of flagellated protozoa containing both free-living and parasitic groups that that maintain their mitochondrial DNA in a specialized domain of the mitochondrion known as the kinetoplast (Vickerman, 1994). Trypanosomatids, as the human-infectious kinetoplastids are called,

have dixenous life cycles that entail cycling between insect vectors and mammals, with the vectors serving as the definitive hosts (Matthews, 2011). This restricts the endemic areas of each disease to the geographical habitats of their respective vectors, although climate change and mass migration are changing these traditional landscapes (Bern and Montgomery, 2009; Claborn, 2010; Lord et al., 2018). *Leishmania* and *T. cruzi* both have an intracellular replicative stage during their infection of mammals, while *T. brucei* remains exclusively extracellular throughout infection. These life cycle differences result in distinct clinical manifestations of disease.

Leishmania are vectored by sandflies and are the most widespread geographically, affecting persons in Asia, Africa, South America, and the Southern United States (Matthews, 2011). Leishmaniasis can take many forms, from painful cutaneous lesions to a deadly visceral disease associated with anemia and the dangerous enlargement of the liver and spleen (Claborn, 2010). Chagas disease is endemic to South and Central America but is an emerging threat in the Southern United States as the triatomine insect vector spreads due to climate change (Bern and Montgomery, 2009). In the majority of patients, Chagas disease is a chronic and life-long infection that results in severe heart disease and debilitating digestive tract abnormalities in a third of cases (Rassi and Marin-Neto, 2010). The initial acute phase of Chagas disease is rarely detected, and treatment of the chronic phase does not appear to improve long-term outcomes (Meymandi et al., 2018). African trypanosomiasis, also known as African sleeping sickness, is currently endemic to Sub-Saharan Africa, which is the native habitat of its tsetse fly vector (Matthews, 2011). Although African trypanosomiasis is not as widespread as leishmaniasis or Chagas disease, it is invariably fatal without treatment in all but a small

subset of asymptomatic individuals (Brun et al., 2010; Capewell et al., 2016). Initial infection presents with general symptoms including fever and malaise, but once the parasite crosses the blood-brain barrier, patients present psychiatric, motor, and sensory disabilities that, if left untreated, will progress into coma and eventual death (Kennedy, 2013).

Treatments for trypanosomatid diseases have historically been acutely toxic and difficult to administer (Barrett and Croft, 2012). There are only two Food and Drug Administration (FDA)-certified treatments for leishmaniasis and Chagas disease. The cutaneous form of leishmaniasis has no formal treatment, while treatment for the visceral form relies on amphotericin B, which has regional and sub-species differences in effectiveness, and miltefosine, which is unsafe for fetal development and is complicated by emerging reports of resistance (Barrett and Croft, 2012). Only nifurtimox and benznidazole are available to treat Chagas disease; both drugs are considered carcinogenic and are not effective in the chronic stage of the disease (Meymandi et al., 2018; Wilkinson and Kelly, 2009). Human African trypanosomiasis treatment is dependent on the *T. brucei* subspecies and disease stage. For late-stage African trypanosomiasis, the arsenical melarsoprol or combinatorial nifurtimox-eflornithine (NECT) are available. Both of these drugs require trained administration and are highly toxic, and resistance has been reported in the field (Wilkinson and Kelly, 2009). A new orally administered drug, fexinidazole, has recently been approved for use against early and late-stage African trypanosomiasis, but it still has harmful side effects in late-stage patients (Lindner et al., 2020), and there is evidence of nifurtimox-fexinidazole cross-

resistance (P De Koning, 2020). The development of new treatments is sorely needed for the many different clinical manifestations of disease caused by these parasites.

Trypanosomatids are an early branching eukaryotic lineage that is highly divergent from animals and fungi, which make up the majority of eukaryotic model systems studied in biology (Burki et al., 2020). As such, it is likely that trypanosomatids have devised unique and essential pathways that could be exploited to design drugs that have minimal impacts on the mammalian host. These unique pathways, from metabolism to cytoskeletal organization, can only be revealed by studying the basic cell biology of trypanosomatids. Moreover, *Leishmania, T. cruzi,* and *T. brucei* also have highly syntenic genomes with a large cohort of genes conserved across the three parasites (Jackson et al., 2015). This conservation is reflected by shared morphologies that the parasites employ during their infection cycle (de Souza, 1999; Gull, 1999; Sunter and Gull, 2017). This degree of conservation raises the possibility that drug targets identified in one species could be exploited for treatments against all three parasites.

In addition to their public health importance, trypanosomes represent a new and exciting model system for cell biology. Our knowledge of the vast majority of biological processes are derived from a handful of model systems that all fall within the same branch on the tree of life—Opisthokonts, which includes fungi and animals. Trypanosomes are separated from humans by ~1 billion years of evolution (Burki et al., 2020), and exhibit characteristics of cell cycle regulation and cytoskeletal organization that are unlike those found in the more widely used “yeast-to-human” range of model systems (Russell et al., 2017). Restricting the majority of life science research to a limited set of yeast-to-human model systems was necessary due to the unavailability of whole-genome sequencing and

the difficulty of developing strategies for genetic manipulation in individual organisms. However, with the advent of high-throughput DNA sequencing and near-global gene editing with CRISPR/Cas9, these limitations have largely been overcome (Alfred and Baldwin, 2015). These technological advancements make restricting research to yeast-to-human model systems limiting to our understanding of eukaryotic cell biology. Studying divergent organisms, such as trypanosomes, will broaden our knowledge of the biodiversity of life and show how evolution has devised unique strategies for survival in diverse ecological niches.

Life cycle morphogenesis tunes trypanosomatids for survival in the host

The basic cell morphology of *T. brucei, T. cruzi,* and *Leishmania* is highly conserved between each species. When not undergoing cell division, every morphotype of each parasite contains one kinetoplast, one nucleus, and one flagellum (**Figure 1**) (Chagas, 1909; Rotureau et al., 2011; Sunter and Gull, 2017). Trypanosomatids differentiate into three basic morphotypes depending on their environment: the trypomastigote, the epimastigote, and the amastigote. The subpellicular microtubule array defines the cell shape of these trypanosomatid morphotypes (**Fig. 2A**). The subpellicular microtubule array is found in essentially all free-living and parasitic kinetoplastids, and is comprised of a single layer of microtubules that encompasses the cell body to create the variety of shapes trypanosomatids take on during their life cycle (Angelopoulos, 1970; Brooker, 1971).

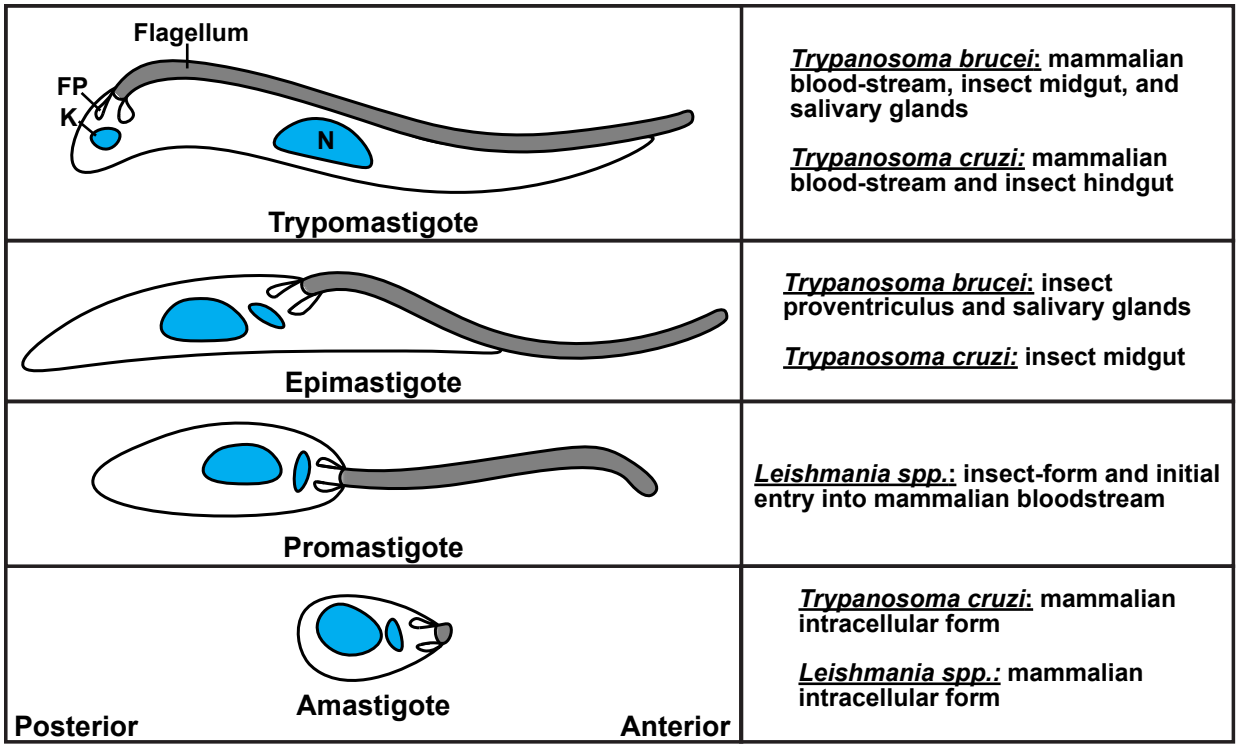

Figure 1. The primary morphologies of human-infectious trypanosomatid parasites. (Left) Schematic of cell structure and topological order of single-copy organelles in each morphotype. The trypomastigote form is characterized by the posterior localization of the mitochondrial DNA aggregate, called the kinetoplast (K), to that of the nucleus (N). An attached flagellum exits from the flagellar pocket (FP) near the cell posterior. In the epimastigote form, the kinetoplast is anterior to the nucleus. While the flagellum is still attached to the cell surface, it also has a long, cell-free overhang. The promastigote form has a similar arrangement of DNA-containing organelles as the epimastigote, but the flagellum is unattached after exiting the flagellar pocket at the cell anterior. The kinetoplast is also positioned anterior to the nucleus in the smaller, more-spherical amastigote form. The flagellum is short and non-motile, and barely protrudes from the flagellar pocket. **(Right)** A list of the life-cycle stages in which the human-infectious trypanosomatids adopt these morphologies.

In each morphotype, the flagellum is nucleated by a basal body and exits the cell body through a structure known as the flagellar pocket, which is an endocytic organelle. In *T. brucei* trypomastigotes and *T. cruzi* epimastigotes, the flagellum emerges onto the cell surface at the cell posterior and is attached to the cell by a series of desmosome-like structures known as the flagellum attachment zone (FAZ) filament (Sunter and Gull,

2016). In *Leishmania* promastigotes, as well as the intracellular amastigotes of both *Leishmania* and *T. cruzi*, the flagellum is not attached to the cell surface; rather, it exits the flagellar pocket located at the cell anterior and is free hanging. The FAZ is still present in promastigotes and amastigotes and attaches the flagellum to the inner surface of the flagellar pocket in both morphotypes (Wheeler et al., 2016).

Within the insect host, *T. brucei* and *T. cruzi* primarily adopt epimastigote and trypomastigote forms, while *Leishmania* are found as promastigotes (**Fig. 1**) (Sharma et al., 2008; Tyler and Engman, 2001; Wheeler et al., 2016). Once transmitted to the mammalian host, *T. brucei* remain extracellular and circulate in the bloodstream or colonize host tissues as trypomastigotes (Capewell et al., 2016; Trindade et al., 2016). In contrast, both *T. cruzi* and *Leishmania* enter host cells and differentiate into amastigote forms after cell entry (Dvorak and Hyde, 1973; Sanyal and Gupta, 1967; Sunter and Gull, 2017; Tyler and Engman, 2001).

These morphological changes specialize trypanosomatid cells for survival in the different environments they inhabit (Wheeler et al., 2013a). The trypomastigote morphology appears to be adapted for motion in crowded bloodstreams and tightly packed tissue compartments (Capewell et al., 2016; Heddergott et al., 2012). As the flagellum beats, the subpellicular array deforms, creating ‘cellular waveforms’ that facilitate swimming in-between blood cells and other biological barriers (Bargul et al., 2016; Sun et al., 2018). Within the mammalian hosts, motility is important for immune evasion; the high velocity reached by *T. brucei* trypomastigotes in blood (more than 20 μm/s) may create a hydrodynamic drag that concentrates host antibodies at the flagellar pocket for rapid uptake and endocytosis (Engstler et al., 2007). Epimastigote and

promastigote morphologies may be primed for attachment to epithelial layers in the insect host, as more of the flagellum is free from the cell body to associate with epithelium and other structures of the insect, such as microvilli and chitin mouthparts, or in the case of *T. cruzi*, the waxy cuticle of the hindgut (Sharma et al., 2008; Tyler and Engman, 2001). These morphologies may facilitate cell division while the flagellum is attached to a substrate. Likewise, the amastigote morphology may be adapted to maximize cell numbers in the crowded environment of the host cell, while minimizing the total amount of surface exposed to host cell factors (Sunter and Gull, 2017). Moreover, the lack of a long flagellum in amastigotes may protect the host cell from damage produced by flagellar beating, which would facilitate amastigote replication (Dvorak and Hyde, 1973).

The subpellicular microtubule array defines cell shape in trypanosomatids

The subpellicular microtubule array is comprised of a single layer of microtubules that are heavily crosslinked to each other and the inner leaflet of the plasma membrane (**Fig. 2 & 3**). Morphological studies have characterized array organization, but little progress has been made towards identifying the molecular mechanisms that create the shape of the array, maintain array microtubules, and segregate the array during cell division.

The subpellicular array is the primary microtubule structure in trypanosomatids. *T. brucei* have no cytoplasmic microtubules, while *T. cruzi* and *Leishmania* have only a small number of cell-cycle regulated cytoplasmic microtubules (Weise et al., 2000). Microtubules are hollow filaments with a dynamic fast growing plus-end and a more stable slow growing minus-end (Akhmanova and Steinmetz, 2015). Several approaches have

shown that the array microtubules in *T. brucei* are highly ordered, with their growing plus-ends oriented towards the cell posterior (Robinson et al., 1995; Sherwin and Gull, 1989a). A microtubule associated protein known as XMAP215 that binds to growing microtubule plus-ends localizes to the posterior of the array in *Leishmania*, suggesting that the polarity of the array is conserved among trypanosomatids (Halliday et al., 2019). The microtubules of the array follow a helical path as they traverse the cell body and are separated by a uniform distance of 18-22 nm (**Fig. 2A**) (Angelopoulos, 1970). Neighboring microtubules are crosslinked by regularly-spaced fibrils at intervals of 12-30 nm (**Fig. 2B-D**) (Bordier et al., 1982; Sherwin and Gull, 1989a; Souto-Padrón et al., 1984). The array microtubules are also attached to the plasma membrane by fibrils spaced at ~20 nm intervals (**Fig. 3**) (Bordier et al., 1982).

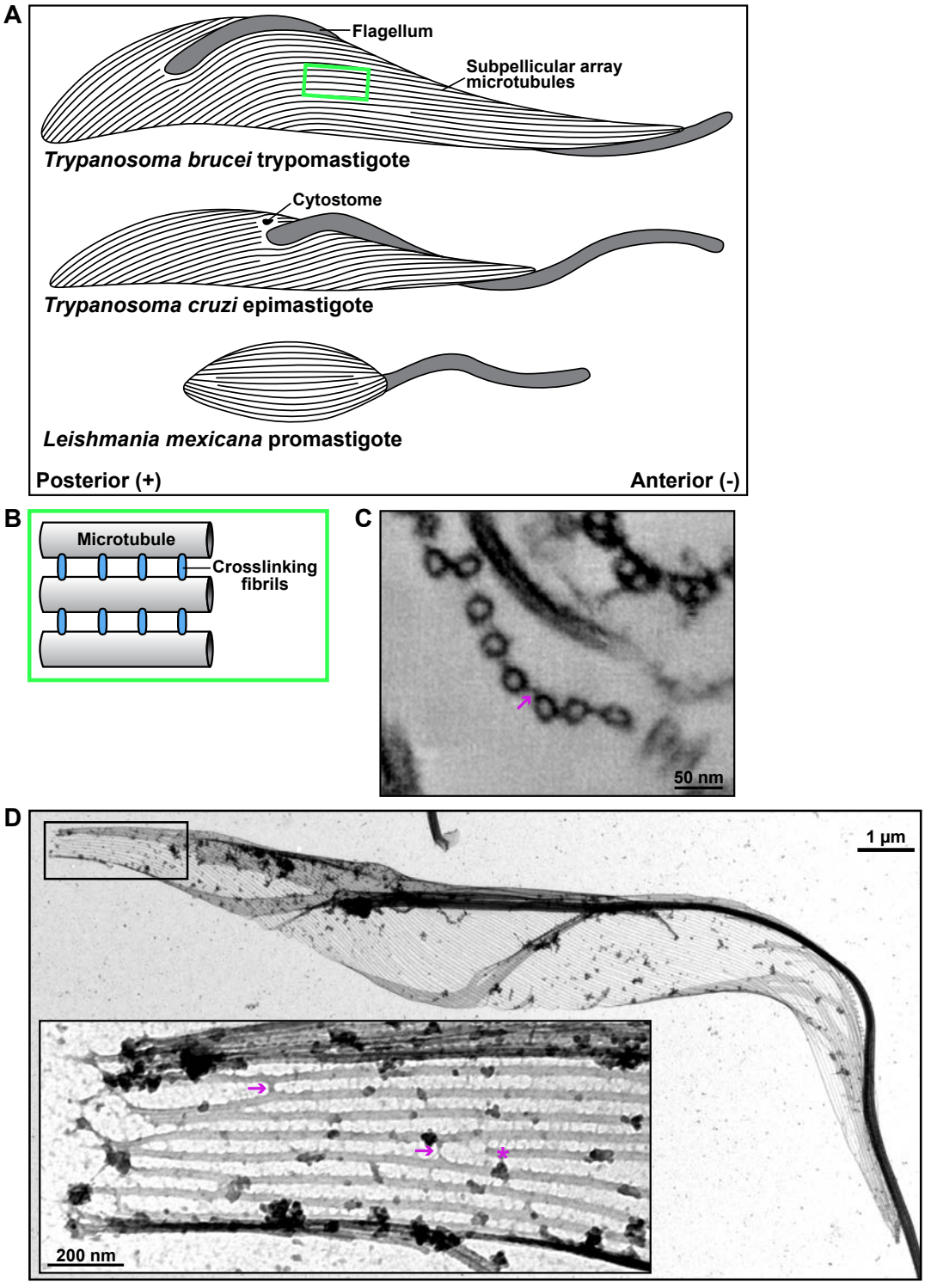

Figure 2. The microtubules of the subpellicular array are extensively crosslinked. (A) Schematics of the arrangement of the subpellicular microtubules in a *Trypanosoma brucei* procyclic-form trypomastigote (top), a *Trypanosoma cruzi* epimastigote (middle), and a *Leishmania mexicana* promastigote (bottom). The growing plus-ends of the microtubules are

oriented towards the cell posterior. In *T. brucei* and *T. cruzi* trypomastigotes and epimastigotes, the array microtubules bend around the flagellar pocket as the flagellum exits onto the cell surface. In *T. cruzi,* the array microtubules also curve around the cytostome, which is an endocytic organelle that forms an opening at the cell surface. In *Leishmania,* the array ends at the flagellar pocket located at the cell anterior. Based on (Alcantara et al., 2014; Angelopoulos, 1970; Sherwin and Gull, 1989a; Sun et al., 2018; Wheeler et al., 2011). **(B)** Schematic of the fibrils that crosslink the microtubules of the array together from the boxed region in (A). **(C)** Tomogram (*z* = 50 nm) of an extracted cytoskeleton of *T. brucei* in which the crosslinks between the array microtubules are visible (arrow). The microtubules of the array are separated from each other by a space of 18-22 nm. Image kindly contributed by Dr. Sue Vaughan and Mr. Timm Mohr. **(D)** Original transmission electron micrograph of a positively-stained procyclic-form *T. brucei* trypomastigote cytoskeleton. The cytoskeleton was critical-point dried and cleaved to remove half of the array. **(Inset)** Higher magnification image of the cell posterior, in which the inter-microtubule crosslinks are clearly shown (arrows). Where a microtubule ends in the array (asterisk), the microtubules on either side of it continue and become crosslinked to each other.

The number of microtubules in the array varies between species and changes depending on the width of the cell body. There are over 100 microtubules in the array in transmission electron microscopy cross sections that traverse the widest point of the cell, which is where the nucleus is located (Meyer and de Souza, 1976; Sanyal and Gupta, 1967). The number of array microtubules decreases as the trypanosomatid cell body narrows towards the tapered posterior and anterior ends. It is not clear how many of the array microtubules span the entire length of the cell body. Transmission electron microscopy has shown that whenever a microtubule ends in the middle of the array, the microtubules on either side continue past it and become crosslinked to each other, maintaining the inter-microtubule distance (**Fig. 2D, asterisk**) (Sherwin and Gull, 1989a).

The continuity of the array is interrupted at specific points in the cell body. In *T. brucei* and *T. cruzi* trypomastigotes and epimastigotes, the flagellar pocket disrupts the array by forming an invagination of the plasma membrane that serves as the flagellum exit site (**Fig. 2A**) (Lacomble et al., 2009). In these morphotypes, the flagellum is attached to the cell surface by the FAZ filament, which is situated between the microtubules of the

array as it traverses the cell body (Sunter and Gull, 2016). *T. cruzi* has an additional interruption created by the cytostome–cytopharynx complex, which is an endocytic organelle (**Fig. 2A**) (Alcantara et al., 2017). Four microtubules associated with the cytostome-cytopharynx complex also interrupt the array as it traverses a specialized membrane domain, known as the pre-oral ridge, that is located between the flagellar pocket and the cytostome-cytopharynx complex. The flagellar pocket and FAZ filament are also present in *Leishmania* promastigotes, but they do not interrupt the array as they are present at the anterior cell tip (Wheeler et al., 2016). In *T. brucei* and *Leishmania,* the flagellar pocket membrane is the only plasma membrane domain that is not in close contact with the array, which makes it the primary site of endo- and exo-cytosis (Lacomble et al., 2009).

T. brucei, T. cruzi, and *Leishmania* have a conserved set of four microtubules, called the microtubule quartet (MtQ), that originates near the basal body of the flagellum and wraps around the flagellar pocket. In *T. brucei* and *T. cruzi* trypomastigotes and epimastigotes, the MtQ intercalates into the array at the point where the flagellum exits the pocket and lies adjacent to the FAZ filament (**Fig. 3A-B**) (Lacomble et al., 2009; Sunter and Gull, 2016). The MtQ in *Leishmania* does not become part of the array and is present on the opposite side of the flagellar pocket to where FAZ filament resides (Wheeler et al., 2016). The MtQ likely has an inverted polarity compared to the array microtubules, as it is nucleated near the basal body and grows towards the cell anterior (Lacomble et al., 2009). This arrangement creates a seam of antiparallel microtubules within the array in *T. brucei* and *T. cruzi* that may facilitate the targeting of protein complexes involved in cell division and morphogenesis. The cytostome-cytopharynx

microtubules in *T. cruzi* also create a seam that may be important for the formation of this organelle during cell division (Alcantara et al., 2017).

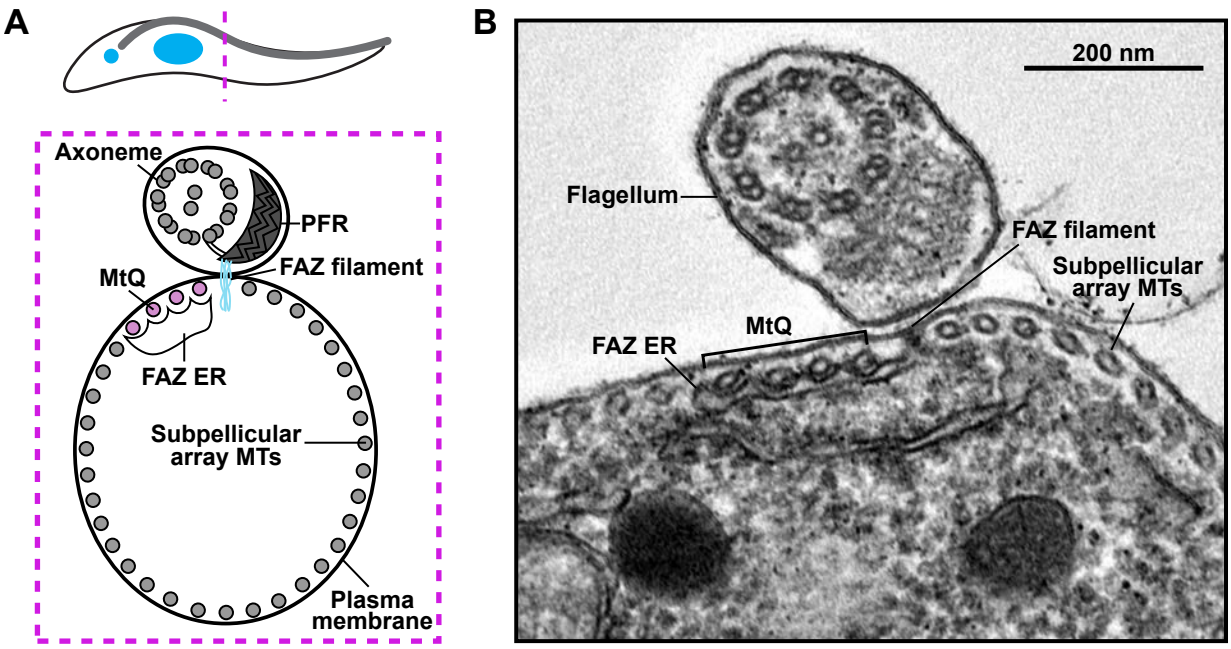

Figure 3. The microtubules of the array are tightly associated with the plasma membrane. **(A)** Schematic of a trypomastigote cross-section, looking from posterior-to-anterior. The array microtubules are located just 10 nm from the plasma membrane. The microtubule quartet (MtQ) has the opposite polarity to the other array microtubules. The flagellum attachment zone (FAZ) filament interrupts the array and attaches the flagellum to the cell surface. PFR; para-flagellar rod. **(B)** Thin section transmission electron micrograph of a *T. brucei* cell in the same orientation as the schematic in (A). Kindly contributed by Dr. Sue Vaughan and Mr. Timm Mohr.

The subpellicular array is extensively remodeled in morphological transitions

The subpellicular microtubule array undergoes significant changes as the parasites transition into different morphologies during the trypanosomatid life cycle. Two primary mechanisms, which are not mutually exclusive, have been shown to alter array morphology: the direct remodeling of array microtubules, and specialized asymmetric cell divisions that result in changes to the shape of the array.

In *T. brucei*, direct microtubule remodeling is responsible for the differentiation of mammalian bloodstream-form trypomastigotes into the insect vector tsetse fly-resident procyclic trypomastigotes (Matthews et al., 1995). In bloodstream-form trypomastigotes, the kinetoplast is in close proximity to the posterior of the array. During differentiation into procyclic-forms, the posterior array lengthens through the extension of pre-existing microtubules or the insertion of new microtubules at the array posterior, which repositions the kinetoplast to a more central location of the cell body to create the procyclic morphology.

The posterior section of the array in procyclic cells lengthens as they migrate towards the proventriculus of the tsetse, producing what are known as mesocyclic trypomastigotes (Rotureau et al., 2011; Van Den Abbeele et al., 1999). In the proventriculus, the nucleus of mesocyclic cells migrates towards the cell posterior as they undergo an asymmetric division that produces two epimastigote daughter cells—one long, which is thought to be terminal, and the other short, which goes on to colonize the salivary glands (Peacock et al., 2018; Sharma et al., 2008). The transition from a trypomastigote to an epimastigote morphotype requires an extensive repositioning of single-copy organelles, resulting in a cell where the kinetoplast, flagellar pocket, and associated flagellum are anterior to the nucleus, along with an extended flagellar overhang (**Fig. 1**). These repositioning events appear to be mediated by delayed growth of the new flagellum and an altered division plane in the subpellicular array (Peacock et al., 2018; Sharma et al., 2008). It is unclear how the new division plane is selected to achieve such an asymmetric partitioning of daughter cells, although RNAi depletion of

certain FAZ components generates epimastigote-like cells (Hayes et al., 2014; McAllaster et al., 2015b; Sunter et al., 2015a).

In *T. cruzi*, the transition from the trypomastigote to the amastigote form in the mammalian host is also accomplished by an extremely asymmetric division event that leads to the expulsion of the trypomastigote flagellum and positions the kinetoplast anterior to the nucleus (Kurup and Tarleton, 2014). After the asymmetric division event, it is not known how the array is altered to become more spherical in the amastigote. There are more microtubules in the cross-sections of *T. cruzi* amastigotes than at any point in the cell body of trypomastigotes, while the inter-microtubule distance is consistent between these two life-cycle stages (Meyer and de Souza, 1976). This suggests that additional microtubules are intercalated into the array to create the spherical amastigote shape.

In *Leishmania,* the transition between promastigote and mammalian-resident amastigote forms does not require significant rearrangement of the kinetoplast and nucleus. Amastigotes are ovoid with a short, non-motile flagellum, but the single copy organelles are retained in the same topological order (**Fig. 1**). It has been shown that *Leishmania* remodel the long promastigote flagellum to the short amastigote flagellum through two pathways: a specialized asymmetric division event in which one daughter cell forms a short and non-motile flagellum, or through the direct remodeling and shortening of the existing flagellum (Wheeler et al., 2015).

It is unclear how *Leishmania* promastigotes remodel their subpellicular array to become more spherical in the amastigote form. During *Leishmania* promastigote cell division, cells initially elongate their cell body before undergoing a drastic reduction in

length while doubling their width just prior to cytokinesis initiation (Wheeler et al., 2011). Rapid depolymerization of array microtubules at the cell posterior, along with the simultaneous insertion of new microtubules at the cell anterior could decrease cell length while increasing cell width in the promastigote division cycle; a similar mechanism could be employed in the differentiation of promastigote to amastigote. Another potential transition mechanism has been suggested by cross sections of promastigote and paramastigote forms of *Herpetomonas samuelpessoi*. The helical pitch of array microtubules is tighter in the more-rounded *H. samuelpessoi* paramastigote morphology, demonstrating the capability of the array to increase microtubule torsion to accommodate additional cell volume (De Andrade and De Almeida, 1980). However, little is known about array ultrastructure and microtubule dynamics during the amastigote differentiation of *T. cruzi* and *Leishmania*, and even less about their return transition into trypomastigotes and promastigotes, respectively. This is an important area of investigation as more genetic tools are developed in these parasites.

It is likely that the choice of differentiation mechanism employed during each life cycle transition reflects the extent of cytoskeletal remodeling taking place. Smaller changes that do not alter the topological order of single-copy organelles are mediated by microtubule growth or remodeling, while topological re-ordering requires a division event. These mechanisms illustrate that even though the array is made up of microtubules that are extensively crosslinked and appear highly persistent, it is not a static structure.

Cytoskeletal replication and cell division in trypanosomatids

The replication of the cytoskeleton is an ordered process in trypanosomatids that takes place in a series of sequential steps. The first step in cytoskeletal replication involves the maturation of the pro-basal body to initiate the growth of a new flagellum (Elias et al., 2007; Sherwin and Gull, 1989b; Wheeler et al., 2011; Wheeler et al., 2016). At the same time, a new microtubule quartet (MtQ) nucleates from the basal body region and extends with the flagellum. In trypomastigotes and epimastigotes, the new flagellum exits through the neck of the flagellar pocket onto the cell surface, while the MtQ is intercalated into the subpellicular array (Lacomble et al., 2009). Once the new flagellum exits from the flagellar pocket, a new FAZ filament is nucleated to attach the new flagellum to the cell surface (Sunter et al., 2015b). In promastigotes and amastigotes, the new flagellum is attached to the flagellar pocket neck by the new FAZ filament (Wheeler et al., 2016). In *T. brucei,* the replicating new flagellum is attached to the old flagellum by a structure called the flagellar connector in insect-resident procyclic forms (Briggs et al., 2004) and the flagellar groove in mammalian-resident bloodstream forms (Hughes et al., 2013). These structures were theorized to facilitate flagellar replication, but recent genetic analysis has shown that they are not required for this process (McAllaster et al., 2015b; Varga et al., 2017). These structures do not appear to be present in *T. cruzi* and *Leishmania* (Elias et al., 2007; Wheeler et al., 2015) and may represent a species-specific adaptation of the flagellum in *T. brucei.*

The replication of the subpellicular microtubule array during cell division has been most thoroughly studied in *T. brucei*, where the addition of new microtubules to the array is cell cycle regulated (Sherwin and Gull, 1989a). New microtubules appear to nucleate

from the sides of existing ones, and extant microtubules are elongated from both the plus and minus ends as detected by an antibody against tyrosinated α-tubulin, which is indicative of microtubule growth (Sherwin and Gull, 1989a). Consistent microtubule polymerization appears to take place throughout the cell cycle at the cell posterior (Halliday et al., 2019; Sherwin and Gull, 1989a; Wheeler et al., 2013b). The array microtubules do not appear to originate or nucleate from one specific point (Sheriff et al., 2014), although many microtubule minus ends are concentrated at the cell anterior in trypomastigotes and epimastigotes, and at the exit of the flagellar pocket in promastigotes. After the nucleation and growth of a new flagellum during cell replication, new microtubules are inserted between the old and new flagella as the width of the cell increases in trypomastigotes and epimastigotes (Elias et al., 2007; Wheeler et al., 2013b). *Leishmania* promastigotes have a unique progression of array growth whereby the array initially elongates and then rapidly shortens as the duplicating cells get rounder (**Fig. 4B**) (Wheeler et al., 2011). In both steps, the overall surface area is maintained. The purpose of this rapid reorganization in *Leishmania* is unknown.

In *T. brucei* and *T. cruzi*, the kinetoplast replicates and divides prior to nuclear mitosis (Elias et al., 2007; Vaughan and Gull, 2008). The kinetoplast is physically linked to the basal body; as the new flagellum grows, the basal bodies separate and pull the replicated kinetoplasts apart (**Fig. 4A & C**) (Lacomble et al., 2010; Robinson and Gull, 1991). In *Leishmania,* the replication phases for the kinetoplast and nucleus are more closely coupled, and nuclear mitosis occurs just prior to kinetoplast segregation (**Fig. 4B**) (Wheeler et al., 2011).

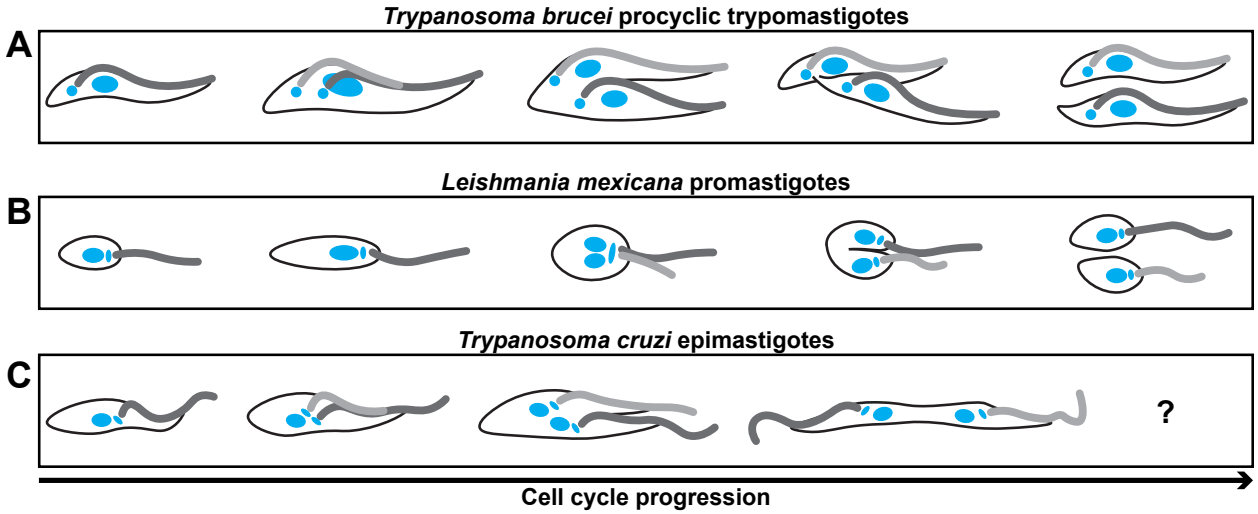

Figure 4. Cell division in trypanosomatid parasites. (A) In a *Trypanosoma brucei* trypomastigote, the kinetoplast replicates prior to the nucleus. The array enlarges to accommodate the increase in cell volume, after which cytokinesis initiates at the cell anterior and progresses towards the cell posterior. Microtubule segregation and bundling separates the subpellicular array, leading to abscission. The division is asymmetric, producing daughter cells with either a rounded or pointed posterior. The old and new flagellum are indicated in dark and light grey, respectively. Based on (Wheeler et al., 2013b). **(B)** The cell body of a *Leishmania mexicana* promastigote lengthens before undergoing a dramatic reduction in cell length while increasing in cell width during replication. The nucleus replicates prior to the kinetoplast. Cytokinesis also proceeds towards the cell posterior. Based on (Wheeler et al., 2011). **(C)** In a *Trypanosoma cruzi* epimastigote, the kinetoplast replicates prior to the nucleus, after which cytokinesis initiates at the cell anterior. The daughter cells are attached end-to-end in the final stage of cytokinesis, but it is currently unknown how *T. cruzi* epimastigotes resolve the array to complete abscission. Based on (Elias et al., 2007).

Cytokinesis is the final step of cell division and physically divides the duplicated organelles and structures into separate daughter cells. The mechanism of cytokinesis is tailored to the cytoskeletal organization and environment of each organism. For example, plant cells use extensive vesicular trafficking along microtubules to deposit new plasma membrane and cell wall material between the two daughter cells, as their cell walls are rigid and inflexible (Müller and Jürgens, 2015). Animal cells lack a cell wall, and thus depend on the force of actomyosin ring constriction to invaginate the plasma membrane in a process called cleavage furrow ingression (Green et al., 2012). Yeast cells use a

mechanism that appears to be a hybrid between plant and animal cell cytokinesis, employing the combined force of actomyosin ring constriction along with cell wall deposition to separate daughter cells (Pollard and Wu, 2010).

In trypanosomatids, the mode and mechanism of cytokinesis is dictated by the presence of the subpellicular microtubule array. Trypanosomatids have developed a unique mechanism of cytokinesis that maintains cell polarity throughout the entire process and does not rely on actomyosin ring constriction. *T. brucei* lacks the non-muscle myosin II required for ring constriction, and actin can be depleted in the insect form of the parasite without affecting cell division (Richards and Cavalier-Smith, 2005; Salcedo et al., 2004). Actin in trypansomatids appears to function primarily in endocytosis and intracellular trafficking (Gupta et al., 2020). Cytokinesis is thus likely to be microtubule-mediated and dominated by processes that sort and remodel microtubules, as the array microtubules do not depolymerize during cell division (Sherwin and Gull, 1989a; Wheeler et al., 2013b).

After the duplication and segregation of the kinetoplast and nucleus, a membrane inflection forms along the long axis of the cell that demarcates the site of future cleavage furrow ingression. This membrane inflection is created by the unidirectional inward curving of the subpellicular array (Elias et al., 2007; Farr and Gull, 2012; Wheeler et al., 2011; Wheeler et al., 2013b; Wheeler et al., 2019). The cleavage furrow begins to ingress in post-mitotic cells, initiating at the tip of the new FAZ filament and progressing along the helical path of the array towards the cell posterior (**Fig. 4**) (Robinson et al., 1995). Throughout this process, the array microtubules must be sorted and bundled to partition them into two discrete arrays (Wheeler et al., 2013b). In *T. brucei*, it has been shown that the inheritance of the array is semi-conservative, providing each daughter cell with a

chimeric structure comprising both old and new microtubules (Sherwin and Gull, 1989a). The daughter cell that contains the newly synthesized flagellum inherits the old cell posterior, while the daughter cell that contains the original flagellum inherits a newly formed posterior derived from microtubule remodeling and sorting at the array mid-zone (Hilton et al., 2018; Wheeler et al., 2013b). *T. brucei* cell division produces non-equivalent daughter cells that rapidly remodel their subpellicular arrays directly after cytokinesis to become more symmetrical, but it is not understood how this is accomplished (Abeywickrema et al., 2019). As the array does not depolymerize in *T. cruzi* and *Leishmania* during cell division (Ambit et al., 2011; Elias et al., 2007; Wheeler et al., 2011), it is likely that array inheritance in these organisms is also semi-conservative. *Leishmania* daughter cells appear much more symmetrical than *T. brucei,* suggesting that the division plane in promastigotes is placed along a more equal axis in promastigotes (Fig. 4B) (Wheeler et al., 2011). In *T. cruzi,* it is not known even on a morphologic level how daughter cells resolve their subpellicular array into two discrete structures, which is an open question in the field (**Fig. 4C**) (Elias et al., 2007; Ramos et al., 2011).

Molecular mechanisms of trypanosomatid cytokinesis

Very little is known about the molecular components involved in trypanosome cytokinesis. What we do know has been derived from the study of *T. brucei,* which is the only trypanosomatid with a high rate of homologous recombination for gene tagging and RNAi machinery for loss of function experiments (Ngô et al., 1998). CRISPR/Cas9 technologies have recently been developed for *T. cruzi* and *Leishmania*, which now opens

the field for targeted investigation of gene function in these parasites (Peng et al., 2014; Sollelis et al., 2015).

Many proteins that comprise the FAZ filament have been implicated in cytokinesis as well as flagellar attachment. Depletion of FAZ filament proteins leads to flagellar detachment and often shortens FAZ filament length (LaCount et al., 2002; Moreira et al., 2017; Sun et al., 2013; Vaughan et al., 2008; Zhou et al., 2011). Disrupting FAZ filament structure leads to the mispositioning of the cleavage furrow, resulting in aberrant cytokinesis and daughter cells that contain unusual DNA content.

One of the first non-FAZ proteins implicated in *T. brucei* cytokinesis was the chromosomal passenger complex kinase TbAUK1. In metazoan systems, the chromosomal passenger complex regulates kinetochore-microtubule attachments during mitosis and specifies the location of actomyosin ring placement through a phosphorylation cascade (Carmena et al., 2012). *T. brucei* has a unique chromosomal passenger complex that consists of TbAUK1, which is the ortholog of metazoan Aurora B kinase, and two novel proteins called TbCPC1 and TbCPC2 (Li et al., 2008; Tu et al., 2006). TbAUK1, TbCPC1, and TbCPC2 are required for proper chromosome segregation during mitosis (Li et al., 2008). Interestingly, TbAUK1 translocates from the nucleus in late anaphase to the tip of the new FAZ just prior to cleavage furrow ingression (Li et al., 2009). This translocation event is necessary for the initiation of cleavage furrow ingression and requires TbAUK1 phosphorylation activity and the presence of TbCPC1 and TbCPC2 (Li et al., 2009).

The morphogenic kinase TbPLK is also required for *T. brucei* cytokinesis. Polo-like kinases are ubiquitous in metazoan systems, and are typically involved in mitosis,

centrosome duplication, and cytokinesis (Zitouni et al., 2014). *T. brucei* TbPLK does not have a role in mitosis, but it is required for the duplication of several cytoskeletal organelles. TbPLK localizes to the basal body, MtQ, flagellar pocket associated structures, and the new FAZ filament during cell division (Ikeda and de Graffenried, 2012; Yu et al., 2012). TbPLK phosphorylation activity is required for basal body segregation and the nucleation and extension of the new FAZ filament (de Graffenried et al., 2013; Hu et al., 2015; Ikeda and de Graffenried, 2012; Lozano-Núñez et al., 2013). Disruption of TbPLK activity leads to detached flagella and inhibits cytokinesis. TbPLK also localizes to the new FAZ tip late in cell division, suggesting that it could have a role in the initiation of cleavage furrow ingression.

A series of proteomic screens were conducted on TbPLK in order to discover potential TbPLK binding partners and substrates involved in *T. brucei* cytokinesis (Hu et al., 2015; McAllaster et al., 2015b). Several cytoskeletal proteins were identified in these screens that corresponded to the localization of TbPLK throughout the cell cycle. Basal body proteins, components of the flagellar pocket apparatus, and FAZ filament proteins were discovered. Of particular interest, one protein was identified that localizes exclusively to the tip of the new FAZ during cell division. This protein, termed TOEFAZ1 (Tip Of the Extending FAZ protein 1), tracks the tip of the new FAZ when it is formed and follows the cleavage furrow as it ingresses during cytokinesis (McAllaster et al., 2015a; Zhou et al., 2016). Depletion of TOEFAZ1 with RNAi blocks TbPLK recruitment to the tip of the new FAZ. Moreover, cells lacking TOEFAZ1 either do not initiate cytokinesis, or their cleavage furrows are misplaced. Interestingly, TOEFAZ1 depletion does not affect mitosis, FAZ elongation, or flagellar attachment. This makes TOEFAZ1 is the first protein

identified in trypanosomatids that functions exclusively in the process of cytokinesis, unlike other proteins that indirectly affect cytokinesis due to their role in the duplication of cytoskeletal structures or mitosis (LaCount et al., 2002; Li et al., 2008; Moreira et al., 2017; Rotureau et al., 2014; Sun et al., 2013; Sunter et al., 2015a; Tu et al., 2006). TOEFAZ1 is conserved across parasitic and free-living kinetoplastids, including *Leishmania* and *T. cruzi*. However, it shares little structural homology to any known proteins, making its specific function unclear.

Microtubule-severing enzymes such as spastin and katanin are also required for cytokinesis in *T. brucei.* Katanin localizes to the new FAZ tip late in cell division and is required for cleavage furrow ingression, while spastin activity is necessary for the final abscission events to separate daughter cells (Benz et al., 2012; Zhou et al., 2018). Recently, a kinetoplastid-specific orphan kinesin called KLIF has been identified in *T. brucei* that is required for array segregation and daughter-cell separation in the final stages of cytokinesis (Hilton et al., 2018; Zhou et al., 2018). These proteins are also present in *T. cruzi* and *Leishmania* (Hilton et al., 2018; McAllaster et al., 2015b), which suggests a conserved cytokinetic mechanism in trypanosomatids, although their function has yet to be tested in these organisms.

Cytokinesis in *T. brucei* requires the faithful replication and segregation of the subpellicular microtubule array in trypanosomatids. Regulators of array microtubules and its shape are essential for the proper progression of cytokinesis and cell viability. In the next sections, we discuss the molecular details of trypanosome tubulin and subpellicular array-associated proteins, both of which are required to maintain array architecture.

Tubulin expression and post translational modifications in trypanosomatids

Microtubules are comprised of α- and β-heterodimer subunits that bind head-to-tail into protofilaments. Typically, thirteen parallel protofilaments associate laterally to form the hollow microtubule filament (Nogales et al., 1999). Microtubules display a property known as dynamic instability, in which they switch stochastically between polymerization and depolymerization states (Mitchison and Kirschner, 1984). Dynamic instability has not been observed in array microtubules; array microtubules are often described as 'highly stable,' but the stability and persistence of the microtubules in the array is unknown and untested (Gull, 1999; Kohl and Gull, 1998; Robinson et al., 1991). The array microtubules do not depolymerize when exposed to cold temperatures (termed 'cold stable'), tolerate detergent extractions when prepared for whole-mount electron microscopy (Alcantara et al., 2014; Angelopoulos, 1970; Sherwin and Gull, 1989b), and remain intact after treatment with microtubule-destabilizing drugs (Ploubidou et al., 1999; Souto-Padron et al., 1993). However, it is not clear if this apparent stability is due to the nature of the microtubules themselves, or to their extensive crosslinking and organization within the array. The biophysical properties of trypanosome tubulin are an open question; it has been purified but is difficult to polymerize into filaments (MacRae and Gull, 1990; Russell et al., 1984; Werbovetz et al., 1999). If the array microtubules are persistent and long-lived, it is unclear how they are replenished or repaired over the lifetime of the cell, which is likely necessary due to the significant strains put on the array by parasite motility in the cases where the flagellum is attached to the cell surface (Bargul et al., 2016; Sun et al., 2018).

The unique stability of subpellicular array microtubules may be reflected in the expression and regulation of trypanosomatid tubulin. Most eukaryotes have multiple copies of α- and β-tubulin genes throughout their genome. In trypanosomatids, these genes are linked together in clustered repeats. In both *T. brucei* and *T. cruzi*, alternating α- and β-tubulin repeats are grouped together within the genome, ranging from 13-17 tandem copies (Maingon et al., 1988; Seebeck et al., 1983). *Leishmania* tubulin genes are also clustered together in upwards of 15 copies, but have separate monotypic arrays of α- or β-tubulin located on different chromosomes (Jackson et al., 2006; Landfear et al., 1983). Phylogenetic analysis has shown that the alternating arrays are the ancestral genome architecture, as they are present in non-parasitic kinetoplastids. As kinetoplastids transcribe their genome polycistronically (Johnson et al., 1987), the repeating array structure ensures high expression levels, which is likely required for the maintenance and assembly of the subpellicular array microtubules. Many eukaryotes also encode a variety of α- and β-tubulin isotypes that have different polymerization dynamics and can be differentially expressed (Vemu et al., 2017). These tubulin isoforms differ primarily in in the sequence of their carboxy-terminal tails, which are charged and disordered (Gadadhar et al., 2017). However, there is no clear evidence that trypanosomatids contain α- or β-tubulin isoforms, as the sequences of the tubulin arrays are all identical (Gallo and Precigout, 1988; Jackson et al., 2006; Schneider et al., 1987).

Trypanosomatids encode a single copy of γ-tubulin in their genome. In metazoan cells, γ-tubulin complexes are responsible for nucleating microtubules at organizing centers, such as centrosomes (Farache et al., 2018). In the subpellicular array, γ-tubulin localizes at the cell anterior where many microtubule minus ends are located, as well as

discrete spots at the minus ends of individual microtubules within the array (Scott et al., 1997). A γ-tubulin complex has been identified in *T. brucei* (γ-TuSC) but does not appear to have a role in subpellicular array biogenesis (Zhou and Li, 2015). The function of γ-tubulin in the array is unknown, although it is important for the assembly of a subset of flagellar axoneme microtubules (McKean et al., 2003).

The trypanosomatid genomes also contain copies of δ-, ε-, and ζ-tubulin (Vaughan et al., 2000; Wickstead and Gull, 2011). These do not appear to be a part of the α/β tandem arrays. Although the localization and function of these tubulins is unknown in trypanosomatids, in *Chlamydomonas* and animal cells, δ-/ε-/ζ-tubulin form a 'module' that is involved in basal body and centriolar structure and orientation (Dutcher and Trabuco, 1998; Turk et al., 2015).

It has recently been discovered that tubulin post-translational modifications comprise a "code" that modifies microtubule dynamics and alters microtubule-associated protein (MAP) binding and behavior (Janke, 2014). The disordered C-terminal tails of tubulin are the most common site of post-translational modifications and MAP interactions. Interestingly, different post-translational modifications and MAPs are enriched in different tubulin structures in *T. brucei* and *T. cruzi*, which suggests that they play a key role in cytoskeletal regulation (Birkett et al., 1992; Gallo and Anderton, 1983; Woods et al., 1989).

The majority of known tubulin post-translational modifications are present in trypanosomatids (**Fig. 5A**). These modifications have been identified with specific antibodies or mass spectrometry; the enzymes involved in the modification pathways are not yet well-described in trypanosomatids. To date, acetylation (Chavan et al., 2007;

Sasse and Gull, 1988; Souto-Padron et al., 1993), detyrosination/tyrosination (Chavan et al., 2007; Gimenez and Machado, 2017; Mattos et al., 2012; Nett et al., 2009; Prasad and Dey, 2000; Sherwin et al., 1987), and phosphorylation (Mattos et al., 2012; Mukhopadhyay et al., 1988; Nett et al., 2009; Prasad and Dey, 2000) have been detected in *T. brucei, T. cruzi,* and *Leishmania*. Poly-glutamylation has been described in *T. brucei* and *Leishmania* (Casanova et al., 2015; Schneider et al., 1997), although poly-glycylation does not appear to be present.

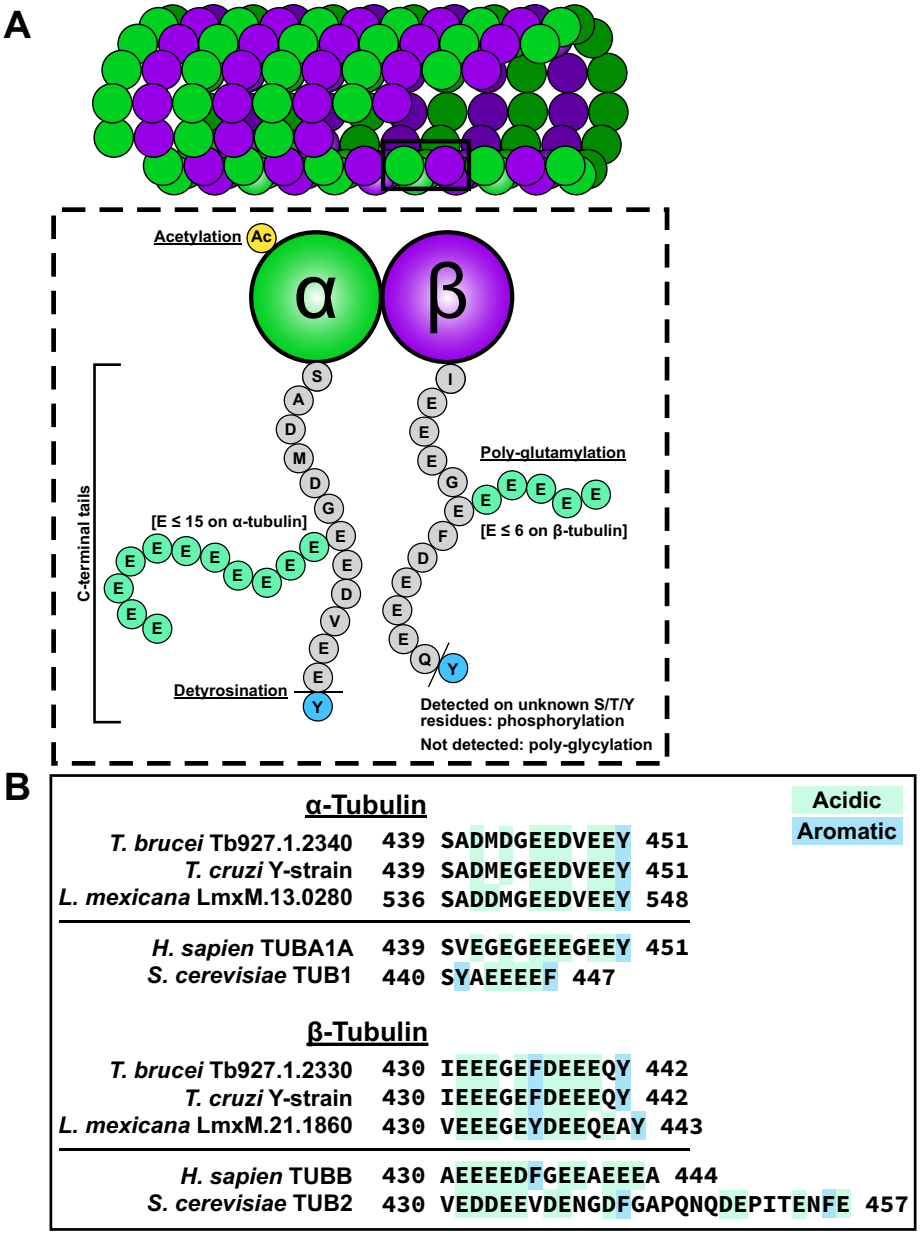

Figure 5. Microtubule modifications found in the trypanosomatid subpellicular array. (A) (Top) A microtubule is a hollow tube made up of tubulin protofilaments, which are comprised of α- and β-tubulin heterodimers (green and purple, respectively. (Bottom) Both α- and β-tubulin subunits have long, intrinsically disordered and highly-charged C-terminal tails that face the cytoplasm, and are the most common site of post-translational modifications. Trypanosomatid microtubules are highly glutamylated on both α- and β-tubulin subunits. The α- and β-tubulin subunits also undergo detyrosination in trypanosomatids, in which the terminal tyrosine residue is cleaved. Unlike most tubulin post-translational modifications, acetylation occurs at an inward-facing site on the α-tubulin subunit. The amino acid sequence of the tails in this schematic is from *Trypanosoma brucei.* **(B)** The amino acid sequences of the cytoplasmic C-terminal tails of α- and β-tubulin from *Trypanosoma brucei, Trypanosoma cruzi* (Y-strain), and *Leishmania mexicana.* The human and yeast sequences are listed beneath for comparison, and acidic and aromatic

charges are indicated. Sequences obtained from (Aslett et al., 2010; Callejas-Hernández et al., 2018).

Acetylated α-tubulin, which is commonly associated with long-lived and stable microtubules, occurs on the microtubule lumen-facing side of the α-tubulin subunit (Janke, 2014). It is found in the subpellicular array as well as the flagellum of *T. brucei, T. cruzi,* and *Leishmania* (Chavan et al., 2007; Sasse and Gull, 1988; Souto-Padron et al., 1993). α-tubulin is acetylated after its incorporation into microtubule polymers (Schneider et al., 1987). The acetylation of α-tubulin appears to weaken inter-protofilament interactions within the microtubule, which increases microtubule flexibility and protects against mechanical stress (Portran et al., 2017). As flagellar beating has been shown to deform the subpellicular array and the cell body in *T. brucei* (Bargul et al., 2016; Sun et al., 2018), acetylation may protect the microtubules in the array from damage and catastrophe. Reduction in α-tubulin acetylation levels also impairs cleavage furrow formation and ingression in bloodstream-form *T. brucei*, although it is unclear by what mechanism (Price et al., 2010).

When α-tubulin is synthesized and polymerized into microtubules, it typically contains a terminal tyrosine residue on its cytoplasmic tail (Nieuwenhuis and Brummelkamp, 2019). Tyrosinated α-tubulin is often used as a marker for newly synthesized microtubules, as the terminal tyrosine is removed by a tubulin carboxypeptidase over time (Kilmartin, 1982; Nieuwenhuis and Brummelkamp, 2019; Sherwin and Gull, 1989a). Soluble α-tubulin can be re-tyrosinated by a tubulin tyrosine ligase, which creates the detyrosination-tyrosination cycle. This cycle is present in *T. brucei* (Schneider et al., 1997; Sherwin and Gull, 1989a; Sherwin et al., 1987), and likely

in *T. cruzi* and *Leishmania* as well, based on the presence of tyrosinated α-tubulin by antibody staining (Chavan et al., 2007; Gimenez and Machado, 2017). The genomes of *T. brucei, T. cruzi*, and *Leishmania* contain many putative tubulin tyrosine ligases, as well as the newly-identified tubulin carboxypeptidase vasohibin (VASH/SVBP) (Aillaud et al., 2017; Aslett et al., 2010; Casanova et al., 2015; van der Laan et al., 2019). Tyrosinated α-tubulin is found at locations within the array that are undergoing microtubule growth, such as the cell posterior and the growing flagellum tip during cell division (Sasse and Gull, 1988; Sherwin and Gull, 1989a; Wheeler et al., 2013b). Newly divided cells elongate and remodel their posterior arrays, which are heavily tyrosinated (Abeywickrema et al., 2019; Wheeler et al., 2013b). During cellular replication in *T. brucei*, the new microtubules that invade between the existing microtubules to enlarge the array are tyrosinated along their entirety (Sherwin and Gull, 1989a). The function of tyrosination is unclear, although in other systems particular kinesins specifically recognize and interact with tyrosinated tubulin (Dunn et al., 2008). Inhibition of detyrosination by depleting TbVASH leads to mitotic and cytokinetic defects, which indicates that the removal of the terminal tyrosine on tubulin is required in these processes (van der Laan et al., 2019). Interestingly, in *T. brucei, T. cruzi*, and *Leishmania*, β-tubulin is also synthesized with a terminal tyrosine residue on its C-terminal tail, which is not found in mammalian or yeast systems (**Fig. 5B**) (Aslett et al., 2010; Nieuwenhuis and Brummelkamp, 2019). In *T. brucei,* it has been shown that this tyrosine can be cleaved (Schneider et al., 1997), which suggests that a detyrosination-tyrosination cycle also exists for β-tubulin in trypanosomatids. The function of the β-tubulin terminal tyrosine, if any, has yet to be investigated.

Both the flagellar and subpellicular array microtubules are poly-glutamylated (Casanova et al., 2015; Schneider et al., 1997). The posterior portion of the array, which grows extensively during cell cycle and differentiation events, is preferentially poly-glutamylated in *T. brucei* trypomastigotes and *L. major* promastigotes (Casanova et al., 2015; Jentzsch et al., 2020). Glutamylation is important for cytokinesis in procyclic *T. brucei,* as decreasing glutamylation levels by depleting glutamylases causes cytokinetic defects (Casanova et al., 2015; Jentzsch et al., 2020). In mammalian systems, poly-glutamylation of up to 10 residues on β-tubulin increases the binding affinity of the microtubule-severing enzyme spastin (Valenstein and Roll-Mecak, 2016). Recent work showing that microtubule severing by spastin and katanin can amplify microtubule number and generate microtubule arrays through their activity (Vemu et al., 2018) may provide a mechanism for the production of the new microtubules that invade the array of dividing trypanosomes. Microtubule severing by katanin is required for cleavage furrow ingression in *T. brucei*, while spastin is necessary for the final abscission event (Zhou et al., 2018).

Tubulin phosphorylation has also been detected in trypanosomatids, but the function of this modification is not known. The tubulin of arsenite-resistant *Leishmania* is hyperphosphorylated (Mukhopadhyay et al., 1988; Prasad and Dey, 2000). In *T. cruzi*, tubulin is dephosphorylated upon parasite interaction with host extracellular matrix proteins (Mattos et al., 2012). These results suggest that tubulin phosphorylation can be regulated by signaling cascades initiated by external stimuli.

These findings indicate that there is a landscape of post-translational modifications across the array that could be used to control the differential recruitment of MAPs and

motors at different times in the cell cycle. This landscape could be driven by levels of microtubule tyrosination. Newly polymerized microtubules are enriched with tyrosinated tubulin (Yu et al., 2015). The detyrosination of α-tubulin preferentially occurs on the microtubule polymer, while re-tyrosination only occurs on free, soluble tubulin. This substrate specificity creates a gradient of tyrosination along the length of individual microtubules, which has been documented in the *T. brucei* subpellicular array (Sherwin and Gull, 1989a). This gradient may act as a rheostat to recruit specific MAPs or modification enzymes that are sensitive to levels of tyrosination. In this fashion, the tubulin code could tune the biophysical properties of array microtubules to account for the local curvature of the cell body, or control how the force generated by flagellar beating is transformed into cell motility.

Subpellicular array regulation by microtubule array-associated proteins and enzymes

In vitro, single microtubules are inherently dynamic and cycle through states of polymerization and depolymerization called ‘rescues’ and ‘catastrophes,’ respectively. Cells regulate this dynamic instability through the activity of tip-binding proteins, molecular motors, and MAPs (Janke, 2014). MAPs can stabilize and bundle microtubules into persistent structures. Few MAPs have been identified in trypanosomatids to date, and little is known about how they function to build, maintain, and remodel the array. As of yet, none of the array-associated proteins identified thus far have been localized to the inter-microtubule crosslinking fibrils that stabilize the array, although some proteins have been found to bundle microtubules in vitro.

In the accompanying table (Table 1), we have listed the proteins currently known to associate with the subpellicular array. The vast majority of these proteins have been identified in *T. brucei* procyclic forms; it is unknown if their functions are conserved in *T. cruzi* or *Leishmania,* although many of these proteins are found in all three species. Although these proteins are broadly referred to in the literature as MAPs, few of them have been shown to bind directly to microtubules or tubulin in vitro, and so caution must be used when applying this term. The array-associated proteins identified thus far have distinct roles in maintaining array architecture, but there is little-to-no mechanistic information on how they function. This area is ripe for research, as the unique functions of these proteins will provide insight into microtubule organization in diverse phyla.

Microtubule array-associated proteins were initially identified through the extraction and solubilization of the array, followed by fractionation and isolation of individual proteins. Some of these proteins, such as a 52 kDa and 33 kDa protein, are able to form crosslinks on mammalian microtubules in vitro with a similar periodicity as found in the subpellicular array (Balaban et al., 1989; Bramblett et al., 1987). This suggests that the fibrils that link microtubules in the array are made up of proteins that bind in a specific orientation along microtubules, thus creating the regular spacing seen in electron micrographs.

Many array-associated proteins appear to have specific localizations across the array. The proteins CAP15 and CAP17, which bundle and stabilize microtubules when expressed ectopically in mammalian cells, localize to the anterior portion of the array (Vedrenne et al., 2002). The recently identified protein PAVE1 preferentially localizes to the posterior array (Hilton et al., 2018), while TbAIR9 is found across the entirety of the

array (May et al., 2012). This distribution pattern suggests that different MAPs are recruited to different parts of the array, perhaps to maintain array shape and facilitate morphogenesis.

In *T. brucei,* several microtubule array-associated proteins are found as paralogous pairs within the genome and are preferentially expressed in either the bloodstream- or procyclic-form of the cell. CAP15 is expressed in bloodstream-forms, while CAP17 is expressed in procyclics (Vedrenne et al., 2002). This pattern is the same for CAP5.5 and CAP5.5V (Olego-Fernandez et al., 2009) and CAP51 and CAP51V (Portman and Gull, 2014). The localization and function of these related proteins is similar in both life cycle stages. The reason for encoding two paralogous proteins with the same function is unclear. Although *T. cruzi* and *L. mexicana* possess homologs of CAP5.5 and CAP51, they do not appear to encode their paralog (Table 1) (Aslett et al., 2010) (Wheeler et al., 2013a). Whether unique paralogous pairs of microtubule array-associated proteins exist in *T. cruzi* or *Leishmania* has yet to be determined. However, the example of paralogs in *T. brucei* presents the possibility that trypanosomatids may differentially regulate microtubule array-associated proteins during life cycle transitions to tune array dynamics in specific life cycle stages. Identification of new proteins in *T. cruzi* and *Leishmania* will be of special interest, as these organisms have both extra- and intra-cellular life cycle stages with vastly different array morphologies.

The microtubules of the array must be organized into a single layer underneath the plasma membrane. This is exemplified by CAP5.5/5.5V and CAP51/51V, which are required to maintain the array microtubules as a single layer in *T. brucei*. When depleted by RNAi, multiple layers of microtubules accumulate underneath the plasma membrane

(Olego-Fernandez et al., 2009; Portman and Gull, 2014). Additionally, the attachment of microtubules to the plasma membrane must also be maintained for correct array organization. The protein WCB, which localizes to the plasma membrane-facing surface of microtubules in extracted cytoskeletons, is one of the proteins that mediates this stable connection (Woods et al., 1992). WCB depletion disrupts array spacing and causes the plasma membrane to bleb across the cell surface; cells divide aberrantly or cease to divide altogether. These results demonstrate the importance of the microtubule-plasma membrane linkage in both array organization and plasma membrane integrity, which appear critical for cell division.

Molecular motors have also been implicated in array biogenesis and remodeling. *L. major* and *T. brucei* genomes encode over 40 kinesins (Wickstead and Gull, 2006). These include kinesins from well-characterized families as well as ungrouped kinetoplastid-specific orphan kinesins. Many of the orphan kinesins characterized thus far have roles in regulating the subpellicular array. In procyclic *T. brucei,* TbKIN-C is found at the extreme posterior of the array and is required to maintain cell shape. Depletion of TbKIN-C results in cells with extended 'nozzle' posteriors (Hu et al., 2012b). TbKIN-D interacts with TbKIN-C and has a similar localization at the posterior tip. Strikingly, TbKIN-D depletion results in the accumulation of multiple layers of microtubules underneath the plasma membrane, similar to the CAP5.5/5.5V and CAP51/51V depletion phenotypes. This suggests that TbKIN-D has a role in remodeling or inserting microtubules into the existing array (Hu et al., 2012a). KLIF, a newly identified orphan kinesin, is required in the final stages of cytokinesis in *T. brucei*. Cells depleted of KLIF stall mid-way through cleavage furrow ingression (Hilton et al., 2018). RNAi against katanin in procyclic *T.*

brucei also stalls the cleavage furrow in a similar manner (Zhou et al., 2018). Interestingly, stalled cleavage furrows were first seen in *T. cruzi* after cells were treated with taxol, which stabilizes microtubules (Baum et al., 1981). These results suggest that microtubules in the array are remodeled by kinesins and microtubule severing enzymes, which have specific functions in maintaining cell shape or segregating the array during cytokinesis. Biophysical characterization of these MAPs, motors, and enzymes is required to determine their mechanism of action and how they localize and function within the context of the array.

Thesis overview and summary of findings

Trypanosomatids cause debilitating diseases in the world's poorest populations. They are under-researched and under-funded (Fitzpatrick et al., 2017), and as such, we lack a basic understanding of how fundamental processes like cell division take place in these organisms. Developing a molecular understanding of their unique cell biology will not only potentially uncover proteins and pathways for therapeutic development, but also broaden our knowledge of how highly divergent organisms differently approach core principles of cell biology, such as cell division and cytoskeletal organization.

The subpellicular microtubule array is a highly conserved and striking feature of trypanosome cell biology. The cell shape produced by the array is essential for cell viability, motility, and pathogenicity. The stability of array microtubules also puts unique constrains on cell division, which must successfully divide the array while maintaining its integrity and cell polarity. However, very little is known about the molecular mechanisms and proteins that drive cytokinesis and maintain cell shape in trypanosomes. The goal of

this thesis research is two-fold: 1) to identify core components of cytokinetic machinery in *T. brucei* and begin to understand their function and 2) to determine the basic principles by which the *T. brucei* subpellicular array is built and maintained.

In Chapter 2, we investigate the function of TOEFAZ1, the first cytokinesis-specific protein discovered in *T. brucei.* TOEFAZ1 is a potential substrate and binding partner of TbPLK and is essential for cytokinesis. It localizes to the new FAZ tip during cell division, which is the location from where cleavage furrow ingression initiates. We determined that TOEFAZ1 consists of three distinct domains, each of which has a separate function. The N-terminal α-helical domain is responsible for protein localization to the new FAZ tip during cell division. The middle intrinsically disordered protein domain mediates the cell-cycle regulation of TOEFAZ1 and is required for TbPLK localization to the new FAZ tip. Interestingly, the intrinsically disordered domain is not required for TOEFAZ1 function or proper cytokinesis. The C-terminal zinc finger domain oligomerizes TOEFAZ1, which is necessary for the protein to localize and function properly. Our data refines the role of TbPLK in trypanosome cytokinesis and suggests that TOEFAZ1 acts as a protein scaffold to recruit and position the molecular machinery that drives cleavage furrow ingression from the new FAZ tip.

In Chapter 3, we determine the function of the protein PAVE1. PAVE1 was identified in a proximity-dependent biotin identification screen of TOEFAZ1, which was conducted to identify proteins involved in cleavage furrow ingression and remodeling of the microtubule array during cell division. PAVE1 localizes to the posterior and ventral edge of the subpellicular array and is necessary to maintain the length of these microtubules. We find that PAVE1 is a component of the inter-microtubule crosslinks at

the array posterior and is specifically added to the extreme posterior end of the array, where microtubule plus-ends are concentrated. PAVE1 and its binding partner PAVE2 form a complex that directly binds the microtubule lattice, making the complex one of the first verified MAPs identified in *T. brucei*. Furthermore, we find that array-associated proteins are differentially localized across the array into specific subdomains: the posterior subdomain to which PAVE1 belongs, the cell middle that encompass the flagellar pocket and nucleus, and the cell anterior. These subdomain localizations are regulated by the protein TbAIR9, and their disruption causes microtubule array defects and inhibits cytokinesis.

Together, these data establish a molecular foundation to understand how cytokinesis takes place in trypanosomes, as well as how the shape of the subpellicular array is created and maintained. These findings enhance our knowledge of the basic cell biology of these divergent organisms, and position trypanosomatids as ideal model systems to investigate cytoskeletal dynamics and organization in an evolutionarily distant branch on the eukaryotic tree of life.

Table 1.

Microtubule array-associated protein	Accession	Organism	Localization	Conservation	Description/ Purported Function	Ref.
p41	Unknown	*T. brucei*	Unknown	Unknown	Has a covalently-bound fatty acid	(Schneider et al., 1988)
52 kDa protein	Unknown	*T. brucei*	Unknown	Unknown	Crosslinks microtubules *in vitro*	(Balaban et al., 1989)
COP33	Unknown	*Crithidia*	Entire subpellicular array	Unknown	Crosslinks microtubules *in vitro*	(Bramblett et al., 1987; Bramblett et al., 1989)
COP61	Unknown	*Crithidia*	Unclear	Unknown	Unknown	(Bramblett et al., 1987; Bramblett et al., 1989)
p15	Unknown	*T. brucei*	Entire subpellicular array	Unknown	Bundles microtubules and co-polymerizes with tubulin *in vitro*	(Balaban and Goldman, 1992)
WCB	Tb927.7.3550	*T. brucei*	Membrane-facing side of entire subpellicular array	Found in *Leishmania* and *T. cruzi*	Crosslinks the plasma membrane to the subpellicular array	(Baines and Gull, 2008)
MARP-1 (p320)	Tb927.10.10360	*T. brucei*	Entire subpellicular array	Found in *Leishmania* and *T. cruzi*	Contains 38 repeats which consist of a microtubule-binding domain; binds microtubules in mammalian cells	(Hemphill et al., 1991; Schneider et al., 1988)
MARP-2	Unknown	*T. brucei*	Unknown	Unknown	Closely related to MARP-1; binds microtubules in mammalian cells with a non-	(Affolter et al., 1994)

					repeat containing C-terminal domain	
Gb4	Tb927.9.2520	*T. brucei*	Microtubule tips at the posterior subpellicular array	Found in *Leishmania* and *T. cruzi*	Large and repetitive	(Rindisbacher et al., 1993)
I/6 autoantigen	Tb927.7.3440	*T. brucei*	Entire subpellicular array	Found in *Leishmania* and *T. cruzi*	Alternatively spliced; may crosslink microtubules	(Detmer et al., 1997)
CAP15/17	Tb927.11.11980 /Tb927.11.16200	*T. brucei*	Anterior subpellicular array	Found only in *T. brucei*	Bundles and stabilizes microtubules in mammalian cells; CAP15 is preferentially expressed in bloodstream-forms; CAP17 is preferentially expressed in procyclic-forms	(Vedrenne et al., 2002)
CAP5.5/5.5V	Tb927.4.3950/ Tb927.8.8330	*T. brucei*	Entire subpellicular array	CAP5.5 found in *Leishmania* and *T. cruzi*	CAP5.5 is preferentially expressed in procyclic-forms; CAP5.5V is preferentially expressed in bloodstream-forms	(Olego-Fernandez et al., 2009)
TbAIR9	Tb927.11.17000	*T. brucei*	Entire subpellicular array	Found in *Leishmania* and *T. cruzi*	Also found in plants	(May et al., 2012)
XMAP215	Tb927.6.3090	*T. brucei*	Positive growing ends of microtubules throughout the subpellicular array	Found in *Leishmania* and *T. cruzi*	Well-known (+)-end tip binding protein in mammalian systems	(Wheeler et al., 2013b)

EB1	Tb927.9.2760	*T. brucei*	Positive growing ends of microtubules throughout the subpellicular array	Found in *T. cruzi*	Well-known (+)-end tip binding protein in mammalian systems	(Sheriff et al., 2014)
CAP51/51V	Tb927.7.2640/ Tb927.7.2650	*T. brucei*	Entire subpellicular array	CAP51 found in *Leishmania* and *T. cruzi*	CAP51 is preferentially expressed in procyclic-forms; CAP51V is preferentially expressed in bloodstream-forms	(Portman and Gull, 2014)
PAVE1	Tb927.8.2030	*T. brucei*	Posterior subpellicular array	Found in *Leishmania* and *T. cruzi*	Predicted coiled-coil	(Hilton et al., 2018)

Table 1. Microtubule array-associated proteins in trypanosomatids.

ACKNOWLEDGEMENTS

The authors would like to thank Dr. Sue Vaughan and Mr. Timm Mohr (Oxford Brookes University) for valuable discussions and for the use of *T. brucei* micrographs. The authors would also like to thank the reviewers for their useful and important insight. Work in CLdG's lab is supported by grants from the National Institutes of Health (1R21AI115089 and 1R01AI112953, to CLdG; and F31AI143163 to ANS).

REFERENCES

Abeywickrema, M., Vachova, H., Farr, H., Mohr, T., Wheeler, R. J., Lai, D.-H., Vaughan, S., Gull, K., Sunter, J. D. and Varga, V. (2019). Non-equivalence in old- and new-flagellum daughter cells of a proliferative division in Trypanosoma brucei. *Mol. Microbiol.* **112**, 1024–1040.

Affolter, M., Hemphill, A., Roditi, I., Müller, N. and Seebeck, T. (1994). The Repetitive Microtubule-Associated Proteins MARP-1 and MARP-2 of Trypanosoma brucei. *J. Struct. Biol.* **112**, 241–251.

Aillaud, C., Bosc, C., Peris, L., Bosson, A., Heemeryck, P., van Dijk, J., Le Friec, J., Boulan, B., Vossier, F., Sanman, L. E., et al. (2017). Vasohibins/SVBP are tubulin carboxypeptidases (TCPs) that regulate neuron differentiation. *Science* **358**, 1448–1453.

Akhmanova, A. and Steinmetz, M. O. (2015). Control of microtubule organization and dynamics: two ends in the limelight. *Nat. Rev. Mol. Cell Biol.* **16**, 711–726.

Alcantara, C. de L., Vidal, J. C., de Souza, W. and Cunha-E-Silva, N. L. (2017). The cytostome-cytopharynx complex of Trypanosoma cruzi epimastigotes disassembles during cell division. *Journal of cell science* **130**, 164–176.

Alcantara, C. L., Vidal, J. C., de Souza, W. and Cunha-E-Silva, N. L. (2014). The three-dimensional structure of the cytostome-cytopharynx complex of Trypanosoma cruzi epimastigotes. *Journal of cell science* **127**, 2227–2237.

Alfred, J. and Baldwin, I. T. (2015). New opportunities at the wild frontier. *Elife* **4**, 24.

Ambit, A., Woods, K. L., Cull, B., Coombs, G. H. and Mottram, J. C. (2011). Morphological events during the cell cycle of Leishmania major. *Eukaryotic Cell* **10**, 1429–1438.

Angelopoulos, E. (1970). Pellicular Microtubules in the Family Trypanosomatidae. *The Journal of Protozoology* **17**, 39–51.

Aslett, M., Aurrecoechea, C., Berriman, M., Brestelli, J., Brunk, B. P., Carrington, M., Depledge, D. P., Fischer, S., Gajria, B., Gao, X., et al. (2010). TriTrypDB: a functional genomic resource for the Trypanosomatidae. *Nucleic Acids Res.* **38**, D457–62.

Baines, A. and Gull, K. (2008). WCB is a C2 domain protein defining the plasma membrane - sub-pellicular microtubule corset of kinetoplastid parasites. *Protist* **159**, 115–125.

Balaban, N. and Goldman, R. (1992). Isolation and characterization of a unique 15 kilodalton trypanosome subpellicular microtubule-associated protein. *Cell Motility and the Cytoskeleton* **21**, 138–146.

Balaban, N., Waithaka, H. K., Njogu, A. R. and Goldman, R. (1989). Isolation of a subpellicular microtubule protein from Trypanosoma brucei that mediates crosslinking of microtubules. *Cell Motility and the Cytoskeleton* **14**, 393–400.

Bargul, J. L., Jung, J., McOdimba, F. A., Omogo, C. O., Adung'a, V. O., Krüger, T., Masiga, D. K. and Engstler, M. (2016). Species-Specific Adaptations of Trypanosome Morphology and Motility to the Mammalian Host. *PLoS Pathog.* **12**, e1005448.

Barrett, M. P. and Croft, S. L. (2012). Management of trypanosomiasis and leishmaniasis. *Br. Med. Bull.* **104**, 175–196.

Baum, S. G., Wittner, M., Nadler, J. P., Horwitz, S. B., Dennis, J. E., Schiff, P. B. and Tanowitz, H. B. (1981). Taxol, a microtubule stabilizing agent, blocks the replication of Trypanosoma cruzi. *PNAS* **78**, 4571–4575.

Benz, C., Clucas, C., Mottram, J. C. and Hammarton, T. C. (2012). Cytokinesis in bloodstream stage Trypanosoma brucei requires a family of katanins and spastin. *PLoS ONE* **7**, e30367.

Bern, C. and Montgomery, S. P. (2009). An estimate of the burden of Chagas disease in the United States. *Clin Infect Dis* **49**, e52–4.

Birkett, C. R., Parma, A. E., Gerke-Bonet, R., Woodward, R. and Gull, K. (1992). Isolation of cDNA clones encoding proteins of complex structures: analysis of the *Trypanosoma brucei* cytoskeleton. *Gene* **110**, 65–70.

Bordier, C., Garavito, R. M. and Armbruster, B. (1982). Biochemical and Structural Analyses of Microtubules in the Pellicular Membrane of Leishmania tropica. *Journal of Protozoology* **29**, 560–565.

Bramblett, G. T., Chang, S. and Flavin, M. (1987). Periodic crosslinking of microtubules by cytoplasmic microtubule-associated and microtubule-corset proteins from a trypanosomatid. *PNAS* 3259–3263.

Bramblett, G. T., Kambadur, R. and Flavin, M. (1989). Immunocytochemical Studies With Antibodies to Three Proteins Prominent in the Isolated Microtubule Cytoskeleton of a Trypanosomatid Cytoskeleton. **13**, 145–157.

Briggs, L. J., McKean, P. G., Baines, A., Moreira-Leite, F., Davidge, J., Vaughan, S. and Gull, K. (2004). The flagella connector of Trypanosoma brucei: an unusual mobile transmembrane junction. *Journal of cell science* **117**, 1641–1651.

Brooker, B. E. (1971). Fine structure of *Bodo saltans* and *Bodo caudatus* (Zoomastigophora: Protozoa) and their affinities with the T*rypanosomatidae*. *Bull. Brit. Mus. Nat. Hist.* **22**, 89–102.

Brun, R., Blum, J., Chappuis, F. and Burri, C. (2010). Human African trypanosomiasis. *Lancet* **375**, 148–159.

Burki, F., Roger, A. J., Brown, M. W. and Simpson, A. G. B. (2020). The New Tree of Eukaryotes. *Trends Ecol Evol* **35**, 43–55.

Callejas-Hernández, F., Rastrojo, A., Poveda, C., Gironès, N. and Fresno, M. (2018). Genomic assemblies of newly sequenced Trypanosoma cruzi strains reveal new genomic expansion and greater complexity. *Sci Rep* **8**, 1–13.

Capewell, P., Cren-Travaillé, C., Marchesi, F., Johnston, P., Clucas, C., Benson, R. A., Gorman, T.-A., Calvo-Alvarez, E., Crouzols, A., Jouvion, G., et al. (2016). The skin is a significant but overlooked anatomical reservoir for vector-borne African trypanosomes. *Elife* **5**, e17716.

Carmena, M., Wheelock, M., Funabiki, H. and Earnshaw, W. C. (2012). The chromosomal passenger complex (CPC): from easy rider to the godfather of mitosis. *Nat. Rev. Mol. Cell Biol.* **13**, 789–803.

Casanova, M., de Monbrison, F., van Dijk, J., Janke, C., Pagès, M. and Bastien, P. (2015). Characterisation of polyglutamylases in trypanosomatids. *International Journal for Parasitology* **45**, 121–132.

Chagas, C. (1909). Nova tripanozomiaze humana. Estudos sobre a morfolojia e o ciclo evolutivo do Schizotrypanum cruzi n. gen., n. sp., ajente etiolojico de nova entidade morbida do homem. *Mem Inst Oswaldo Cruz* **1**.

Chavan, H. D., Singh, G. and Dey, C. S. (2007). Confocal microscopic investigation of tubulin distribution and effect of paclitaxel on posttranslationally modified tubulins in sodium arsenite resistant Leishmania donovani. *Experimental Parasitology* **116**, 320–326.

Claborn, D. M. (2010). The biology and control of leishmaniasis vectors. *J Glob Infect Dis* **2**, 127–134.

De Andrade, P. P. and De Almeida, D. F. (1980). Herpetomonas samuelpessoai: role of subpellicular microtubules in shape transitions of trypanosomatids. *Experimental Parasitology* **50**, 57–66.

de Graffenried, C. L., Anrather, D., Raußendorf, Von, F. and Warren, G. (2013). Polo-like kinase phosphorylation of bilobe-resident TbCentrin2 facilitates flagellar inheritance in Trypanosoma brucei. *Mol. Biol. Cell* **24**, 1947–1963.

de Souza, W. (1999). A Short Review on the Morphology of *Trypanosoma cruzi*: from 1909 to 1999. *Mem Inst Oswaldo Cruz* **94**, 17–36.

Detmer, E., Hemphill, A., Müller, N. and Seebeck, T. (1997). The Trypanosoma brucei autoantigen I/6 is an internally repetitive cytoskeletal protein. *Eur. J. Cell Biol.* **72**, 378–384.

Dunn, S., Morrison, E. E., Liverpool, T. B., Molina-París, C., Cross, R. A., Alonso, M. C. and Peckham, M. (2008). Differential trafficking of Kif5c on tyrosinated and detyrosinated microtubules in live cells. *Journal of cell science* **121**, 1085–1095.

Dutcher, S. K. and Trabuco, E. C. (1998). The UNI3Gene Is Required for Assembly of Basal Bodies of Chlamydomonasand Encodes δ-Tubulin, a New Member of the Tubulin Superfamily. *Mol. Biol. Cell* **9**, 1293–1308.

Dvorak, J. A. and Hyde, T. P. (1973). *Trypanosoma cruzi:* Interaction with vertebrate host cells in vitro: I. Individual interactions at the cellular and subcellular levels. *Experimental Parasitology* **34**, 268–283.

Elias, M. C., da Cunha, J. P. C., de Faria, F. P., Mortara, R. A., Freymüller, E. and Schenkman, S. (2007). Morphological events during the Trypanosoma cruzi cell cycle. *Protist* **158**, 147–157.

Engstler, M., Pfohl, T., Herminghaus, S., Boshart, M., Wiegertjes, G., Heddergott, N. and Overath, P. (2007). Hydrodynamic flow-mediated protein sorting on the cell surface of trypanosomes. *Cell* **131**, 505–515.

Farache, D., Emorine, L., Haren, L. and Merdes, A. (2018). Assembly and regulation of γ-tubulin complexes. *Open Biol* **8**, 170266.

Farr, H. and Gull, K. (2012). Cytokinesis in trypanosomes. *Cytoskeleton (Hoboken)* **69**, 931–941.

Fèvre, E. M., Wissmann, B. V., Welburn, S. C. and Lutumba, P. (2008). The burden of human African trypanosomiasis. *PLoS Negl Trop Dis* **2**, e333.

Fitzpatrick, C., Nwankwo, U., Lenk, E., de Vlas, S. J. and Bundy, D. A. P. (2017). *An Investment Case for Ending Neglected Tropical Diseases*. 3rd ed. (eds. Holmes, K. K., Bertozzi, S., Bloom, B. R., and Jha, P. International Bank for Reconstruction and Development.

Gadadhar, S., Bodakuntla, S., Natarajan, K. and Janke, C. (2017). The tubulin code at a glance. *Journal of cell science* **130**, 1347–1353.

Gallo, J.-M. and Anderton, B. H. (1983). A subpopulation of trypanosome microtubules recognized by a monoclonal antibody to tubulin. *The EMBO Journal* **2**, 479–483.

Gallo, J.-M. and Precigout, E. (1988). Tubulin expression in trypanosomes. *Biology of the Cell* **64**, 137–143.

Gimenez, A. M. and Machado, E. E. (2017). *Trypanosoma cruzi:* Morphological and Microtubular Changes Related to Epimastigote Differentiation under Hyperosmotic Stress. *SOJ Microbiology and Infectious Disease* **4**, 1–6.

Green, R. A., Paluch, E. and Oegema, K. (2012). Cytokinesis in Animal Cells. *Annu. Rev. Cell Dev. Biol.* **28**, 29–58.

Gull, K. (1999). The Cytoskeleton of Trypanosomatid Parasites. *Annu. Rev. Microbiol.* **53**, 629–655.

Gupta, C. M., Ambaru, B. and Bajaj, R. (2020). Emerging Functions of Actins and Actin Binding Proteins in Trypanosomatids. *Front. Cell Dev. Biol.* **8**, 216.

Halliday, C., Billington, K., Wang, Z., Madden, R., Dean, S., Sunter, J. D. and Wheeler, R. J. (2019). Cellular landmarks of Trypanosoma brucei and Leishmania mexicana. *Molecular and Biochemical Parasitology* **230**, 24–36.

Hayes, P., Varga, V., Olego-Fernandez, S., Sunter, J., Ginger, M. L. and Gull, K. (2014). Modulation of a cytoskeletal calpain-like protein induces major transitions in trypanosome morphology. *The Journal of Cell Biology* **206**, 377–384.

Heddergott, N., Krüger, T., Babu, S. B., Wei, A., Stellamanns, E., Uppaluri, S., Pfohl, T., Stark, H. and Engstler, M. (2012). Trypanosome motion represents an adaptation

to the crowded environment of the vertebrate bloodstream. *PLoS Pathog.* **8**, e1003023.

Hemphill, A., Lawson, D. and Seebeck, T. (1991). The Cytoskeletal Architecture of Trypanosoma brucei. *The Journal of Parasitology* **77**, 603–612.

Hilton, N. A., Sladewski, T. E., Perry, J. A., Pataki, Z., Sinclair-Davis, A. N., Muniz, R. S., Tran, H. L., Wurster, J. I., Seo, J. and de Graffenried, C. L. (2018). Identification of TOEFAZ1-interacting proteins reveals key regulators of Trypanosoma brucei cytokinesis. *Mol. Microbiol.* **109**, 306–326.

Hu, H., Hu, L., Yu, Z., Chasse, A. E., Chu, F. and Li, Z. (2012a). An orphan kinesin in trypanosomes cooperates with a kinetoplastid-specific kinesin to maintain cell morphology by regulating subpellicular microtubules. *Journal of cell science* **125**, 4126–4136.

Hu, H., Zhou, Q. and Li, Z. (2015). A novel basal body protein and Polo-like kinase substrate is required for basal body segregation and flagellum adhesion in Trypanosoma brucei. *J. Biol. Chem.* **290**, jbc.M115.674796–25022.

Hu, L., Hu, H. and Li, Z. (2012b). A kinetoplastid-specific kinesin is required for cytokinesis and for maintenance of cell morphology in Trypanosoma brucei. *Mol. Microbiol.* **83**, 565–578.

Hughes, L., Towers, K., Starborg, T., Gull, K. and Vaughan, S. (2013). A cell-body groove housing the new flagellum tip suggests an adaptation of cellular morphogenesis for parasitism in the bloodstream form of Trypanosoma brucei. *Journal of cell science* **126**, 5748–5757.

Ikeda, K. N. and de Graffenried, C. L. (2012). Polo-like kinase is necessary for flagellum inheritance in Trypanosoma brucei. *Journal of cell science* **125**, 3173–3184.

Jackson, A. P., Otto, T. D., Aslett, M., Armstrong, S. D., Bringaud, F., Schlacht, A., Hartley, C., Sanders, M., Wastling, J. M., Dacks, J. B., et al. (2015). Kinetoplastid Phylogenomics Reveals the Evolutionary Innovations Associated with the Origins of Parasitism. *Curr. Biol.* **26**, 161–172.

Jackson, A. P., Vaughan, S. and Gull, K. (2006). Evolution of tubulin gene arrays in Trypanosomatid parasites: genomic restructuring in *Leishmania*. *BMC Genomics* **7**, 1–14.

Janke, C. (2014). The tubulin code: molecular components, readout mechanisms, and functions. *The Journal of Cell Biology* **206**, 461–472.

Jentzsch, J., Sabri, A., Speckner, K., Lallinger-Kube, G., Weiss, M. and Ersfeld, K. (2020). Microtubule polyglutamylation is important for regulating cytoskeletal architecture and motility in Trypanosoma brucei. *Journal of cell science* **133**, jcs248047.

Johnson, P. J., Kooter, J. M. and Borst, P. (1987). Inactivation of Transcription by UV Irradiation of T. brucei Provides Evidence for a Multicistronic Transcription Unit Including a VSG Gene. *Cell* **51**, 273–381.

Kennedy, P. G. (2013). Clinical features, diagnosis, and treatment of human African trypanosomiasis (sleeping sickness). *The Lancet Neurology* **12**, 186–194.

Kilmartin, J. V. (1982). Rat monoclonal antitubulin antibodies derived by using a new nonsecreting rat cell line. *The Journal of Cell Biology* **93**, 576–582.

Kohl, L. and Gull, K. (1998). Molecular architecture of the trypanosome cytoskeleton. *Molecular and Biochemical Parasitology* **93**, 1–9.

Kurup, S. P. and Tarleton, R. L. (2014). The Trypanosoma cruzi Flagellum Is Discarded via Asymmetric Cell Division following Invasion and Provides Early Targets for Protective CD8+ T Cells. *Cell Host & Microbe* **16**, 439–449.

Lacomble, S., Vaughan, S., Gadelha, C., Morphew, M. K., Shaw, M. K., McIntosh, J. R. and Gull, K. (2009). Three-dimensional cellular architecture of the flagellar pocket and associated cytoskeleton in trypanosomes revealed by electron microscope tomography. *Journal of cell science* **122**, 1081–1090.

Lacomble, S., Vaughan, S., Gadelha, C., Morphew, M. K., Shaw, M. K., McIntosh, J. R. and Gull, K. (2010). Basal body movements orchestrate membrane organelle division and cell morphogenesis in Trypanosoma brucei. *Journal of cell science* **123**, 2884–2891.

LaCount, D. J., Barrett, B. and Donelson, J. E. (2002). Trypanosoma brucei FLA1 is required for flagellum attachment and cytokinesis. *J. Biol. Chem.* **277**, 17580–17588.

Landfear, S. M., McMahon-Pratt, D. and Wirth, D. F. (1983). Tandem arrangment of tubulin genes in the protozoan parasite Leishmania enriettii. *Mol. Cell. Biol.* **3**, 1070–1076.

Li, Z., Lee, J. H., Chu, F., Burlingame, A. L., Günzl, A. and Wang, C. C. (2008). Identification of a novel chromosomal passenger complex and its unique localization during cytokinesis in Trypanosoma brucei. *PLoS ONE* **3**, e2354.

Li, Z., Umeyama, T. and Wang, C. C. (2009). The Aurora Kinase in Trypanosoma brucei plays distinctive roles in metaphase-anaphase transition and cytokinetic initiation. *PLoS Pathog.* **5**, e1000575.

Lindner, A. K., Lejon, V., Chappuis, F., Seixas, J., Kazumba, L., Barrett, M. P., Mwamba, E., Erphas, O., Akl, E. A., Villanueva, G., et al. (2020). New WHO guidelines for treatment of gambiense human African trypanosomiasis including fexinidazole: substantial changes for clinical practice. *Lancet Infect Dis* **20**, e38–e46.

Lord, J. S., Hargrove, J. W., Torr, S. J. and Vale, G. A. (2018). Climate change and African trypanosomiasis vector populations in Zimbabwe's Zambezi Valley: A mathematical modelling study. *PLoS Med* **15**, e1002675.

Lozano-Núñez, A., Ikeda, K. N., Sauer, T. and de Graffenried, C. L. (2013). An analogue-sensitive approach identifies basal body rotation and flagellum attachment zone elongation as key functions of PLK in Trypanosoma brucei. *Mol. Biol. Cell* **24**, 1321–1333.

MacRae, T. H. and Gull, K. (1990). Purification and assembly in vitro of tubulin from Trypanosoma brucei brucei. *Biochem. J.* **265**, 87–93.

Maingon, R., Gerke, R., Rodriguez, M., Urbina, J., Hoenicka, J., Negri, S., Aguirre, T., Nehlin, J., Knapp, T. and Crampton, J. (1988). The tubulin genes of Trypanosoma cruzi. *European Journal of Biochemistry* **171**, 285–589.

Matthews, K. R. (2011). Controlling and coordinating development in vector-transmitted parasites. *Science* **331**, 1149–1153.

Matthews, K. R., Sherwin, T. and Gull, K. (1995). Mitochondrial genome repositioning during the differentiation of the African trypanosome between life cycle forms is microtubule mediated. *Journal of cell science* **108**, 2231–2239.

Mattos, E. C., Schumacher, R. I., Colli, W. and Alves, M. J. M. (2012). Adhesion of Trypanosoma cruzi trypomastigotes to fibronectin or laminin modifies tubulin and paraflagellar rod protein phosphorylation. *PLoS ONE* **7**, e46767.

May, S. F., Peacock, L., Almeida Costa, C. I. C., Gibson, W. C., Tetley, L., Robinson, D. R. and Hammarton, T. C. (2012). The Trypanosoma brucei AIR9-like protein is cytoskeleton-associated and is required for nucleus positioning and accurate cleavage furrow placement. *Mol. Microbiol.* **84**, 77–92.

McAllaster, M. R., Ikeda, K. N., Lozano-Núñez, A., Anrather, D., Unterwurzacher, V., Gossenreiter, T., Perry, J. A., Crickley, R., Mercadante, C. J., Vaughan, S., et al. (2015a). Proteomic identification of novel cytoskeletal proteins associated with TbPLK, an essential regulator of cell morphogenesis in Trypanosoma brucei. *Mol. Biol. Cell* **26**, 3013–3029.

McAllaster, M. R., Ikeda, K. N., Lozano-Núñez, A., Anrather, D., Unterwurzacher, V., Gossenreiter, T., Perry, J. A., Crickley, R., Mercadante, C. J., Vaughan, S., et al. (2015b). Proteomic identification of novel cytoskeletal proteins associated with TbPLK, an essential regulator of cell morphogenesis in Trypanosoma brucei. *Mol. Biol. Cell* **26**, 3013–3029.

McKean, P. G., Baines, A., Vaughan, S. and Gull, K. (2003). γ-tubulin functions in the nucleation of a discrete subset of microtubules in the eukaryotic flagellum. *Curr. Biol.* **13**, 598–602.

Meyer, H. and de Souza, W. (1976). Electron Microscopic Study of *Trypanosoma cruzi* Periplast in Tissue Cultures. I. Number and Arrangement of the Peripheral Microtubules in the Various Forms of the Parasite's Life Cycle. *The Journal of Protozoology* **23**, 385–390.

Meymandi, S., Hernandez, S., Park, S., Sanchez, D. R. and Forsyth, C. (2018). Treatment of Chagas Disease in the United States. *Curr Treat Options Infect Dis* **10**, 373–388.

Mitchison, T. and Kirschner, M. (1984). Dynamic instability of microtubule growth. *Nature* **312**, 237–242.

Moreira, B., Da Fonseca, C. K., Hammarton, T. C. and Baqui, M. M. A. (2017). Giant FAZ10 is required for flagellum attachment zone stabilization and furrow positioning in *Trypanosoma brucei*. *Journal of cell science* **130**, 1179-1193.

Mukhopadhyay, N. K., Saha, A. K., Lovelace, J. K., Da Silva, R., Sacks, D. L. and Glew, R. H. (1988). Comparison of the Protein Kinase and Acid Phosphatase Activities of Five Species of *Leishmania*. *The Journal of Protozoology* **35**, 601–607.

Müller, S. and Jürgens, G. (2015). Plant cytokinesis-No ring, no constriction but centrifugal construction of the partitioning membrane. *Semin. Cell Dev. Biol.*

Nett, I. R. E., Martin, D. M. A., Miranda-Saavedra, D., Lamont, D., Barber, J. D., Mehlert, A. and Ferguson, M. A. J. (2009). The Phosphoproteome of Bloodstream Form Trypanosoma brucei, Causative Agent of African Sleeping Sickness. *Molecular & Cellular Proteomics* **8**, 1527–1538.

Ngô, H., Tschudi, C., Gull, K. and Ullu, E. (1998). Double-stranded RNA induces mRNA degradation in Trypanosoma brucei. *PNAS* **95**, 14687–14692.

Nieuwenhuis, J. and Brummelkamp, T. R. (2019). The Tubulin Detyrosination Cycle: Function and Enzymes. *Trends in Cell Biology* **29**, 80–92.

Nogales, E., Whittaker, M., Milligan, R. A. and Downing, K. H. (1999). High-resolution model of the microtubule. *Cell* **96**, 79–88.

Olego-Fernandez, S., Vaughan, S., Shaw, M. K., Gull, K. and Ginger, M. L. (2009). Cell morphogenesis of Trypanosoma brucei requires the paralogous, differentially expressed calpain-related proteins CAP5.5 and CAP5.5V. *Protist* **160**, 576–590.

P De Koning, H. (2020). The Drugs of Sleeping Sickness: Their Mechanisms of Action and Resistance, and a Brief History. *Trop Med Infect Dis* **5**, 14.

Peacock, L., Kay, C., Bailey, M. and Gibson, W. (2018). Shape-shifting trypanosomes: Flagellar shortening followed by asymmetric division in Trypanosoma congolense from the tsetse proventriculus. *PLoS Pathog.* **14**, e1007043.

Peng, D., Kurup, S. P., Yao, P. Y., Minning, T. A. and Tarleton, R. L. (2014). CRISPR-Cas9-mediated single-gene and gene family disruption in Trypanosoma cruzi. *MBio* **6**, e02097–14.

Ploubidou, A., Robinson, D. R., Docherty, R. C., Ogbadoyi, E. O. and Gull, K. (1999). Evidence for novel cell cycle checkpoints in trypanosomes: kinetoplast segregation and cytokinesis in the absence of mitosis. *Journal of cell science* **112**, 4641–4650.

Pollard, T. D. and Wu, J.-Q. (2010). Understanding cytokinesis: lessons from fission yeast. *Nat. Rev. Mol. Cell Biol.* **11**, 1–7.

Portman, N. and Gull, K. (2014). Identification of paralogous life-cycle stage specific cytoskeletal proteins in the parasite Trypanosoma brucei. *PLoS ONE* **9**, e106777.

Portran, D., Schaedel, L., Xu, Z., Théry, M. and Nachury, M. V. (2017). Tubulin acetylation protects long-lived microtubules against mechanical ageing. *Nat. Cell Biol.* **19**, 391–398.

Prasad, V. and Dey, C. S. (2000). Tubulin is hyperphosphorylated on serine and tyrosine residues in arsenite-resistant Leishmania donovani promastigotes. *Parasitol. Res.* **86**, 876–880.

Price, H. P., Peltan, A., Stark, M. and Smith, D. F. (2010). The small GTPase ARL2 is required for cytokinesis in Trypanosoma brucei. *Molecular and Biochemical Parasitology* **173**, 123–131.

Ramos, T. C. P., Freymüller-Haapalainen, E. and Schenkman, S. (2011). Three-dimensional reconstruction of Trypanosoma cruzi epimastigotes and organelle distribution along the cell division cycle. *Cytometry A* **79**, 538–544.

Rassi, A. and Marin-Neto, J. A. (2010). Chagas disease. *Lancet* **375**, 1388–1402.

Richards, T. A. and Cavalier-Smith, T. (2005). Myosin domain evolution and the primary divergence of eukaryotes. *Nature* **436**, 1113–1118.

Rindisbacher, L., Hemphill, A. and Seebeck, T. (1993). A repetitive protein from Trypanosoma brucei which caps the microtubules at the posterior end of the cytoskeleton. *Molecular and Biochemical Parasitology* **58**, 83–96.

Robinson, D. R. and Gull, K. (1991). Basal body movements as a mechanism for mitochondrial genome segregation in the trypanosome cell cycle. *Nature* **352**, 731–733.

Robinson, D. R., Sherwin, T., Ploubidou, A., Byard, E. H. and Gull, K. (1995). Microtubule polarity and dynamics in the control of organelle positioning, segregation,

and cytokinesis in the trypanosome cell cycle. *The Journal of Cell Biology* **128**, 1163–1172.

Robinson, D., Beattie, P., Sherwin, T. and Gull, K. (1991). Microtubules, tubulin, and microtubule-associated proteins of trypanosomes. *Meth. Enzymol.* **196**, 285–299.

Rotureau, B., Blisnick, T., Subota, I., Julkowska, D., Cayet, N., Perrot, S. and Bastin, P. (2014). Flagellar adhesion in Trypanosoma brucei relies on interactions between different skeletal structures in the flagellum and cell body. *Journal of cell science* **127**, 204–215.

Rotureau, B., Subota, I. and Bastin, P. (2011). Molecular bases of cytoskeleton plasticity during the Trypanosoma brucei parasite cycle. *Cellular Microbiology* **13**, 705–716.

Russell, D. G., Miller, D. and Gull, K. (1984). Tubulin heterogenicity in the trypanosome Crithidia fasciculata. *Mol. Cell. Biol.* **4**, 779–790.

Russell, J. J., Theriot, J. A., Sood, P., Marshall, W. F., Landweber, L. F., Fritz-Laylin, L., Polka, J. K., Oliferenko, S., Gerbich, T., Gladfelter, A., et al. (2017). Non-model model organisms. *BMC Biol.* **15**, 55.

Salcedo, J. A. G., Morga, D. P., Gijón, P., Dilbeck, V., Pays, E. and Nolan, D. P. (2004). A differential role for actin during the life cycle of Trypanosoma brucei. *The EMBO Journal* **23**, 780–789.

Sanyal, A. B. and Gupta, Sen, P. C. (1967). Fine structure of Leishmania in dermal leishmanoid. *Transactions of the Royal Society of Tropical Medicine and Hygiene* **61**, 211–216.

Sasse, R. and Gull, K. (1988). Tubulin post-translational modifications and the construction of microtubular organelles in Trypanosoma brucei. *Journal of cell science* **90**, 577–589.

Schneider, A., Eichenberger, W. and Seebeck, T. (1988). A microtubule-binding protein of Trypanosoma brucei which contains covalently bound fatty acid. *J. Biol. Chem.* **263**, 6472–6475.

Schneider, A., Plessmann, U. and Weber, K. (1997). Subpellicular and flagellar microtubules of Trypanosoma brucei are extensively glutamylated. *Journal of cell science* 431–437.

Schneider, A., Sherwin, T., Sasse, R., Russell, D. G., Gull, K. and Seebeck, T. (1987). Subpellicular and Flagellar Microtubules of Trypanosoma brucei brucei Contain the Same **α-Tubulin Isoforms**. *The Journal of Cell Biology* **104**, 431–438.

Scott, V., Sherwin, T. and Gull, K. (1997). γ-tubulin in trypanosomes: molecular characterisation and localisation to multiple and diverse microtubule organising centres. *Journal of cell science* **110**, 157–168.

Seebeck, T., Whittaker, P. A., Imboden, M. A., Hardman, N. and Braun, R. (1983). Tubulin genes of Trypanosoma brucei: A tightly clustered family of alternating genes. *PNAS* **80**, 4634–4638.

Sharma, R., Peacock, L., Gluenz, E., Gull, K., Gibson, W. and Carrington, M. (2008). Asymmetric Cell Division as a Route to Reduction in Cell Length and Change in Cell Morphology in Trypanosomes. *Protist* **159**, 137–151.

Sheriff, O., Lim, L.-F. and He, C. Y. (2014). Tracking the biogenesis and inheritance of subpellicular microtubule in Trypanosoma brucei with inducible YFP-α-tubulin. *Biomed Res Int* **2014**, 1–12.

Sherwin, T. and Gull, K. (1989a). Visualization of Detyrosination along Single Microtubules Reveals Novel Mechanisms of Assembly during Cytoskeletal Duplication in Trypanosomes. *Cell* **57**, 211–221.

Sherwin, T. and Gull, K. (1989b). The cell division cycle of Trypanosoma brucei brucei: timing of event markers and cytoskeletal modulations. *Philosophical Transactions of the Royal Society B: Biological Sciences* **323**, 573–588.

Sherwin, T., Schneider, A., Sasse, R., Seebeck, T. and Gull, K. (1987). Distinct localization and cell cycle dependence of COOH terminally tyrosinolated alpha-tubulin in the microtubules of Trypanosoma brucei brucei. *The Journal of Cell Biology* **104**, 439–446.

Sollelis, L., Ghorbal, M., MacPherson, C. R., Martins, R. M., Kuk, N., Crobu, L., Bastien, P., Scherf, A., Lopez-Rubio, J.-J. and Sterkers, Y. (2015). First efficient CRISPR-Cas9-mediated genome editing in Leishmania parasites. *Cellular Microbiology* **17**, 1405–1412.

Souto-Padron, T., Cunha-E-Silva, N. L. and Souza, W. de (1993). Acetylated alpha-tubulin in *Trypanosoma cruzi*: immunocytochemical localization. *Mem Inst Oswaldo Cruz* **88**, 517–528.

Souto-Padrón, T., de Souza, W. and Heuser, J. E. (1984). Quick-freeze, deep-etch rotary replication of *Trypanosoma cruzi* and *Herpetomonas megaseliae*. *Journal of cell science* **69**, 167–178.

Sun, S. Y., Kaelber, J. T., Chen, M., Dong, X., Nematbakhsh, Y., Shi, J., Dougherty, M., Lim, C. T., Schmid, M. F., Chiu, W., et al. (2018). Flagellum couples cell shape to motility in Trypanosoma brucei. *Proc. Natl. Acad. Sci. U.S.A.* **115**, E5916–E5925.

Sun, S. Y., Wang, C., Yuan, Y. A. and He, C. Y. (2013). An intracellular membrane junction consisting of flagellum adhesion glycoproteins links flagellum biogenesis to cell morphogenesis in Trypanosoma brucei. *Journal of cell science* **126**, 520–531.

Sunter, J. and Gull, K. (2017). Shape, form, function and Leishmania pathogenicity: from textbook descriptions to biological understanding. *Open Biol* **7**, 170165–13.

Sunter, J. D. and Gull, K. (2016). The Flagellum Attachment Zone: "The Cellular Ruler" of Trypanosome Morphology. *Trends Parasitol.* **32**, 309–324.

Sunter, J. D., Benz, C., Andre, J., Whipple, S., McKean, P. G., Gull, K., Ginger, M. L. and Lukeš, J. (2015a). Flagellum attachment zone protein modulation and regulation of cell shape in Trypanosoma brucei life cycle transitions. *Journal of cell science* **128**, jcs.171645–3130.

Sunter, J. D., Varga, V., Dean, S. and Gull, K. (2015b). A dynamic coordination of flagellum and cytoplasmic cytoskeleton assembly specifies cell morphogenesis in trypanosomes. *Journal of cell science* **128**, 1580–1594.

Torres-Guerrero, E., Quintanilla-Cedillo, M. R., Ruiz-Esmenjaud, J. and Arenas, R. (2017). Leishmaniasis: a review. *F1000Res* **6**, 750.

Trindade, S., Rijo-Ferreira, F., Carvalho, T., Pinto-Neves, D., Guegan, F., Aresta-Branco, F., Bento, F., Young, S. A., Pinto, A., Van Den Abbeele, J., et al. (2016). Trypanosoma brucei Parasites Occupy and Functionally Adapt to the Adipose Tissue in Mice. *Cell Host & Microbe* **19**, 837–848.

Tu, X., Kumar, P., Li, Z. and Wang, C. C. (2006). An aurora kinase homologue is involved in regulating both mitosis and cytokinesis in Trypanosoma brucei. *J. Biol. Chem.* **281**, 9677–9687.

Turk, E., Wills, A. A., Kwon, T., Sedzinski, J., Wallingford, J. B. and Stearns, T. (2015). Zeta-Tubulin Is a Member of a Conserved Tubulin Module and Is a Component of the Centriolar Basal Foot in Multiciliated Cells. *Curr. Biol.* **25**, 2177–2183.

Tyler, K. M. and Engman, D. M. (2001). The life cycle of Trypanosoma cruzi revisited. *International Journal for Parasitology* **31**, 473–481.

Valenstein, M. L. and Roll-Mecak, A. (2016). Graded Control of Microtubule Severing by Tubulin Glutamylation. *Cell* **164**, 911–921.

Van Den Abbeele, J., Claes, Y., van Bockstaele, D., Le Ray, D. and Coosemans, M. (1999). Trypanosoma brucei spp. development in the tsetse fly: characterization of the post-mesocyclic stages in the foregut and proboscis. *Parasitology* **118**, 469–478.

van der Laan, S., Lévêque, M. F., Marcellin, G., Vezenkov, L., Lannay, Y., Dubra, G., Bompard, G., Ovejero, S., Urbach, S., Burgess, A., et al. (2019). Evolutionary Divergence of Enzymatic Mechanisms for Tubulin Detyrosination. *Cell Rep* **29**, 4159–4171.e6.

Varga, V., Moreira-Leite, F., Portman, N. and Gull, K. (2017). Protein diversity in discrete structures at the distal tip of the trypanosome flagellum. *Proc. Natl. Acad. Sci. U.S.A.* **114**, E6546–E6555.

Varikuti, S., Jha, B. K., Volpedo, G., Ryan, N. M., Halsey, G., Hamza, O. M., McGwire, B. S. and Satoskar, A. R. (2018). Host-Directed Drug Therapies for Neglected Tropical Diseases Caused by Protozoan Parasites. *Front Microbiol* **9**, 2655.

Vaughan, S. and Gull, K. (2008). The structural mechanics of cell division in Trypanosoma brucei. *Biochem Soc Trans* **36**, 421–424.

Vaughan, S., Attwood, T., Navarro, M., Scott, V., McKean, P. and Gull, K. (2000). New tubulins in protozoal parasites. *Curr. Biol.* **10**, R258–9.

Vaughan, S., Kohl, L., Ngai, I., Wheeler, R. J. and Gull, K. (2008). A repetitive protein essential for the flagellum attachment zone filament structure and function in Trypanosoma brucei. *Protist* **159**, 127–136.

Vedrenne, C., Giroud, C., Robinson, D. R., Besteiro, S., Bosc, C., Bringaud, F. and Baltz, T. (2002). Two related subpellicular cytoskeleton-associated proteins in Trypanosoma brucei stabilize microtubules. *Mol. Biol. Cell* **13**, 1058–1070.

Vemu, A., Atherton, J., Spector, J. O., Moores, C. A. and Roll-Mecak, A. (2017). Tubulin isoform composition tunes microtubule dynamics. *Mol. Biol. Cell* **28**, 3564–3572.

Vemu, A., Szczesna, E., Zehr, E. A., Spector, J. O., Grigorieff, N., Deaconescu, A. M. and Roll-Mecak, A. (2018). Severing enzymes amplify microtubule arrays through lattice GTP-tubulin incorporation. *Science* **361**, eaau1504–14.

Vickerman, K. (1994). The evolutionary expansion of the trypanosomatid flagellates. *International Journal for Parasitology* **24**, 1317–1331.

Weise, F., Stierhof, Y. D., Kühn, C., Wiese, M. and Overath, P. (2000). Distribution of GPI-anchored proteins in the protozoan parasite Leishmania, based on an improved

ultrastructural description using high-pressure frozen cells. *Journal of cell science* **113 Pt 24**, 4587–4603.

Werbovetz, K. A., Brendle, J. J. and Sackett, D. L. (1999). Purification, characterization, and drug susceptibility of tubulin from Leishmania. *Molecular and Biochemical Parasitology* **98**, 53–65.

Wheeler, R. J., Gluenz, E. and Gull, K. (2015). Basal body multipotency and axonemal remodelling are two pathways to a 9+0 flagellum. *Nat Commun* **6**, 1–10.

Wheeler, R. J., Gluenz, E. and Gull, K. (2011). The cell cycle of Leishmania: morphogenetic events and their implications for parasite biology. *Mol. Microbiol.* **79**, 647–662.

Wheeler, R. J., Gluenz, E. and Gull, K. (2013a). The limits on trypanosomatid morphological diversity. *PLoS ONE* **8**, e79581.

Wheeler, R. J., Gull, K. and Sunter, J. D. (2019). Coordination of the Cell Cycle in Trypanosomes. *Annu. Rev. Microbiol.* **73**, 133–154.

Wheeler, R. J., Scheumann, N., Wickstead, B., Gull, K. and Vaughan, S. (2013b). Cytokinesis in Trypanosoma brucei differs between bloodstream and tsetse trypomastigote forms: implications for microtubule-based morphogenesis and mutant analysis. *Mol. Microbiol.* **90**, 1339–1355.

Wheeler, R. J., Sunter, J. D. and Gull, K. (2016). Flagellar pocket restructuring through the *Leishmania* life cycle involves a discrete flagellum attachment zone. *Journal of cell science* **129**, 854–867.

Wickstead, B. and Gull, K. (2006). A “Holistic” Kinesin Phylogeny Reveals New Kinesin Families and Predicts Protein Functions. *Mol. Biol. Cell* **17**, 1734–1743.

Wickstead, B. and Gull, K. (2011). The evolution of the cytoskeleton. *The Journal of Cell Biology* **194**, 513–525.

Wilkinson, S. R. and Kelly, J. M. (2009). Trypanocidal drugs: mechanisms, resistance and new targets. *Expert Rev Mol Med* **11**, e31.

Woods, A., Baines, A. J. and Gull, K. (1992). A high molecular mass phosphoprotein defined by a novel monoclonal antibody is closely associated with the intermicrotubule cross bridges in the Trypanosoma brucei cytoskeleton. *Journal of cell science* **103**, 665–675.

Woods, A., Sherwin, T., Sasse, R., MacRae, T. H., Baines, A. J. and Gull, K. (1989). Definition of individual components within the cytoskeleton of Trypanosoma brucei by a library of monoclonal antibodies. *Journal of cell science* **93**, 491–500.

World Health Organization (2013). Research Priorities for Chagas Disease, Human African Trypanosomiasis and Leishmaniasis. *WHO Technical Report Series* **975**, 1–116.

Yu, I., Garnham, C. P. and Roll-Mecak, A. (2015). Writing and Reading the Tubulin Code. *J. Biol. Chem.* **290**, 17163–17172.

Yu, Z., Liu, Y. and Li, Z. (2012). Structure-function relationship of the Polo-like kinase in Trypanosoma brucei. *Journal of cell science* **125**, 1519–1530.

Zhou, Q. and Li, Z. (2015). The γ-tubulin complex in Trypanosoma brucei: molecular composition, subunit interdependence and requirement for axonemal central pair protein assembly. *Mol. Microbiol.* **98**, 667–680.

Zhou, Q., An, T., Pham, K. T. M., Hu, H. and Li, Z. (2018). The CIF1 protein is a master orchestrator of trypanosome cytokinesis that recruits several cytokinesis regulators to the cytokinesis-initiation site. *J. Biol. Chem.* **293**, 16177–16192.

Zhou, Q., Gu, J., Lun, Z.-R., Ayala, F. J. and Li, Z. (2016). Two distinct cytokinesis pathways drive trypanosome cell division initiation from opposite cell ends. *PNAS* 201601596–15.

Zhou, Q., Liu, B., Sun, Y. and He, C. Y. (2011). A coiled-coil- and C2-domain-containing protein is required for FAZ assembly and cell morphology in Trypanosoma brucei. *Journal of cell science* **124**, 3848–3858.

Zitouni, S., Nabais, C., Jana, S. C., Guerrero, A. and Bettencourt-Dias, M. (2014). Polo-like kinases: structural variations lead to multiple functions. *Nat. Rev. Mol. Cell Biol.* **15**, 433–452.

Chapter 2:

Functional analysis of TOEFAZ1 uncovers protein domains essential for cytokinesis in *Trypanosoma brucei*

Originally published in *Journal of Cell Science*, 2017

Vol. 130, Issue 22, pages 3918-3932.

Functional analysis of TOEFAZ1 uncovers protein domains essential for cytokinesis in *Trypanosoma brucei*

Amy N. Sinclair-Davis[1], Michael R. McAllaster[1, ¶], and Christopher L. de Graffenried[1*]

1. Department of Molecular Microbiology and Immunology, Brown University, Providence, RI, 02912

*To whom correspondence should be addressed. Phone: +1 (401) 863-9775

E-mail: Christopher_degraffenried@Brown.edu.

¶ Current address: Department of Pathology and Immunology, Washington University School of Medicine, St. Louis, MO 63110.

Abbreviations: FAZ, flagellum attachment zone; TOEFAZ1, tip of the extending FAZ protein 1; TF1, TOEFAZ1; FP, flagellar pocket; FPC, flagellar pocket collar; MtQ, microtubule quartet; FC, flagellar connector; TbPLK, *Trypanosoma brucei* polo-like kinase; BioID, proximity-dependent biotinylation; CIF1, cytokinetic initiation factor 1; IDP, intrinsically disordered protein; ZnF, zinc finger; disuccinimidyl suberate, (DSS); WCL, whole cell lysate; nt, nucleotide; SD, standard deviation

Abstract

The parasite *Trypanosoma brucei* is highly polarized, including a flagellum that is attached along the cell surface by the flagellum attachment zone (FAZ). During cell division, the new FAZ positions the cleavage furrow, which ingresses from the anterior tip of the cell towards the posterior. We recently identified Tip Of the Extending FAZ protein 1 (TOEFAZ1) as an essential protein in trypanosome cytokinesis. We analyzed the localization and function of TOEFAZ1 domains using overexpression and RNAi complementation. TOEFAZ1 comprises three domains with separable functions: an N-terminal α-helical domain that may be involved in FAZ recruitment, a central intrinsically disordered domain that retains the morphogenic kinase TbPLK at the new FAZ tip, and a C-terminal zinc finger domain necessary for TOEFAZ1 oligomerization. Both the N-terminal and C-terminal domains are essential for TOEFAZ1 function, but TbPLK retention at the FAZ is not necessary for cytokinesis. The feasibility of alternate cytokinetic pathways that do not employ TOEFAZ1 are also assessed. Our results show that TOEFAZ1 is a multimeric scaffold for recruiting proteins that control the timing and location of cleavage furrow ingression.

INTRODUCTION

The protozoan parasite *Trypanosoma brucei* is the causative agent of African sleeping sickness in humans and nagana in cattle, both of which are sources of substantial hardship in sub-Saharan Africa (Fèvre et al., 2008). *T. brucei* is an obligate extracellular pathogen that has evolved a unique cell morphology as a means to survive within its mammalian and insect hosts (Gull, 1999). Trypanosomes have a long, tapered cell body shaped by a subpellicular microtubule array that underlies the cell surface (**Fig. 1A)** (Anderson and Ellis, 1965; Vickerman, 1962). A single flagellum nucleates near the posterior end of the cell and is attached along the cell body, extending towards the cell anterior (Langousis and Hill, 2014). The attachment and positioning of the flagellum are essential for proper motility and evasion of the host immune response (Engstler et al., 2007; Heddergott et al., 2012). Along with replicating and partitioning cellular organelles, cell division in *T. brucei* must faithfully transmit this complex cellular morphology to ensure the viability of daughter cells (Farr and Gull, 2012; Wheeler et al., 2013). Unlike many other organisms, trypanosomes maintain their high degree of polarity throughout cell division, which puts unique constraints on this process.

The cytoskeletal components associated with the flagellum play an important role in maintaining cell morphology (**Fig. 1A**). A single basal body nucleates the flagellum from the base of the cell surface invagination known as the flagellar pocket (FP), which is the only compartment in trypanosomes that is competent for endo- or exo-cytosis. The top of the FP is tightly apposed to the flagellar membrane by a series of cytoskeletal structures including the flagellar pocket collar (FPC), the hook complex, and the centrin arm (Bonhivers et al., 2008; He et al., 2005; Morriswood, 2015; Morriswood and Schmidt, 2015). Once the flagellum emerges from the FP it is attached to the cell surface by the flagellum attachment zone (FAZ), which is made up of a series of junctional complexes similar to desmosomes, and a set of four unique microtubules that have opposing polarity to the microtubules present in the subpellicular array (Sunter and Gull, 2016; Robinson et al., 1995). These microtubules, known as the microtubule quartet (MtQ), nucleate near the basal

body, wrap around the side of the FP, traverse the hook complex and FPC, and then extend beside the FAZ filament as part of the subpellicular array (Lacomble et al., 2009).

Cytokinesis, the late cell cycle event that segregates duplicated organelles and cytoplasm to produce daughter cells, proceeds via a unique mechanism in *T. brucei* (**Fig. 1B**). In most eukaryotes, the motor protein nonmuscle myosin II and actin filaments arranged in an actomyosin ring provide the force necessary to separate daughter cells (Fenix et al., 2016; Glotzer, 2005; Laplante et al., 2016). Trypanosomes appear to lack a nonmuscle myosin II homolog and actin is not essential in the insect-resident (procyclic) form of the parasite, suggesting that the protein does not participate in a core conserved function such as cell division (García-Salcedo et al., 2004). Instead, the trypanosome cleavage furrow initiates from the anterior tip of the new FAZ and progresses towards the cell posterior along an indentation in the cell membrane known as the cleavage furrow fold. (**Fig. 1B**, **inset**). The posterior end of the cell contains plus-end microtubule binding proteins such as XMAP215 and is a major microtubule nucleation site for the subpellicular array (Wheeler et al., 2013). A new nucleation site forms during division to delimit the subpellicular microtubule arrays of the two daughter cells (Robinson et al., 1995; Sherwin et al., 1987). The assembly of the nascent cell posterior for the cell containing the old flagellum and FAZ is a separate event from cleavage furrow ingression, although the two events happen in concert to complete cytokinesis.

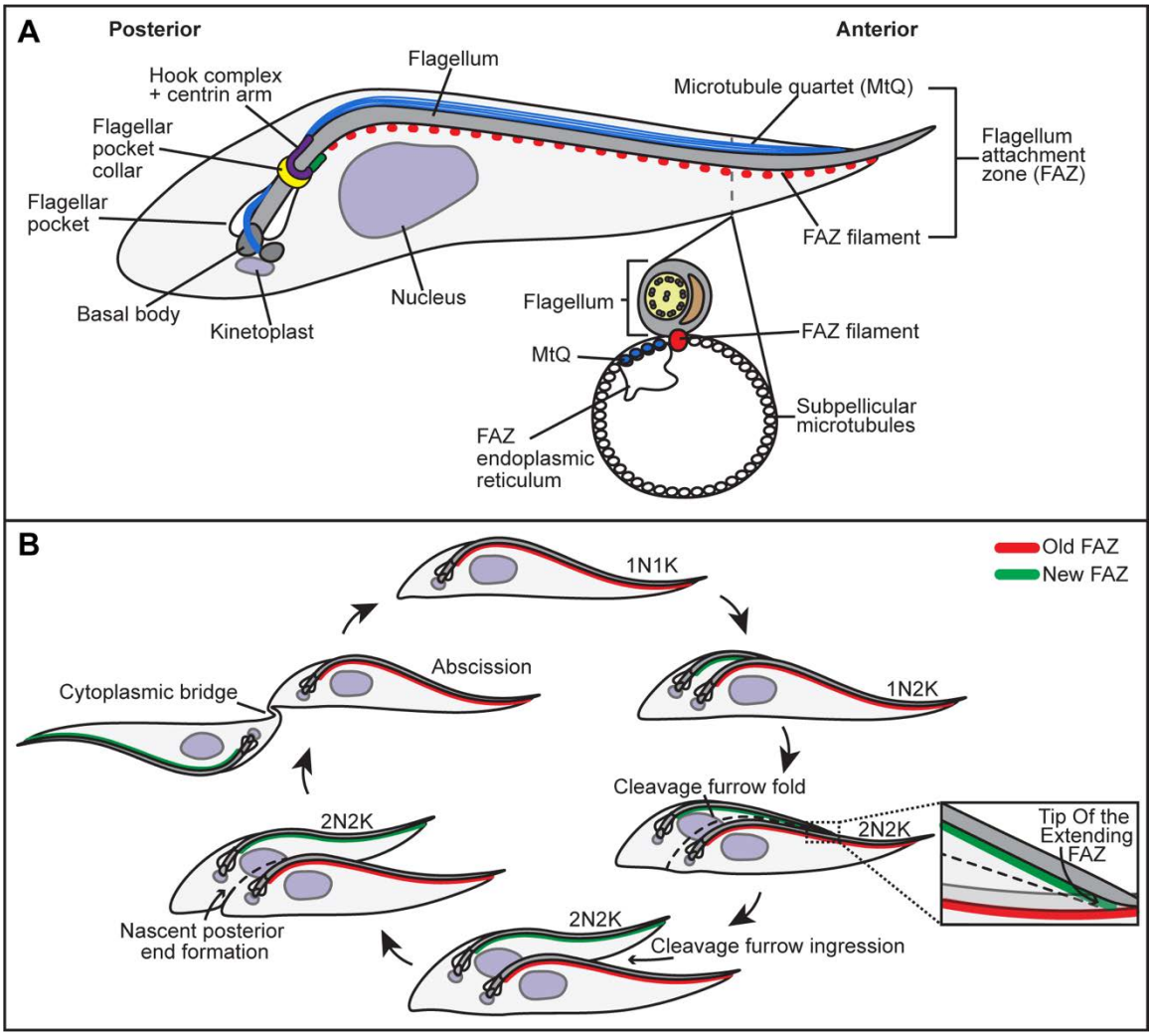

Figure 1. Schematic of the cytoskeleton and cell cycle of *Trypanosoma brucei*. (**A**) Key cytoskeletal structures involved in this work. (**B**) The cell cycle in *T. brucei*.

While cytokinesis in trypanosomes has been well described morphologically, little is known about the specific proteins that are involved. Due to a lack of conserved cytokinetic components, this process is likely to be mechanistically unique. Removing essential FAZ components or perturbing cytoskeletal structures that are necessary for new FAZ assembly causes cleavage furrow misplacement or an outright block in cytokinesis (He et al., 2005; Sunter et al., 2015; Vaughan et al., 2008). Depleting proteins involved in flagellar assembly, such as IFT components, yields shorter daughter cells, most likely due to misplaced furrow ingression caused by a shortened new FAZ (Kohl et al., 2003). Recently, the polo-like kinase homolog in trypanosomes,

named TbPLK, was shown to localize to the anterior tip of the new FAZ during cell division; inhibiting TbPLK activity early in the cell cycle blocks cytokinesis, suggesting that the kinase may have some mechanistic role in this process (Hammarton et al., 2007; Ikeda and de Graffenried, 2012; Li et al., 2010; Lozano-Núñez et al., 2013; Yu et al., 2012).

We recently conducted a screen that employed phosphoproteomics and proximity-dependent biotin identification (BioID) to identify novel TbPLK interactors and substrates (McAllaster et al., 2015). One of our candidate proteins, which we named Tip Of the Extending FAZ protein 1 (TOEFAZ1), colocalizes with TbPLK at the tip of the new FAZ during cell division (McAllaster et al., 2015; Zhou et al., 2016a). Depletion of TOEFAZ1 blocks recruitment of TbPLK to the tip of the new FAZ and causes substantial defects in cytokinesis, initially producing many anucleate and multinucleate cells followed by a block in cell division. TOEFAZ1 is the first protein identified in *T. brucei* that appears to have a specific role in cytokinesis, as its depletion does not cause additional defects in new FAZ or cytoskeletal assembly. Subsequent work by others chose an alternate name for the protein (Cytokinetic Initiation Factor 1; CIF1) and proposed that in its absence an alternate "back-up" cytokinetic mechanism could produce a furrow that ingresses from posterior to anterior to generate viable daughter cells (Zhou et al., 2016a).

TOEFAZ1 is conserved among kinetoplastids but lacks clear homologs in other organisms such as yeast and mammals. The protein contains three distinct domains: an N-terminal α-helical domain, a central intrinsically disordered protein (IDP) domain, and a C-terminal zinc finger (ZnF) domain (Mezulis et al., 2015; Xu et al., 2014). We sought to determine how the protein functions by dissecting the contribution of each domain using both overexpression and RNAi complementation strategies. We show that the N-terminal domain may function as a protein interaction domain that interacts with other FAZ proteins to localize TOEFAZ1. The IDP domain controls the timing of protein expression during the cell cycle and TbPLK retention at the tip of the new FAZ, but is not essential. The C-terminal ZnF domain is a homo-oligomerization domain that is necessary but not sufficient for TOEFAZ1 recruitment to the tip of the new FAZ. We further

show that cells lacking TOEFAZ1 rapidly develop aberrant DNA states that are not consistent with further productive cell divisions, calling into question the viability of alternate cytokinetic pathways.

RESULTS

Localization of TOEFAZ1 during cell division

TOEFAZ1 localizes to the tip of the extending FAZ and subsequently to the ingressing cleavage furrow. To further characterize its localization, we studied the distribution of the protein compared to two monoclonal antibodies: L3B2, which detects the FAZ filament protein FAZ1, and 1B41, which recognizes a subset of beta tubulin that is present in the FAZ, most likely in the MtQ (Gallo et al., 1988; Kohl et al., 1999; Vaughan et al., 2008). We generated cells where TOEFAZ1 was endogenously tagged at its N-terminus with three copies of the HA epitope and stained them with 1B41, anti-FAZ1, and anti-HA. **Fig. 2A** shows a panel of cells at different cell cycle stages. Trypanosomes maintain a mitochondrial DNA aggregate known as the kinetoplast as well as a nucleus; tracking the distribution of these DNA-containing organelles allows the cell cycle state to be easily distinguished. During the cell cycle, a cell that contains one nucleus and one kinetoplast (1N1K) first duplicates its kinetoplast (1N2K), and then its nucleus (2N2K), before cytokinesis produces two daughter cells with a single copy of each organelle (**Fig. 1B**). Early in the cell cycle, the 1B41 and FAZ1 labeling patterns are in close proximity and similar in length and cells lack TOEFAZ1 labeling (**Fig. 2A,i**). TOEFAZ1 appears just as the new FAZ can be resolved, which is most easily seen by the bright anterior 1B41 labeling on the new FAZ tip (**Fig. 2A,ii, asterisk**). As the new FAZ continues to elongate, the 1B41 signal extends slightly beyond the most anterior labeling visible for FAZ1 and comes in close proximity to the old FAZ. In contrast, there is a distinct gap in the FAZ1 labeling between the new and old FAZ (**Fig. 2A, iii,iv**). The TOEFAZ1 signal accumulates on the bright puncta at the anterior end of the 1B41 signal on the new FAZ, which matches the gap between FAZ1 signals (**Fig. 2A, iii,iv**). TOEFAZ1 is present at the tip of the new

FAZ until cleavage furrow ingression, when the protein localizes along the furrow (**Fig. 2A,v**) (McAllaster et al., 2015; Zhou et al., 2016a).

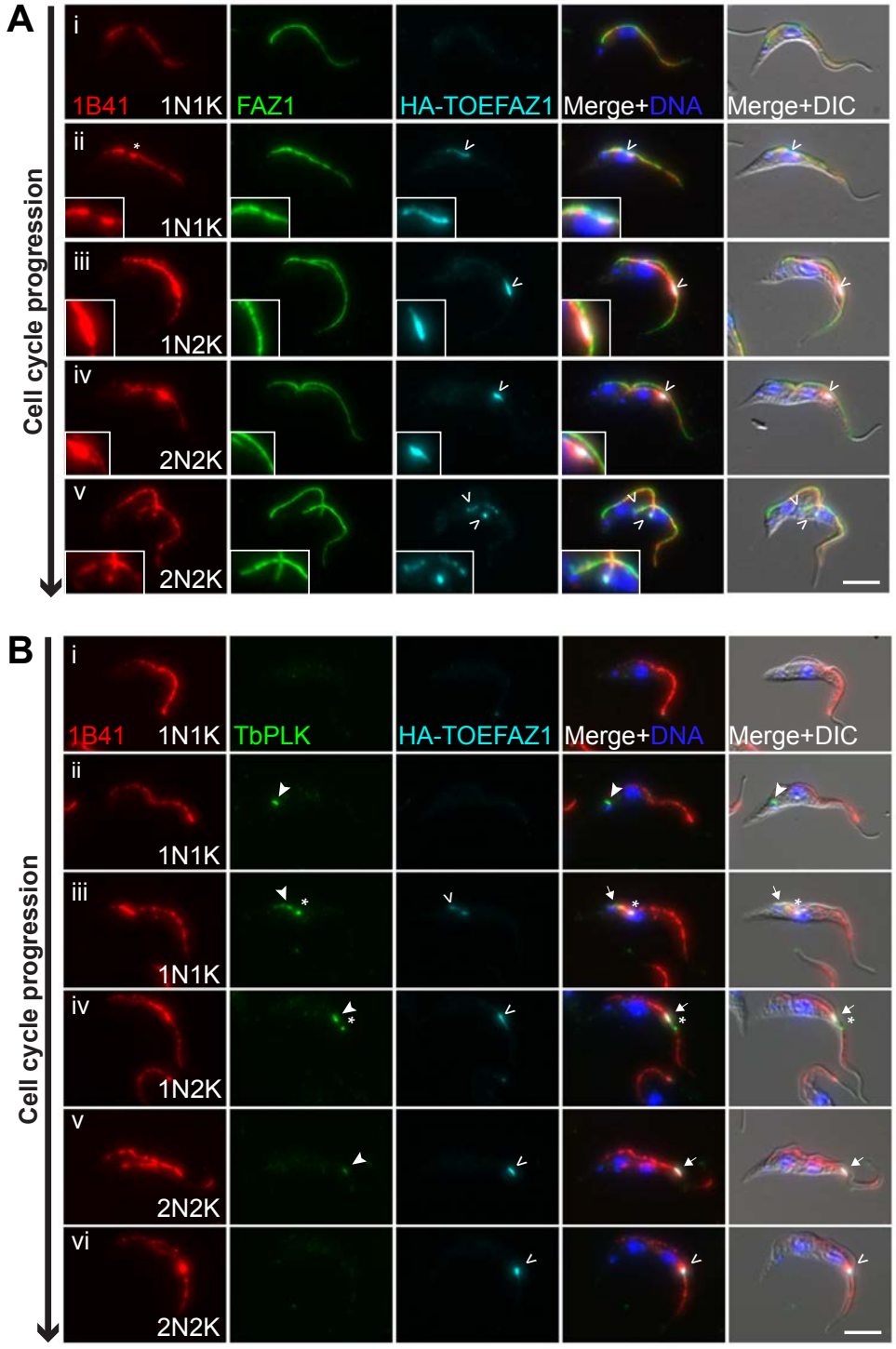

Figure 2. TOEFAZ1 localizes to the tip of the new FAZ and the cleavage furrow. (**A**) Cells were methanol-fixed and labeled with 1B41 (red), anti-FAZ1 (green), and anti-HA (HA-TOEFAZ1;

cyan). Arrowheads point to TOEFAZ1 localization. The asterisk in panel ii indicates the new FAZ tip labeled by 1B41. (**B**) The same cell line as in (A) was methanol-fixed and stained with 1B41 (red), anti-TbPLK (green) and anti-HA (HA-TOEFAZ1; cyan). Asterisks in panels iii-iv point to TbPLK FC labeling, filled-in arrowheads indicate TbPLK FAZ labeling, and empty arrowheads indicate HA-TOEFAZ1 localization. DAPI was used to label DNA (blue). Scale bars: 5 μm.

We compared the localization of TOEFAZ1 and TbPLK in relation to the FAZ marker 1B41 to mark the migration pattern of the two proteins. At early stages of the cell cycle cells do not express TbPLK or TOEFAZ1 (**Fig. 2B,i**). TbPLK initially appears on the basal body, hook complex, and centrin arm, all of which are proximal to the flagellar pocket (**Fig. 2B, ii,iii, arrowhead**). TOEFAZ1 first localizes to the anterior end of the TbPLK signal, which is most likely the centrin arm and/or hook complex (**Fig. 2B,iii, empty arrowhead**). This also coincides with the bright puncta of 1B41 signal. As the new FAZ extends, TbPLK and TOEFAZ1 are present on the tip of the extending structure, with TbPLK also on the flagella connector (FC) that links the tip of the new flagellum to the old flagellum (**Fig. 2B,iv, asterisk**) (McAllaster et al., 2015; Moreira-Leite et al., 2001; Zhou et al., 2016a). As the cell cycle progresses, the TbPLK signal at the tip of the FAZ begins to decline, while the TOEFAZ1 signal remains constant (**Fig. 2B,v**). TbPLK is absent from the tip of the new FAZ once cleavage furrow ingression initiates (**Fig. 2B,vi**).

Overexpression of individual TOEFAZ1 domains

TOEFAZ1 comprises three distinct domains: an N-terminal α-helical domain (aa 1-319), a central IDP domain (aa 320-649), and a C-terminal ZnF domain containing two zinc finger motifs (aa 650-790) (**Fig. 3A**). As a first test of protein function, we expressed each domain individually using the doxycycline-inducible vector pLEW100 (**Fig. 3A**) (Wirtz et al., 1999). Each domain was tagged at its N-terminus with three copies of the Ty1 epitope tag and induction of domain expression was assessed by anti-Ty1 western blotting (**Fig. 3B**). None of the expression constructs caused growth defects, showing that they lacked dominant negative properties (**Fig. S1**). Full-length TOEFAZ1 migrates at a substantially higher molecular weight than the expected 93 kDa, most likely due to posttranslational modifications (**Fig. 3B**) (McAllaster et al., 2015; Zhou

et al., 2016a). Similarly, all three domains appear at a higher molecular weight than expected (**Fig. 3B**). This is likely due to phosphorylation; 9 phosphosites have been detected in the N-terminal domain and at least 21 in the IDP domain (Urbaniak et al., 2012; Urbaniak et al., 2013).

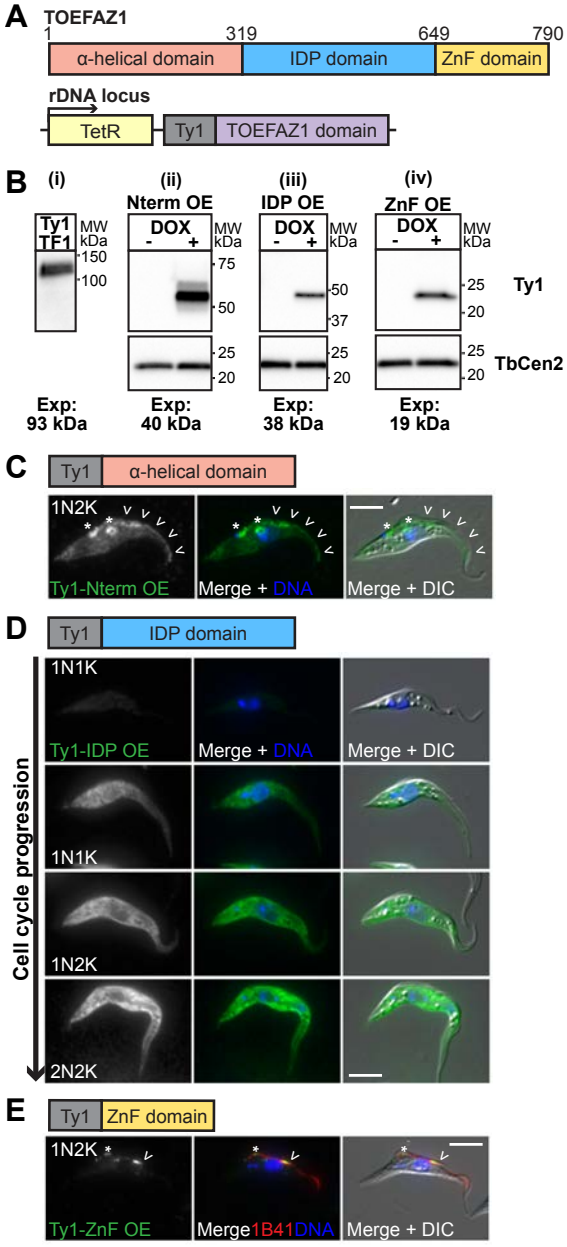

Figure 3. Overexpression of TOEFAZ1 domains reveals separable functions. (**A**) Schematic of TOEFAZ1 domain organization (top) and the doxycycline-inducible domain overexpression strategy (bottom). (**B**) Anti-Ty1 western blots of 427 cells expressing 3x-Ty1-TOEFAZ1 from the endogenous locus (**i**) and 29-13 cells containing the 3X-Ty1 tagged domain overexpression constructs that were treated with either 70% ethanol (-DOX) or doxycycline (+DOX) for 1 day (**ii-iv**). Blots ii-iv were stripped and re-probed with TbCentrin2 as a loading control. The expected

mass of each construct (tag + domain) is indicated. (**C-E**) Overexpression cell lines were induced as in (B) and collected for immunofluorescence with anti-Ty1 labeling (Ty1-TOEFAZ1 domain; green). DAPI was used to label DNA (blue). (**C**) N-terminus domain cells were paraformaldehyde-fixed. Asterisks indicate ring-like structures and arrowheads mark FAZ labeling. (**D**) IDP domain cells were paraformaldehyde-fixed. (**E**) ZnF domain cells were methanol-fixed and stained with 1B41 to mark the FAZ (red). Scale bars: 5 μm.

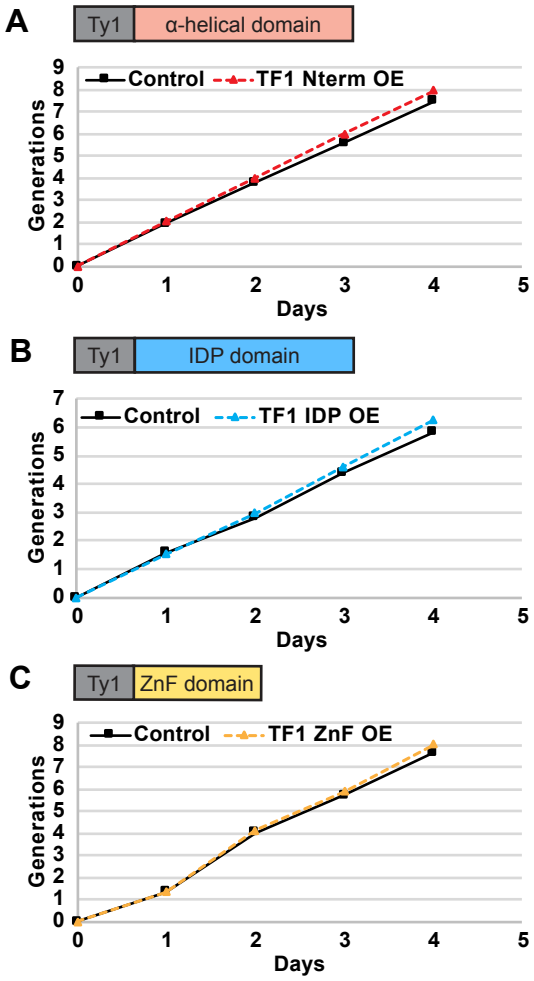

Figure S1. TOEFAZ1 domain overexpression does not cause a growth defect. Cell growth was recorded in 29-13 cells harboring the 3X-Ty1 N-terminal domain **(A)**, the 3X-Ty1 IDP domain **(B)**, and the 3X-Ty1 ZnF domain **(C)** overexpression constructs after induction. Curves are representative of 2-3 independent clones.

The localization of each domain was assessed by immunofluorescence microscopy. The N-terminal α-helical domain was expressed at all cell cycle stages and had primarily a diffuse

cytoplasmic localization, although some of the protein formed ring-like structures that were frequently in close proximity to the kinetoplast (**Fig. 3C, asterisks**). A portion of the protein also localized to the full length of the FAZ (**Fig. 3C, arrowheads**). The ring structures and FAZ labeling were susceptible to detergent extraction, suggesting that the N-terminal domain is not tightly associated with the cytoskeleton. The IDP domain localized exclusively to the cytoplasm, but was not expressed in the majority of 1N1K cells early in the cell cycle. Expression of the IDP was evident in cells where the kinetoplast had begun to divide and in 1N2K and 2N2K cells (**Fig. 3D**), which corresponds to the cell cycle window when full-length TOEFAZ1 is normally expressed (**Fig. 2A**). Considering that the IDP domain is being overexpressed from a vector that lacks the native 5' and 3' UTRs for TOEFAZ1, it is unlikely that translational control could be responsible for the observed cell cycle-restricted expression. The C-terminal ZnF domain localized primarily to the tip of the new FAZ (**Fig. 3E**), but the domain was also present along the length of the old and new FAZ, suggesting that it was not able to maintain as tight a localization with the FAZ tip structure as the full-length protein (**Fig. 3E, asterisk**). The protein localized to the cytoplasm in cells that were not dividing.

TOEFAZ1 RNAi complementation analysis

To better understand the function of each domain within TOEFAZ1, we devised an RNAi complementation strategy that allows us to generate cells expressing only truncated forms of the protein that lack individual domains (**Fig. 4A**). We assembled an RNAi hairpin against the native TOEFAZ1 DNA sequence (nt 578-1090) in the doxycycline-inducible vector pTrypSon using Gibson Assembly (McAllaster et al., 2016). The plasmid was integrated into cells carrying the necessary machinery for doxycycline induction (29-13), and then one allele of TOEFAZ1 was endogenously tagged with a triple-Ty1 tag at its N-terminus. This cell line, carrying the TOEFAZ1 RNAi hairpin and a natively coded, Ty1-tagged WT TOEFAZ1 allele, was the base cell line used for all further modifications. We then recoded a segment of the TOEFAZ1 gene (nt 4-1096) so that the DNA sequence uses different codons than the native gene but still encodes the same

amino acids, making it insensitive to the RNAi hairpin that targets the native coding sequence (Horn, 2008). Thus, induction of RNAi should selectively deplete the mRNA produced from the native allele. The recoded sequence was included in an endogenous tagging construct that also introduces a triple-HA tag onto the N-terminus of TOEFAZ1. Because the two versions of the gene are differentially epitope tagged we can readily distinguish the native from recoded alleles.

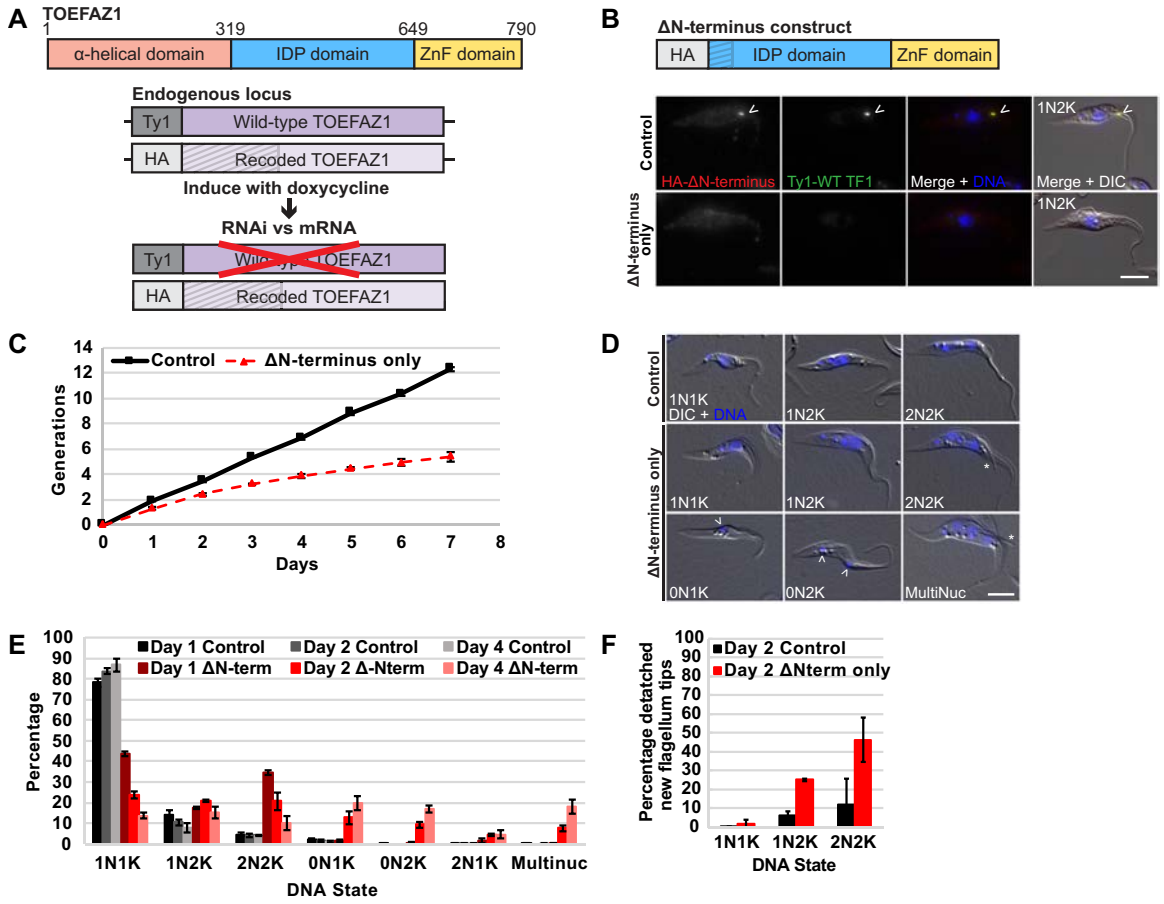

Figure 4. The TOEFAZ1 N-terminal domain is required for stable localization to the new FAZ tip. (**A**) Schematic of TOEFAZ1 RNAi complementation strategy. Gray stripes indicate the recoded segment of the gene. (**B**) ΔN-terminus cells in the endogenously-tagged 3X-Ty1 TOEFAZ1 RNAi background were treated with vehicle control or doxycycline (ΔN-terminus only) for 1 day. Cells were methanol-fixed and labeled with anti-HA (HA-ΔN-terminus; red), anti-Ty1 (Ty1-WT TOEFAZ1; green), and DAPI for DNA (blue). Arrowheads indicate TOEFAZ1 construct localization. (**C**) The ΔN-terminus cell line was treated as in (B) and cell number was monitored every 24 hours. The curve represents the average of three independent experiments. (**D**) Control and ΔN-terminus only cells from (C) were paraformaldehyde-fixed and stained with DAPI for DNA (blue) after 2 days of TOEFAZ1 depletion. Asterisks indicate detached new flagellum tip. (**E**) Quantification of DNA state in control cells (black-grey) and ΔN-terminus only cells (dark-light red). 300 cells were counted per condition for three independent experiments. (**F**) Quantification

of detached new flagellum tips after 2 days of TOEFAZ1 depletion in control and ΔN-terminus only cells as in (E). Scale bars: 5 μm. Error bars are the SD.

As a proof of principle, we introduced full-length TOEFAZ1 with the recoded segment tagged with HA into our base cell line. Induction of RNAi by addition of doxycycline effectively depleted the native copy of the protein, as assessed by anti-Ty1 immunofluorescence and western blotting, but the protein produced from the recoded HA-tagged allele localized effectively to the tip of the new FAZ and resisted depletion (**Fig. S2, A,B**). Cells expressing only the recoded allele grew at the same rate as cells carrying a native copy of the gene, which shows that the recoded allele is fully functional and that our RNAi hairpin has no off-target effects (**Fig. S2C**).

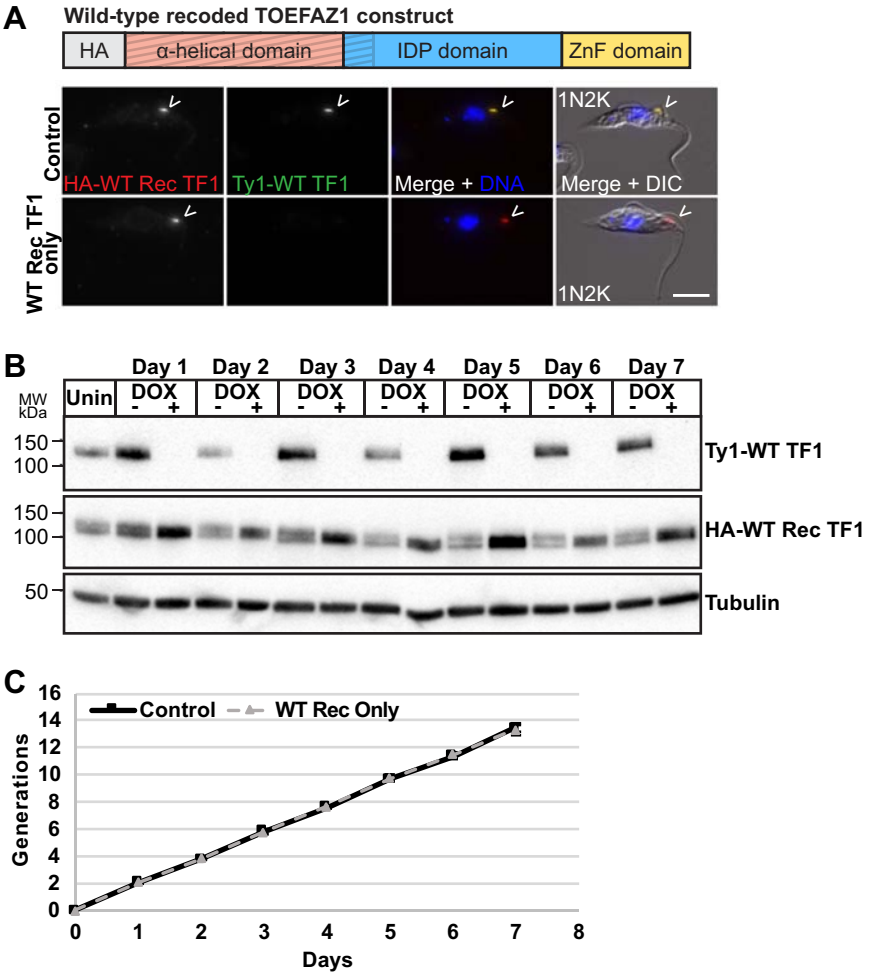

Figure S2. Recoded TOEFAZ1 complements WT TOEFAZ1 function. (A) Nucleotides 4-1096 of TOEFAZ1 were recoded and transfected into the endogenously tagged 3X-Ty1 TOEFAZ1

RNAi cell line. TOEFAZ1 RNAi was induced for 1 day, followed by methanol-fixation and staining with anti-HA (HA-WT Rec TOEFAZ1; red) and anti-Ty1 (Ty1-TOEFAZ1; green). DAPI was used to label DNA (blue). Arrowheads indicate TOEFAZ1 construct localization. Scale bar: 5 μm. **(B)** Western blot of the WT Recoded TOEFAZ1 cell line after induction of TOEFAZ1 RNAi. Lysates were collected every 24 hours. The blot was probed with anti-Ty1 (Ty1-TOEFAZ1), stripped and re-probed with anti-HA (HA-WT Rec TOEFAZ1), and stripped and re-probed with anti-tubulin as a loading control. **(C)** TOEFAZ1 was depleted in the WT Recoded TOEFAZ1 cell line and cell growth was recorded for three independent experiments. Error bars are the SD.

With the efficacy of the RNAi complementation strategy established, we introduced RNAi-insensitive mutants of TOEFAZ1 into our base cell line to observe the effect of removing individual domains of the protein. We confirmed the correct integration of each of these domain mutant cell lines by western blotting, loci PCR, and sequencing of the modified locus (**Fig. S3**). Our first mutant, termed ΔN-terminus, removed the N-terminal α-helical domain from TOEFAZ1. Immunofluorescence with anti-Ty1 and anti-HA antibodies showed that ΔN-terminus TOEFAZ1 mutant colocalized with WT TOEFAZ1 (**Fig. 4B**). Depletion of the WT TOEFAZ1 by RNAi caused the rapid loss of Ty1 signal by western blotting (**Fig. S3A**) and immunofluorescence (**Fig. 4B**), while the HA signal, which detected the mutant RNAi-insensitive protein, remained detectable by western. In the absence of full-length TOEFAZ1, the ΔN-terminus mutant was no longer able to localize to the tip of the new FAZ, suggesting that the mutant relies on the presence of the full-length protein for localization (**Fig. 4B**). After one day of WT protein depletion, cells expressing only the ΔN-terminus TOEFAZ1 display significant cell division defects, including slow growth and an increase in the number of 2N2K cells (**Fig. 4 C,E**). After two days, DNA counting of cells expressing only the ΔN-terminus TOEFAZ1 showed increasing cytokinetic defects, with 1N1K cells making up only 24% of the population and an elevated number of 1N2K and 2N2K cells (21% and 20%, respectively; **Fig. 4 D,E**). Aberrant cells containing no nuclei (0N1K, 0N2K) or multinucleate cells also appeared. Four days after depletion of the wild-type protein, 1N1K cells comprise only 14% of the population, while the anucleate and multinucleate cells make up over 62% of the population. We also noted that nearly half of the 2N2K cells in the experimental

condition had detached new flagella tips after two days of RNAi induction, which suggested that the FC had resolved before cleavage furrow ingression, as we previously saw in the case of full-length TOEFAZ1 depletion (**Fig. 4F**) (McAllaster et al., 2015). This indicates that cleavage furrow ingression is likely delayed in cells expressing only the ΔN-terminus construct, although it is not formally known if FC resolution is independent of cleavage furrow ingression.

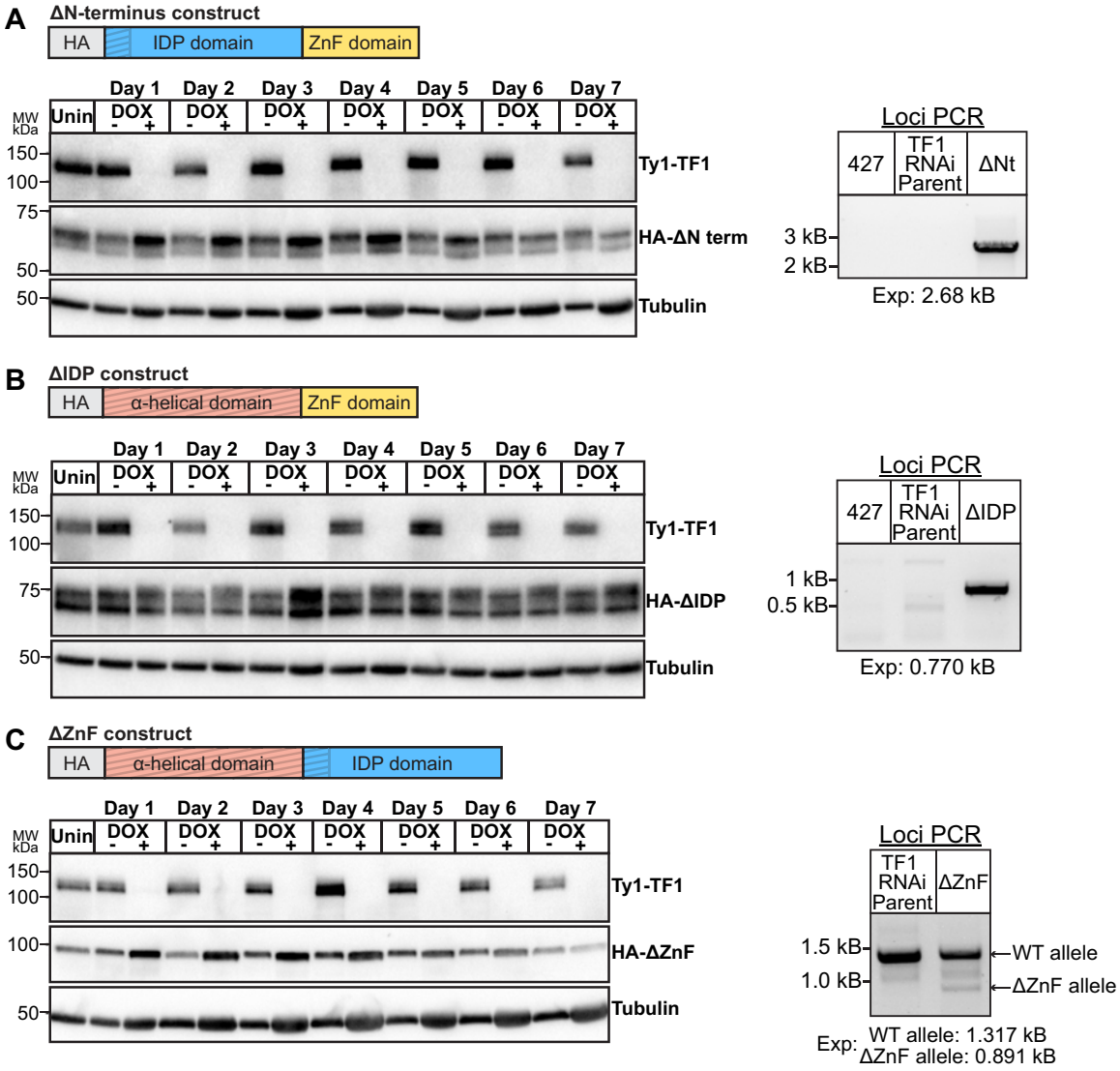

Figure S3. TOEFAZ1 domain mutant constructs are expressed upon RNAi induction. On the left are western blots of TOEFAZ1 RNAi inductions. TOEFAZ1 domain mutant cell lines were induced and lysates were collected every 24 hours. For (A-C), blots were labeled with anti-Ty1 (Ty1-TOEFAZ1), stripped and re-probed with anti-HA (HA-domain construct), and stripped and re-probed with anti-tubulin for a loading control. On the right are loci PCRs demonstrating the

correct integration of each domain mutant construct. The N-terminus **(A)**, the IDP **(B)**, and the ZnF **(C)** cell lines.

We next generated a cell line that contained a recoded, mutant TOEFAZ1 allele that lacked the IDP domain. Depletion of the WT allele proceeded with similar kinetics to the cell line containing the ∆N-terminus TOEFAZ1 construct (**Fig. S3B**). The mutant protein was able to localize to the tip of the new FAZ in the presence or absence of the full-length TOEFAZ1 (**Fig. 5A**), although the ∆IDP protein had an additional labeling pattern in some cells just to the posterior side of the extending FAZ (**Fig. 5A, asterisk**). Surprisingly, the IDP domain of TOEFAZ1 does not appear to be essential to cell viability, as cells expressing only the ∆IDP mutant had just a 10% deficit in doubling rate (**Fig. 5B**). After three days of RNAi induction, ∆IDP mutant cells had slightly lower levels of 1N1K cells compared to controls (62% vs. 80% 1N1Ks, respectively) and a concomitant increase in 2N2K cells; there was also a small but noticeable population of zoid cells (**Fig. 5C**). These results argue that while the ∆IDP TOEFAZ1 mutant can support near-wild type levels of growth, there is still a small delay or defect in cytokinesis. This cytokinetic defect is further evidenced by the premature release of the FC in almost 40% of the ∆IDP 2N2K cell population (**Fig. 5D**). We also noticed additional TOEFAZ1 labeling in the posterior of 1N1K cells, which most likely corresponds to the point at which cleavage furrow ingression terminates prior to nascent posterior end formation (**Fig. 5E, arrowhead**).

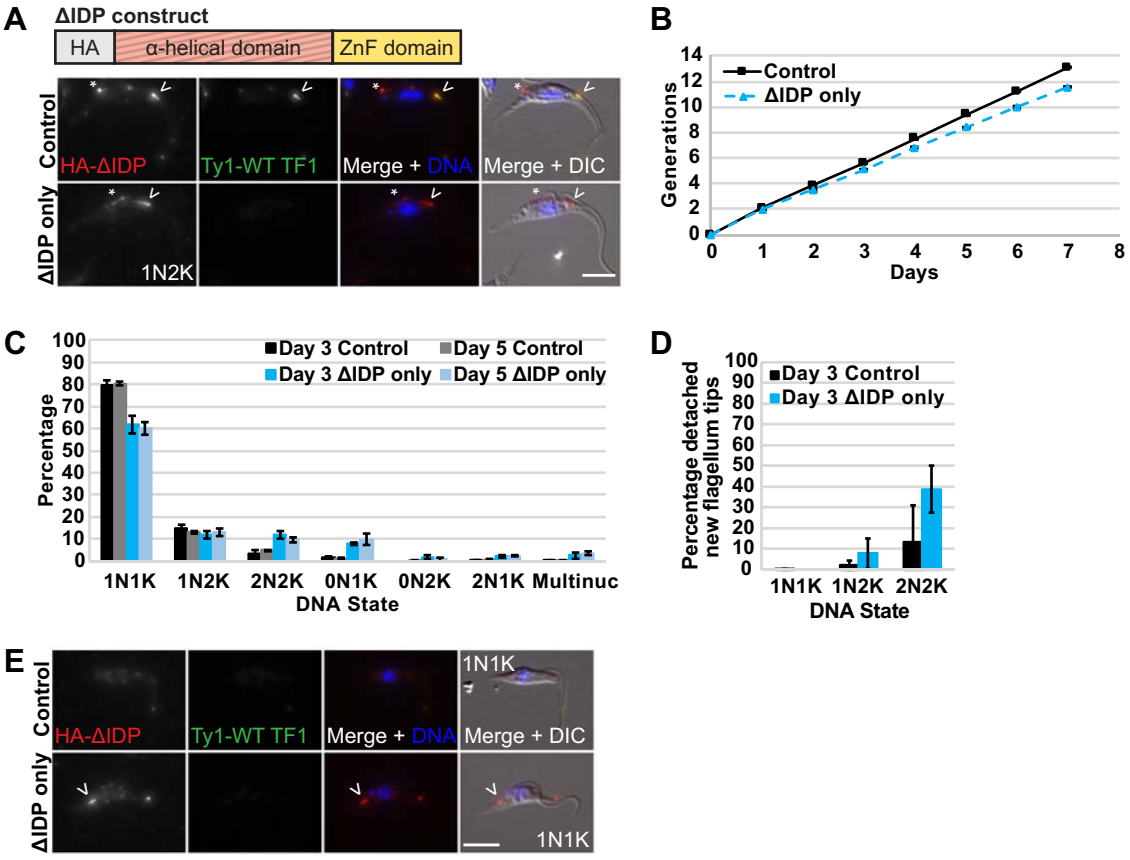

Figure 5. The ΔIDP construct complements WT TOEFAZ1 function. The same analyses as in Fig. 4 were performed on the ΔIDP cell line. (**A**) ΔIDP cells were fixed after 2 days of TOEFAZ1 RNAi and labeled as in Fig. 4B. Asterisk indicates posterior labeling by the ΔIDP protein. (**B**) ΔIDP cells were induced and cell growth was monitored. The curve is the average of three independent experiments. (**C**) Quantification of DNA state after TOEFAZ1 depletion in control (black-grey) and ΔIDP only (dark-light blue) cells. 300 cells were counted for each condition for three independent experiments. (**D**) Quantification of detached new flagellum tips in control and ΔIDP only cells after 3 days of TOEFAZ1 depletion as in (C). (**E**) Control and ΔIDP only cells after 2 days of TOEFAZ1 depletion were methanol-fixed and labeled as in (A). Arrowhead indicates ΔIDP protein labeling in the cell posterior. Scale bars: 5 μm. Error bars are the SD.

Finally, we generated cells lacking the TOEFAZ1 C-terminal ZnF domain using our complemented RNAi strategy. Induction of RNAi with doxycycline led to a rapid depletion of the full-length, native coding protein, while the HA-tagged recoded protein persisted (**Fig. S3C**). This mutant was unable to localize to the tip of the new FAZ in the presence or absence of the full-length protein (**Fig. 6A**). Cells expressing only the ΔZnF version of TOEFAZ1 began to show a

rapid decline in the rate of cell division, with minimal growth observed after 4 days of RNAi depletion of the full-length protein (**Fig. 6B**). Assessment of cell cycle stage and morphology showed a similar pattern as to what was observed for cells lacking the N-terminal α-helical domain. There was an initial increase in 2N2K cells, followed by the appearance of anucleate and multinucleate cells, which make up 63% of the population after four days of TOEFAZ1 RNAi induction (**Fig. 6C**). Over 40% of 2N2K cells had prematurely detached new flagella tips, suggesting a delay or defect in cleavage furrow ingression (**Fig. 6D**). This result suggests that the ZnF domain is absolutely required for TOEFAZ1 localization to the new FAZ tip and for its proper function.

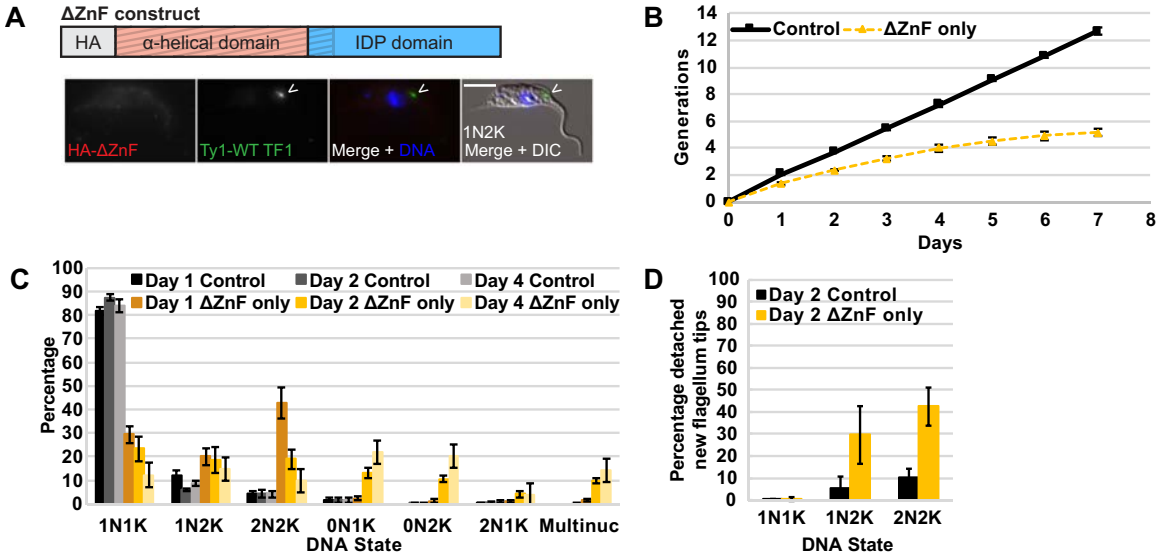

Figure 6. The ΔZnF construct does not localize to the new FAZ tip. The ΔZnF cell line was analyzed as in Fig. 4. (**A**) Uninduced ΔZnF cells were methanol-fixed and prepared as in Fig. 4B. (**B**) TOEFAZ1 RNAi was induced in ΔZnF cells and cell growth was monitored. The curve is the average of three independent experiments. (**C**) Quantification of DNA state in control (black-grey) and ΔZnF only cells (gold-yellow) after WT TOEFAZ1 depletion. 300 cells were counted per condition for three independent experiments. (**D**) The percentage of detached new flagellum tips was quantified in control and ΔZnF only cells after 2 days of TOEFAZ1 depletion as in (C). Scale bar: 5 μm. Error bars are the SD.

The ability of the TOEFAZ1 mutant lacking the IDP domain to support cell growth raised the possibility that the N-terminal domain and the C-terminal ZnF domain could function together in *trans*, either by forming a complex or by performing their functions independently. To test this possibility, we altered our RNAi complementation strategy to allow for individual expression of the two TOEFAZ1 domains (**Fig. S4A**). We tagged one of the native TOEFAZ1 alleles at its N-terminus with the GFP variant mClover3 so that we could use the HA and Ty1 epitope tags for the individual domains (Bajar et al., 2016). We modified the second TOEFAZ1 allele so that it contained a recoded version of the N-terminal domain tagged with HA and the ZnF domain tagged with Ty1, each with its own start and stop codons. The two domains were separated by an intergenic sequence from the tubulin locus, which allows the two segments to be transcribed from a single promoter but processed into two unique mRNAs (Imboden et al., 1987). The three variants of the protein could be detected individually by western blotting with anti-HA, anti-Ty1, and antibodies against GFP. Depletion of the full-length mClover3-tagged TOEFAZ1 by RNAi proceeded similarly to the Ty1-tagged protein in our conventional RNAi complementation approach, leaving cells expressing only the separate N-terminal and ZnF domains (**Fig. S4B**). In control cells, the Ty1-tagged ZnF domain and full-length mClover3-TOEFAZ1 proteins were able to localize to the new FAZ tip, but no signal was evident for the HA-tagged N-terminal domain (**Fig. S4C**), although we could observe protein expression by anti-HA western blotting. Depletion of the full-length TOEFAZ1 caused the mislocalization of the ZnF domain (**Fig. S4C**). The loss of WT TOEFAZ1 caused a rapid slowdown in growth, with kinetics similar to the ∆N-terminus and ∆ZnF mutants in previous experiments (**Fig. S4D**). This result suggests that these domains cannot operate in *trans* and need to be physically linked to function.

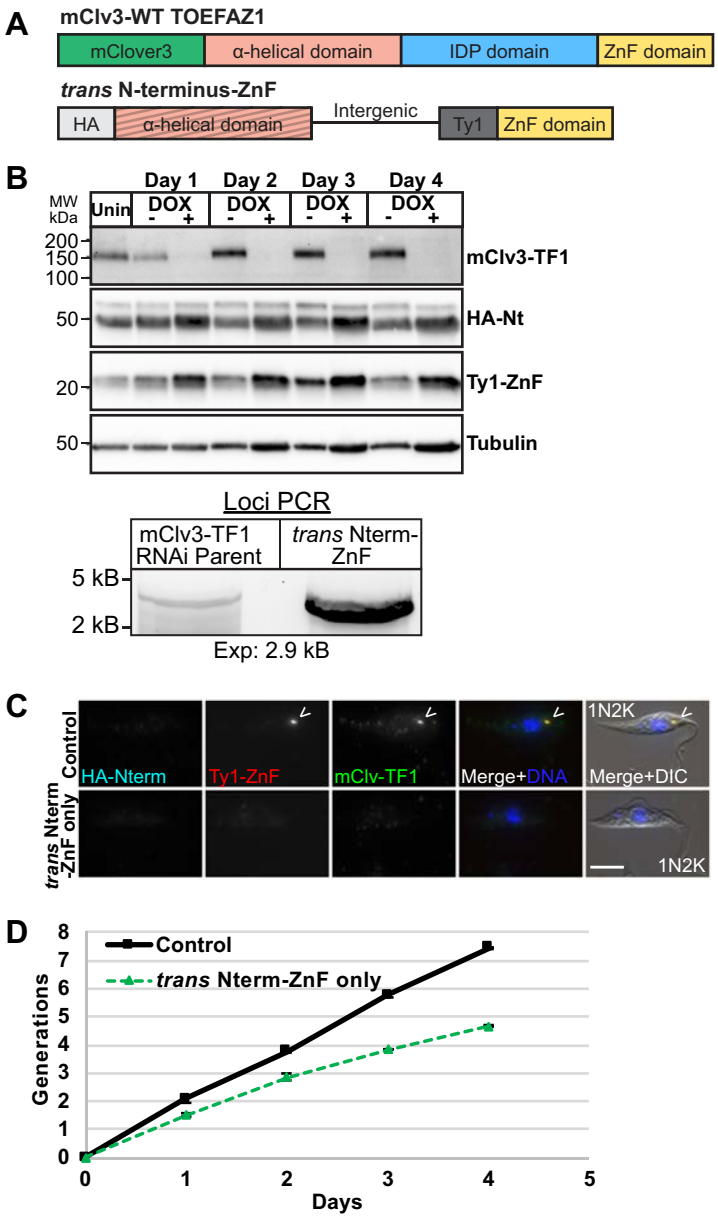

Figure S4. TOEFAZ1 N-terminal domain and C-terminal ZnF do not operate in trans. (A) Schematic of the TOEFAZ1 endogenous locus in the trans N-terminus-ZnF cell line. **(B)** Top: western blot of the trans N-terminus-ZnF cell line induction. The blot was cut and probed using anti-GFP (mClv3-TOEFAZ1), anti-HA (HA-N-terminus), and anti-Ty1 (Ty1-ZnF). The blot was then stripped and re-probed with anti-tubulin as a loading control. Bottom: loci PCR showing the correct integration of the trans construct. **(C)** After 1 day of TOEFAZ1 RNAi induction, cells were methanol-fixed and labeled with anti-HA (HA-N-terminus; cyan), anti-Ty1 (Ty1-ZnF; red), anti-GFP (mClv3-TOEFAZ1; green), and DAPI was used to stain DNA (blue). Arrowheads indicate TOEFAZ1 construct localization. Scale bar: 5 μm. **(D)** Cell growth was monitored in the trans N-terminus-ZnF cell line after RNAi induction. Curve is the average of three independent experiments. Error bars are the SD.

The cell line expressing the individual domains of TOEFAZ1 provided an opportunity to test the oligomerization characteristics of the ZnF domain, as the Ty1-tagged ZnF domain localizes to the new FAZ tip only when full-length TOEFAZ1 is present (**Fig. S4C**). We added the 8-atom crosslinker disuccinimidyl suberate (DSS) or a vehicle control (DMSO) to lysates and determined the oligomerization state of the Ty1-tagged ZnF domain (**Fig. S5A**). In lysates treated with vehicle control, the ZnF domain migrates at its expected size (19 kDa). In the presence of DSS, we observed higher order species that migrated at the expected molecular weight of a ZnF tetramer and a second higher-order species. We also tested if the ZnF domain was able to oligomerize with full-length TOEFAZ1 (**Fig. S5B**). We treated live cells with DSS or DMSO, followed by lysis and immunoprecipitation with GFP-Trap resin to capture full-length mClover3-tagged TOEFAZ1. In the presence of DSS, we were able to capture the Ty1-tagged ZnF domain with GFP-Trap resin, showing that the domain can interact with full-length TOEFAZ1. Blotting the immunoprecipitated fractions with anti-GFP also showed that the full-length TOEFAZ1 formed an oligomer in the presence of DSS.

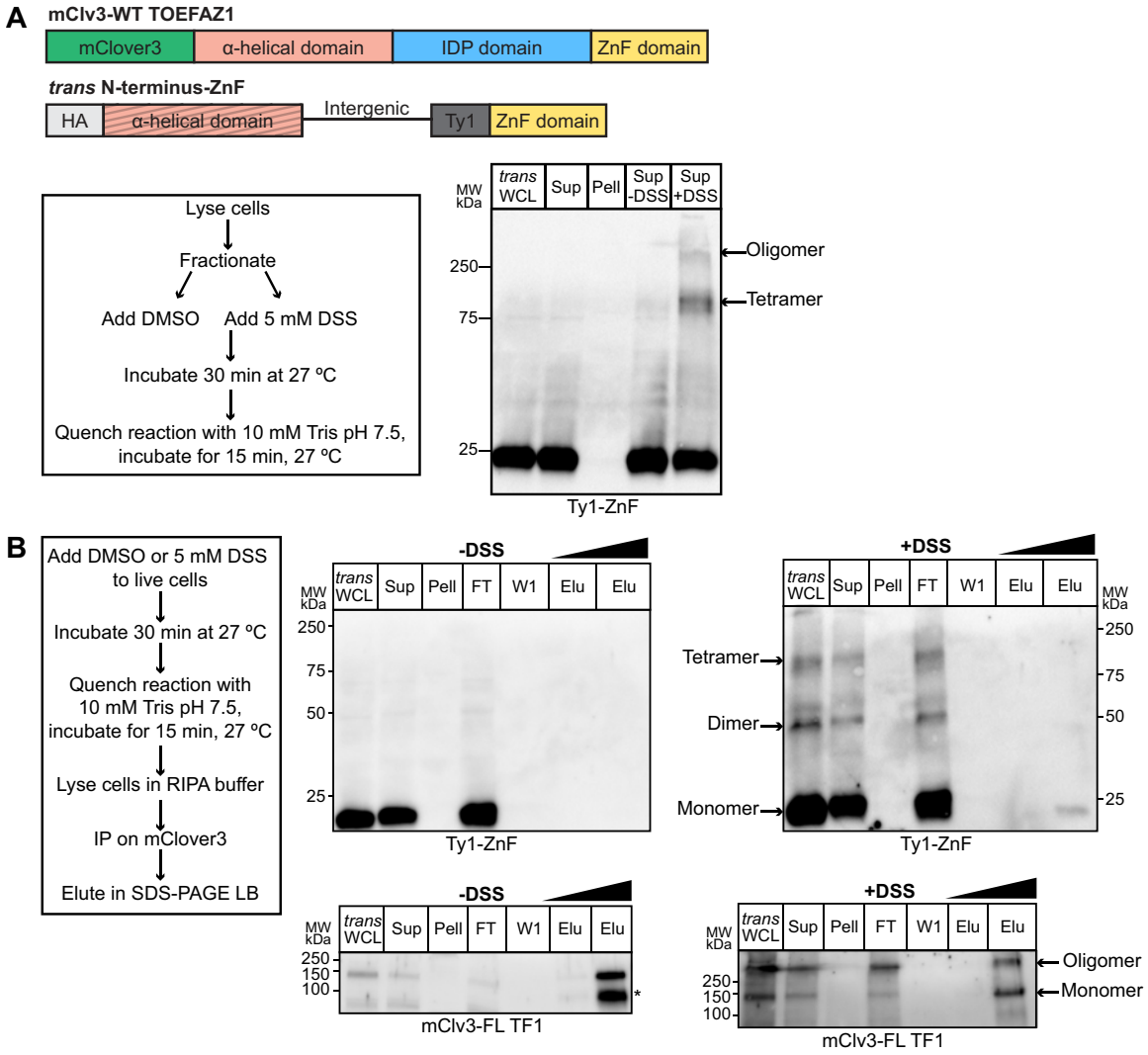

Figure S5. TOEFAZ1 ZnF domain oligomerizes and associates with full-length protein. (A) Disuccinimidyl suberate (DSS) was used to crosslink clarified trans cell line lysates. The reaction was quenched with Tris pH 7.5 and diluted in SDS-PAGE loading buffer. Samples were then separated by SDS-PAGE and western blotted with anti-Ty1 antibody (Ty1-ZnF). **(B)** Whole cells from the trans cell line were treated with vehicle control or DSS and lysed in RIPA buffer, after which the mClv3-FL TOEFAZ1 was immunoprecipitated. Samples were taken at each step of immunoprecipitation: WCL, whole cell lysate; Sup, clarified supernatant input; Pell, pellet; FT, flow-through; W1, first wash. Samples were diluted in SDS-PAGE loading buffer and separated by SDS-PAGE and transferred to nitrocellulose for western blotting with anti-Ty1 (Ty1-ZnF) and anti-GFP (mClv3-FL TOEFAZ1) antibodies. Elution lanes are equal volume (1.8%) and 40% elution, respectively. Asterisk indicates degradation product.

To address the differences in localization observed when the domains are overexpressed, we generated cells expressing the individual N-terminal and C-terminal domains of TOEFAZ1 at

endogenous levels. We integrated HA-tagged, RNAi-resistant versions of the N-terminal α-helical domain and the C-terminal ZnF domain into the base cell line for our RNAi complementation approach (**Fig. S6**). After confirming correct integration, we checked the localization pattern of the individual domains (**Fig. S6 A,B**). The N-terminal α-helical domain on its own was not able to localize to the tip of the new FAZ either in the presence or absence of the full-length protein (**Fig. S6A**), as was the case with the ΔZnF mutant and *trans* cell line (**Figs. 6A, S4C**), suggesting that the FAZ labeling and ring structures we observed previously arise only when the protein is expressed at high levels (**Fig. 3C**). The ZnF on its own was able to localize to the new FAZ tip as long as full-length TOEFAZ1 was present in cells (**Fig. S6B**), as is the case with the ΔN-terminal mutant and the *trans* cell line (**Figs. 4B, S4C**). When the protein was localized, it showed a high degree of colocalization with native, full length TOEFAZ1, which suggests that the broader expression pattern along the length of the FAZ observed previously (**Fig. 3E**) is also due to overexpression.

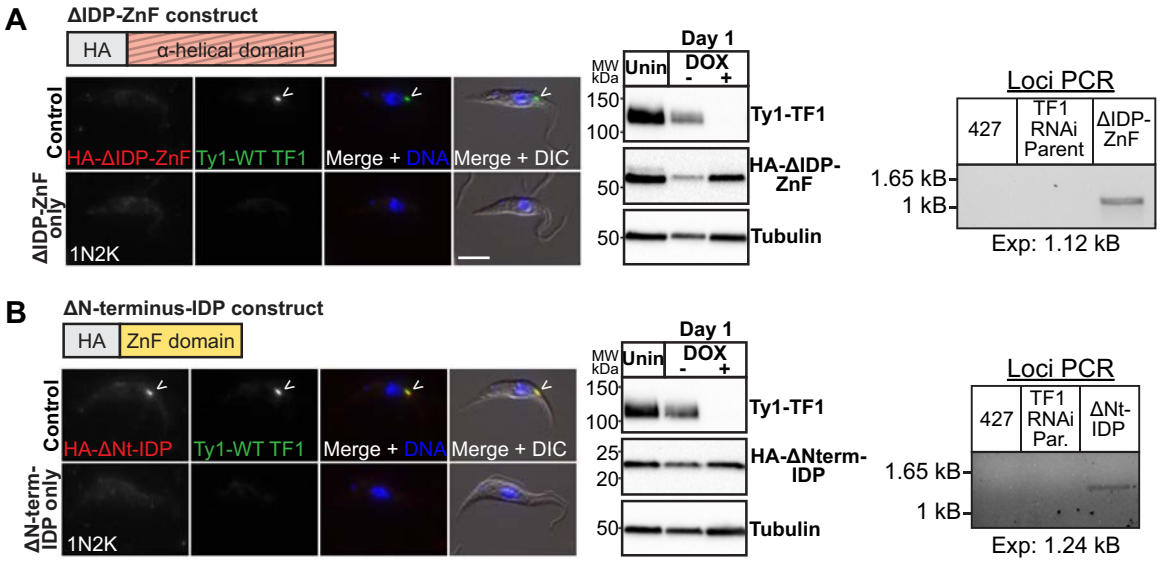

Figure S6. Characterization of endogenous expression of TOEFAZ1 N-terminal and ZnF domains. (A) The second allele of the base 3X-Ty1 TOEFAZ1 RNAi cell line was replaced with only the recoded N-terminal domain (ΔIDP-ZnF construct). TOEFAZ1 RNAi was induced for 1 day and cells were prepared for immunofluorescence as in Fig. 4B. Arrowheads indicate TOEFAZ1 construct localization. **(B)** Identical analysis as in (A) for the ΔN-terminus-IDP cell line, in which only the ZnF domain is present on the second allele. To the right of the

microscopy in (A) and (B) is a western blot from each cell line after 1 day of TOEFAZ1 RNAi and a loci PCR demonstrating the correct integration of the domain mutant constructs. The western blotting scheme is the same as Fig. S2B. Scale bars: 5 μm.

TbPLK localization in TOEFAZ1 domain mutants

We next assessed the localization of TbPLK in cells expressing only the domain deletion mutants of TOEFAZ1. We classified TbPLK localization into four categories based upon its localization pattern throughout the cell cycle (**Fig. 2B**): no TbPLK expression (none); localization to the basal body, centrin arm, and hook complex (pocket); FAZ exclusively or FAZ and FC (FAZ/FC); or exclusively to the FC (FC). We first looked at cells expressing only the ΔIDP TOEFAZ1 mutant because it maintained localization to the FAZ tip and these cells showed only a slight growth defect, which made it possible that TbPLK localization was not altered. In control conditions where the full-length TOEFAZ1 was present, TbPLK localized to the pocket region early in the cell cycle, then was present on the tip of the new FAZ and FC as those structures migrate during later stages in cell division (**Fig. 7 A,B**). In cells expressing only the ΔIDP mutant after five days of RNAi induction, TbPLK recruitment to the pocket region was the same as in control cells. However, recruitment of the kinase to the tip of the new FAZ was blocked, similarly to what is observed when full-length TOEFAZ1 is depleted from cells (McAllaster et al., 2015; Zhou et al., 2016a). This block is remarkable because the ΔIDP mutant cells grow at nearly the same rate as control cells, which strongly argues that TbPLK localization to the tip of the new FAZ at later cell cycle stages is dispensable for growth and more specifically for cytokinesis.

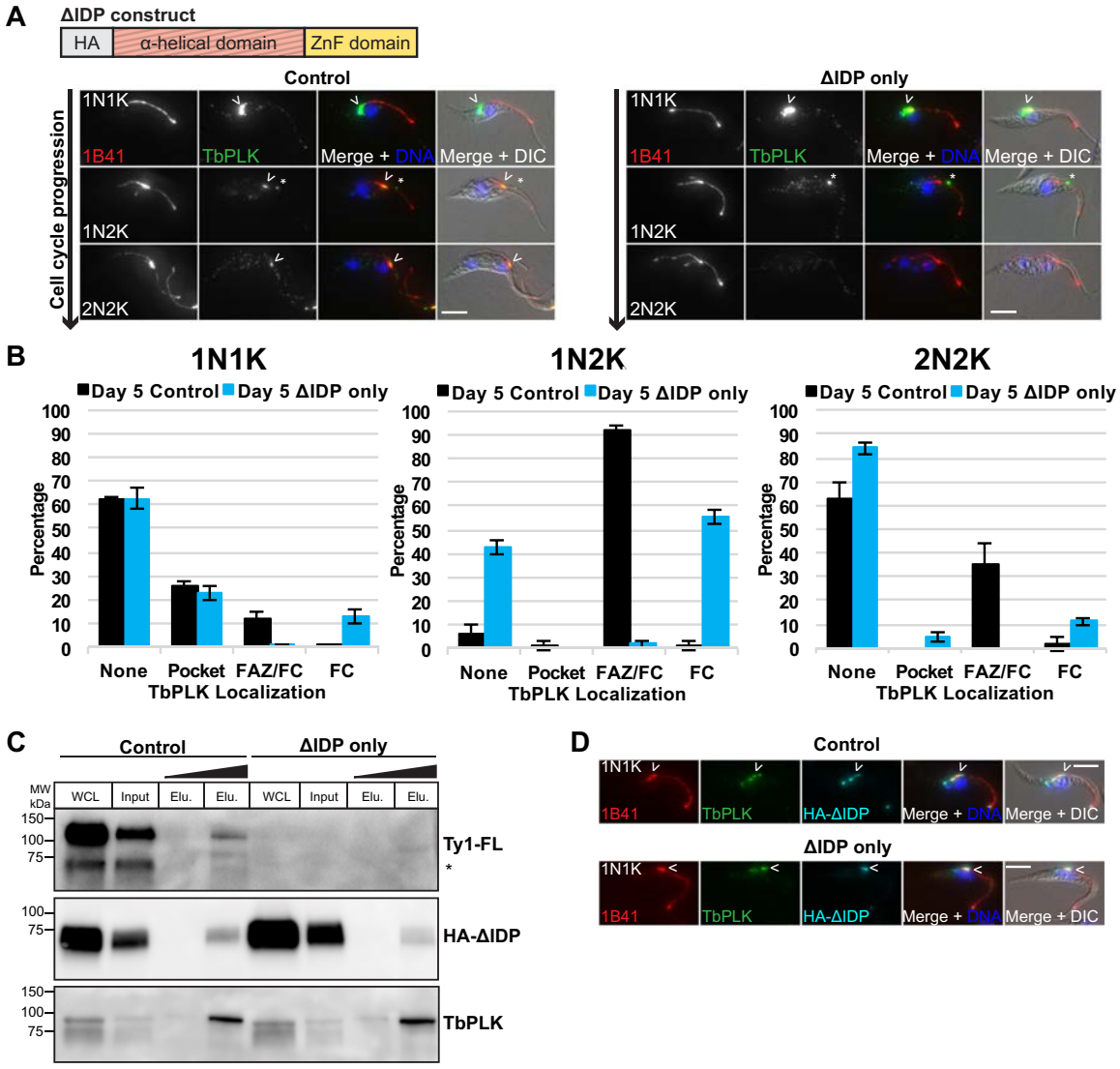

Figure 7. The IDP domain is required to maintain TbPLK localization at the new FAZ tip. (**A**) Control and ΔIDP only cells were methanol-fixed and labeled with 1B41 (red) and anti-TbPLK (green) after 5 days of TOEFAZ1 depletion. Arrowheads indicate TbPLK localization. Asterisks mark TbPLK FC labeling. (**B**) Quantification of TbPLK localization in cells from (A). 300 cells per condition from three independent experiments were counted. Error bars are the SD. (**C**) TOEFAZ1 RNAi was induced in ΔIDP cells for 3 days and cells were collected for TbPLK immunoprecipitation. Both input and immunoprecipitated fractions were western blotted with antibodies against Ty1 (Ty1-FL TOEFAZ1), HA (HA-ΔIDP) and TbPLK. Elution fractions are equal volume (1.2%) and 20% elution, respectively. Asterisk indicates degradation product. WCL; whole cell lysate. (**D**) ΔIDP cells were methanol-fixed and stained with 1B41 (red), anti-TbPLK (green), and anti-HA (HA-ΔIDP; cyan) after 2 days of WT TOEFAZ1 depletion. Arrowheads indicate ΔIDP and TbPLK colocalization at the short new FAZ tip. DAPI was used to stain DNA (blue). Scale bars: 5 μm.

We also determined TbPLK localization in cells expressing only the ΔN-terminus or ΔZnF mutants of TOEFAZ1 (**Fig. S7**). Because both of these mutants were unable to localize to the new FAZ tip on their own, it was likely that TbPLK recruitment would be blocked, as we saw previously with full-length TOEFAZ1 depletion (McAllaster et al., 2015). As expected, exclusive expression of either mutant led to a near-total block of TbPLK recruitment to the new FAZ tip, while the kinase was still able to localize to the pocket region early in the cell cycle.

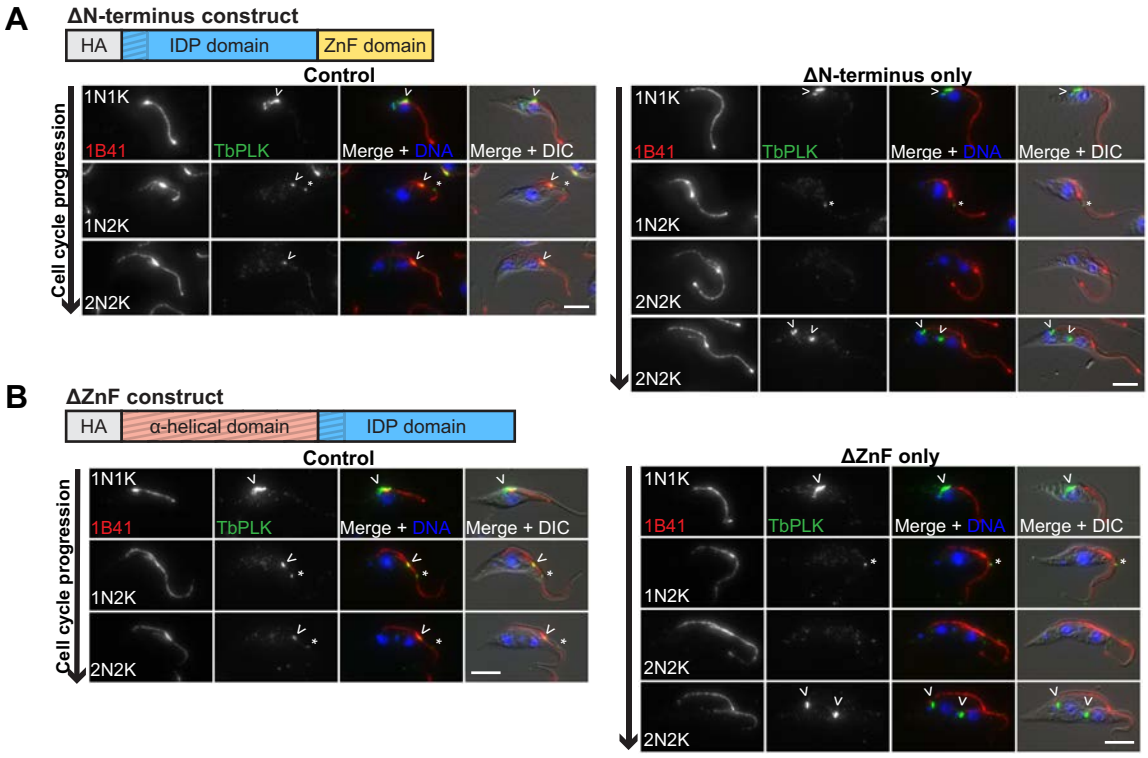

C

DNA State 24 hrs		No labeling	Pocket	FAZ/FC	FC only
ΔN-terminus HA IDP domain ZnF domain					
% 1N1K	Control	64 ± 4	24 ± 5	12 ± 3	0.3 ± 0.2
	ΔN only	39 ± 9	35 ± 6	2 ± 1	24 ± 7
% 1N2K	Control	13 ± 2	0 ± 0	87 ± 2	0 ± 0
	ΔN only	48 ± 9	0.8 ± 1	2 ± 2	49 ± 6
% 2N2K	Control	61 ± 5	0 ± 0	38 ± 4	1 ± 3
	ΔN only	79 ± 6	17 ± 4	0 ± 0	4 ± 2
ΔZnF HA α-helical domain IDP domain					
% 1N1K	Control	57 ± 1	30 ± 2	13 ± 1	0 ± 0
	ΔZnF only	39 ± 6	41 ± 1	5 ± 2	15 ± 8
% 1N2K	Control	11 ± 12	1 ± 2	88 ± 12	0 ± 0
	ΔZnF only	48 ± 5	2 ± 2	0.5 ± 1	49 ± 3
% 2N2K	Control	71 ± 1	0 ± 0	29 ± 1	0 ± 0
	ΔZnF only	72 ± 2	25 ± 4	0.3 ± 0.5	3 ± 2

Figure S7. TbPLK does not localize to the new FAZ tip when only the ΔN-terminus and ΔZnF constructs are present. TOEFAZ1 RNAi was induced for 1 day in the ΔN-terminus **(A)** and ΔZnF **(B)** cell lines. Cells were methanol-fixed and stained with 1B41 (red) and anti-TbPLK (green). DAPI was used to stain DNA (blue). Arrowheads indicate TbPLK localization. Scale bars: 5 μm. **(C)** Summary of TbPLK localization in cells expressing only the ΔN-terminus and ΔZnF constructs after 1 day of WT TOEFAZ1 depletion (red and gold lettering, respectively; corresponding controls in black). TbPLK localization was counted in 300 cells per condition in three independent experiments, and the numbers are the mean ± SD.

We decided to determine whether the IDP domain was absolutely necessary for interaction with TbPLK, as TbPLK no longer localizes to the new FAZ tip at later cell cycle stages in cells expressing only the ∆IDP protein, even though the ∆IDP protein is present at this location. Mapping this interaction was complicated by the fact that TOEFAZ1 forms oligomers (**Fig. S5B**), so it was essential to perform the experiment in the cells expressing only the ∆IDP mutant. We induced RNAi against the wild-type protein for 3 days in the ∆IDP cell line and then performed anti-TbPLK immunoprecipitations. We blotted the eluted proteins from both immunoprecipitations with anti-Ty1 and anti-HA to identify the WT full-length and ∆IDP TOEFAZ1, respectively (**Fig. 7C**). We were able to immunoprecipitate both full-length TOEFAZ1 and ∆IDP TOEFAZ1 under control conditions. Interestingly, in cells expressing only the ∆IDP TOEFAZ1, TbPLK precipitation was still able to capture ∆IDP TOEFAZ1. Immunofluorescence examination using antibodies to detect the FAZ, TbPLK, and the HA-tagged ∆IDP protein in cells only expressing the ∆IDP mutant showed that TbPLK co-localized with the ∆IDP protein at the early stages of cell division, when TbPLK localizes to the pocket region just as the new FAZ is being formed (**Fig. 7D**). These experiments demonstrate that the IDP domain is not essential for TbPLK interaction, but is necessary to maintain the kinase on the new FAZ tip at later points in the cell cycle.

Cell cycle analysis of TOEFAZ1 RNAi cells

Several of the TOEFAZ1 domain mutant cell lines show significant decreases in growth and aberrant DNA content in the absence of full-length protein. While this is consistent with our

previous work, it contrasts with other reports where a diminished but constant growth rate is observed in the absence of TOEFAZ1 (Zhou et al., 2016a). It is possible that the isolated domains that remain in our experiments exert some additional dominant-negative effect that is lacking when TOEFAZ1 is completely removed, but we did not observe any detrimental phenotype from overexpression of individual domains (**Fig. S1**). To address this discrepancy, we tagged the second TOEFAZ1 allele in our base cell line with a triple-HA tag but did not alter the codon usage, retaining its sensitivity to our TOEFAZ1 RNAi hairpin. We referred to this cell line as our double-tag line and used it in conjunction with our previously constructed cell line containing an HA-tagged TOEFAZ1 allele resistant to RNAi (now referred to as add-back line) to probe the effect of complete protein depletion (**Fig. 8A**).

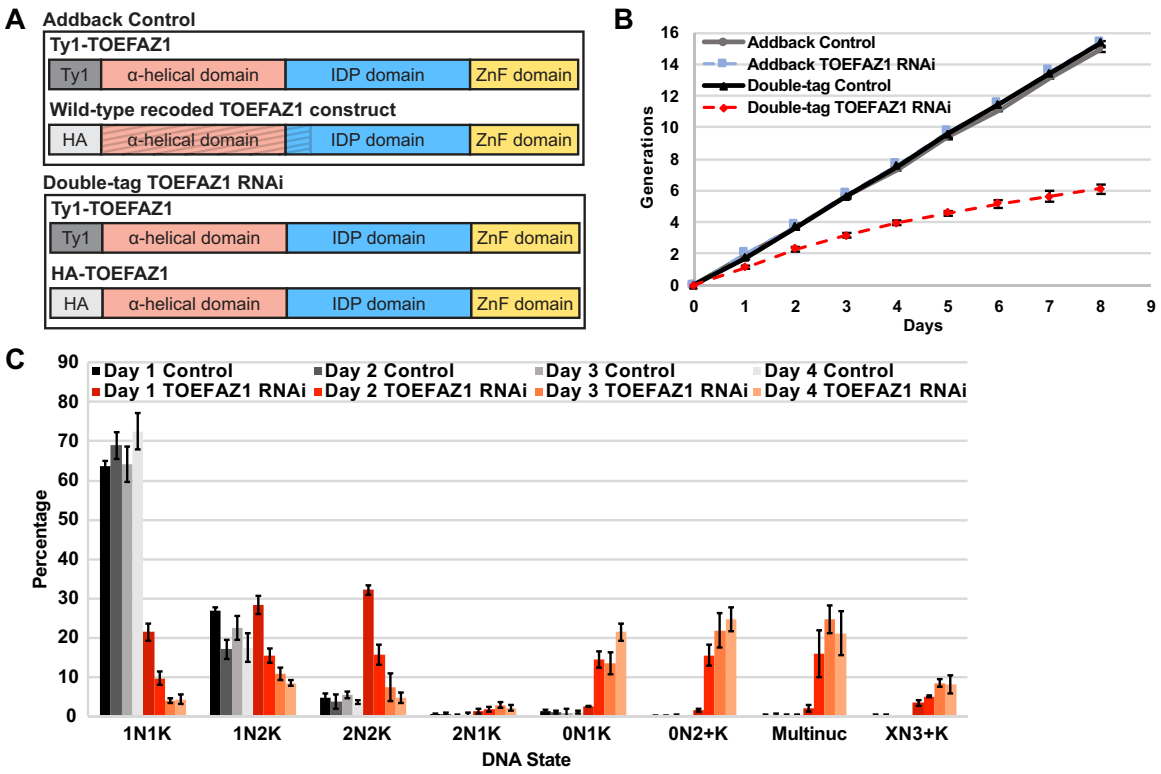

Figure 8. TOEFAZ1 RNAi causes severe cytokinetic defects. All analyses are the same as in Fig. 4. (**A**) Schematic of the TOEFAZ1 endogenous locus in addback control (top) and double-tagged TOEFAZ1 RNAi cell lines (bottom). (**B**) TOEFAZ1 RNAi was induced in addback control and double-tag RNAi lines and cell growth was monitored. The curve is the average of three independent experiments. (**C**) Quantification of DNA state in control (black-grey) and TOEFAZ1-

depleted cells (dark-light red) in the double-tag cell line. 300 cells per condition were quantified for three independent experiments. 0N2+K: no nuclei and 2+ kinetoplasts; XN3+K: 1-2 nuclei and 3+ kinetoplasts. Error bars are the SD.

We induced TOEFAZ1 RNAi in the add-back and double-tag cell lines and monitored parasite growth, DNA state, and morphology over the course of 8 days. The add-back cell line grew at the same rate both in the presence or absence of TOEFAZ1 RNAi induction, as in our previous experiment, showing that our RNAi is specific (**Fig. 8B**). In the double-tag cell line, induction of TOEFAZ1 RNAi caused a rapid decrease in cell growth. Over the 8 days of the experiment the growth of TOEFAZ1-depleted cells continued to decrease, and from day 6 to day 8 the cells were not able to complete a single doubling. Western blotting of lysates from both the add-back and double-tag lines showed that the RNAi insensitive allele was preserved in the add-back line while both copies of TOEFAZ1 were depleted in the double-tag line, as expected (**Fig. S8**).

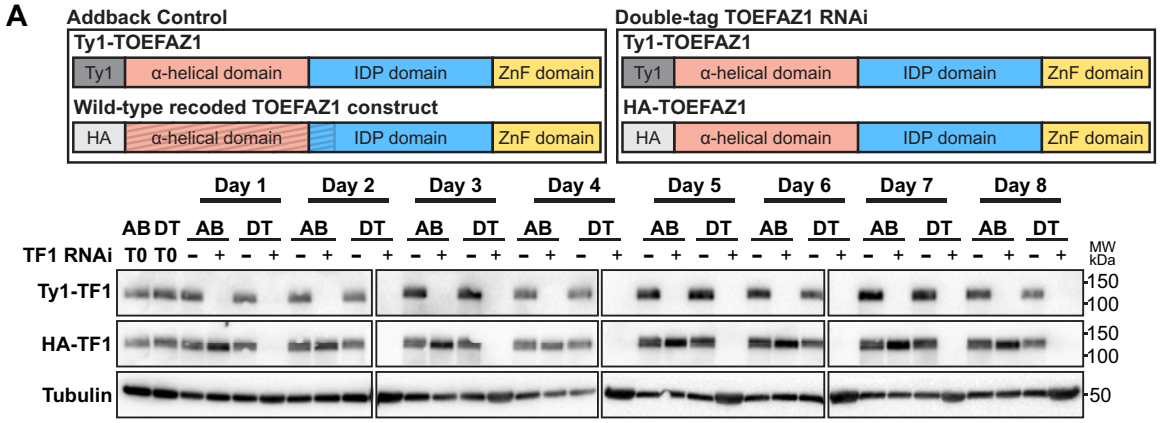

Figure S8. WT TOEFAZ1 is depleted while the recoded addback control remains during TOEFAZ1 RNAi. (A) TOEFAZ1 RNAi was induced in both the addback control and double-tagged TOEFAZ1 cell lines. Lysates were collected and western blotting was performed as described in Fig. S2B.

We focused our DNA and morphologic analysis on the double-tag cell line because it was the only cell line to show growth defects (**Fig. 8B**). After one day of depletion, cells lacking TOEFAZ1 showed a substantially diminished number of 1N1K cells and began to accumulate at

the 2N2K stage, suggesting a delay in cytokinesis (**Fig. 8C**). After two days, the population of 2N2K cells decreased and anucleate cells containing only kinetoplasts became prevalent. Multinucleate cells began to appear as well. This trend continued on days three and four, with anucleate cells now comprising more than half the population and cells with conventional DNA states making up fewer than 20% of the total cells. Many of these conventional cells may have contained normal DNA states (i.e. 1N1K, 1N2K, and 2N2K), but showed a wide range of abnormal morphologies that were difficult to categorize. Quantitating DNA state and morphology after day 4 was not possible due to the complexity of observed morphologies and large multinucleate cells.

DISCUSSION

In this work, we have dissected the function of the three modular domains of TOEFAZ1. The N-terminal domain has low affinity for the FAZ and cytoskeleton, the IDP domain retains TbPLK at the new FAZ tip, and the C-terminal ZnF domain is involved in TOEFAZ1 oligomerization. TOEFAZ1 most likely functions as a scaffold for organizing and assembling different protein complexes to perform their functions at different stages of cell division. The protein is unlikely to function as a direct initiator of cytokinesis but rather helps to recruit and localize other factors that are responsible for this process.

The N-terminal α-helical domain has low affinity for the cytoskeletal elements to which TOEFAZ1 targets during cell division (**Fig. 3C**). The N-terminal domain is likely to interact with other proteins on the tip of the new FAZ, although it cannot localize when expressed at endogenous levels (**Fig. S6A**). Among potential N-terminal binding partners is the protein CIF2, which was identified in a BioID screen with TOEFAZ1 and is essential for recruitment of the protein to the tip of the new FAZ (Zhou et al., 2016b). It is likely that TOEFAZ1 is part of a larger complex that is responsible for the timing and positioning of cleavage furrow ingression, and that the N-terminal domain is responsible for these interactions. The N-terminal domain has two predicted coiled-coil regions that could act as a stable scaffold for protein association (Zhou et al., 2016a).

The weak interaction of the isolated N-terminal domain at endogenous levels may be due to its monomeric state; since TOEFAZ1 appears to be an oligomer, the presence of additional copies of the N-terminal domain in the same complex may boost binding affinity and specificity in the full-length protein. However, we cannot exclude the possibility that the N-terminal domain mislocalizes under high expression levels, although its localization pattern shares similarities to the wild-type protein.

The TOEFAZ1 IDP domain is important for protein degradation at the end of cell division and for maintaining interaction with TbPLK, although neither of these functions is essential. IDP domains are unstructured and flexible domains that can adopt specific conformations upon binding to another protein, allowing them to bind to different partners (Malaney et al., 2013; Wright and Dyson, 2015). IDPs have also been thought of as flexible coils or springs that provide the motion necessary for protein function or as separation between functional domains (Young et al., 2001). IDPs are common sites for posttranslational modifications, especially phosphorylation (Bah et al., 2015). There are several potential TbPLK phosphosites on TOEFAZ1, although these sites appear to be clustered in the N-terminus (McAllaster et al., 2015). Depletion of full-length TOEFAZ1 blocks recruitment of TbPLK to the tip of the new FAZ without interfering with kinase localization to the pocket region or FC. Thus, our immunoprecipitation data **(Fig. 7C)** and others' work suggests that TbPLK recruits TOEFAZ1 to the tip of the FAZ, and TOEFAZ1 maintains this interaction (McAllaster et al., 2015; Zhou et al., 2016a). However, small molecule inhibition of TbPLK in synchronized cells shows that kinase activity is not necessary late in the cell cycle (Li et al., 2010; Lozano-Núñez et al., 2013). We now formally show that the presence of TbPLK at the new FAZ tip is not essential for cytokinesis to proceed, as TOEFAZ1 lacking the IDP domain is able to support near wild-type growth without maintaining TbPLK at this location. The essential functions of TbPLK appear to be restricted to early cell cycle events, such as duplication of the FPC, basal body rotation, and nucleation of the new FAZ (Ikeda and de Graffenried, 2012; Lozano-Núñez et al., 2013). It is possible that TbPLK is loaded onto the new FAZ tip during its

initial assembly and remains there as a consequence of this early event without having a discrete function.

The IDP domain is heavily phosphorylated and its expression is regulated during the cell cycle, most likely via proteolysis (**Fig. 3D**). There are a series of potential degradation motifs in the IDP, including a D-box (aa 366-369), a phosphodependent degron (aa 198-204), and a PEST domain (aa 399-411) (Lindon and Pines, 2004 ; Al-Zain et al., 2015; Li et al., 2012). Similar motifs were recently shown to control the stability of TbPLK via a ubiquitin-mediated degradation pathway (Hu et al., 2017). TOEFAZ1 lacking the IDP domain appears to persist in cells that have completed cytokinesis in a location similar to where the cleavage furrow ends, which is likely where the protein is removed and degraded (**Fig. 5E**). While the IDP is not required for TOEFAZ1 function, the N-terminal and C-terminal domains are not able to work in *trans*, either by associating with one another or performing their functions individually, so they must be present on the same polypeptide chain in order to function (**Fig. S4**). This strongly argues that the individual domains cannot interact with one another in cells and that the IDP domain acts as a physical linker to coordinate the function the N-terminal and ZnF domains of TOEFAZ1.

The ZnF domain in TOEFAZ1 plays an important role in assembling the protein into higher order structures (**Fig. S5**). Zinc fingers are ubiquitous folds in eukaryotes and have expanded their early-described function as nucleic acid binding domains to encompass many different types of interactions (Bates et al., 2008; Gamsjaeger et al., 2007). The full range of zinc fingers in trypanosomes has not been established, although the parasite contains many of the CCCH type, which are involved in binding and stabilizing mRNAs (Kramer et al., 2010). Some zinc fingers have been shown to interact exclusively with other proteins. For example, the C-terminal zinc finger domain in the transcription factor Ikaros has been shown to function as a highly specific dimerization domain that excludes closely-related proteins (Laity et al., 2001; McCarty et al., 2003). We propose that the TOEFAZ1 ZnF domain plays a similar role by oligomerizing the protein. This higher order structure now includes at least two copies of the N-terminal localization

domain that can interact with other proteins to localize TOEFAZ1. The ZnF domain can recruit itself to the tip of the new FAZ, but only if full-length TOEFAZ1 is also present (**Fig. S6B**). This likely means that the ZnF domain does not contain localization information on its own but relies on the N-terminal domain to target it to the correct cellular location once the protein is oligomerized.

Our data suggest that TOEFAZ1 is not absolutely essential for cytokinetic furrow ingression but is required for its correct timing and positioning (**Fig. 8C**). The appearance of anucleate cells in the TOEFAZ1 domain mutants as well as in complete TOEFAZ1 depletion conditions shows that a cytokinetic event must occur in the absence of the protein. The lack of an increasing 2N1K population argues against zoid production from 2N2K cells, which has been seen in cells lacking TbCentrin4 (Shi et al., 2008). A possible source for the anucleate population are multinucleate cells that expel zoids due to incorrect furrow positioning. An additional possibility is premature cytokinesis in 1N2K cells. Cells that do not complete abscission, the last step of cytokinesis, have been shown to restart the cell cycle, although these cells have already undergone cleavage furrow ingression and are only connected by a small posterior segment (Wheeler et al., 2013). In parasites lacking TOEFAZ1, 2N2K cells delayed in cleavage furrow ingression began to re-express TbPLK even though they have not yet completed the previous round of cell division **(Fig. S7**) (McAllaster et al., 2015). This indicates that the cytoplasmic cell cycle stage in these cells has progressed beyond their corresponding cytokinetic state. If cells with an “advanced” cytoplasmic state complete division after an initial delay in cleavage furrow ingression, the daughter cells would be primed to start division prematurely. We occasionally observed TOEFAZ1-depleted 1N2K cells with what appeared to be cleavage furrow folds and released FCs, suggesting that these cells were attempting to undergo cytokinesis to produce a 1N1K cell and a zoid. This constant cytoplasmic cycling combined with a delay in cleavage furrow ingression would lead to increasing asynchrony between the cell cycle events tasked with organelle duplication and those that partition them, which would result in cells with such aberrant

DNA states that viable cells could no longer be produced. This mimics the decreasing viability of cell divisions that we observe in our cell counting experiments.

Others have shown that TOEFAZ1 depletion blocks cleavage furrow ingression in the anterior-posterior direction, and suggested that this triggers a novel cytokinetic pathway in which a furrow ingresses from the posterior end of the cell towards the anterior to produce viable cells (Zhou et al., 2016a). We occasionally saw cells in our TOEFAZ1-depleted lines that had multiple posteriors while lacking clear ingression from the anterior end, which could be classified as posterior "furrows." However, it should be noted that nascent posterior end formation is an essential cell division event that creates a new posterior end for the cell containing the old flagellum and FAZ (Robinson et al., 1995; Wheeler et al., 2013). Taking these data together, it is more likely that the reported "back-up" cytokinetic mechanism is the result of nascent posterior end formation and subsequent subpellicular microtubule remodeling, and is not the reverse ingression of a posterior cleavage furrow. As the cleavage furrow fold is still produced in TOEFAZ1-depleted cells (Zhou et al., 2016a), cells could pull apart along the fold at the point of nascent posterior end formation due to the force of flagellar beating. In essentially every published image of a "backup" cytokinetic event in trypanosomes, the cells have already begun to replicate their kinetoplasts and even their nuclei beyond the 2N2K state (Zhou et al., 2016a; Zhou et al., 2016b). This indicates that "backup" cytokinesis is either an extremely slow process or is triggered after a prolonged delay, both of which would lead to asynchrony between cytoplasmic and cytokinetic states. While some organisms do employ alternate cytokinetic pathways to account for differences in growth conditions or defective proteins, these cells tend to lack a high degree of polarity and frequently use adherence to a surface as a mechanism to separate daughter cells (Choudhary et al., 2013; Gerisch and Weber, 2000; Rancati et al., 2008; Uyeda and Nagasaki, 2004). The inability of trypanosomes to sustain growth in the absence of TOEFAZ1 strongly argues that this method of cell division cannot be relied upon to provide viable progeny. The differences in our results compared to others that have depleted TOEFAZ1 could reflect a

difference in RNAi targeting efficiency or rate of depletion, although we note that we have shown the specificity of our RNAi hairpin with an add-back control. Long-term live cell imaging, which is still a challenge in *T. brucei,* will be required to determine the contribution of the “back up” cytokinesis to *T. brucei* cell division.

The primary function of TOEFAZ1 is to correctly position cytokinetic components to direct cleavage furrow ingression along the correct plane and at the correct time. The fact that cell division events can occur along an incorrect plane in the cell highlights the malleability of the cytoskeleton, but also emphasizes the importance of the precise placement of the cleavage furrow. Future research is needed to identify the molecular components that drive furrow ingression, remodel the surrounding membrane, and modify the subpellicular microtubule corset. The function of TOEFAZ1 homologs in the related kinetoplastids *Leishmania* and *T. cruzi*, which have FAZ homologs but do not attach most of their flagella, also remains to be studied (Wheeler et al., 2016).

MATERIALS AND METHODS

Cell Culture

Wild-type procyclic *T. brucei brucei* 427 strain cells were used to perform experiments, as well as 427 cells that were modified to carry doxycycline-inducible machinery (29-13) (Wirtz et al., 1999). 427 cells were passaged in Beck's Medium (Hyclone—GE Healthcare, Logan, Utah) supplemented with 10% fetal calf serum (Gemini Bioproducts—West Sacramento, CA), while 29-13 cells were passaged in Beck's Medium supplemented with 15% doxycycline-free fetal calf serum, 50 μg mL^{-1} hygromycin (ThermoFisher Scientific—Waltham, MA), and 15 μg mL^{-1} neomycin (Sigma-Aldrich—St. Louis, MO). 427 and 29-13 media also included 10 μg mL^{-1} gentamycin (ThermoFisher Scientific) and 500 μg mL^{-1} penicillin-streptomycin-glutamine (Hyclone). All cells were maintained at 27 °C. Cells were counted using a particle counter (Z2 Coulter Counter, Beckman Coulter—Brea, CA).

Antibodies

Antibodies are from the following sources and used at the following dilutions: anti-Ty1 (1:300) from Cynthia He (National University of Singapore, Singapore), 1B41 (1:1000) from Linda Kohl (Centre National de la Recherche Scientifique, Paris, France), and anti-FAZ1 (1:150) from Keith Gull (Oxford University, Oxford, United Kingdom). The anti-HA antibody (1:500) was purchased from Sigma-Aldrich (clone 3F10) and the anti-α tubulin (1:50,000) from ThermoFisher Scientific (clone B-5-1-2). The anti-TbPLK (1:150) and anti-TbCentrin2 (1:250) antibodies, as well as the anti-GFP polyclonal antibody (1:10,000), was previously described (de Graffenried et al., 2008; Ho et al., 2006; Ikeda and de Graffenried, 2012).

Cloning and Cell Line Construction

All constructs were created by PCR amplification of inserts using Q5 polymerase (NEB—Ipswich, MA) followed by either restriction-ligation or Gibson Assembly into a sequencing vector (PCR4Blunt) or pLEW100 as previously described (McAllaster et al., 2016). Each DNA construct was validated by sequencing and transfected into cells using an electroporator (GenePulser xCell, Bio-Rad—Hercules, CA). Clonal cell lines were created by selection and limiting dilution.

Domain constructs for overexpression. The endogenous sequence corresponding to each domain of TOEFAZ1 (N-terminus: nt 1-957, IDP: nt 958-1947, ZnF: nt 1948-2376) was PCR amplified and inserted into a pLEW100 vector that contained a 5' triple-Ty1 epitope tag. Overexpression pLEW100 constructs were linearized with *Not*I for transfection into the doxycycline-inducible 29-13 cell line and selected with 40 μg mL^{-1} Zeocin (Invivogen—San Diego, CA). Isolated clones were induced and screened by western blotting and immunofluorescence microscopy.

Endogenous tagging and mutant domain constructs for functional RNAi. Endogenous tagging of TOEFAZ1 with triple-Ty1, triple-HA, and mClover3 tags was carried out by targeting the tag to the TOEFAZ1 locus using 500 bp of the 5' UTR and the first 500 bp of the TOEFAZ1 coding sequence. The endogenous tagging constructs were digested with *Pac*I and *Nsi*I for transfection into either 427 cells or 29-13 cells carrying the doxycycline-inducible TOEFAZ1 RNAi construct (McAllaster et al., 2015), and selected with either 20 μg mL^{-1} blasticidin (Invivogen) for the triple-Ty1 and mClover3 constructs or 1 μg mL^{-1} puromycin (Invivogen) for the triple-HA construct. For endogenous

tagging in the 29-13 cell line, selection with blasticidin was used at a concentration of 10 μg mL^{-1}.

The recoded TOEFAZ1 sequence was generated using nt 4-1096 of the published TOEFAZ1 5' coding sequence (427 accession Tb427tmp.01.7450) (Aslett et al., 2009). Optimal *T. brucei* codons were used when possible (Horn, 2008). To create the RNAi-insensitive domain constructs, the recoded TOEFAZ1 sequence that overlapped with the N-terminal and IDP domains was amplified and annealed to the remaining endogenous TOEFAZ1 sequence for each domain construct. For the *trans* N-terminus-ZnF construct, the tubulin intergenic sequence was inserted between the recoded N-terminus and endogenous ZnF domain sequence.

Domain constructs were assembled into a sequencing vector containing a 5' triple-HA tag, were digested as above and transfected into the doxycycline-inducible TOEFAZ1 RNAi cell line containing an endogenous triple-Ty1 or mClover3-tagged TOEFAZ1. Domain analysis constructs were targeted to the second endogenous TOEFAZ1 allele using 500 bp of the 5' UTR and either 500 bp of 3' coding sequence (wild-type recoded control, ΔIDP, and ΔN-terminus constructs) or 3' UTR (ΔZnF, ΔN-terminus-IDP, ΔIDP-ZnF, and *trans* N-terminus-ZnF constructs). Clonal cell lines were selected with 1 μg mL^{-1} puromycin (while maintaining selection for the initial endogenous tag and the inducible TOEFAZ1 RNAi construct with 10 μg mL^{-1} blasticidin and 10 μg mL^{-1} Zeocin, respectively) and isolated clones were screened for proper recombination by endogenous locus PCR of genomic DNA, western blotting, and immunofluorescence microscopy. Domain truncation cell lines were further validated by sequencing of the endogenous locus.

Overexpression and RNAi

Cultures for overexpression and RNAi time courses were seeded at a density of 1 x 10^6 cells mL^{-1} and induced with 1 µg mL^{-1} doxycycline (ThermoFisher Scientific) or treated with 70% ethanol as a vehicle control. Cells were maintained as above and reseeded with fresh media and doxycycline or ethanol every 48 h. Cells were counted every 24 h, and samples were collected for western blotting and immunofluorescence microscopy as needed. For domain overexpression cell lines, the generation plots are representative of 2-3 independent clones. For functional RNAi analyses, the generation plot represents the average count of three independent experiments, and the error bars are the standard deviation.

Immunofluorescence

Cells were collected by centrifugation, washed in PBS, and centrifuged onto coverslips. Cells were fixed in -20 °C methanol for 20 min, followed by air-drying or direct rehydration in PBS. Cells were washed in PBS and blocked for either 1 h room temperature (RT) or 4 °C overnight in blocking buffer (3% bovine serum albumin or 5% goat serum diluted in PBS). Coverslips were incubated with primary antibodies diluted in blocking buffer for 1 h RT, washed three times in PBS, and were re-blocked for 20 minutes RT. Coverslips were then incubated in Alexa 647, 568-, and 488-conjugated secondary antibodies (Life Technologies—ThermoFisher Scientific) as above, washed in PBS, and mounted onto glass slides in DAPI-Fluoromount G (Southern Biotech—Birmingham, AL). For DNA state and morphology quantification, cells were harvested as above, fixed in 4% paraformaldehyde in PBS for 20 minutes RT, washed in PBS, and either mounted directly or stained for immunofluorescence as above. Coverslips were imaged with a Zeiss Axio

Observer.Z1 equipped with an ORCA-Flash 4.0 CMOS camera using a Plan-Apochromat 100x/1.4 oil lens. The microscope was controlled using the ZEN 2 PRO program. All immunofluorescence images (with the exception of **Fig. 3C,D**) are maximum projections of the Z-stack as signals were on different focal planes. The DIC image was overlayed on the merge. When comparing presence or absence of immunofluorescence signal between cells, the images were set to have the same look-up tables. All images were analyzed and quantified in ImageJ (National Institutes of Health—Bethesda, MD), and assembled for publication in Adobe Photoshop and Illustrator (CC 2017).

Western Blotting

Cells were collected for lysate by centrifugation, washed with PBS, and resuspended in SDS-PAGE loading buffer. A total of 2.5 x 10^6 cell equivalents of lysate/lane was separated by SDS-PAGE, transferred onto a nitrocellulose membrane, and blocked for 1 h RT in blocking buffer (5% (w/v) non-fat dried milk dissolved in Tris-buffered saline (TBS) containing 0.1% Tween-20). Blots were incubated overnight at 4 °C with primary antibodies diluted in blocking buffer. Blots were then washed in TBS containing 0.1% Tween-20 and incubated for 1 h RT with secondary antibodies conjugated to horseradish peroxidase (Jackson ImmunoResearch—West Grove, PA) diluted in blocking buffer. Blots were washed and then imaged using Clarity Western ECL Substrate (BioRad) and a BioRad Gel Doc XR+ system. When required, blots were stripped with Restore Western Blot Stripping Buffer (ThermoFisher Scientific), washed, re-blocked, and incubated with antibodies for detection and imaged as above. All western blot images are representative of two independent experiments.

Crosslinking and Immunoprecipitation

Crosslinking of cell lysates. 2.7 x 10^8 *trans* N-terminus—ZnF cells were harvested, washed in PBS, and resuspended in 700 µL of cold amine-free lysis buffer (10 mM $NaPO_4$, 150 mM NaCl, 0.5% glucose, 7.0% sucrose, and 0.5% NP-40 with protease and phosphatase inhibitors). Cells were lysed using the gentleMACS Dissociator (Miltenyi Biotec—Auburn, CA), and lysates were clarified by centrifugation at 17,000 x G for 20 min at 4 ºC. The supernatant was separated into two equal fractions to which either 5 mM DSS (ThermoFisher Scientific) or DMSO was added. Lysates were incubated for 30 min at RT, and crosslinking was quenched using 10 mM Tris pH 7.5. The crosslinked lysates were diluted in SDS-PAGE loading buffer, and samples were separated using SDS-PAGE and western blotted as above. The western blot is representative of three independent experiments.

Crosslinking of whole cells followed by immunoprecipitation. 3.5 x 10^8 *trans* N-terminus—ZnF cells were washed twice with cold HBSS and gently resuspended in 3.6 mL of HBSS. The cell suspension was separated into equal fractions to which DMSO or 5 mM DSS was added. Cells were incubated at RT and the crosslinking reaction was quenched as above. Cells were then pelleted and resuspended in cold RIPA buffer (50 mM Tris pH 7.4, 150 mM NaCl, 2 mM EDTA, 1.0% NP-40, 0.5% Na-deoxycholate, 0.1% SDS with protease and phosphatase inhibitors). Cells were lysed and the lysate was clarified as above. The supernatant was gently rotated with 30 µL of GFP-Trap MA bead slurry (Chromotek—Hauppauge, NY) for 1 h at 4 ºC. The beads were washed 3X with cold RIPA buffer and bound proteins were eluted by incubating the beads at 99 ºC for 10 minutes in SDS-PAGE loading buffer. Samples were separated using SDS-PAGE and transferred to nitrocellulose for western blotting as above. The western blot is

representative of three independent experiments.

Immunoprecipitation of TbPLK. The ΔIDP domain mutant cell line was treated with either 70% ethanol or 1 μg mL^{-1} doxycycline to induce TOEFAZ1 RNAi for 3 d. 250 x 10^6 cells from each condition were harvested, washed with PBS, and resuspended in 650 μL of cold lysis buffer (10 mM $NaPO_4$, 150 mM NaCl, 0.5% glucose, 7.0% sucrose, and 0.5% NP-40 with protease and phosphatase inhibitors). The cells were lysed and the lysate was clarified by centrifugation as above. 30 μL of rat anti-TbPLK antibody was added to each supernatant and then gently rotated for 2 h at 4 ºC. 50 μL of anti-rat IgG magnetic bead slurry (NEB) was added to each condition and rotated for 45 min RT. The beads were then washed 3X in lysis buffer and bound proteins were eluted in SDS-PAGE loading buffer as described above. Samples were separated using SDS-PAGE and western blotted as above. The western blot is representative of two independent experiments.

Quantification and statistics

For DNA, morphology, and immunofluorescence quantification, 300 cells were counted for both control and RNAi conditions per time point for three independent experiments. All error bars represent the standard deviation of three independent experiments unless otherwise stated. Counts were analyzed and graphed in Excel (Microsoft).

ACKNOWLEDGMENTS

We would like to thank Nicholas Hilton and Jenna Perry for comments on the manuscript, Rebecca Page for TOEFAZ1 domain analysis, Richard Bennett for the use of his microscope, and Dan Weinreich and Sam Obado for helpful discussions. This work was funded by the NIH (RO1 AI112953-01 to CLD; ANS-D was supported by 5 T32 GM 7601-37).

AUTHOR CONTRIBUTIONS

ANS-D, MRM, and CLdG performed the conception and design of the study; ANS-D performed the experiments; ANS-D and CLdG performed analysis or interpretation of the data; ANS-D and CLdG wrote the manuscript.

REFERENCES

Al-Zain, A., Schroeder, L., Sheglov, A. and Ikui, A. E. (2015). Cdc6 degradation requires phosphodegron created by GSK-3 and Cdk1 for SCFCdc4 recognition in Saccharomyces cerevisiae. *Mol. Biol. Cell* **26**, 2609–2619.

Aslett, M., Aurrecoechea, C., Berriman, M., Brestelli, J., Brunk, B. P., Carrington, M., Depledge, D. P., Fischer, S., Gajria, B., Gao, X., et al. (2009). TriTrypDB: a functional genomic resource for the Trypanosomatidae. *Nucleic Acids Res.* **38**, D457–D462.

Bah, A., Vernon, R. M., Siddiqui, Z., Krzeminski, M., Muhandiram, R., Zhao, C., Sonenberg, N., Kay, L. E. and Forman-Kay, J. D. (2015). Folding of an intrinsically disordered protein by phosphorylation as a regulatory switch. *Nature* **519**, 106–109.

Bajar, B. T., Wang, E. S., Lam, A. J., Kim, B. B., Jacobs, C. L., Howe, E. S., Davidson, M. W., Lin, M. Z. and Chu, J. (2016). Improving brightness and photostability of green and red fluorescent proteins for live cell imaging and FRET reporting. *Sci. Rep.* **6**, 1–12.

Bates, D. L., Chen, Y., Kim, G., Guo, L. and Chen, L. (2008). Crystal Structures of Multiple GATA Zinc Fingers Bound to DNA Reveal New Insights into DNA Recognition and Self-Association by GATA. *J. Mol. Biol.* **381**, 1292–1306.

Choudhary, A., Lera, R. F. and Martowicz, M. L. (2013). Interphase cytofission maintains genomic integrity of human cells after failed cytokinesis.

de Graffenried, C. L., Ho, H. H. and Warren, G. (2008). Polo-like kinase is required for Golgi and bilobe biogenesis in Trypanosoma brucei. *J. Cell Biol.* **181**, 431–438.

Farr, H. and Gull, K. (2012). Cytokinesis in trypanosomes. *Cytoskeleton (Hoboken)*.

Fenix, A. M., Taneja, N., Buttler, C. A., Lewis, J., Van Engelenburg, S. B., Ohi, R. and Burnette, D. T. (2016). Expansion and concatenation of non-muscle myosin IIA filaments drive cellular contractile system formation during interphase and mitosis. *Mol. Biol. Cell* **27**, 1465–1478.

Fèvre, E. M., Wissmann, B. V., Welburn, S. C. and Lutumba, P. (2008). The burden of human

African trypanosomiasis. *PLoS Negl Trop Dis* **2**, e333.

Gallo, J. M., Précigout, E. and Schrével, J. (1988). Subcellular sequestration of an antigenically unique beta-tubulin. *Cell Motil. Cytoskeleton* **9**, 175–183.

GAMSJAEGER, R., LIEW, C., LOUGHLIN, F., CROSSLEY, M. and MACKAY, J. (2007). Sticky fingers: zinc-fingers as protein-recognition motifs. *Trends in Biochemical Sciences* **32**, 63–70.

García-Salcedo, J. A., Pérez-Morga, D., Gijón, P., Dilbeck, V., Pays, E. and Nolan, D. P. (2004). A differential role for actin during the life cycle of Trypanosoma brucei. *EMBO J.* **23**, 780–789.

Gerisch, G. and Weber, I. (2000). Cytokinesis without myosin II. *Curr. Opin. Cell Biol.* **12**, 126–132.

Glotzer, M. (2005). The molecular requirements for cytokinesis. *Science* **307**, 1735–1739.

Gull, K. (1999). The cytoskeleton of trypanosomatid parasites. *Annu. Rev. Microbiol.* **53**, 629–655.

Hammarton, T. C., Kramer, S., Tetley, L., Boshart, M. and Mottram, J. C. (2007). Trypanosoma brucei Polo-like kinase is essential for basal body duplication, kDNA segregation and cytokinesis. *Mol. Microbiol.* **65**, 1229–1248.

He, C. Y., Pypaert, M. and Warren, G. (2005). Golgi duplication in Trypanosoma brucei requires Centrin2. *Science* **310**, 1196–1198.

Ho, H. H., He, C. Y., de Graffenried, C. L., Murrells, L. J. and Warren, G. (2006). Ordered assembly of the duplicating Golgi in Trypanosoma brucei. *Proc. Natl. Acad. Sci. U.S.A.* **103**, 7676–7681.

Horn, D. (2008). Codon usage suggests that translational selection has a major impact on protein expression in trypanosomatids. *BMC Genomics* **9**, 2.

Hu, H., Zhou, Q., Han, X. and Li, Z. (2017). CRL4WDR1 Controls Polo-like Kinase Protein Abundance to Promote Bilobe Duplication, Basal Body Segregation and Flagellum

Attachment in Trypanosoma brucei. *PLoS Pathog.* **13**, e1006146–24.

Ikeda, K. N. and de Graffenried, C. L. (2012). Polo-like kinase is necessary for flagellum inheritance in Trypanosoma brucei. *J. Cell. Sci.* **125**, 3173–3184.

Imboden, M. A., Laird, P. W., Affolter, M. and Seebeck, T. (1987). Transcription of the intergenic regions of the tubulin gene cluster of Trypanosoma brucei: evidence for a polycistronic transcription unit in a eukaryote. *Nucleic Acids Res.* **15**, 7357–7368.

Kohl, L., Robinson, D. and Bastin, P. (2003). Novel roles for the flagellum in cell morphogenesis and cytokinesis of trypanosomes. *EMBO J.* **22**, 5336–5346.

Kohl, L., Sherwin, T. and Gull, K. (1999). Assembly of the paraflagellar rod and the flagellum attachment zone complex during the Trypanosoma brucei cell cycle. *J. Eukaryot. Microbiol.* **46**, 105–109.

Kramer, S., Kimblin, N. C. and Carrington, M. (2010). Genome-wide in silico screen for CCCH-type zinc finger proteins of Trypanosoma brucei, Trypanosoma cruzi and Leishmania major. *BMC Genomics* **11**, 283.

Lacomble, S., Vaughan, S., Gadelha, C., Morphew, M. K., Shaw, M. K., McIntosh, J. R. and Gull, K. (2009). Three-dimensional cellular architecture of the flagellar pocket and associated cytoskeleton in trypanosomes revealed by electron microscope tomography. *J. Cell. Sci.* **122**, 1081–1090.

Laity, J. H., Lee, B. M. and Wright, P. E. (2001). Zinc finger proteins: new insights into structural and functional diversity. *Current Opinion in Structural Biology* **11**, 39–46.

Langousis, G. and Hill, K. L. (2014). Motility and more: the flagellum of Trypanosoma brucei. *Nat. Rev. Microbiol.* **12**, 505–518.

Laplante, C., Huang, F., Tebbs, I. R., Bewersdorf, J. and Pollard, T. D. (2016). Molecular organization of cytokinesis nodes and contractile rings by super-resolution fluorescence microscopy of live fission yeast. *Proc Natl Acad Sci USA* **113**, E5876–E5885.

Li, B., Hu, Q., Xu, R., Ren, H., Fei, E., Chen, D. and Wang, G. (2012). Hax-1 is rapidly degraded

by the proteasome dependent on its PEST sequence. *BMC Cell Biol.* **13**, 20.

Li, Z., Umeyama, T., Li, Z. and Wang, C. C. (2010). Polo-like kinase guides cytokinesis in Trypanosoma brucei through an indirect means. *Eukaryotic Cell* **9**, 705–716.

Lindon, C. and Pines, J. (2004). Ordered proteolysis in anaphase inactivates Plk1 to contribute to proper mitotic exit in human cells. *J. Cell Biol.* **164**, 233–241.

Lozano-Núñez, A., Ikeda, K. N., Sauer, T. and de Graffenried, C. L. (2013). An analogue-sensitive approach identifies basal body rotation and flagellum attachment zone elongation as key functions of PLK in Trypanosoma brucei. *Mol. Biol. Cell* **24**, 1321–1333.

Malaney, P., Pathak, R. R., Xue, B., Uversky, V. N. and Davé, V. (2013). Intrinsic Disorder in PTEN and its Interactome Confers Structural Plasticity and Functional Versatility. *Sci. Rep.* **3**, 215–14.

McAllaster, M. R., Ikeda, K. N., Lozano-Núñez, A., Anrather, D., Unterwurzacher, V., Gossenreiter, T., Perry, J. A., Crickley, R., Mercadante, C. J., Vaughan, S., et al. (2015). Proteomic identification of novel cytoskeletal proteins associated with TbPLK, an essential regulator of cell morphogenesis in Trypanosoma brucei. *Mol. Biol. Cell* **26**, 3013–3029.

McAllaster, M. R., Sinclair-Davis, A. N., Hilton, N. A. and de Graffenried, C. L. (2016). A unified approach towards Trypanosoma brucei functional genomics using Gibson assembly. *Mol. Biochem. Parasitol.* **210**, 13–21.

McCarty, A. S., Kleiger, G., Eisenberg, D. and Smale, S. T. (2003). Selective dimerization of a C2H2 zinc finger subfamily. *Molecular Cell* **11**, 459–470.

Mezulis, S., Yates, C. M., Wass, M. N., Sternberg, M. J. E. and Kelley, L. A. (2015). The Phyre2 web portal for protein modeling, prediction and analysis. *Nat Protoc* **10**, 845–858.

Moreira-Leite, F. F., Sherwin, T., Kohl, L. and Gull, K. (2001). A trypanosome structure involved in transmitting cytoplasmic information during cell division. *Science* **294**, 610–612.

Rancati, G., Pavelka, N., Fleharty, B., Noll, A., Trimble, R., Walton, K., Perera, A., Staehling-Hampton, K., Seidel, C. W. and Li, R. (2008). Aneuploidy Underlies Rapid Adaptive

Evolution of Yeast Cells Deprived of a Conserved Cytokinesis Motor. *Cell* **135**, 879–893.

Robinson, D. R., Sherwin, T., Ploubidou, A., Byard, E. H. and Gull, K. (1995). Microtubule polarity and dynamics in the control of organelle positioning, segregation, and cytokinesis in the trypanosome cell cycle. *J. Cell Biol.* **128**, 1163–1172.

Sherwin, T., Schneider, A., Sasse, R., Seebeck, T. and Gull, K. (1987). Distinct localization and cell cycle dependence of COOH terminally tyrosinolated alpha-tubulin in the microtubules of Trypanosoma brucei brucei. *J. Cell Biol.* **104**, 439–446.

Shi, J., Franklin, J. B., Yelinek, J. T., Ebersberger, I., Warren, G. and He, C. Y. (2008). Centrin4 coordinates cell and nuclear division in T. brucei. *J. Cell. Sci.* **121**, 3062–3070.

Sunter, J. D. and Gull, K. (2016). The Flagellum Attachment Zone: "The Cellular Ruler" of Trypanosome Morphology. *Trends in Parasitology* **32**, 309–324.

Sunter, J. D., Varga, V., Dean, S. and Gull, K. (2015). A dynamic coordination of flagellum and cytoplasmic cytoskeleton assembly specifies cell morphogenesis in trypanosomes. *J. Cell. Sci.* **128**, 1580–1594.

Urbaniak, M. D., Guther, M. L. S. and Ferguson, M. A. J. (2012). Comparative SILAC Proteomic Analysis of Trypanosoma brucei Bloodstream and Procyclic Lifecycle Stages. *PLoS ONE* **7**, e36619.

Urbaniak, M. D., Martin, D. M. A. and Ferguson, M. A. J. (2013). Global quantitative SILAC phosphoproteomics reveals differential phosphorylation is widespread between the procyclic and bloodstream form lifecycle stages of Trypanosoma brucei. *J. Proteome Res.* **12**, 2233–2244.

Uyeda, T. Q. and Nagasaki, A. (2004). Variations on a theme: the many modes of cytokinesis. *Curr. Opin. Cell Biol.* **16**, 55–60.

Vaughan, S., Kohl, L., Ngai, I., Wheeler, R. J. and Gull, K. (2008). A repetitive protein essential for the flagellum attachment zone filament structure and function in Trypanosoma brucei. *Protist* **159**, 127–136.

Wheeler, R. J., Scheumann, N., Wickstead, B., Gull, K. and Vaughan, S. (2013). Cytokinesis in Trypanosoma brucei differs between bloodstream and tsetse trypomastigote forms: implications for microtubule-based morphogenesis and mutant analysis. *Mol. Microbiol.* **90**, 1339–1355.

Wheeler, R. J., Sunter, J. D. and Gull, K. (2016). Flagellar pocket restructuring through the Leishmania life cycle involves a discrete flagellum attachment zone. *J. Cell. Sci.* **129**, 854–867.

Wirtz, E., Leal, S., Ochatt, C. and Cross, G. A. (1999). A tightly regulated inducible expression system for conditional gene knock-outs and dominant-negative genetics in Trypanosoma brucei. *Mol. Biochem. Parasitol.* **99**, 89–101.

Wright, P. E. and Dyson, H. J. (2015). Intrinsically disordered proteins in cellular signalling and regulation. *Nature Publishing Group* **16**, 18–29.

Xu, D., Jaroszewski, L., Li, Z. and Godzik, A. (2014). FFAS-3D: improving fold recognition by including optimized structural features and template re-ranking. *Bioinformatics* **30**, 660–667.

Young, M. A., Gonfloni, S., Superti-Furga, G., Roux, B. and Kuriyan, J. (2001). Dynamic coupling between the SH2 and SH3 domains of c-Src and Hck underlies their inactivation by C-terminal tyrosine phosphorylation. *Cell* **105**, 115–126.

Yu, Z., Liu, Y. and Li, Z. (2012). Structure-function relationship of the Polo-like kinase in Trypanosoma brucei. *J. Cell. Sci.* **125**, 1519–1530.

Zhou, Q., Gu, J., Lun, Z.-R., Ayala, F. J. and Li, Z. (2016a). Two distinct cytokinesis pathways drive trypanosome cell division initiation from opposite cell ends. *Proc Natl Acad Sci USA* **113**, 3287–3292.

Zhou, Q., Hu, H. and Li, Z. (2016b). An EF-hand-containing Protein in Trypanosoma brucei Regulates Cytokinesis Initiation by Maintaining the Stability of the Cytokinesis Initiation Factor CIF1. *Journal of Biological Chemistry* **291**, 14395–14409.

Chapter 3:

The *Trypanosoma brucei* subpellicular microtubule array is organized into functionally discrete subdomains defined by microtubule associated proteins

Modified from its original submission to *PloS Pathogens* (submitted November 2020, currently under review)

Figure 1 and Supplemental Figure 1 are excerpted from Hilton *et al.* Identification of TOEFAZ1-interacting proteins identifies key regulators of *Trypanosoma brucei* cytokinesis. *Molecular Microbiology,* 2018. Vol. 109, Issue 3, pp. 306-326.

The work in Figure 1 D & E were conducted in collaboration with Zemplen Pataki

The work in Figure 6 and Supplementary Figure 3 was performed by Christine T. Huynh

The *Trypanosoma brucei* subpellicular microtubule array is organized into functionally discrete subdomains defined by microtubule associated proteins

Amy N. Sinclair[1], Christine T. Huynh[1], Thomas E. Sladewski[1], Jenna L. Zuromski[2], Amanda E. Ruiz[2], and Christopher L. de Graffenried[1*]

1. Department of Molecular Microbiology and Immunology, Brown University, Providence, RI, 02912
2. Department of Pathology and Laboratory Medicine, Center for International Health Research, Brown University, Providence, RI 02903

Short title: Subpellicular array subdomains in *T. brucei*

Abbreviations: Flagellum attachment zone (FAZ), microtubule associated protein (MAP), proximity-dependent biotin identification (BioID), nucleus (N), kinetoplast (K), immunogold electron microscopy (iEM), transmission electron microscopy (TEM), scanning electron microscopy (SEM), RNA interference (RNAi), mNeonGreen (mNG), maltose binding protein (MBP), total internal reflection fluorescence microscopy (TIRF)

ABSTRACT

Microtubules are inherently dynamic cytoskeletal polymers whose length and activity can be altered to perform essential functions in eukaryotic cells, such as providing tracks for intracellular trafficking and forming the mitotic spindle. Microtubules can be bundled to create more stable structures that collectively propagate force, such as in the flagellar axoneme, which provides motility. The subpellicular microtubule array of the protist parasite *Trypanosoma brucei,* the causative agent of African sleeping sickness, is a remarkable example of a highly specialized microtubule bundle, comprising a single microtubule layer that is crosslinked to each other and the plasma membrane. The array microtubules appear to be highly stable and remain intact throughout the cell cycle, but very little is known about the pathways that tune microtubule properties in trypanosomatids. Here, we show that the subpellicular microtubule array is organized into subdomains that consist of differentially localized array-associated proteins. We characterize the localization and function of the array-associated protein PAVE1, which is a component of the inter-microtubule crosslinking fibrils present within the posterior subdomain. PAVE1 functions to stabilize these microtubules to produce the tapered cell posterior. PAVE1 and the newly identified PAVE2 form a complex that binds directly to the microtubule lattice. TbAIR9, which localizes to the entirety of the subpellicular array, is necessary for retaining PAVE1 within the posterior subdomain, and also maintains array-associated proteins in the middle and anterior subdomains of the array. The arrangement of proteins within the array is likely to tune the local properties of the array microtubules and create the asymmetric shape of the cell, which is essential for parasite viability.

INTRODUCTION

Trypanosoma brucei is the causative agent of African trypanosomiasis, which affects both humans and livestock in Sub-Saharan Africa (Fitzpatrick et al., 2017). A key contributor to *T. brucei* pathogenesis is the highly asymmetric shape of its cell body, which is essential for parasite survival within both insect and mammalian hosts. The trypomastigote form of *T. brucei* has a bore-like shape and tapered ends, with a broader cell posterior and a narrower, pointed anterior end (Figure 1A). This shape is produced by a single layer of microtubules that underlies the plasma membrane called the subpellicular array (Angelopoulos, 1970; Vickerman, 1962). A single flagellum is attached to the cell surface by the flagellum attachment zone (FAZ), which is comprised of a filament that is inserted between the subpellicular microtubules. The FAZ filament follows the left-handed helical path of the array microtubules as they traverse the cell body (Sunter and Gull, 2016). As the flagellum beats, it deforms the subpellicular microtubule array and creates 'cellular waveforms' that define the distinctive corkscrew-like motility pattern of *T. brucei* (Bargul et al., 2016; Heddergott et al., 2012; Sun et al., 2018). This specialized motility is essential for parasite escape from high-flow blood vessels and capillaries into low-flow compartments, which leads to the invasion of epithelial and adipose tissues that facilitate persistent host infection and dissemination back to the insect vector (Caljon et al., 2016; Capewell et al., 2016; Dóró et al., 2019; Trindade et al., 2016). The microtubules of the subpellicular array must be able to withstand and propagate the force generated by the flagellum, which is not uniformly distributed along the cell body (Sun et al., 2018). The ability to regulate microtubule dynamics and flexibility

within different domains of the array would allow the parasite to optimize the transmission of energy generated by the flagellar beat and channel it into productive motility.

Early morphological studies using electron microscopy revealed that the subpellicular array is a complex structure that is highly conserved among trypanosomatids (Angelopoulos, 1970; Brooker, 1971). The microtubules of the array are uniformly oriented with the same polarity, with their growing plus-ends facing the broader cell posterior (Halliday et al., 2019; Robinson et al., 1995; Sheriff et al., 2014). The array microtubules are spaced apart at a uniform distance of 18-20 nm and are extensively crosslinked to each other and the plasma membrane by regularly spaced fibrils (Bordier et al., 1982; Sherwin and Gull, 1989a; Souto-Padrón et al., 1984). The widest point of the cell body, which is near the nucleus, can contain over 100 microtubules. As the cell tapers toward the posterior and anterior ends, microtubules terminate in a stepwise fashion that maintains the inter-microtubule distance and consistent spacing between crosslinking fibrils while creating the asymmetric shape of the trypanosome cell body.

Microtubules are rigid, hollow polymers made up of α- and β-tubulin heterodimer subunits that bind and hydrolyze GTP. They exhibit a property known as dynamic instability wherein they undergo GTPase-dependent cycles of depolymerization (‘catastrophes’) and growth (‘rescues’) (Mitchison and Kirschner, 1984). This property allows for the rapid reorganization of internal cytoskeletal networks and is essential for cell migration, intracellular transport, and division (Janke, 2014). Microtubules are organized and regulated by microtubule associated proteins (MAPs) and motor proteins such as kinesins to control their dynamic instability. Many MAPs crosslink microtubules into bundles that can propagate and withstand force, such as the bundles found at the

mitotic spindle, ciliary axoneme, and neuronal axon (Forth et al., 2014; Kwan et al., 2008; Rubinstein et al., 2009; Sanchez et al., 2011). Tubulin subunits have intrinsically disordered and highly charged C-terminal tails that are heavily decorated with post-translational modifications, which serve as binding sites for many MAPs (Janke and Bulinski, 2011; Song and Brady, 2015). Other MAPs recognize specific structural conformations of the microtubule lattice, such as the incompletely polymerized and more open lattice found at microtubule plus-ends (Bechstedt et al., 2014; Reid et al., 2019).

The subpellicular microtubule array is a fascinating example of a specialized microtubule bundle. Dynamic instability has not been observed in microtubules of the array, most likely due to their extensive crosslinking (**Fig. 1A**). Some crosslinking proteins in other systems are known to promote microtubule flexibility (Portran et al., 2013), which may explain the apparent longevity of array microtubules as they respond to forces produced by the flagellar beat. However, very little is known about the structure and function of the inter-microtubule crosslinking fibrils that organize the array, or how MAPs may regulate array microtubules. Fewer than twenty non-motor proteins have been identified that associate with the subpellicular array (Sinclair and de Graffenried, 2019). The function of many of these has yet to be determined, but a subset have been described as microtubule stabilizers or potential crosslinkers that are required for proper cell division (Balaban et al., 1989; Bramblett et al., 1987; May et al., 2012; Vedrenne et al., 2002) and the arrangement of array microtubules in a single layer underneath the plasma membrane (Baines and Gull, 2008; Olego-Fernandez et al., 2009; Portman and Gull, 2014). However, the precise mechanism these proteins employ to localize to the array and perform their function has not been established. Understanding how *T. brucei* MAPs bind

to microtubules will have important implications in trypanosomatid cell biology and provide a more fundamental understanding of how cytoskeletal filaments are organized among diverse phyla.

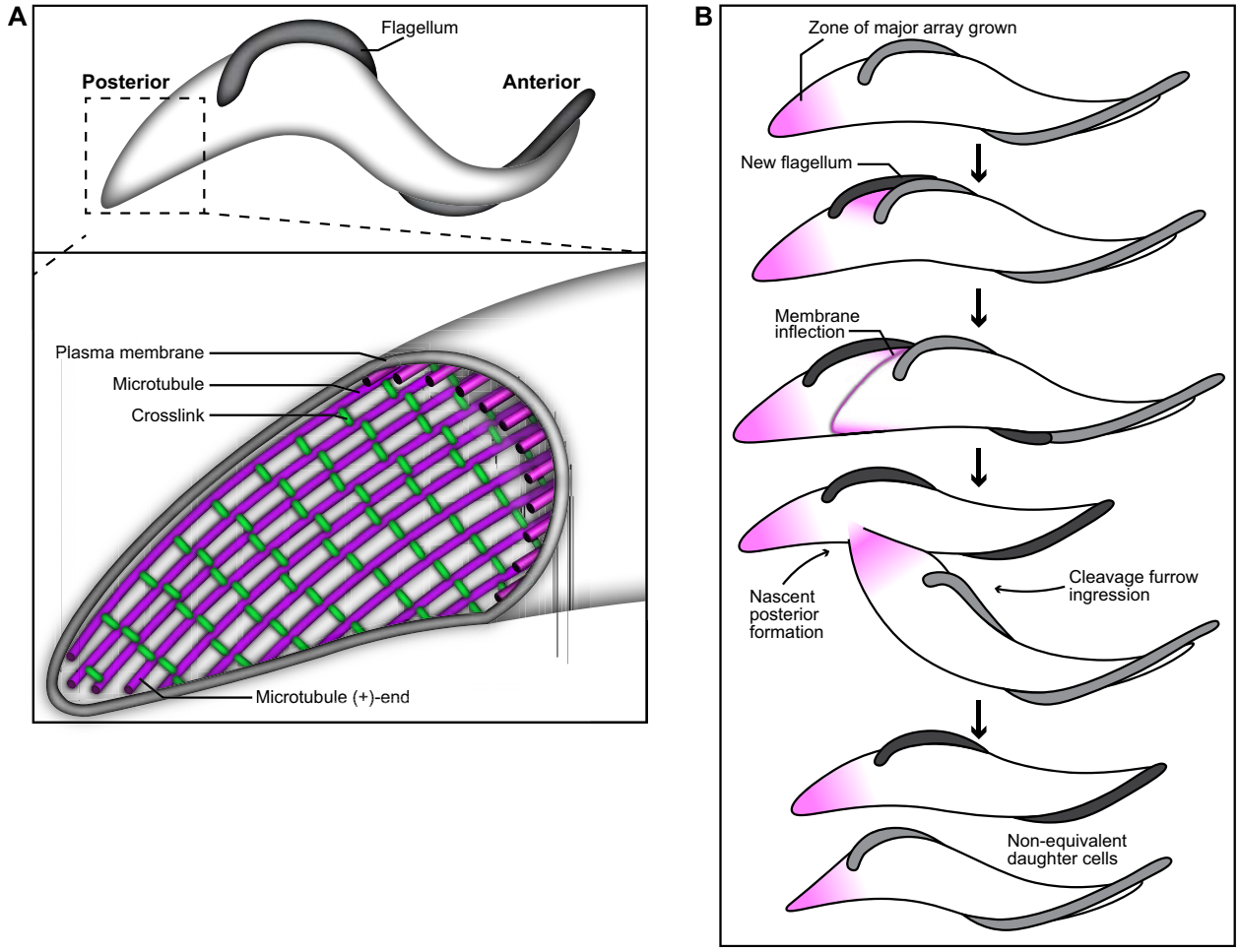

Figure 1. Schematics of the cytoskeleton and cell division in *Trypanosoma brucei*. (A) The subpellicular array is a single layer of microtubules purple) that underlies the plasma membrane. The microtubules are crosslinked to each other by regularly spaced fibrils (green). The (+)-growing ends of array microtubules face the cell posterior. **(B)** Array microtubules appear to be consistently polymerizing at the posterior end of the cell (purple shading). As the new flagellum is nucleated, new microtubules are inserted between the old and new flagellum to increase cell width. A membrane inflection forms that demarcates the path of cleavage furrow ingression, which follows the helical path of array microtubules. Cleavage furrow ingression initiates at the cell anterior, and nascent posterior end formation remodels the array at the cell midzone to resolve the subpellicular array into two distinct structures to complete cytokinesis.

The array microtubules appear highly stable and remain intact throughout the cell cycle, which requires that many aspects of *T. brucei* cell division include microtubule remodeling processes that duplicate and segregate the array (Robinson et al., 1995; Sherwin and Gull, 1989b). During cell division, extant microtubules are elongated and short, new microtubules are inserted between them to lengthen and widen the array (Sherwin and Gull, 1989a). At later stages of the cell cycle, new microtubules are inserted in between the old and new flagellum to widen the cell body (**Fig. 1B**) (Wheeler et al., 2013). Microtubule polymerization also appears to occur continuously at the cell posterior throughout the cell cycle, suggesting that the array microtubules may be consistently turning over tubulin subunits to maintain cell length and shape (Abeywickrema et al., 2019; Sheriff et al., 2014; Wheeler et al., 2013). Cytokinesis proceeds via a cleavage furrow that initiates at the cell anterior and follows the helical path of the array microtubules towards the cell posterior to divide the cell on its long axis (**Fig. 1B**) (Robinson et al., 1995; Sherwin and Gull, 1989b; Wheeler et al., 2019).

Subpellicular array morphogenesis is an inherent part of cell division in trypanosomatids. To identify key regulators of cytokinesis and the subpellicular array, we recently conducted a proximity-dependent biotin identification (BioID) screen using cytokinetic protein TOEFAZ1 as the bait (Hilton et al., 2018). TOEFAZ1 is a scaffold protein that recruits cytokinetic regulators to the site of cleavage furrow initiation and tracks the cleavage furrow as it ingresses, and is thus likely to come into close contact with proteins involved in subpellicular array morphogenesis (Sinclair-Davis et al., 2017). We identified several proteins in this screen that regulate TOEFAZ1 and also remodel the subpellicular array during cell division. Here, we establish the function of PAVE1

(Tb927.8.2030), which was a top hit in the TOEFAZ1 interaction screen. PAVE1 is found exclusively in kinetoplastids and localizes to the posterior and ventral edge of the array (Hilton et al., 2018). We show that PAVE1 is required for the formation of the more broadly tapered end of the cell posterior and determine that PAVE1 is a component of the inter-microtubule crosslinking fibrils present in the posterior array and is essential for stabilizing these microtubules. PAVE1, in complex with its binding partner PAVE2, binds directly to the microtubule lattice, demonstrating that PAVE1 and PAVE2 together form a true kinetoplastid-specific MAP. The previously identified protein TbAIR9 (May et al., 2012) forms a complex with PAVE1 and PAVE2 and regulates the distribution of array-associated proteins to specific regions of the subpellicular array that we term subdomains. Our work shows that the subpellicular array contains a landscape of differentially localized array-associated proteins that likely function to locally tune the biophysical characteristics of array microtubules. These results update the long-standing view of the subpellicular array as a static arrangement of microtubules. Our work suggests that the array is a dynamic, multidomain structure that plays an essential role in cell morphogenesis and motility.

RESULTS

PAVE1 defines the posterior subdomain of the subpellicular array

A BioID screen using TOEFAZ1 as the bait protein identified almost 500 novel interactors (Hilton et al., 2018). The candidate gene Tb927.8.2030 was selected for further analysis because a statistically significant interactor of TOEFAZ1 and had no purported function or reported localization (Hilton et al., 2018). We appended three copies

of the Ty1 epitope tag to the N-terminus of Tb927.8.2030 at its endogenous locus and localized the gene with anti-Ty1 immunofluorescence. Strikingly, Tb927.8.2030 localized to the posterior end of the subpellicular array, with a preference for the ventral edge of the cell (using the flagellum to establish a dorsal-ventral axis), and so we termed this protein PAVE1 (Posterior And Ventral Edge protein 1) (**Figure 2A**). We studied the localization pattern of PAVE1 throughout the *T. brucei* cell cycle. *T. brucei* contain one nucleus (N) and one kinetoplast (K; the mitochondrial DNA aggregate) early in the cell cycle (1N1K). Cells first duplicate their kinetoplast (1N2K) before undergoing nuclear mitosis (2N2K) prior to initiating cytokinesis. PAVE1 localized to the posterior array of cells early in the cell cycle (1N1K) with its labeling density declining as the array widens near the location of the kinetoplast. In 2N2K cells, PAVE1 signal extends past the midzone of the cell towards the more anterior-located nucleus. PAVE1 collected at the site of nascent posterior formation in cells actively undergoing cytokinesis (**Fig. 2A, asterisk**), which is the location of extensive microtubule remodeling that leads to the creation of the new posterior end for the old flagellum containing daughter cell (Wheeler et al., 2013). This localization pattern suggests that PAVE1 is stably associated with the array microtubules at the posterior end of the cell throughout the cell cycle and is recruited to the nascent posterior end during its formation. PAVE1 is also found along the cleavage furrow, where it colocalizes with TOEFAZ1 as it tracks the ingressing furrow (**Fig. 2B**).

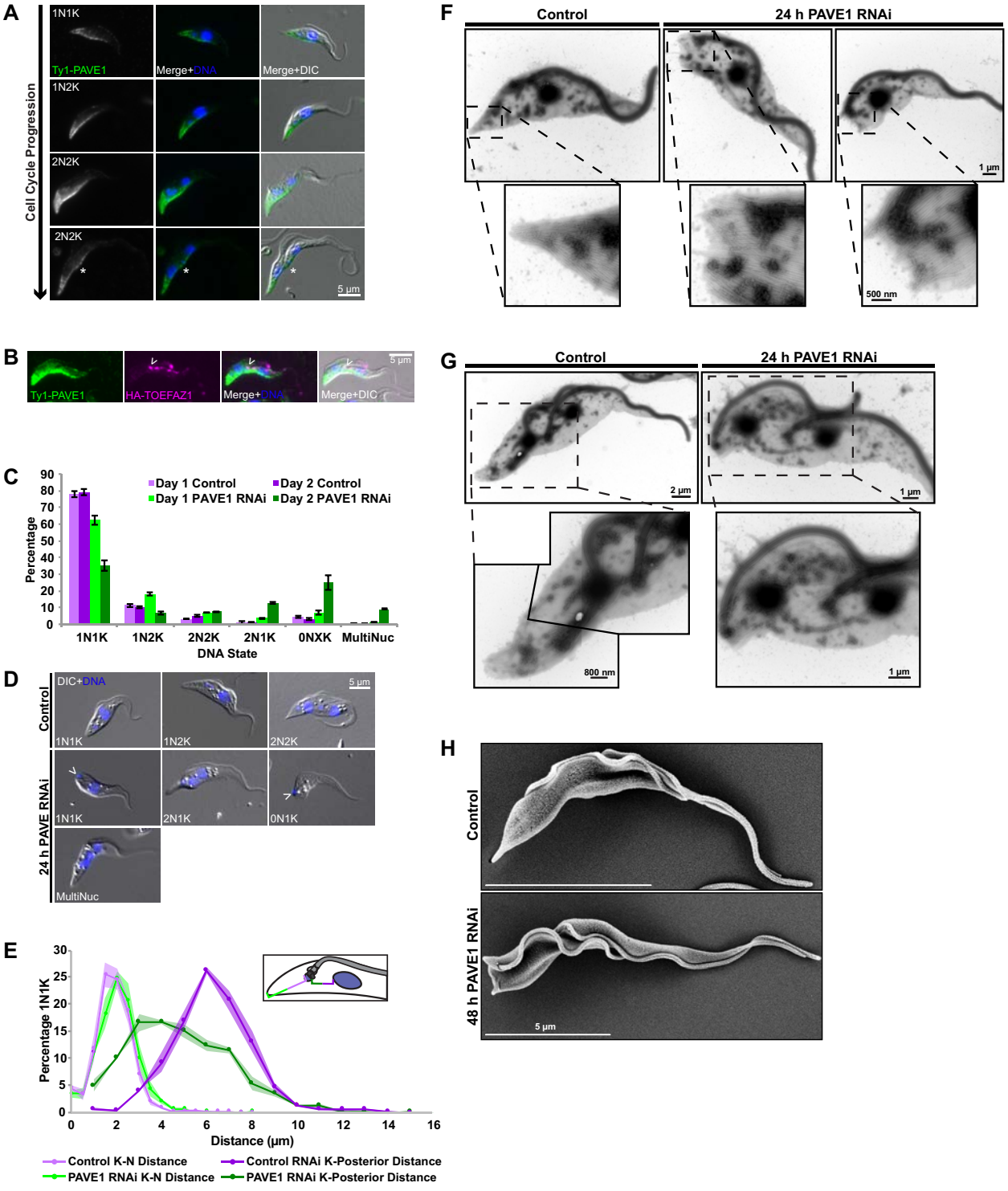

Figure 2. PAVE1 is required for to maintain the length and shape of the posterior subpellicular array. (A) Cells containing endogenously-tagged Ty1-PAVE1 were fixed in methanol and stained with anti-Ty1 antibodies for epifluorescence microscopy. DAPI was used to label the DNA. **(B)** A cleaving cell fixed in methanol containing endogenously-tagged Ty1-PAVE1 and HA-TOEFAZ1 shows TOEFAZ1 in close proximity to PAVE1 at the apex of the

cleavage furrow. **(C)** Quantification of DNA states in control and PAVE1 RNAi cells after 1 and 2 d of RNAi induction. Bars represent the mean and the error bars are the S.D. 300 cells in both control and PAVE1 RNAi conditions from N=3 independent biological replicates were counted at each time point. **(D)** PAVE1 RNAi was induced for 1 d, after which control and PAVE1-depleted cells were fixed with paraformaldehyde and examined by epifluorescence microscopy. **(E)** The kinetoplast-to-posterior (K-posterior) and the kinetoplast-to-nucleus (K-N) distance was measured in control and PAVE1 RNAi cells from (D). 200 cells were counted in each condition. Shaded regions are the S.E. **(F)** Control and PAVE1 RNAi cells after 1 d of RNAi induction were extracted and negatively stained for transmission electron microscopy. **(G)** Dividing cells in control and PAVE1-depleted cells as imaged by transmission electron microscopy. Cells were prepared as in (F). (**H**) Control and PAVE1 RNAi cells induced for 2 d were fixed in suspension with glutaraldehyde and examined by scanning electron microscopy.

PAVE1 is conserved in trypanosomatids but is not found in other domains of life. We depleted PAVE1 using RNA interference (RNAi) to determine its function. Cell growth began to decline after two days of PAVE1 RNAi, and cell division ceased after four days (**Supplemental Figure 1A & B**). We quantified cell cycle progression in control and PAVE1 RNAi cells (**Figure 2C**). After one day of PAVE1 depletion, we saw an increase in 1N2K and 2N2K cells. After two days of PAVE1 RNAi induction, we saw an accumulation of multinucleated cells, as well as cells with two nuclei and one kinetoplast (2N1K) and cells that lacked nuclei (0NXK). This suggests that in cells that were able to divide, the cleavage furrow was misplaced and incorrectly segregated nuclear content.

In addition to these cell division defects, we saw that in many cells depleted of PAVE1, the posterior edge of the cell body directly abutted the kinetoplast (**Fig. 2D, empty arrowheads**). This suggested that either the posterior subpellicular array was shorter in cells depleted of PAVE1, or that the kinetoplast had migrated farther away from the nucleus. To distinguish between these two possibilities, we measured the distance between the kinetoplast and posterior cell edge, as well as between the nucleus and the kinetoplast, in control and PAVE1-depleted 1N1K cells after 24 h of PAVE1 RNAi (**Fig.**

2E). We used DIC imaging to demarcate the cell body and DAPI to label the kinetoplast and nucleus. In control cells, we found that the median distance between the posterior cell edge and the kinetoplast was 6.7 μm, with 90% of distances falling between 4 and 9 μm. In PAVE1 RNAi cells, the median distance was 5.3 μm, and more than 30% of cells contained kinetoplasts that were within 3 μm of the posterior cell edge. By contrast, the distance between the nucleus and kinetoplast was the same in both control and PAVE1 RNAi cells. This result suggests that in the absence of PAVE1, the posterior subpellicular array shortens without affecting the placement of the kinetoplast or nucleus.

We examined this posterior truncation phenotype in more detail using transmission electron microscopy (TEM). We extracted the cytoskeleton of control and PAVE1 RNAi cells, stained them with aurothioglucose as a negative stain, and imaged the whole-mount cytoskeletons with TEM. Control cells had a tapered posterior array characterized by the successive truncation of microtubules to an organized point (**Fig. 2F**). By contrast, PAVE1 RNAi cells entirely lacked the tapered portion of the posterior array. The microtubules still appeared to maintain consistent inter-microtubule distance, but the array ended abruptly in close proximity to the basal body. This suggests that PAVE1 is necessary to maintain the microtubules at the tapered posterior array.

We next examined the subpellicular array in dividing cells by TEM. In 2N2K control cells, the posterior subpellicular array was extended and came to a tapered point (**Fig. 2G**). In 2N2K cells depleted of PAVE1, the posterior array was blunted as in PAVE1 RNAi 1N1K cells (**Fig. 2F**). This illustrates that cells lacking PAVE1 maintain blunted posterior ends throughout the cell cycle. To determine the state of the plasma membrane at the truncated posterior ends, we fixed control and PAVE1 RNAi cells in suspension and

examined them by scanning electron microscopy (SEM) (**Fig. 2H**). Similar to our whole-mount TEM analysis, the cell body and membrane tapered to a point at the posterior of control cells. In PAVE1 RNAi cells, the cell posterior was blunted near the point where the flagellum exited onto the cell surface, which is similar to the location of posterior truncation seen by previous DIC and TEM analysis. Interestingly, the membrane was intact and stretched over the blunted posterior end.

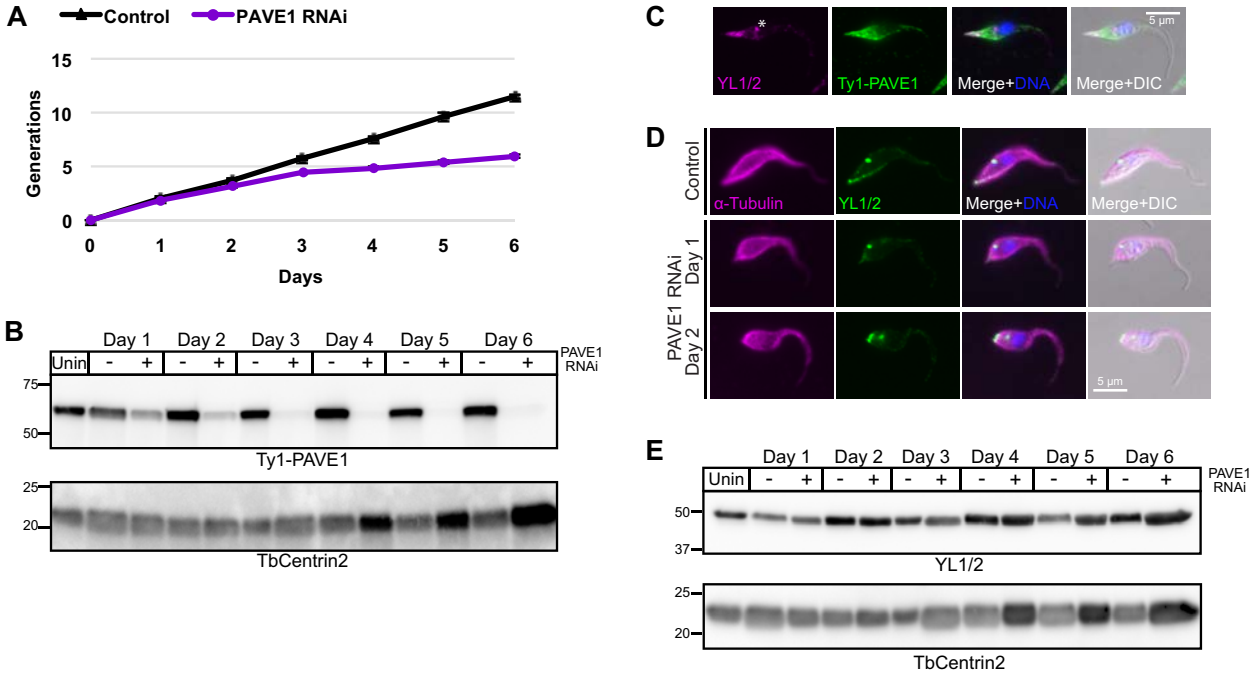

Figure S1. PAVE1 does not affect tubulin polymerization at the cell posterior. (A) Generation plot of control and PAVE1 RNAi cells after RNAi induction. Cell density was monitored every 24 h. Plot is the average of three independent biological replicates with the S.D. **(B)** Western blot of lysates from control and PAVE1 RNAi cells every 24 h during PAVE1 RNAi induction. Anti-Ty1 antibody was used to follow the depletion of Ty1-PAVE1. TbCentrin2 was used as a loading control. **(C)** Ty1-PAVE1 cells were fixed in methanol and labeled with anti-Ty1 antibody and YL1/2, which recognizes tyrosinated tubulin. The asterisk is denoting a pool of tyrosinated tubulin at the basal body. **(D)** Control and PAVE1 RNAi cells during 1 and 2 d of RNAi induction were fixed in methanol and stained with anti-α-tubulin and YL1/2 antibody. **(E)** Western blot of lysates prepared from control and PAVE1 RNAi cells. YL1/2 antibody was used to determine tyrosinated tubulin levels during PAVE1 RNAi. TbCentrin2 was used as a loading control.

The posterior array truncation phenotype could arise from the inability to polymerize microtubules at the array posterior in cells depleted of PAVE1. Microtubules are consistently polymerized at the posterior array throughout the cell cycle, as evidenced by the localization of YFP-tubulin and YL1/2 antibody staining (Sheriff et al., 2014; Sherwin and Gull, 1989a; Wheeler et al., 2013). The antibody YL1/2 recognizes the terminal tyrosine residue of alpha-tubulin (Kilmartin, 1982). Terminal tyrosination is a hallmark of newly polymerized tubulin and is considered a marker of array growth during the cell cycle. Ty1-PAVE1 and YL1/2 colocalize at the array posterior, although Ty1-PAVE1 signal extends more anterior than YL1/2 signal (**Supp. Fig. 1C**). YL1/2 also labels a pool of tyrosinated tubulin present at the basal body (**Supp. Fig. 1C, asterisk**). To test if the microtubules of the posterior array are no longer able to polymerize in the absence of PAVE1, we performed immunofluorescence with α-tubulin and YL1/2 antibodies on control and PAVE1 RNAi cells. In both control cells and PAVE1 RNAi cells, YL1/2 labeled the cell posterior (**Supp. Fig. 1D**). In PAVE1 RNAi cells, the pattern of YL1/2 labeling was altered and reflected the more rounded, truncated posterior present in these cells. Western blotting analysis also showed no difference in tyrosinated tubulin levels (**Supp. Fig. 1E**). This suggests that PAVE1 has a role in stabilizing the microtubules of the posterior array and does not function in microtubule nucleation or polymerization.

PAVE1 localizes to the inter-microtubule crosslinks of the subpellicular array at the cell posterior

PAVE1 localizes to the posterior array and is required to form the tapered array at this location. Depletion of PAVE1 does not affect other portions of the array, suggesting that the posterior portion of the array is a unique subdomain. As a potential MAP, PAVE1 may localize to specific regions of individual microtubules at the posterior subpellicular array to carry out its function. We performed negative-stain immunogold electron microscopy (iEM) on extracted cytoskeletons prepared from cells containing Ty1-tagged PAVE1 to obtain high-resolution localization information (**Fig. 3A**). The 20 nm gold particles labeling Ty1-PAVE1 localized to the posterior portion of the subpellicular array with very little labeling on the cell anterior. However, it was not possible to determine if PAVE1 preferentially bound a specific region of individual microtubules. When whole-mount cytoskeletons are imaged by TEM, both the top and bottom layers of the array are visible, which results in a cross-hatching pattern that makes it difficult to distinguish individual microtubules. To address this problem, we generated subpellicular array sheets from immunogold-labeled cytoskeletons (Sherwin and Gull, 1989a). Extracted whole-mount immunogold-labeled cytoskeletons were positively stained with uranyl acetate, critical point dried, and cleaved using double-sided tape to 'unroof' the cell and remove the top layer of the subpellicular array (**Fig. 3B**).

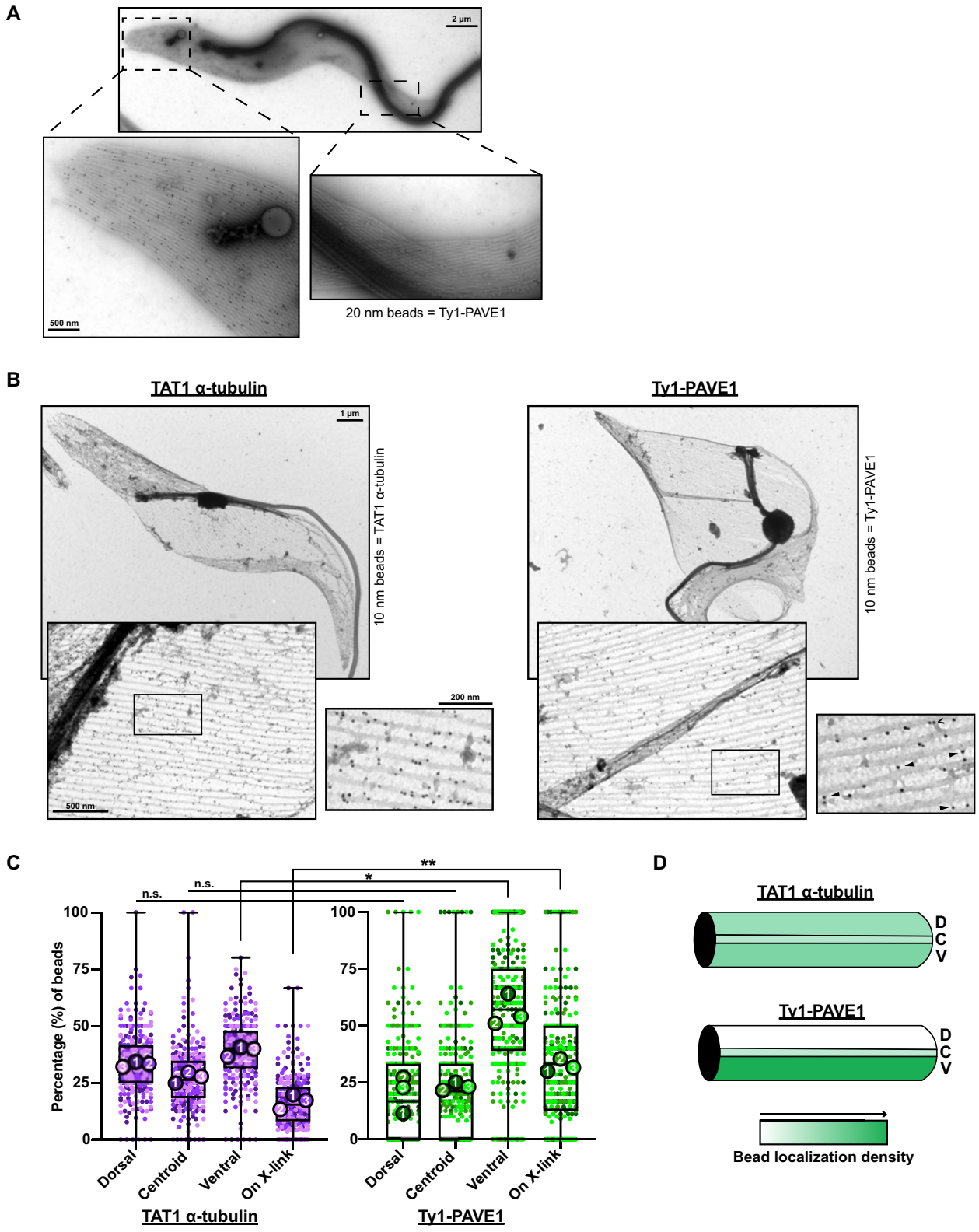

Figure 3. PAVE1 is a component of the inter-microtubule crosslinks of the cell posterior. **(A)** Whole-mount extracted cytoskeleton immunogold-labeled for Ty1-PAVE1 with 20 nm beads. **(B)** (Left) A subpellicular array sheet from WT 427 control cells immunogold-labeled with 10 nm

beads against TAT1, which recognizes trypanosome α-tubulin. (Right) A subpellicular array sheet immunogold-labeled for Ty1-PAVE1 with 10 nm beads. Empty arrowheads are pointing to ventrally localized Ty1-PAVE1 beads, and solid arrows are marking Ty1-PAVE1 beads on preserved inter-microtubule crosslinking fibrils. **(C)** Quantification of immunogold label distribution along individual microtubules in subpellicular sheets represented as a Superplot (Lord et al., 2020), which shows each individual measurement in each biological replicate. The replicates are color-coded and the average is illustrated as large circles. TAT1 α-tubulin—Ty1-PAVE1 dorsal:dorsal and centroid:centroid distributions are not significantly different (P=0.0542 and P=0.0741, respectively). *P=0.0146, **P=0.0032. P-values are calculated from unpaired two-tailed Student's *t*-tests using the averages from N=3 independent biological replicates. 3 subpellicular sheets in both TAT1 control and Ty1-PAVE1 conditions from N=3 independent biological replicates were quantified. **(D)** Heat map of α-tubulin and Ty1-PAVE1 immunogold label distribution on individual microtubules.

To determine if PAVE1 had a unique and polarized labeling pattern along individual microtubules, we compared PAVE1 distribution to the localization pattern of the TAT1 antibody, which recognizes *T. brucei* α-tubulin (**Fig. 3B, left**). We developed a semi-automated macro in ImageJ that allowed us to quantify the localization of immunogold labeling (**Supp. Fig. 2**). Subpellicular sheets were oriented along their dorsal-ventral axis using the intact flagellum as a fiducial marker. Gold beads were then classified as localizing to the dorsal, centroid, or ventral regions of individual array microtubules. We found that in comparison to TAT1 labeling, PAVE1 preferentially localized to the outside ventral walls of the array microtubules at the cell posterior, as well as to the inter-microtubule crosslinks that remained after sheet preparation (**Fig. 3C & D**). Many crosslinks were disrupted in the sheet preparation, leaving small protrusions on the outside microtubule wall (**Fig. 3B, open arrowhead**). The ventral localizations of PAVE1 often occurred on these protrusions, likely indicating that PAVE1 was on a crosslink that was disrupted. This localization pattern suggests that PAVE1 may be part of the inter-microtubule crosslinking fibrils present in the posterior subdomain of the array.

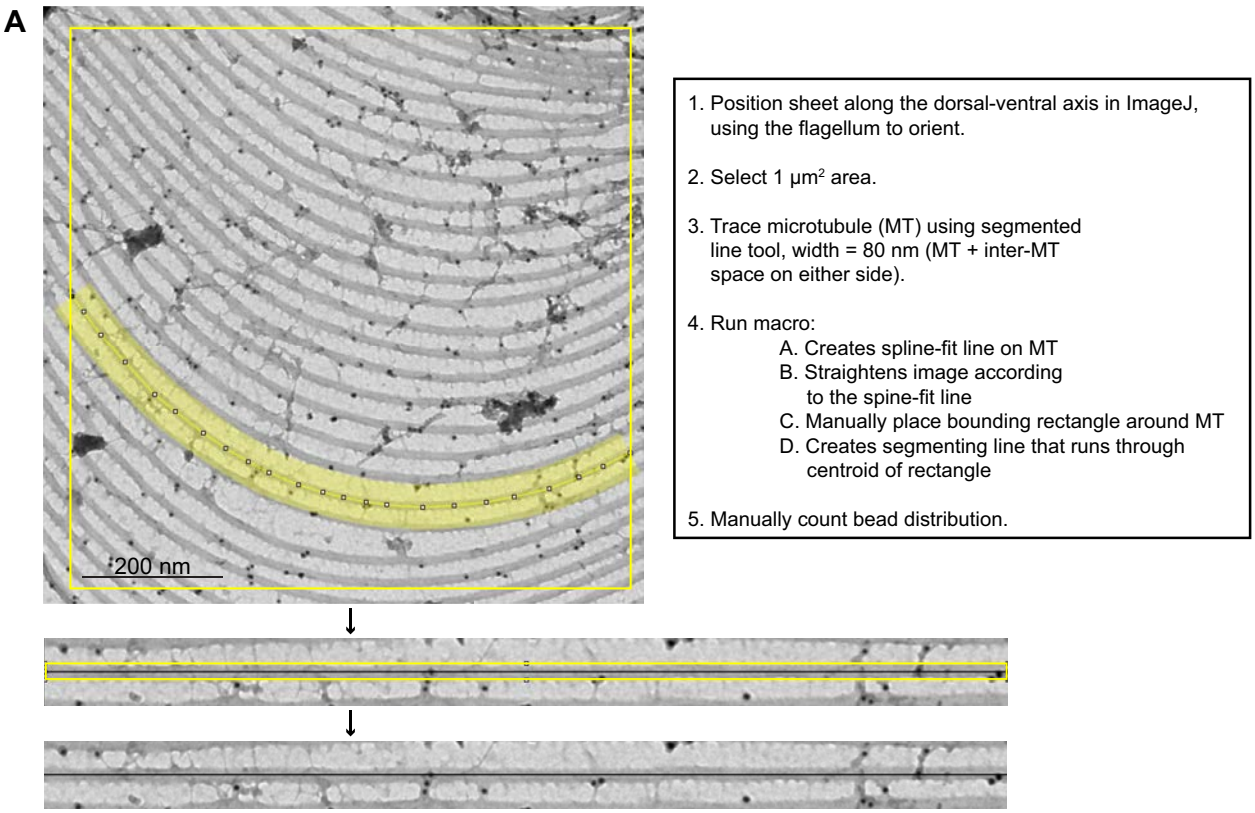

Figure S2. Quantification methodology used to classify immunogold label distribution in subpellicular array sheets. (A) A semi-automated macro was written in ImageJ to facilitate the classification gold bead distribution as dorsal, centroid, or ventral, as well as cross-link associated, along individual microtubules of subpellicular array sheets.

PAVE1 maintains microtubule length at the posterior subpellicular array

Nothing is currently known about how the microtubule crosslinking fibrils are assembled or remodeled as new tubulin dimers are added to the plus-ends present at the cell posterior. To determine how PAVE1 and the inter-microtubule crosslinks are incorporated into the array at the cell posterior, we developed a capping assay using HaloTag technology, which allows the irreversible conjugation of a dye to a specific fusion protein (Los et al., 2008). We appended the HaloTag protein to the N-terminus of one of the endogenous PAVE1 alleles, then incubated an exponentially growing culture with a cell-permeable HaloTag substrate containing the far-red fluor JF646 to covalently label

all the HaloTag-PAVE1 present in the cell. The remaining JF646-conjugated substrate was then washed out of the culture and replaced with a substrate linked to the rhodamine analog TMR, which is only able to label newly synthesized HaloTag-PAVE1 (**Fig. 4A**). Cells were then harvested, fixed, and imaged using epifluorescence microscopy. The fluorescence intensity of each fluor-conjugated version of PAVE1 was analyzed using a line scan placed along the ventral edge of the cell body of 1N1K cells (**Fig. 4B**). This two-color labeling approach allowed us to localize where newly synthesized PAVE1 was added to the array and how its distribution changed over time. We designated T=0 h as the point when the TMR substrate was added to the media for our subsequent analysis.

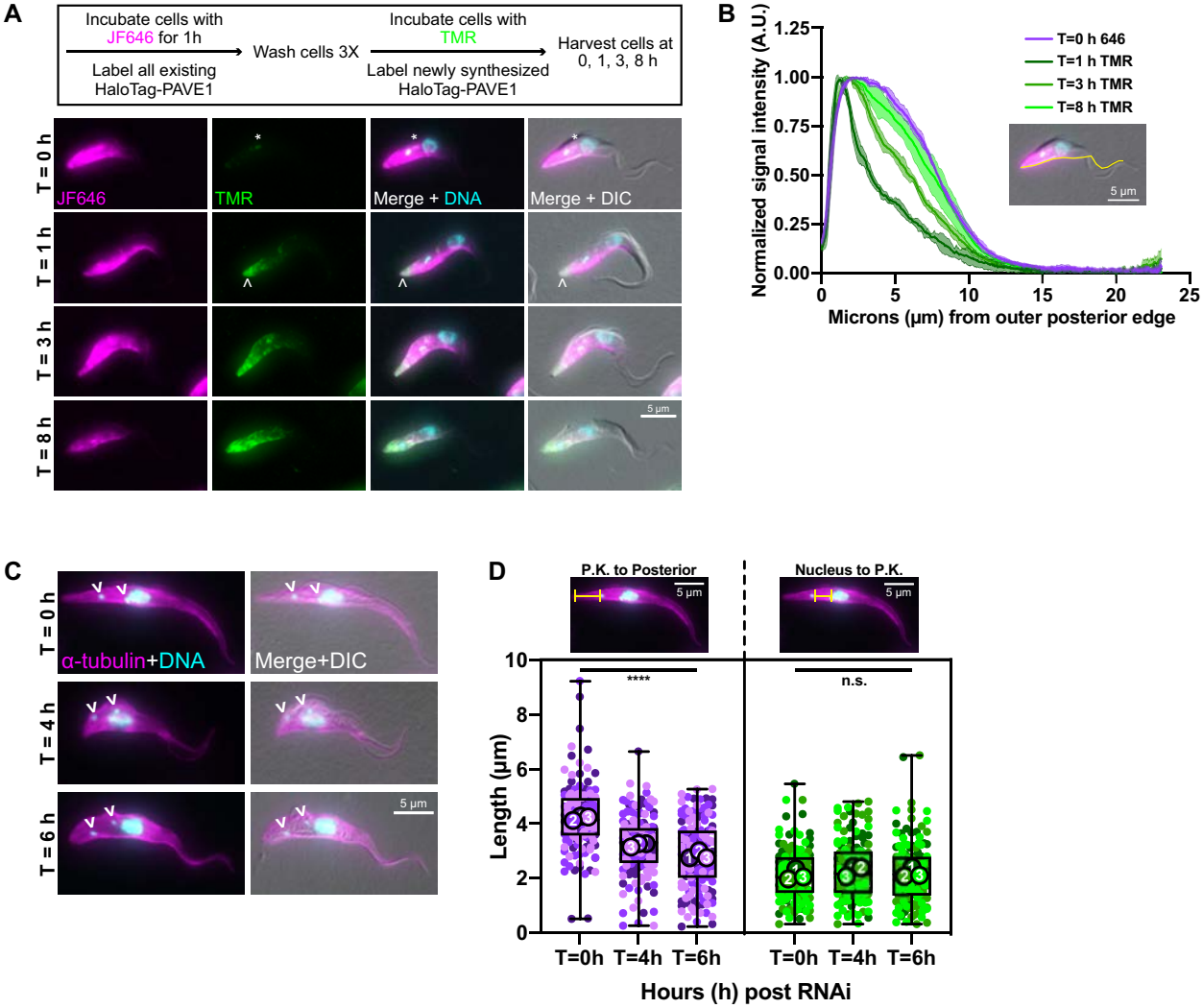

Figure 4. PAVE1 is added to and stabilizes the microtubules at the extreme posterior end of the array. (A) HaloTag-PAVE1 cells were fixed in paraformaldehyde at T=0 h, T=1 h, T=3 h, and T=8 h after the addition of HaloTag ligand conjugated to TMR to cell culture in the capping assay. Asterisk represents background labeling of the endomembrane system. Empty arrowhead is pointing to the earliest addition of HaloTag-PAVE1, represented by TMR labeling, at the extreme cell posterior. **(B)** Fluorescence intensity quantification of HaloTag ligand labeling along the ventral edge of the cell body at T=0 h, T=1 h, T=3 h, and T=8 h after TMR substrate addition. Fluorescence intensity was normalized to 1 at each time point in order to illustrate the shape of the curve. 50 1N1K cells at each time point from N=3 independent biological replicates were measured. **(C)** PAVE1 RNAi was induced and cells were harvested, fixed in methanol, and stained with anti-α-tubulin after T=0 h, T=4 h, and T=6 h of PAVE1 RNAi induction. 1N2K cells were selected for analysis as they completed cytokinesis prior to PAVE1 depletion. **(D)** Superplot of the measured distances between the posterior kinetoplast to outer posterior edge of the subpellicular array, and the posterior edge of the nucleus to the posterior kinetoplast in control and PAVE1 RNAi cells. One-way ANOVAs were calculated using the averages from N=3 independent biological replicates. ****P<0.0001, n.s. P=0.5653. 50 1N2K cells were measured at each time point from N=3 independent biological replicates.

At T=0 h, the JF646 signal labeled the posterior and ventral edge of cells in a similar pattern to what was observed with Ty1-PAVE1 immunofluorescence. There was an additional punctum of JF646 and TMR signal near the endomembrane system (**Fig. 4A, asterisk**), which was likely due to endocytosis of the HaloTag substrate. At T=1 h, the TMR signal was greatest at the extreme posterior end of the cell and rapidly declined towards the cell anterior (**Fig. 4B**). This suggested that new HaloTag-PAVE1 was added to the posterior subpellicular array at the same location that microtubule polymerization occurs throughout the cell cycle (Sheriff et al., 2014; Sherwin and Gull, 1989a). At T=3 h, the TMR signal began to increase past the extreme posterior end. This demonstrated that HaloTag-PAVE1 moved toward the cell anterior over time. At the latest time point T=8 h, which was approximately the duration of one cell cycle, the TMR signal was similar to the original JF646 signal. Moreover, the JF646 signal intensity declined at T=8 while the TMR

signal intensity increased, which suggested that there was turnover of HaloTag-PAVE1 on the array.

Depletion of PAVE1 using RNAi truncates the subpellicular array until the posterior cell edge directly abuts the kinetoplast (**Fig. 2F**). We performed an RNAi time course to test if PAVE1 is required to maintain the microtubules of the posterior array, or if the array truncation seen in PAVE1-depleted cells is the result of aberrant cell division. Considering that cultured *T. brucei* cells are asynchronous and that there are currently no established methods for synchronizing these cells that are compatible with RNAi, we developed a strategy to identify cells that had completed cell division prior to PAVE1 RNAi induction. We induced PAVE1 RNAi in log-phase cell cultures and harvested cells after 4 or 6 h of RNAi induction and restricted our analysis to 1N2K cells to select for cells that had progressed well into G1 phase at the time of PAVE1 depletion. The cell cycle for the 29.13 line carrying the PAVE1 RNAi hairpin is 12.9 h. Previous studies have shown that 1N2K cells would have initiated cell division approximately 10.8 h (0.84 units) prior to the time of harvest (Sherwin and Gull, 1989b). Selecting 1N2K cells allowed us to eliminate any confounding effects on array morphology from cytokinesis and the posterior end remodeling that occurs in G1 phase immediately following cytokinesis, as these cells will have already completed these processes prior to PAVE1 RNAi induction (Abeywickrema et al., 2019; Wheeler et al., 2013). Thus, any defects observed in the array of 1N2K cells would be the direct result PAVE1 depletion without the combined effects of the major subpellicular array remodeling that occurs during the latest stages of cell division (**Fig. 4C**).

We visualized the array microtubules using immunofluorescence microscopy with an anti-α-tubulin antibody and measured the length of the array from the more posterior kinetoplast to the posterior edge of the cell in PAVE1 RNAi and control 1N2K cells. We found that the posterior array of PAVE1 RNAi cells at T=4 h were significantly shorter than T=0 h cells by an average of 0.99 ± 0.12 µm (**Fig. 4D**). Moreover, the average posterior array length of PAVE1 RNAi cells at T=6 h was 1.38 ± 0.23 µm shorter than T=0 h cells. However, the length of the array between the nucleus and posterior kinetoplast was the same at all three time points, which indicates that PAVE1 RNAi did not cause repositioning of the kinetoplast within the cell body or a shortening of the array at the cell midzone. This data suggests that PAVE1 is required to maintain the extended, tapering portion of microtubules at the cell posterior independent of its potential function during formation of the nascent cell posterior during cell division.

PAVE1 immunoprecipitation reveals two potential interacting partners

The inter-microtubule crosslinking fibrils are approximately 6 nm in diameter and span the 18-20 nm distance between microtubules (Souto-Padrón et al., 1984). We were curious if PAVE1 was part of a complex of proteins that formed the inter-microtubule crosslinks at the cell posterior. To determine if PAVE1 had interacting partners, we endogenously tagged both PAVE1 alleles with the fluorescent protein mNeonGreen (mNG) at their N-termini (**Fig. 5A**) and immunoprecipitated mNG-PAVE1 using mNeonGreenTrap antibody. Fractions of the eluate examined by SDS-PAGE and subsequent silver staining showed two primary unique bands compared to the control eluate (**Fig. 5B**). Mass spectrometry analysis of on-bead tryptic digests generated from mNG-PAVE1 and control immunoprecipitations revealed two potential interacting

partners whose predicted molecular weight matched that of the unique bands on the silver-stained gel (**Table 1**). These potential interactors were an uncharacterized protein (Tb927.9.11540, predicted MW 51 kDa) and TbAIR9 (Tb927.11.17000, predicted MW 110 kDa).

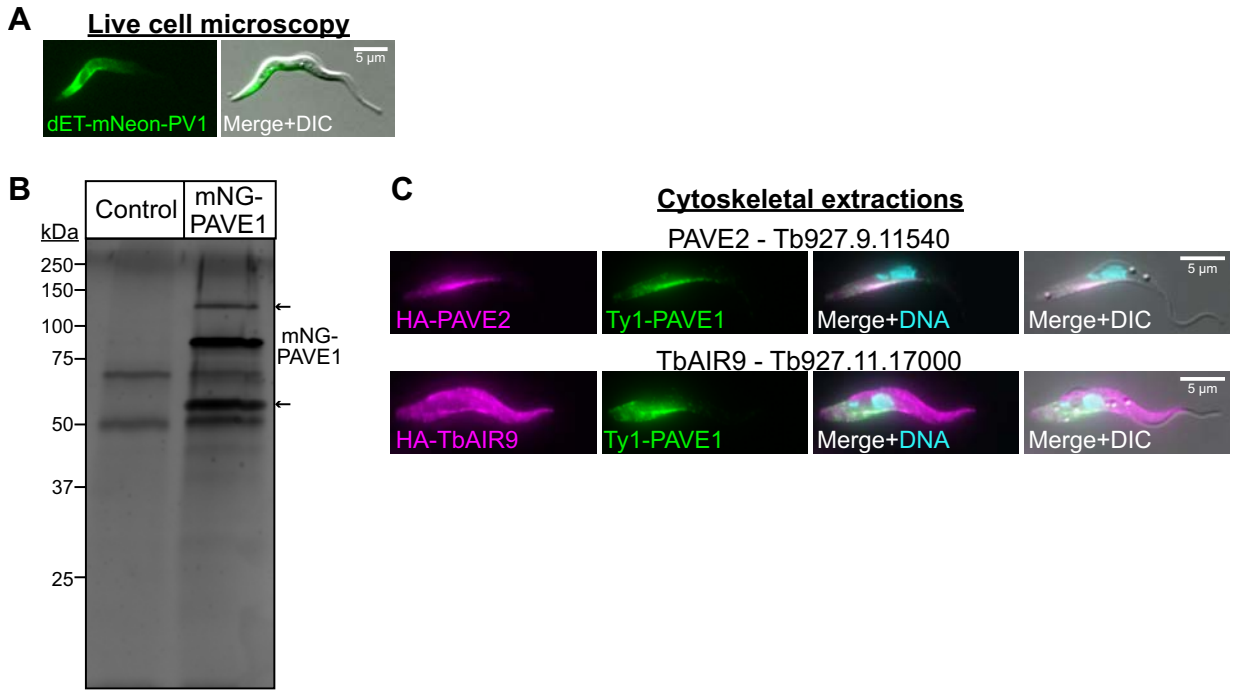

Figure 5. Immunoprecipitation of mNeonGreen-PAVE1 reveals two interacting partners. **(A)** Representative image of a live *T. brucei* cells expressing mNeonGreen-PAVE1 from both endogenous loci. **(B)** dET-mNeon-PAVE1 cells were harvested, lysed, and sonicated to solubilize cytoskeletal proteins. Clarified supernatant was batch-bound with magnetic camelid nanobodies against mNeonGreen. Beads were washed 6X and bound proteins were analyzed by mass spectrometry. Gel is a representative silver-stained SDS-PAGE gel of the elution from the mNeonGreen immunoprecipitation in control and mNeonGreen-PAVE1 samples. Both lanes are 50% of input material. Arrows indicate the two major unique protein bands present in the mNeonGreen-PAVE1 sample not present in WT 427 controls. **(C)** The two potential interacting partners of PAVE1 identified in the mNeonGreen-PAVE1 immunoprecipitation were endogenously tagged with the HA epitope tag. The cytoskeleton was extracted and cells were processed for immunofluorescence to co-localize each protein with Ty1-PAVE1.

We appended triple-HA epitope tags to the N-termini of the potential interactors in a cell line already harboring Ty1-tagged PAVE1, then performed cytoskeletal extractions

followed by immunofluorescence microscopy. The uncharacterized HA-tagged protein Tb927.9.11540 was stably associated with the cytoskeleton and co-localized with Ty1-PAVE1, so we termed this new protein PAVE2 (**Fig. 5C, top**). HA-TbAIR9 was stably associated with the entire array, as previously reported (May et al., 2012). There was more intense staining of HA-TbAIR9 at the anterior portion of the array, where the Ty1-PAVE1 signal is minimal (**Fig. 5C, bottom**).

PAVE1 and PAVE2 require each other for stability and localization

Like PAVE1, PAVE2 is conserved in kinetoplastids and has no homologs in other domains of life. PAVE2 was also identified as a potential interactor of the cytokinetic regulator TOEFAZ1 in the same proximity-dependent biotinylation screen that identified PAVE1 (Hilton et al., 2018). To test its function, we conducted RNAi against PAVE2 and found that cells were unable to divide after 4 d of RNAi induction (**Supp. Fig. 3A & B**). PAVE2 RNAi led to an accumulation of multinucleated cells (MultiN), cells with two nuclei and one kinetoplast (2N1K), and anucleate zoids (0N1K) (**Fig. 6 A & B**), which is similar to the cell division defect observed in PAVE1 RNAi (**Fig. 2C**).

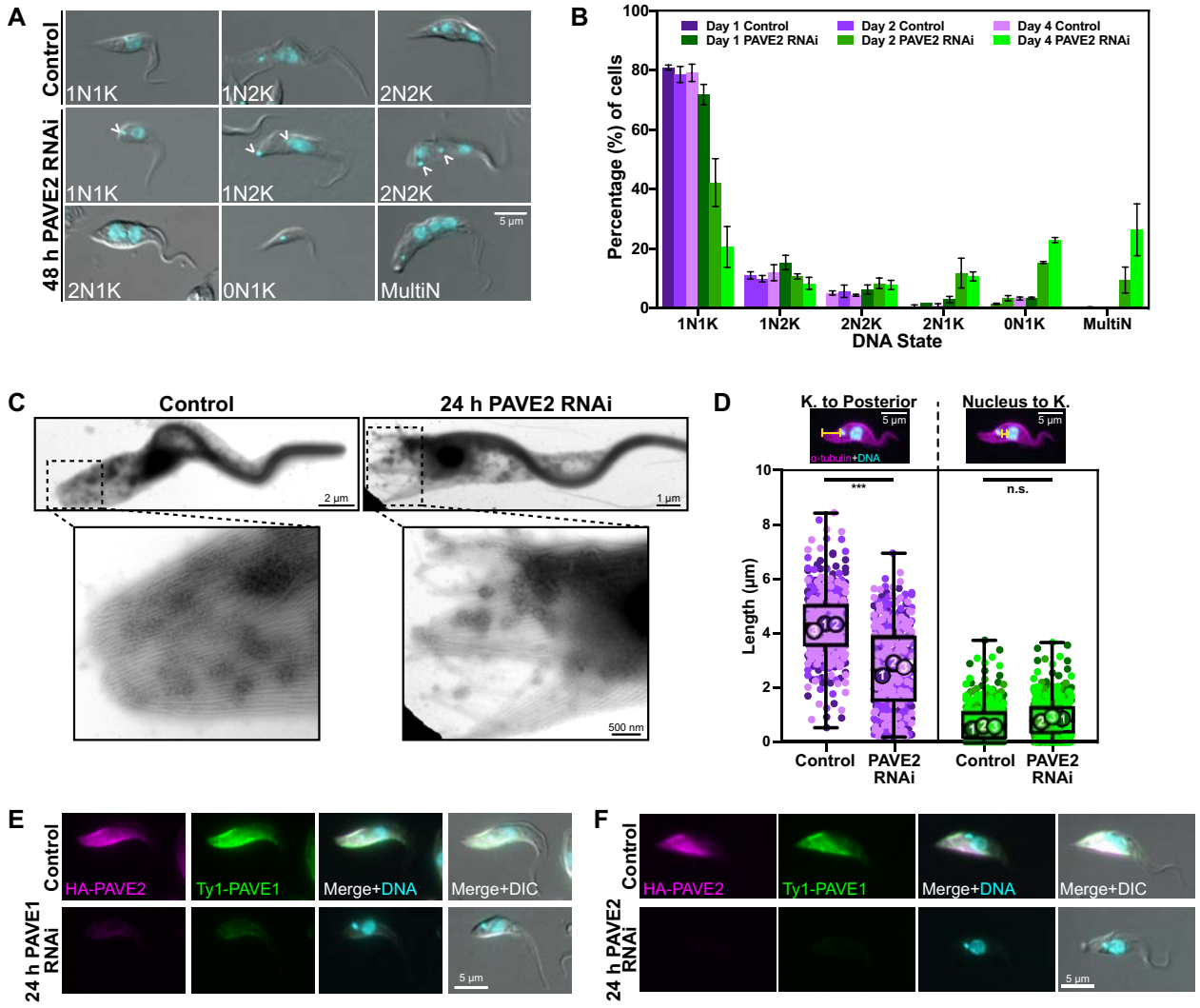

Figure 6. PAVE2 phenocopies PAVE1. (A) PAVE2 RNAi was induced for two days, after which control and PAVE2-depleted cells were fixed with paraformaldehyde and examined by epifluorescent microscopy. **(B)** Quantification of DNA states in control and PAVE2 RNAi cells after 1, 2, and 4 d of RNAi induction. Bars represent the mean and the error bars are the S.D. 300 cells in both control and PAVE2 RNAi conditions from N=3 independent biological replicates were counted at each time point. **(C)** Whole-mount transmission electron microscopy of control and PAVE2 RNAi cells after 1 d of PAVE2 depletion. **(D)** PAVE2 RNAi was induced for 1 d and cells were harvested, fixed in paraformaldehyde, and stained with anti-α-tubulin to demarcate the subpellicular array. Superplot is of the measured distance between the kinetoplast and the outer posterior edge of the array, and the posterior edge of the nucleus to the kinetoplast of 1N1K cells in control and PAVE2 RNAi conditions. 100 1N1K cells were measured for both control and PAVE2 RNAi conditions in N=3 independent biological replicates. Unpaired two-tailed Student's *t*-tests were performed using the averages from N=3 independent biological replicates. ***P=0.0006. n.s. P=0.0753. **(E)** Control and PAVE1 RNAi cells were fixed in paraformaldehyde and stained after 1 d of PAVE1 depletion. PAVE2 does not localize to the array in the absence

of PAVE1. **(F)** Control and PAVE2 RNAi cells were fixed in paraformaldehyde and stained after 1 d of PAVE2 depletion. PAVE1 does not localize to the array in the absence of PAVE2.

Strikingly, we saw that PAVE2 depletion resulted in cell bodies whose posterior ends directly abutted the kinetoplast (**Fig. 6A, empty arrowheads**). This mirrored the PAVE1 RNAi posterior truncation phenotype (**Fig. 2 D & E**). The microtubules of truncated posterior arrays in PAVE2 RNAi cells were also disorganized in comparison to control cells when analyzed by TEM (**Fig. 6C**). We measured the length of the posterior array in control and PAVE2 RNAi cells to confirm the truncation phenotype. We found that the mean distance between the kinetoplast and posterior end of 1N1K cells was an average of 1.62 $\pm$ 0.31 µm shorter than controls after 24 h of RNAi induction, while the distance between the nucleus and kinetoplast remained constant (**Fig. 6D**). This suggested the posterior truncation phenotype was not due to aberrant kinetoplast placement or defects in the array at other locations but to the specific destabilization of microtubules at the posterior array, which phenocopies PAVE1 RNAi.

Both PAVE1 and PAVE2 RNAi result in the truncation of the posterior array, which suggests that these proteins may have a shared function or may form a complex. We depleted PAVE1 using RNAi and determined the localization of PAVE2 to establish if PAVE2 relied on PAVE1 for localization or stability within the cell. We found that HA-tagged PAVE2 localization to the posterior subpellicular array decreased as Ty1-PAVE1 protein levels decreased (**Fig. 6E**). Western blot analysis showed that PAVE2 protein levels also decreased during PAVE1 RNAi (**Supp. Fig. 3C**). We also found that the inverse relationship existed as well; when PAVE2 was depleted by RNAi, PAVE1 no longer localized to the posterior array (**Fig. 6F**) and its levels were reduced (**Supp. Fig.**

3D). These results suggest that PAVE1 and PAVE2 require each other for localization and protein stability inside the cell.

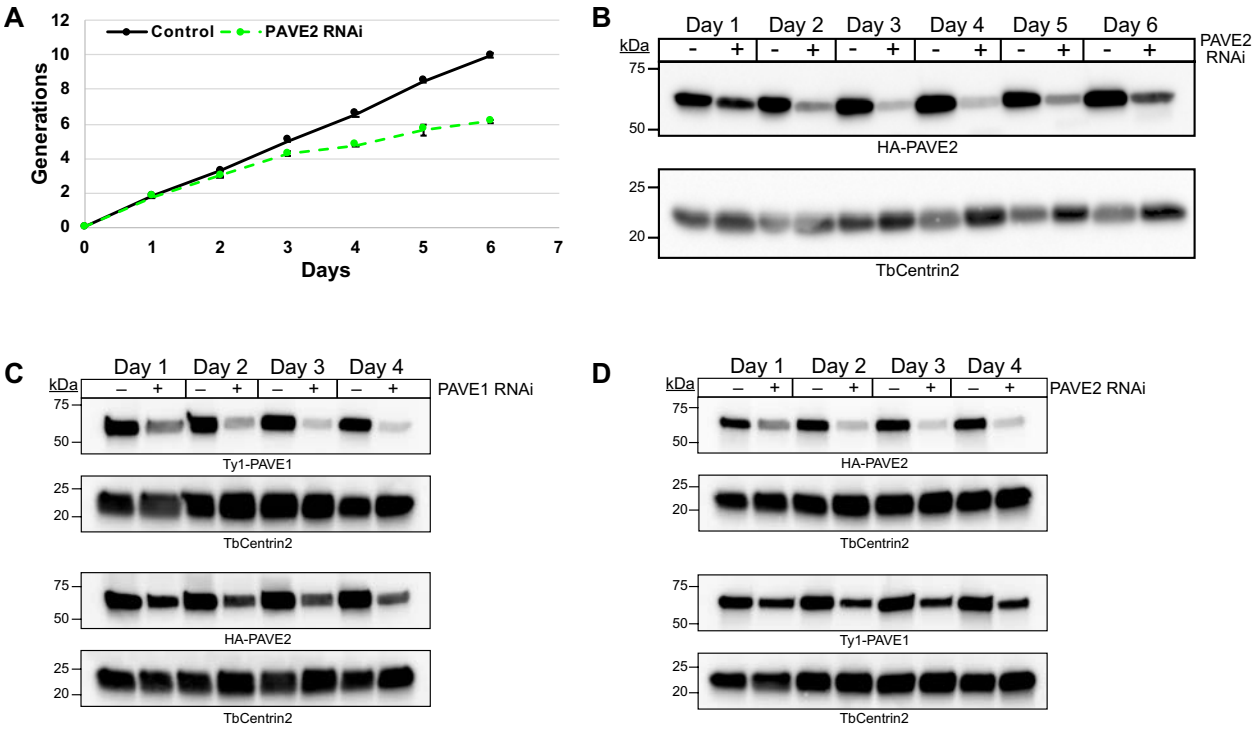

Figure S3. PAVE1 and PAVE2 require each other for stability in vivo. (A) Generation plot of cell growth after induction of PAVE2 RNAi. The cell density was monitored every 24 h in control and PAVE2 RNAi conditions. The curve is the mean of N=3 independent biological replicates. **(B)** Lysates were collected every 24 h from control and PAVE2 RNAi cells during 6 d of PAVE2 depletion. Lysates were western blotted with antibodies against HA and TbCentrin2 as a loading control. **(C)** Lysates from control and PAVE1 RNAi cells in which PAVE2 is endogenously tagged were collected for western blotting every 24 h during PAVE1 depletion. Duplicate lysates were western blotted, as PAVE1 and PAVE2 are the same molecular weight. **(D)** Lysates from control and PAVE2 RNAi cells in which PAVE1 is endogenously tagged were collected for western blotting every 24 h during PAVE2 depletion. The lysates were blotted in duplicates as in (C).

PAVE1 and PAVE2 form a microtubule-associated complex *in vitro*

The interdependence of PAVE1 and PAVE2 *in vivo* (**Fig. 6**) and the near-stoichiometric levels of PAVE2 pulled down in the PAVE1 immunoprecipitation (**Fig. 5B**) suggest that the two proteins may form a protein complex. To test this, we co-expressed PAVE1 and PAVE2 recombinantly in *Escherichia coli.* The solubility-promoting maltose

binding protein (MBP) followed by an oligo-His tag and TEV protease site was appended to the N-terminus of mNG-PAVE1, while a Strep peptide tag was added to the N-terminus of PAVE2. Lysates from *E. coli* co-expressors were incubated with nickel resin, followed by elution of the captured proteins and treatment with TEV protease to cleave the MBP-oligoHis tag from mNG-PAVE1. Subsequent capture of the eluate with Strep-Tactin resin resulted in a pure complex of mNG-PAVE1 and Strep-PAVE2, which we termed the PAVE complex (**Fig. 7A, left**). Attempts to purify either PAVE1 or PAVE2 on their own were not successful, which suggests that these proteins require each other for proper folding. The purified PAVE complex was diluted into a low salt buffer and then clarified by an ultracentrifuge to test its solubility. The majority of the complex remained in solution, suggesting that the PAVE complex is highly soluble (**Fig. 7A, right**). These expression results, combined with their relationship in vivo, suggest that PAVE1 and PAVE2 form a hetero-oligomer that is responsible for the construction and maintenance of the tapered cell posterior.

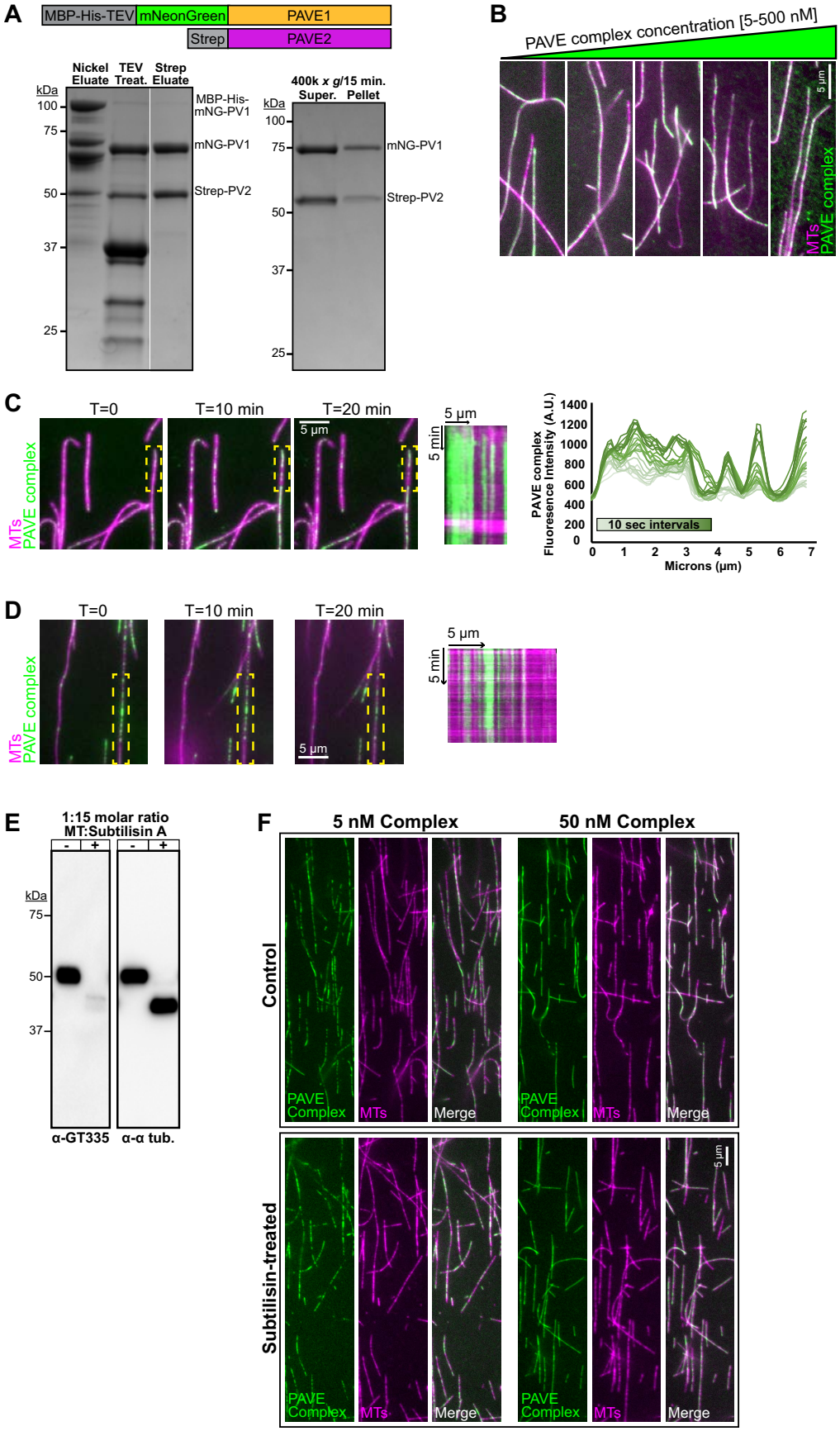
A
MBP-His-TEV
mNeonGreen
PAVE1
Strep
PAVE2
Nickel Eluate
TEV Treat.
Strep Eluate
kDa
100
75
50
37
25
MBP-His-mNG-PV1
mNG-PV1
Strep-PV2
400k x g/15 min.
Super.
Pellet
B
PAVE complex concentration [5-500 nM]
5 µm
MTs
PAVE complex
C
T=0
T=10 min
T=20 min
5 µm
5 min
PAVE complex Fluorescence Intensity (A.U.)
10 sec intervals
Microns (µm)
D
E
1:15 molar ratio
MT:Subtilisin A
α-GT335
α-α tub.
F
5 nM Complex
50 nM Complex
Control
Subtilisin-treated
PAVE Complex
MTs
Merge

Figure 7. PAVE1 and PAVE2 form a complex in vitro that binds the microtubule lattice. (A) (Left) Coomassie-stained SDS-PAGE gel demonstrating the co-purification of mNeonGreen-PAVE1 and Strep-PAVE2 from *E. coli* cells. *E. coli* cells co-expressing [MBP-oligoHis-TEV]-nNeonGreen-PAVE1 and Strep-PAVE2 constructs were harvested, lysed, and clarified supernatant were batch-bound with Ni-NTA resin. The eluate was treated with TEV protease and allowed to interact with Strep-Tactin XT resin. Proteins were eluted using 50 mM biotin. The Strep eluate is 4 µg of protein. (Right) The PAVE complex was diluted into a low salt buffer containing 50 mM NaCl and ultracentrifuged. Equal fractions of both the supernatant and pellet were separated on an SDS-PAGE gel and stained with Coomassie blue. **(B)** 5, 50, 100, 200, and 500 nM clarified PAVE complex was allowed to interact with Taxol-stabilized bovine microtubules labeled with the Cy5 fluor for 20 min RT. The PAVE complex-microtubule solution was settled onto a blocked flow cell and unbound protein was washed away. The flow cell was imaged using epifluorescence microscopy. **(C)** (Left) A PEGylated flow cell was blocked and Taxol-stabilized bovine Cy5-microtubules were allowed to attach to the flow cell surface. 5 nM clarified PAVE complex was added to the flow cell chamber and immediately imaged using TIRF microscopy. Images were taken every 10 sec for 20 min. (Middle) Kymograph of PAVE complex on the microtubule outlined in yellow. (Right) Fluorescence intensity line scan of the microtubule outlined in yellow for the first 4 min 10 sec of TIRF imaging. **(D)** (Left) 5 nM clarified PAVE complex was mixed with Taxol-stabilized bovine Cy5-microtubules for 10 min RT to pre-seed patches. The PAVE complex-microtubule mixture was flowed into a blocked and PEGylated flow cell and allowed to attach to the flow cell surface. Unbound protein was washed away and the flow cell was immediately imaged using TIRF microscopy. Images were taken every 10 sec for 20 min. (Right) Kymograph of PAVE complex on the microtubule outlined in yellow. **(E)** Control microtubules and microtubules treated with subtilisin A were collected for western blotting. The post-translational modification of glutamylation is no longer present on subtilisin-treated microtubules, as detected with the antibody GT335, and there is a molecular weight shift showing that the C-terminal tails have been cleaved, as detected with anti-α-tubulin. **(F)** PAVE complex was incubated with control or subtilisin-treated Taxol-stabilized bovine Cy5-microtubules as in (B) and imaged using epifluorescence. There is no difference in PAVE complex binding to subtilisin-treated microtubules cleaved of their C-terminal tails in comparison to control, indicating that the PAVE complex binds directly to the microtubule lattice.

To determine if the PAVE complex can bind directly to microtubules, we incubated purified complex in solution with microtubules polymerized from bovine brain tubulin labeled with Cy5 dye. The PAVE complex-microtubule mixture was added to a flow cell and allowed to attach to the surface, after which unbound protein was washed away and the flow cell was imaged using epifluorescence microscopy. The PAVE complex bound to microtubules at concentrations as low as 5 nM (**Fig. 7B**). However, the PAVE complex

did not crosslink microtubules into higher order structures such as bundles, regardless of the concentration of PAVE complex used or the length of the incubation. Although PAVE1, and thus PAVE2 as a direct binding partner, localize to the inter-microtubule crosslinks of the *T. brucei* posterior subpellicular array in vivo, they do not appear to have the capacity to crosslink microtubules in vitro. This suggests that PAVE1 and PAVE2 are a necessary component of the inter-microtubule crosslinks at the posterior array but are not sufficient to form these crosslinks.

Although the PAVE complex cannot bundle microtubules, we observed that it localized to microtubules in patches even at high nanomolar concentrations, rather than being distributed in a uniform manner along the length of the microtubule (**Fig. 7B**). To determine how these patches form, we performed total internal reflection fluorescence (TIRF) microscopy to image the PAVE complex binding to microtubules. Cy5-labelled microtubules were attached to a flow cell, after which 5 nM PAVE complex was added into the chamber and immediately imaged using TIRF microscopy (**Movie 1**). We saw that the PAVE complex bound to microtubules in discrete patches; these patches did not grow over time, although they did increase in intensity (**Fig. 7C, middle and right**). Moreover, the PAVE complex patches were highly persistent. When patches were pre-seeded on microtubules in solution, added to a flow cell, and unbound complex was washed away, the pre-seeded patches remained for greater than 20 min (**Fig. 7D, Movie 2**). These results demonstrate that the PAVE complex binds to microtubules in static patches, which suggests that the complex may recognize specific regions of microtubules.

Microtubules have many post-translational modifications (PTMs), which can differentially recruit MAPs or affect MAP behavior (Song and Brady, 2015). Most microtubule PTMs occur on their highly disordered and charged C-terminal tails. We cleaved the C-terminal tails from bovine Cy5-labelled microtubules using subtilisin protease (Rodionov et al., 1990) to establish if the PAVE complex recognized tail-associated PTMs, which could explain its patchy localization pattern. We confirmed the removal of tubulin C-terminal tails by subtilisin using western blotting analysis (**Fig. 7E**). We found that glutamylation, which is a modification that occurs exclusively on the C-terminal tail of α- and β-tubulin, was significantly reduced by subtilisin treatment. Blotting with anti-tubulin antibody also showed that the protease-treated tubulin had undergone a molecular weight shift, indicating that the C-terminal tail had been removed. We incubated the PAVE complex with control and subtilisin-treated microtubules and found no difference in the intensity or pattern of binding, regardless of the concentration of PAVE complex used (**Fig. 7F**). These results suggest that the PAVE complex binds directly to the microtubule lattice and may recognize a specific lattice structure rather than a post-translational modification in the tubulin tails.

TbAIR9 controls the distribution of PAVE1 in the subpellicular array

TbAIR9, which localizes to the entire subpellicular array, was also identified as a potential PAVE1 interactor in our immunoprecipitation analysis (**Fig. 5C, bottom**). TbAIR9 shares sequence similarity with the microtubule associated protein AIR9 found in *Arabidopsis thaliana,* which has a role in positioning the phragmoplast during plant cytokinesis (Buschmann et al., 2006). We tested whether depleting TbAIR9 had an effect on PAVE1. We conducted RNAi against TbAIR9 in a cell line where TbAIR9 was tagged

with HA and PAVE1 was tagged with Ty1. Cells lacking TbAIR9 developed aberrant cell morphologies and ceased to divide, as previously reported (**Supp. Fig. 4A & B**) (May et al., 2012). After 24 h of RNAi induction, HA-tagged TbAIR9 signal remained at the cell anterior while the cell posterior lacked the protein (**Supp. Fig. 4C**). In uninduced control cells, Ty1-tagged PAVE1 strongly localized to the posterior and ventral edge of the cell, while in the absence of TbAIR9, PAVE1 lost its preference for this subdomain and spread throughout the entirety of the array (**Fig. 8A**). A line scan measuring PAVE1 intensity placed along the ventral edge of TbAIR9 RNAi cells showed that PAVE1 labeling was less intense at the cell posterior and more intense at the cell anterior in comparison to control cells (**Fig. 8B**). PAVE1 protein levels were not altered, indicating that TbAIR9 depletion only affected the ability of PAVE1 to localize to the posterior subdomain (**Fig. 8C**). Depleting PAVE1 from cells did not affect TbAIR9 stability or localization, except for its absence at the posterior subpellicular array in cells where the posterior was truncated (**Supp. Fig. 4D & E**).

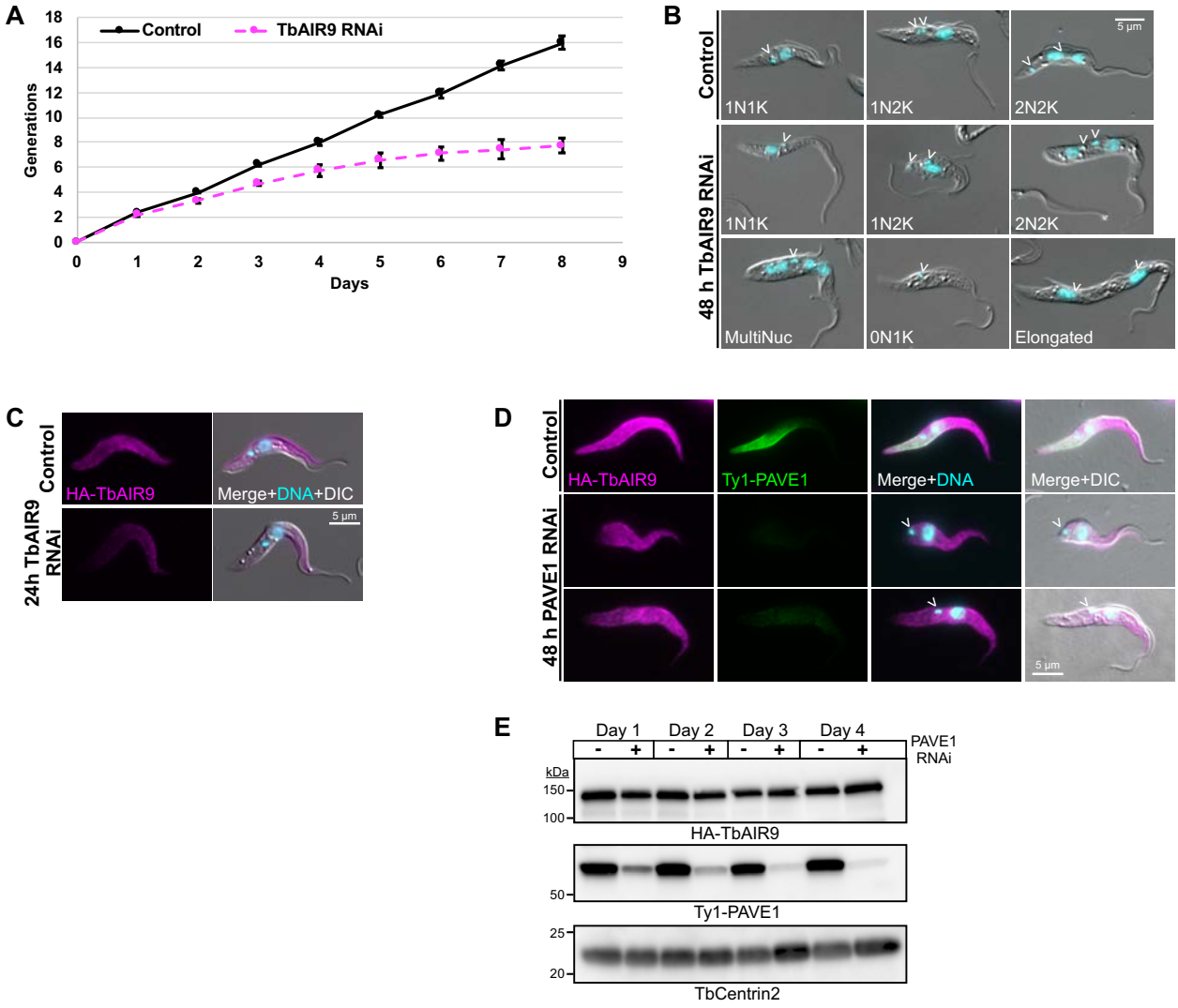

Figure S4. TbAIR9 does not require PAVE1 for localization or stability in vivo. (A) Generation plot of cell growth after induction of TbAIR9 RNAi. Cell concentration was monitored in control and TbAIR9 RNAi cells every 24 h. The curve is the mean of N=3 independent biological replicates. **(B)** Control and TbAIR9 RNAi cells were fixed in paraformaldehyde after 2 d of TbAIR9 depletion. Images are representative morphologies in control and TbAIR9 RNAi conditions. The epimastigote-like morphotype and elongated cell bodies were common in cells depleted of TbAIR9, as previously reported [(May et al., 2012)]. Open arrowheads indicate the kinetoplast. **(C)** Control and TbAIR9 RNAi cells were fixed with paraformaldehyde and stained after 24 h of TbAIR9 depletion. TbAIR9 localization initially disappears from the cell posterior during TbAIR9 RNAi, as previously reported. **(D)** PAVE1 RNAi was induced in cells in which TbAIR9 is endogenously tagged with the HA epitope tag. Cells were collected for fixation in paraformaldehyde after 2 d of PAVE1 depletion and stained for epifluoresence microscopy. The localization pattern of TbAIR9 does not change after PAVE1 depletion. **(E)** Lysates were collected from control and PAVE1 RNAi cells in which TbAIR9 is endogenously tagged every 24 h during PAVE1 depletion and western blotted. TbAIR9 stability is not affected by PAVE1 depletion.

The mis-localization of PAVE1 could be due to the disruption of inter-microtubule crosslinks during TbAIR9 depletion. To determine if crosslinks are still formed in cells depleted of TbAIR9, we created subpellicular array sheets of uninduced control and TbAIR9 RNAi cytoskeletons immunogold-labeled for Ty1-PAVE1 (**Fig. 8D**). In control cells, crosslinks were present throughout the array and PAVE1 localized to those present at the cell posterior (**Fig. 8D, left**). In TbAIR9 RNAi cells, crosslinks were also still present in the entire array (**Fig. 8D, right**). However, PAVE1 now localized to the crosslinks at both the posterior and anterior ends of the cell. This result suggests that TbAIR9 is not necessary to build the inter-microtubule crosslinks present in the array but is required to properly confine the distribution of PAVE1 to the cell posterior.

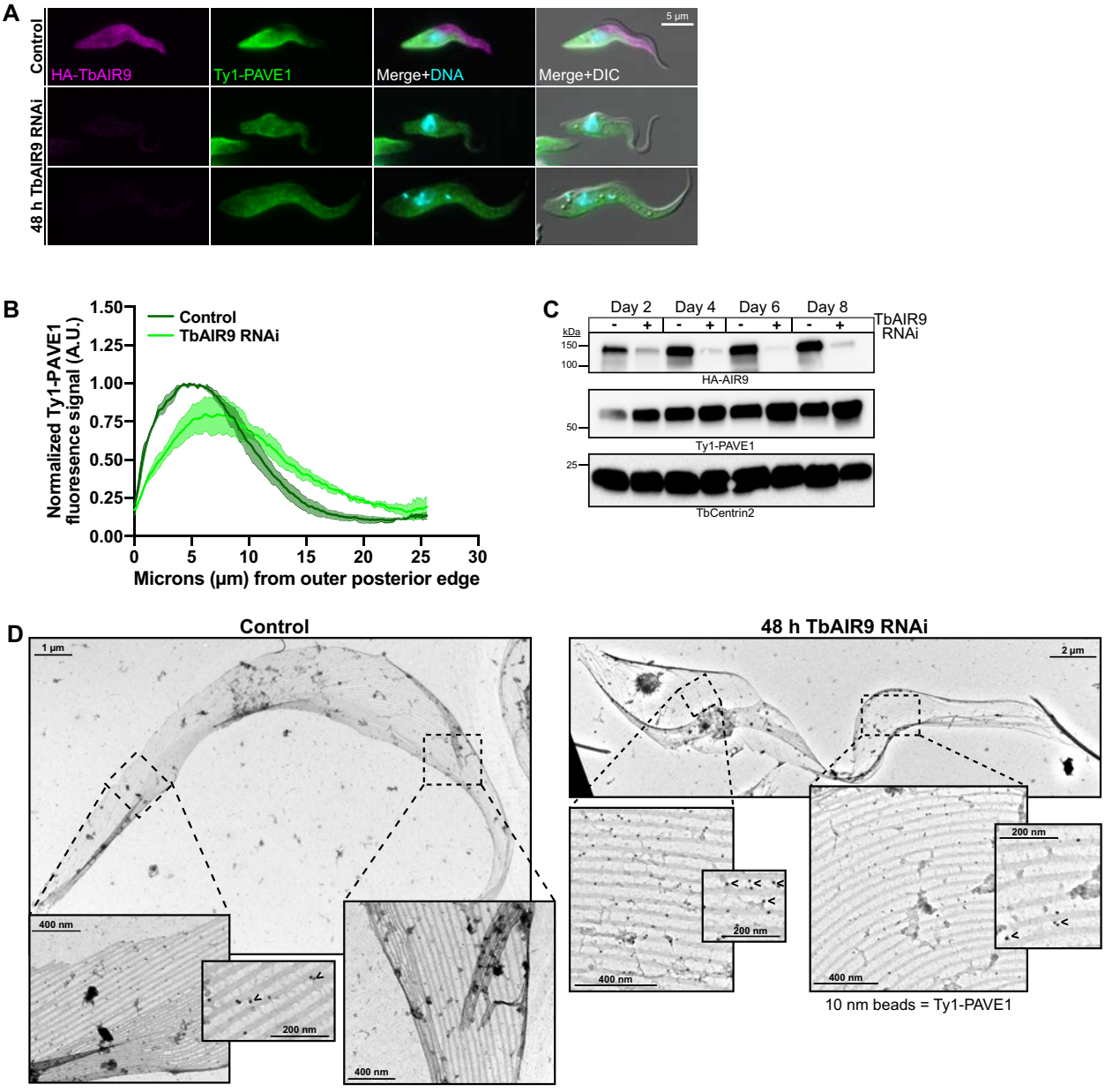

Figure 8. TbAIR9 confines PAVE1 to the crosslinks at the cell posterior. (A) Control and TbAIR9 RNAi cells were fixed in paraformaldehyde and stained after 2 d of TbAIR9 depletion. Ty1-PAVE1 signal appears spread throughout the array in the absence of TbAIR9. **(B)** The fluorescence signal intensity of Ty1-PAVE1 was measured along the ventral side of control and TbAIR9 RNAi cells after 2 d of TbAIR9 depletion. The signal intensities were normalized to the maximum control intensity, averaged, and plotted with the S.D. 50 1N1K cells in both control and TbAIR9 RNAi conditions from N=3 independent biological replicates were measured. Ty1-PAVE1 signal is more evenly distributed throughout the array in TbAIR9 depleted cells than in control cells. **(C)** TbAIR9 RNAi was induced and lysates were collected every 48 h from control and TbAIR9 depleted cells. Lysates were separated by SDS-PAGE and transferred to nitrocellulose for western blotting. Ty1-PAVE1 signal remains stable during TbAIR9 depletion.

(D) Subpellicular array sheets of control and TbAIR9 RNAi cells after 2 d of TbAIR9 depletion immunogold labeled against Ty1-PAVE1 with 10 nm beads. Ty1-PAVE1 localizes to the inter-microtubule crosslinks at both the posterior and anterior ends of the array in the absence of TbAIR9.

TbAIR9 is a global regulator of subpellicular array-associated protein localization

The striking redistribution of PAVE1 throughout the array during TbAIR9 depletion led us to consider that TbAIR9 may regulate the localization of other cytoskeletal proteins in the subpellicular array. To test this, we identified two proteins that localized to different domains of the array using the whole-genome localization database TrypTag (Dean et al., 2017).

Tb927.9.10790 is a 33 kDa protein annotated by TrypTag as localizing to the middle of the subpellicular array. This protein is found only within the genomes of *T. brucei* and *T. cruzi* with no homologs present in other domains of life. Tb927.11.1840 is a 45 kDa protein that localizes to the anterior array in TrypTag and appears to be unique to kinetoplastids (Aslett et al., 2010). We endogenously tagged both proteins at their C-termini and performed immunofluorescence on extracted cytoskeletons. Both 10790-Ty1 and 1840-Ty1 were stably associated with the cytoskeleton and localized to the midzone and anterior domains of the array, respectively (**Fig. 9A**).

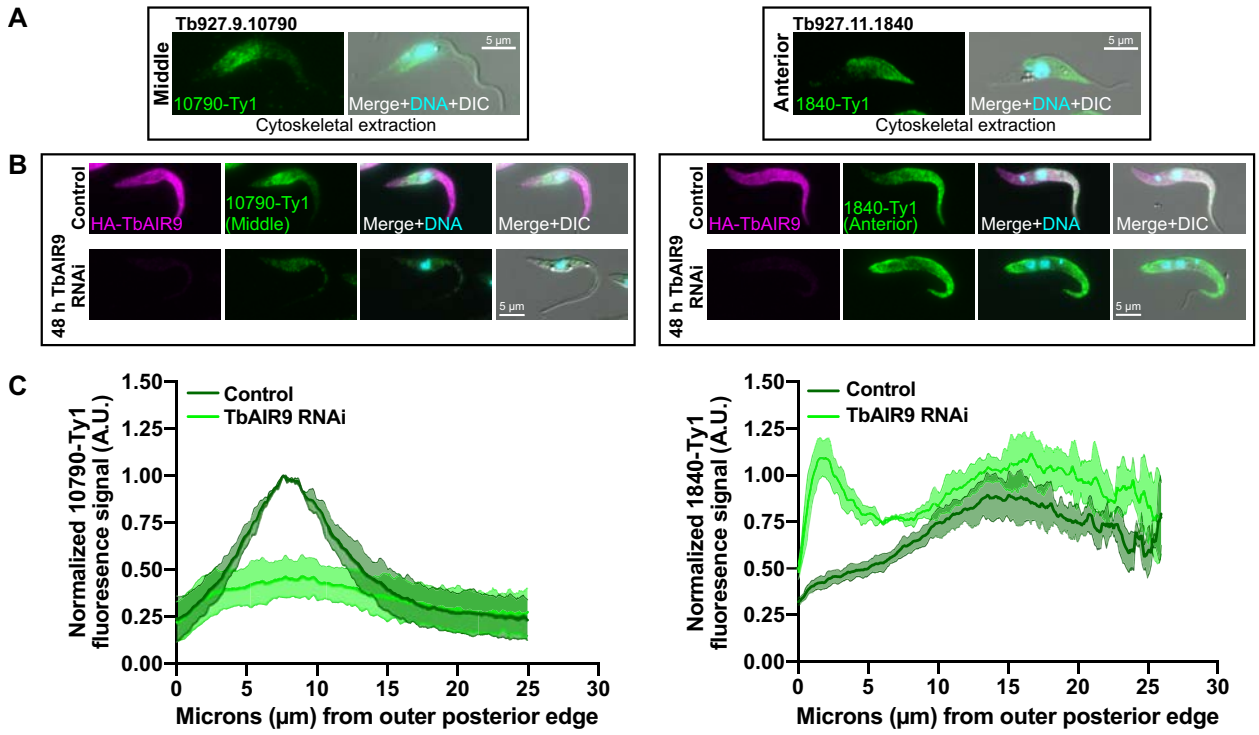

Figure 9. TbAIR9 maintains the localization array-associated proteins at specific domains. **(A)** Identification of array-associated proteins from TrypTag that localize to the middle (Tb927.9.10790, left) and anterior (Tb927.11.1840, right) domains of the subpellicular array. Both proteins were tagged at their C-terminus with Ty1 and cytoskeletal extractions followed by immunofluorescence with anti-Ty1 antibody was perfomed. Both proteins remained bound to the array in cytoskeletal extractions. **(B)** Cell lines containing 10790-Ty1 (left) and 1840-Ty1 (right) endogenous tags were fixed in paraformaldehyde and stained after 2 d of TbAIR9 depletion. 10790-Ty1 signal is depleted and spread throughout the cell body in the absence of TbAIR9, while 1840-Ty1 signal is detected at the posterior and anterior ends in TbAIR9 depleted cells. **(C)** Quantification of 10790-Ty1 (left) and 1840-Ty1 (right) fluorescent signal intensity along the ventral side of the cell body in TbAIR9 RNAi cells after 2 d of TbAIR9 depletion. The signal intensities were normalized to the maximum control values and plotted with the S.D. 50 1N1K cells in both control and TbAIR9 RNAi conditions from N=3 independent biological replicates were measured.

We next determined if TbAIR9 is necessary to confine the distribution of 10790 and 1840 to their respective domains of the subpellicular array, as it does in confining PAVE1 to the array posterior (**Fig. 8**). We induced TbAIR9 RNAi and localized 10790 and 1840 using immunofluorescence microscopy. We found that upon TbAIR9 depletion, 10790 is weakly distributed throughout the array (**Fig. 9B & C, left**), while 1840 localized

to both the posterior and anterior array, with weaker signal at the array midzone (**Fig. 9B & C, right**). TbAIR9 RNAi decreased the protein levels of 10790 (**Supp. Fig. 5A**), while 1840 protein levels increased (**Supp. Fig. 5B**). These results suggest that TbAIR9 functions to organize and confine array-associated proteins to distinct domains within the array.

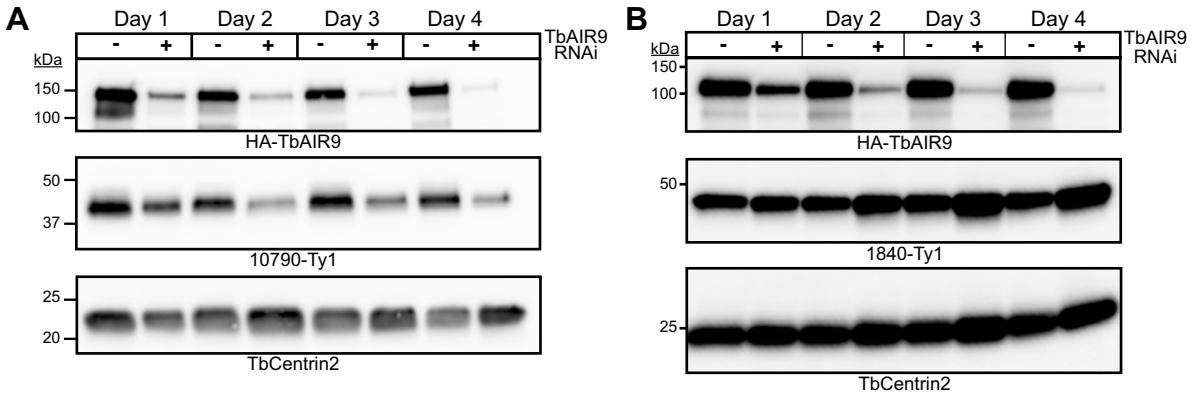

Figure S5. TbAIR9 depletion has differing effects on protein stability of array-associated proteins. (A) Lysates were collected from control and TbAIR9 RNAi cells in which Tb927.9.10790 was endogenously tagged every 24 h during TbAIR9 depletion and western blotted. 10790-Ty1 protein levels decrease during TbAIR9 depletion. **(B)** Lysates were collected from control and TbAIR9 RNAi cells in which Tb927.11.1840 was endogenously tagged every 24 h during TbAIR9 depletion and western blotted. 1840-Ty1 protein levels are stable and increase during TbAIR9 depletion.

DISCUSSION

In this work, we have characterized a series of proteins that appear to localize to and regulate the inter-microtubule crosslinking fibrils of the subpellicular array, which previously had no known components. These results show that the subpellicular array is organized into subdomains that are likely defined by microtubule crosslinks with unique protein compositions, which may differentially structure the array to shape *T. brucei* cells and alter the local properties of the microtubules. Asymmetric protein localization within the basal bodies of *Tetrahymena* stabilizes them against ciliary beating forces (Bayless

et al., 2016) and is required for basal body replication and positioning in *Paramecium* (Bengueddach et al., 2017; Ruiz et al., 2005). *T. brucei* may employ a similar mechanism on a broader scale across the array to withstand the forces from flagellar beating and maintain array shape.

PAVE1 was identified in a BioID screen of TOEFAZ1 (Hilton et al., 2018). Although PAVE1 does not appear to have a direct role in cytokinesis, it is required to maintain the length and shape of the posterior subpellicular array (**Fig. 2**). PAVE1 depletion does result in a cytokinetic defect (**Fig. 2C**), but this result is a secondary phenotype. Cells lacking PAVE1 develop truncated posterior arrays, which likely inhibits the proper replication of the array and leads to the misplacement of the cleavage furrow during cytokinesis. This phenotype illustrates the close relationship between cytokinesis and subpellicular array structure in *T. brucei.*

Our quantitative iEM shows that PAVE1 preferentially localizes to the ventral side of the subpellicular microtubules and the inter-microtubule crosslinks at the cell posterior (**Fig. 3B-D**). While our 'unroofing' approach disrupts many of the inter-microtubule crosslinking fibrils, the spacing and length of the structures we observe coincide with the placement of the inter-microtubule crosslinks found by others in subpellicular array sheets (Sherwin and Gull, 1989a; Woods et al., 1992). Currently, there are no methods available for immuno-labeling intact inter-microtubule crosslinks, which are best visualized using electron tomography or quick-freeze deep-etch EM (Hemphill et al., 1991; Souto-Padrón et al., 1984; Sun et al., 2018). The specific localization of PAVE1 to the ventral side of microtubules suggests that the crosslinking fibrils are composed of asymmetrically distributed proteins and that PAVE1 contacts the microtubule on one side of the crosslink.

This placement argues that there must be other proteins that span the inter-microtubule distance and contact the dorsal side of the adjacent microtubule to complete the crosslink. This is in line with our in vitro data, which show that the PAVE complex is not able crosslink microtubules into bundles in solution, most probably because the complex cannot assemble a complete span that can contact two microtubules simultaneously (**Fig. 7B**). Instead, our data suggest that the PAVE complex is an essential component of the ventral microtubule interface of the crosslinks at the cell posterior. The asymmetric composition of array crosslinks has also been suggested by the array-associated protein WCB, which preferentially localizes to one side of the plasma-membrane facing surface of array microtubules (Baines and Gull, 2008; Woods et al., 1992). Additional proteins that can contribute to the assembly of a complete crosslink are currently being sought.

PAVE1 is initially loaded onto the subpellicular microtubules at the extreme posterior end of the cell (**Fig. 4A**). The growing plus-ends of subpellicular array microtubules are concentrated at this location throughout the cell cycle (Sherwin and Gull, 1989a; Wheeler et al., 2013). The microtubule plus-ends are recruitment sites for new tubulin dimers, which are preferentially loaded with GTP and still contain the terminal tyrosine residue on their C-terminal tails (Kilmartin, 1982). Removing the C-terminal tails with subtilisin had no effect on the avidity or pattern of PAVE complex binding to microtubules, which argues that the complex binds directly to the microtubule lattice (**Fig. 7F**). It is intriguing that the PAVE complex binds to microtubules in patches, even at high concentrations of protein (**Fig. 7B**). The PAVE complex is unlikely to be a microtubule plus-end binding protein, as its localization is not exclusive microtubules that still contain terminal tyrosination (**Supp. Fig. 1C**). Recently, it has been suggested that several MAPs,

including the plus-end binder EB1 and the neuronal MAP doublecortin, preferentially recognize more open and irregular conformations of the microtubule lattice, which are often present at microtubule plus-ends and sites of curvature or damage (Bechstedt and Brouhard, 2012; Bechstedt et al., 2014; Reid et al., 2019). The neuronal MAP tau also forms concentration-dependent condensates on the GDP-lattice of microtubules, especially at sites of curvature, which protects the microtubule from the action of severing enzymes (Siahaan et al., 2019; Tan et al., 2019). It is possible that PAVE1 may recognize irregularities in the microtubule lattice, which are concentrated at the polymerizing end of the microtubule where the lattice is incomplete. Finally, it is also possible that polymerizing microtubule ends are the only places with free microtubule binding sites in the subpellicular array, as sites located more anterior in the array are already occupied with different MAPs.

Our HaloTag capping assay shows that the inter-microtubule crosslinks are not static within the array (**Fig. 4A**). PAVE1 migration towards the anterior end suggests two possible mechanisms of inter-microtubule crosslink movement. One possibility is that the inter-microtubule crosslinks remain associated with specific parts of the microtubule lattice and that the microtubules turn over as new tubulin is added to the cell posterior, which moves the crosslinks toward the anterior end of the cell. The other possibility is that inter-microtubule crosslinks can diffuse along the microtubules and that the selective recruitment of new PAVE1 to the extreme posterior end drives the movement of extant crosslinks specifically towards the cell anterior. Our in vitro results suggest that the PAVE complex forms persistent contacts with microtubules and does not diffuse along their lengths (**Fig 7C &D**). This, along with the fact that new tubulin subunits are constantly

added to the cell posterior, argues that PAVE1 is forming persistent contacts with the microtubules that anchor the crosslinks in place and suggests the former possibility of crosslink movement. The rapid rate of posterior end retraction upon PAVE1 depletion (**Fig. 4C**) argues that new inter-microtubule crosslinks are constantly being assembled and are essential for retaining the extended shape of the cell. Since the subpellicular microtubules do not appear to undergo catastrophes that shorten them, this observation requires that cells that are not undergoing cell division have some process that truncates or removes tubulin subunits from the array at a rate similar to that which tubulin is added to the posterior end. Recently, it has been theorized that the microtubules of the array may 'slide' to the anterior end of the cell to accommodate remodeling events after cell division, which could be suggestive of a microtubule treadmilling process in the array (Abeywickrema et al., 2019).

Since PAVE1 does not localize to the anterior end of the cell, some mechanism must exist to remove it from the microtubule crosslinks once the crosslinks reach the cell midzone. It is currently unknown if the crosslinks are remodeled by replacing subdomain-specific proteins such as PAVE1/2 with other proteins, or if new crosslinks are constructed at each subdomain, which would require a mechanism for installing them within the local array subdomain. It would also require that each subdomain of the subpellicular array have specialized sites for the local construction of different microtubule crosslinks, which have not been observed yet.

TbAIR9 is associated with the PAVE complex, which argues that the protein is also a component of the inter-microtubule crosslinks (**Figure 5B**). The trypanosomatid homolog of AIR9 differs from its plant counterpart in that it lacks a microtubule binding

domain at its N-terminus and has fewer A9 repeats at its C-terminus, which are Ig-like domains that likely serve as sites for protein-protein interactions (Buschmann et al., 2007). The absence of the microtubule binding domain suggests that TbAIR9 is recruited to the microtubules by other proteins, such as the PAVE complex, likely via the A9 repeats.

The broad distribution of TbAIR9 across the array (**Fig. 5C**) suggests that it may be a universal component that makes up a core part of the microtubule crosslinking fibrils, whose behavior are then locally tuned by proteins that interact with TbAIR9. While the PAVE complex does not appear to bind to post-translational modifications on the C-terminal tail of tubulin, other subpellicular components may use them to localize to different regions of the array and then form associations with core crosslink-associated proteins such as TbAIR9. Tubulin post-translational modifications such as polyglutamylation and tyrosination have different distribution patterns along the array and may serve as landmarks for recruiting specific MAPs (Casanova et al., 2015; Jentzsch et al., 2020; Sherwin and Gull, 1989a; Wheeler et al., 2013).

In *Arabidopsis*, AtAIR9 localizes to the cortical microtubules, which are analogous to the subpellicular array in that they underlie the plasma membrane. Cortical array microtubules in plants primarily control the distribution of cellulose synthetase and possibly act as tracks for membrane traffic (Dixit and Cyr, 2004). Deletion of AtAIR9 does not produce a phenotype, but a strong synthetic effect is observed with the simultaneous deletion of a second microtubule-binding protein known as TANGLED1, which produces plants with disorganized cortical microtubules and twisted roots (Mir et al., 2018). Depletion of TbAIR9 did not cause the crosslinks to disappear (**Fig. 8D**), so TbAIR9

function must be focused on controlling the distribution of proteins along the array (**Fig. 9**). The phenotype of TbAIR9 depletion is complex, producing anucleate and multinucleated cells with elongated and epimastigote-like morphologies (**Supp. Fig. 4B**) (May et al., 2012). Our data show that TbAIR9 depletion results in the mislocalization PAVE1 (**Fig. 8**) and two newly identified array-associated proteins, Tb927.9.10790 and Tb927.11.1840 (**Fig. 9**). Each of these proteins is confined to different subdomains of the array in wild-type cells, but the subdomain architecture is lost or scrambled in the absence of TbAIR9. This suggests that the TbAIR9 RNAi phenotype is the result of the inability to locally regulate microtubule properties in these subdomains, which appears to have a strong effect on parasite cell division.

Our work has highlighted the potential functions of a set of proteins that are components of the inter-microtubule crosslinking fibrils within the subpellicular array. These crosslinks appear consist of different protein components that likely have discrete functions in order to locally tune array dynamics. While the PAVE complex appears to function to maintain the length and shape of the array microtubules at the cell posterior, the functions of Tb927.9.10790 and Tb927.11.1840 are yet to determined. Future work is also needed to discover how TbAIR9 organizes these proteins into defined domains across the array. The TrypTag database contains many previously unidentified proteins that appear to localize to the subpellicular array; some are present along the whole array, and others localize to subdomains. It is interesting to note that the distribution patterns of some of these proteins are more complex, including more variety along the dorsal and ventral sides. Uncovering the function of these proteins is essential to understanding

subpellicular array biogenesis and how this structure maintains its shape throughout the cell cycle and during the cell body waveforms created by *T. brucei* motility.

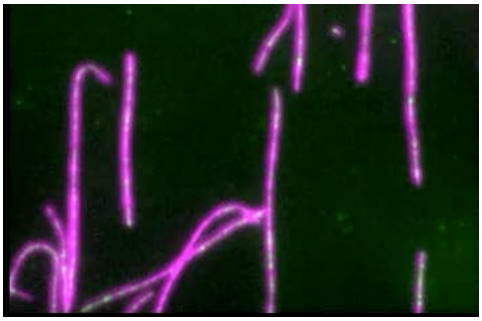

Movie 1. The PAVE complex binds to microtubules in patches. TIRF microscopy of 5 nM PAVE complex binding to Taxol-stabilized Cy5-labeled bovine microtubules. Images were taken every 10 sec for 20 min. Movie is 10 frames per second.

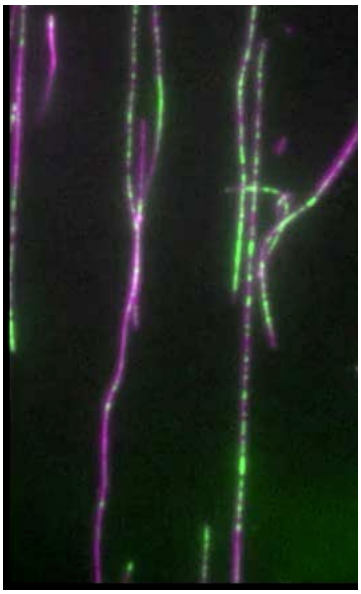

Movie 2. PAVE complex patches are highly stable. TIRF microscopy of 5 nM PAVE complex patches pre-seeded for 10 min on Taxol-stabilized Cy5-labeled bovine microtubules. Unbound protein was washed out prior to imaging. Images were taken every 10 sec for 20 min. Movie is 10 frames per second.

A.

Replicate 1			Total Unique Peptide Count	Total Unique Peptide Count
Identified Proteins	**Accession Number**	**Molecular Weight**	**WT Control**	**mNeon-PAVE1**
mNeon_PAVE1	Tb927.8.2030	75 kDa	0	32
PAVE2	Tb927.9.11540	51 kDa	0	25
AIR9-like protein	Tb927.11.17000	110 kDa	0	9
Tubulin beta chain	Tb927.1.2330	50 kDa	10	12
Tubulin alpha chain	Tb927.1.2340	50 kDa	10	12

B.

Replicate 2			Total Unique Peptide Count	Total Unique Peptide Count
Identified Proteins	**Accession Number**	**Molecular Weight**	**WT Control**	**mNeon-PAVE1**
mNeon_PAVE1	Tb927.8.2030	75 kDa	0	56
PAVE2	Tb927.9.11540	51 kDa	0	47
AIR9-like protein	Tb927.11.17000	110 kDa	0	32
Tubulin beta chain	Tb927.1.2330	50 kDa	14	21
Tubulin alpha chain	Tb927.1.2340	50 kDa	16	21
Cluster of Heat shock protein 70	Tb927.11.11330	75 kDa	2	14
RNA helicase	Tb927.11.15460	81 kDa	3	9
Mitochondrial carrier protein	Tb927.10.14840	34 kDa	5	8
ATP synthase subunit beta	Tb927.3.1380	56 kDa	2	8
40S ribosomal protein S2	Tb927.10.14710	29 kDa	5	8
Gim5B	Tb927.9.11600	26 kDa	4	7
Paraflagellar rod component, putative	Tb927.10.15250	58 kDa	2	5
Chaperonin Hsp60	Tb927.10.6510	60 kDa	3	5

Table 1. Proteins identified by mass spectrometry in the mNeonGreen-PAVE1 immunoprecipitations. Replicate 1 **(A)** and Replicate 2 **(B)**. Proteins with at least 5 total peptides in the mNeonGreen elution are listed.

MATERIALS AND METHODS

Antibodies

Antibodies are from the following sources and were used at the following dilutions: anti-Ty1 (1:1000) from Sebastian Lourido (Massachusetts Institute of Technology—Boston, MA), TAT1 (1:100) from Jack Sunter (Oxford Brookes University—Oxford, United Kingdom). YL1/2 (1:4,000) was purchased from ThermoFisher Scientific (Waltham, MA, cat# MA1-80017) and anti-α tubulin (1:10,000) was also purchased from ThermoFisher Scientific (clone B-5-1-2). Anti-HA antibody (1:500) was purchased from Sigma-Aldrich (St. Louis, MA, clone 3F10). GT335 (1:25,000) was purchased from Adipogen (San Diego, CA, cat# AG-20B-0020-C100). Anti-TbCentrin2 (1:150) antibody was previously described (de Graffenried et al., 2013).

Cell Culture

Wild-type procyclic *T. brucei brucei* 427 strain cells and the doxycycline-inducible 29-13 *T. brucei* cell line (Wirtz, 1999) were used to perform experiments. 427 cells were passaged in Beck's Medium (Hyclone—GE Healthcare, Logan, Utah) supplemented with 10% fetal calf serum (Gemini Bioproducts—West Sacramento, CA), while 29-13 cells were passaged in Beck's Medium supplemented with 15% doxycycline-free fetal calf serum (R&D Systems—Minneapolis, MN), 50 μg mL^{-1} hygromycin (ThermoFisher Scientific), and 15 μg mL^{-1} G418 (Sigma-Aldrich). 427 and 29-13 media also included 10 μg mL^{-1} gentamycin (ThermoFisher Scientific) and 500 μg mL^{-1} penicillin-streptomycin-glutamine (ThermoFisher Scientific). All cells were maintained at 27 °C. Cells were counted using a particle counter (Z2 Coulter Counter, Beckman Coulter—Brea, CA).

Cloning and Cell Line Construction

All constructs were created by PCR amplification of inserts from *T. brucei* genomic DNA using Q5 polymerase (NEB—Ipswich, MA) followed by either restriction-ligation or Gibson Assembly into a sequencing vector (PCR4Blunt) or a modified pLEW100 for long-hairpin RNAi (lhRNAi) generation as previously described (McAllaster et al., 2016). Each DNA construct was validated by sequencing and transfected into cells using an electroporator (GenePulser xCell, Bio-Rad—Hercules, CA). Clonal cell lines were created by selection and limiting dilution. Cell lines were validated with western blotting and loci PCRs. All sequences were obtained from TriTrypDB (Aslett et al., 2010).

RNAi constructs. Sequences for RNAi were selected from the coding sequence of the target protein using the RNAit online tool (https://dag.compbio.dundee.ac.uk/RNAit/) (Redmond et al., 2003). 400-600 base pairs were used to create lhRNAi constructs as follows: PAVE1 (Tb927.8.2030)—bp 97-543; PAVE2 (Tb927.9.11540)—bp 514-1112; TbAIR9 (Tb927.11.17000)—bp 1868-2303. Constructs were linearized for transfection with NotI (NEB) and transfected into the 29-13 cell line, after which clonal populations were obtained by selection with 40 μg ml^{-1} Zeocin (Life Technologies—Carlsbad, CA).

Endogenous tagging constructs. Endogenous tagging constructs were created using Gibson Assembly into the PCR4Blunt sequencing vector. N-terminal tagging constructs (PAVE1, PAVE2, TbAIR9) were targeted to their respective endogenous loci using last 500 bp of 5' UTR and first 500 bp of the coding sequence. C-terminal tagging constructs (Tb927.9.10790, Tb927.11.1840) were targeted to their loci using the last 500 bp of the coding sequence followed by the first 500 bp of the 3' UTR. Endogenous tagging constructs were excised using PacI and NsiI (NEB) and transfected into either the 427 or

29-13 cell lines, and clonal populations were selected using 10 μg mL^{-1} blasticidin or 1 μg mL^{-1} puromycin.

Image Acquisition for Fluorescence Microscopy

Epifluorescence acquisition. Images were acquired using a Zeiss Axio Observer.Z1 microscope (Carl Zeiss Microscopy—Oberkochen, Germany) using an 100X/1.4 NA Plan-Apochromat oil lens with an ORCA-Flash 4.0 V2 CMOS camera (Hamamatsu—Shizuoka, Japan). *Z*-stacks were acquired for each image.

Total Internal Reflection Fluorescence acquisition. Images were acquired at RT with the same Zeiss Axio Observer.Z1 microscope described above, equipped with a spinning illumination ring VectorTIRF system which includes a 405/488/561/640 quad band dichroic filter (Intelligent Imaging Innovations, Inc.—Denver, CO) and an Alpha Plan-Apochromat 100X/1.46 NA oil TIRF objective. Samples were excited using 488 nm 150mW and 647 nm 120mW lasers at 20% power. Images were acquired every 10 sec for 20 min using a Prime 95B Back Illuminated Scientific CMOS camera (Teledyne Photometrics—Tuscon, AZ) and a Definite Focus.2 system (Carl Zeiss Microscopy) for automatic focus correction.

SlideBook 6 digital microscopy software (Intelligent Imaging Innovations, Inc.) was used to manipulate the microscope and acquire images. Images were analyzed with ImageJ (National Institutes of Health—Bethesda, MD) and exported to Adobe Photoshop and Illustrator (CC 2020) for publication.

Immunofluorescence Microscopy

Cells were harvested from culture by centrifugation at 2400 *x g* for 5 min and washed with PBS. Cells were centrifuged onto coverslips and fixed as per the conditions

below. All fixation conditions for each experiment are specified in the text and figure legends. After fixation, cells were washed 3X with PBS and blocked using 5% goat serum (ThermoFisher) in PBS. Coverslips were then incubated with primary antibody diluted into blocking buffer for 1 hr RT, after which they were washed 3X with PBS and incubated with secondary antibody conjugated to Alexa Fluor -647, -568, and -488 (Life Technologies) diluted into blocking buffer for 1 hr RT. Coverslips were washed for a final 3X with PBS and mounted for epifluorescence imaging using Fluoromount-G with DAPI (Southern Biotech—Birmingham AL).

Methanol fixation. After cells were centrifuged onto coverslips, excess PBS was wicked away with tissue paper and the coverslips were quickly plunged into ice-cold methanol at 20 ˚C for 20 min.

Paraformaldehyde fixation. Coverslips were inverted onto a drop of 4% paraformaldehyde in PBS for 20 min RT in a humidified chamber. Cells were permeabilized by moving the coverslip to a drop of 0.25% NP-40 (IPEGAL CA-630, Sigma Aldrich) in PBS for 5 min RT.

Cytoskeletal extraction. Coverslips were inverted onto a drop of cytoskeletal extraction buffer (0.1 M PIPES pH 6.9, 2 mM EGTA, 1 mM $MgSO_4$, 0.1 mM EDTA, 0.25% NP-40) for 2 min RT. Coverslips were then quickly washed 6X with PBS and fixed for 20 min RT with 4% paraformaldehyde in PBS.

Transmission Electron Microscopy

Whole-mount extracted cytoskeletons preparation. Cells were harvested by centrifugation at 800 *x g* and washed 3X with PBS. Cells were briefly spun onto glow-discharged formvar- and carbon-coated grids (Electron Microscopy Sciences—

Hatchfield, PA) at 800 *x g.* Grids were floated on two subsequent drops of cytoskeletal extraction buffer (0.1 M PIPES pH 6.9, 2 mM EGTA, 1 mM $MgSO_4$, 0.1 mM EDTA, 1% NP-40) for 3 min RT each drop, and then briefly washed in a drop of extraction buffer without detergent. Grids were fixed in a drop of 2.5% glutaraldehyde in PBS for 5 min RT, after which they were washed with distilled water and negatively stained with 1% aurothioglucose (Sigma Aldrich).

Immunogold labeling. Whole-mount extracted cytoskeletons were prepared as above, but prior to fixation, cells were blocked by quickly moving the grids through 5 drops of blocking buffer (2% bovine serum albumin in PBS). Grids were incubated for 1 hr RT in primary antibody diluted in blocking buffer, after which they were washed 5X with blocking buffer. Grids were then incubated with 10 nm or 20 nm gold-conjugated secondary antibodies (BBI Solutions—Newport, United Kingdom) diluted in blocking buffer for 1 h RT. Grids were fixed and stained as above. *Subpellicular sheeting.* Cells were prepared for sheeting as described in (Sherwin and Gull, 1989a). After cells were spun onto grids and extracted as above, the grids were gently fixed in a primary fixative of 3.2% paraformaldehyde in cellular extraction buffer without detergent for 5 min RT. The paraformaldehyde was then quenched by incubating the grids in 20 mM glycine in PBS for 5 min RT. Grids were blocked and immunogold labeled as above. After labeling, grids were fixed with 2.5% glutaraldehyde in PBS for 5 min RT, washed 2X with distilled water, and positively stained in a drop of 2% aqueous uranyl acetate for 45 min RT. Grids were dehydrated in an ethanol series and critical point dried. The top layer of the subpellicular array was removed to ‘unroof’ the cells by inverting the grid onto double-sided tape, applying gentle pressure, and then lifting the grid off the tape.

Image acquisition for TEM. Images were taken on a Phillips 410 transmission electron microscope at 100 kV equipped with a 1k x 1k Advantage HR CCD camera from Advanced Microscopy Techniques (AMT) using AMT imaging software. Images were analyzed in ImageJ and exported to Adobe Photoshop and Illustrator for processing.

Quantification of immunogold label distribution on subpellicular sheets. Micrographs of subpellicular sheets in which the flagellum was still attached were analyzed in ImageJ. The sheets were oriented along the dorsal-ventral axis using the flagellum as a fiducial marker. A 1 μm^2 area of the sheet was selected for analysis. Each microtubule within the 1 μm^2 area was traced using the segmented line tool. A semi-automated macro was written in ImageJ which converted the segmented line into a spline-fit line and straightened the microtubule according to the spline curve. A rectangle was placed on the bounding edges of the straightened microtubule and its centroid was calculated and plotted. The location of each gold bead on the microtubule was manually counted as dorsal (above the centroid line), centroid (touching the centroid line) or ventral (below the centroid line), as well whether the gold bead localized to an inter-microtubule crosslink. Three subpellicular array sheets were analyzed per N=3 independent biological replicates for each experiment. The data were recorded in Microsoft Excel and statistical tests were performed and the data graphed using Prism 8 (Graphpad).

Scanning Electron Microscopy

Cells were pre-fixed in culture with 2.5% glutaraldehyde for 10 min at 27 ˚C and were harvested by gentle centrifugation at 800 x g and washed 3X with 100 mM sodium cacodylate ($C_2H_7AsO_2$) pH 7.4. Cells were then fixed with 2.5% glutaraldehyde diluted in 100 mM sodium cacodylate pH 7.4 for 2 h RT, after which the cells were washed 3X with

100 mM sodium cacodylate pH 7.4 and settled onto glass coverslips. Cells were dehydrated in an ethanol series, critical point dried, and sputter-coated with gold. Slips were imaged using a Thermo Apreo VS SEM at 5 kV with a 0.20 nA current and a working distance of 5.9 mm.

HaloTag Capping Assay

HaloTag (Los et al., 2008) substrate conjugated to JF646 (Promega—Madison, WI) was added to a culture of 2 x 10^6 cell mL^{-1} log-phase HaloTag-PAVE1 cells at a final concentration of 2 μM for 1 h at 27 ˚C. Cells were collected by centrifugation at 2400 *x g* and washed 3X with Beck's Medium. Cells were resuspended at 2 x 10^6 cell mL^{-1} in complete media and HaloTag substrate conjugated to TMR (Promega) was added at a final concentration of 5 μM. Cells were harvested at T=0 h, T=1 h, T=3 h, and T=8 h of TMR substrate addition by centrifugation at 2400 *x g*. Cells were washed 3X with HBSS, centrifuged onto coverslips, and fixed for 20 min RT with 4% paraformaldehyde in PBS. Coverslips were washed 3X with PBS and mounted with Fluoromount-G containing DAPI.

Image acquisition and fluorescence intensity analysis. Images were captured using epifluorescence as above. Maximum projections of each *Z*-stack were created and background-corrected using rolling ball background subtraction (radius = 100 pixels). The ventral edge of 50 1N1K cells per time point was traced using the segmented line tool. The fluorescence intensity along each line for HaloTag substrates conjugated to JF646 and TMR were recorded and exported to Microsoft Excel. The average pixel intensity and S.D. at each position along the line was calculated and normalized to 1 from N=3 independent biological replicates and graphed using Prism 8 software.

RNAi

Log-phase cultures of 29-13 cells containing lhRNAi constructs were seeded at 1 x 10^6 cell mL^{-1}. RNAi was induced in using 1 µg mL^{-1} doxycyline (ThermoFisher Scientific) or 70% ethanol as a vehicle control. Cell growth was recorded every 24 h unless otherwise noted, and samples were collected for western blotting or immunofluorescence. RNAi cultures were re-seeded every 48 h in fresh media and doxycycline or ethanol was added as above. All RNAi generation plots represent three independent biological replicates and the error bars are the S.D.

PAVE1 and PAVE2 RNAi image analysis. Control and RNAi cells were fixed in methanol or paraformaldehyde and stained as above. Maximum projections of each *Z*-stack were created for analysis*. For the PAVE1 RNAi*: Cells were harvested and fixed in paraformaldehyde and stained with DAPI to detect DNA. For DNA statet analysis, 300 cells were counted in control and RNAi conditions in N=3 independent biological replicates. For posterior end measurements, 200 1N1K cells were measured in control and PAVE1 RNAi conditions in N=3 independent biological replicates. *For the PAVE1 RNAi 1N2K time course*: cells were harvested and fixed in methanol after T=0 h, 4 h, and 6 h after RNAi induction. Only 1N2K cells were selected for analysis, as these cell types have progressed over halfway through the cell cycle at the time of harvest (Sherwin and Gull, 1989c), and defects in the array would be due solely to PAVE1 RNAi, and not defects in cytokinesis or G1 subpellicular array remodeling. 50 1N2K cells per each time point in N=3 independent biological replicates were measured. The distance from the posterior kinetoplast to the outer posterior edge of the subpellicular array, as well as the posterior nucleus edge to the posterior kinetoplast, were measured. *For PAVE2 RNAi*: Cells were harvested and fixed in paraformaldehyde. For DNA state analysis, 300 cells for each time

point in control and PAVE2 RNAi conditions were counted in N=3 independent biological replicates. For posterior end measurements, 100 1N1K cells in control and Day 1 PAVE2 RNAi conditions were measured as above in N=3 independent biological replicates. Data were recorded in Microsoft Excel and statistical tests were conducted and the data graphed using Prism 8.

PAVE1, Tb927.9.10790, Tb927.11.1840 fluorescence intensity analysis during TbAIR9 RNAi. Control and TbAIR9 RNAi cells were harvested after two days of RNAi induction and fixed in paraformaldehyde and stained as above. The ventral side of 1N1K cells was traced using the segmented line tool, and fluorescence intensities were recorded and analyzed as above and normalized to the maximum control value. 50 1N1K cells each were measured in control and TbAIR9 RNAi conditions for N=3 independent biological replicates.

SDS-PAGE and Western Blotting

T. brucei cells were collected by centrifugation at 2400 *x g*, washed with PBS, lysed in SDS-PAGE lysis buffer and incubated for 10 min at 99 ˚C. 3 x 10^6 cell equivalents/lane were separated by SDS-PAGE and transferred to a nitrocellulose membrane. Blots were blocked with 5% (w/v) non-fat dry milk dissolved in TBS containing 0.1% Tween-20 and incubated overnight at 4 ˚C with primary antibody diluted in blocking buffer. Blots were washed 3X with TBS containing 0.1% Tween-20 and incubated for 1 hr RT with secondary antibody conjugated to horseradish peroxidase diluted into blocking buffer (Jackson ImmunoResearch—West Grove, PA). Blots were washed a final 3X and imaged using Clarity Western ECL substrate (BioRad) and a BioRad Gel Doc XR+ system.

Immunoprecipitation of mNeonGreen-PAVE1

Both endogenous alleles of PAVE1 were tagged at their N-termini with mNeonGreen (Shaner et al., 2013) as described above. 3-8.0 x 10^8 WT 427 control and mNeonGreen-PAVE1 cells were harvested and lysed in lysis buffer [10 mM Na_3PO_4 pH 7.4, 150 mM NaCl, 0.5% glycerol, 7% sucrose, and 0.5% NP-40 with 1 mM DTT; 1mM PMSF and 1X HALT (ThermoFisher) were added as protease inhibitors]**.** Cytoskeletal proteins were solubilized with sonication, after which the lysate was clarified by centrifugation at 17.1K *x g* for 20 min at 4 ˚C*.* Cleared supernatant material was diluted by half to decrease the concentration of detergent and incubated with magnetic beads conjugated to the camelid nanobody mNeonGreen-Trap (Chromotek—Munich, Germany) for 1 hr 4 ˚C. The beads were washed 6X with lysis buffer without glycerol, sucrose, and detergent. Beads were immediately processed for mass spectrometry, or bound proteins were eluted by adding SDS-PAGE lysis buffer and incubating the beads at 99 ˚C for 10 min. Eluted proteins were separated by SDS-PAGE and the gel was silver stained (ThermoFisher Scientific) for imaging.

Mass spectrometry

On-beads sample preparation of control and mNeonGreen-PAVE1 immunoprecipitates. The supernatants from mNeonGreen-PAVE1 and corresponding 427 WT control immunoprecipitations were removed and replaced with 100 µL 0.1 M ammonium bicarbonate in water. Cys residues were reduced and alkylated using 5 mM dithiothreitol in 0.1 M ammonium bicarbonate for 1.5 hr, and 10 mM iodoacetamide in 0.1 M ammonium for 45 min in the dark, respectively. Both reactions proceeded at 37°C in a thermal mixer. A 16 hr, 37°C on-beads tryptic digestion was performed on a thermal mixer

with constant agitation using a 1:20 (w/w) enzyme:protein ratio for Promega modified sequencing grade trypsin. Tryptic peptides were then removed and the digestion was quenched by the addition of concentrated formic acid to yield a final pH of 3. Proteolytic peptides were desalted using Pierce™ C18 Spin Columns (ThermoFisher Scientific) per manufacturer's instruction, dried to completion, resuspended in 0.1% formic acid in water (Solvent A) and quantified using a Thermo Scientific Nanodrop Spectrophotometer.

Mass spectrometry-based proteomics analysis. mNeonGreen-PAVE1 and WT 427 control peptide sample concentrations were matched using Solvent A prior to injection onto a Waters 75 µm x 250 mm BEH C18 analytical column using a Thermo Scientific Ultimate 3000 RSLCnano ultra-high performance liquid chromatography system directly coupled to a Thermo Scientific Q Exactive HF Orbitrap mass spectrometer. A 1 hr, linear reversed-phase gradient (Solvent B: 0.1% formic acid in acetonitrile) at 300 nL/min flow was used to separate peptides prior to mass analysis. Peptides were ionized directly into the Q Exactive HF via nanoflow electrospray ionization. High energy collision dissociation (HCD) MS/MS peptide interrogation was achieved using a top 15 data-dependent acquisition method in positive ESI mode. All raw data were searched against the Uniprot *T. brucei* reference proteome (identifier AUP000008524, database accessed 09/11/2018 and updated 04/27/2018) plus the full mNeonGreen-PAVE1 protein sequence using the MaxQuant software suite (Cox and Mann, 2008). Search parameters included the following: 1% false discovery rate cutoff at the protein and peptide-spectrum match levels, trypsin cleavage specificity with 2 missed cleavages, 5 amino acids/peptide minimum, and the "LFQ" algorithm was used to provide label-free quantitation. All other MaxQuant

parameters were kept at default values. Search output files were compiled into Scaffold Q+S (Proteome Software, Inc.) for data visualization and further analysis.

Recombinant Expression and Purification of the PAVE Complex

For recombinant expression in bacteria, the entire coding sequences of PAVE1 and PAVE2 were amplified from *T. brucei* genomic DNA. The solubility-enhancing maltose-binding protein (MBP) was fused to an oligo-His tag followed by a TEV protease site and appended to the N-terminus of mNeonGreen-PAVE1. The MBP-oligoHis-TEV-mNeonGreen-PAVE1 construct was inserted into a MalpET expression vector containing kanamycin resistance. The Strep-tag (Schmidt and Skerra, 2007) peptide sequence was appended to the N-terminus of PAVE2 and inserted into a pOKD5 expression vector containing ampicillin resistance. Both vectors were co-transformed into BL21 (DE3) bacteria. 0.5 L of cells were grown to mid-log phase (OD_{600} ~0.6) and overexpression of the proteins were induced by adding 0.4 mM IPTG at 16 ˚C overnight. Cells were collected by centrifugation and lysed in lysis buffer [100 mM Tris pH 8.0, 300 mM NaCl, 0.5% NP-40, 0.5 mM DTT, with the addition of 1 mM PMSF and 1X HALT]. After sonication, the lysate was clarified by centrifugation at 17K *x g* and the supernatant was batch-incubated for 45 min at 4 ˚C with 3 mL of Ni-NTA agarose resin that had been pre-treated with 0.5 M imidazole pH 7.4 followed by equilibration with lysis buffer (ThermoFisher Scientific). The protein-bound resin was passed over a column and washed with 20 column volumes of Wash10 buffer [100 mM Tris pH 8.0, 300 mM NaCl, 0.5 mM DTT, 10 mM imidazole] followed by 20 column volumes of Wash30 buffer [100 mM Tris pH 8.0, 300 mM NaCl, 0.5 mM DTT, 30 mM imidazole]. Bound proteins were eluted in 1 mL fractions using elution buffer [100 mM Tris pH 8.0, 300 mM NaCl, 0.5 mM DTT, 200 mM imidazole]. Peak

fractions were pooled and dialyzed overnight at 4 ˚C into Strep buffer [100 mM Tris pH 8.0, 150 mM NaCl, 1 mM EDTA]. Dialyzed fractions were treated with TEV protease (1:25 molar ratio) to remove the MBP-oligoHis-TEV fusion from mNeonGreen-PAVE1 for 5 hr RT, after which the complex was passed over Strep-Tactin XT resin (IBA Lifesciences—Goettingen, Germany). Bound complex was eluted using Buffer BXT containing 50 mM biotin (IBA Lifesciences). Protein samples were diluted into SDS-PAGE lysis buffer and incubated at 99 ˚C for 10 min for separation by SDS-PAGE and Coomassie staining. Purified PAVE complex was then dialyzed into storage buffer [100 mM Tris pH 8.0, 300 mM NaCl, 1 mM DTT, 50% glycerol] overnight at 4 ˚C. This preparation typically yielded ~200 µg of total protein that was stable for several months at -20 ˚C.

In vitro Microtubule Interaction Assays

Microtubules were polymerized from cycled bovine tubulin (PurSolutions—Nashville, TN) mixed with Cy5-labled bovine tubulin (PurSolutions) and stabilized with 10 µM Taxol (Cytoskeleton Inc.—Denver, CO) as previously described (Sladewski et al., 2018), (Hilton et al., 2018). The PAVE complex was clarified to remove aggregates by ultracentrifugation at 400K *x g* at 2 ˚C.

In-solution microtubule binding experiments. 5-500 nM PAVE complex was mixed with microtubules diluted in blocking buffer [10 mM imidazole pH 7.4, 50 mM KCl, 1 mM EGTA, 4 mM $MgCl_2$ supplemented with 2 mg mL^{-1} κ-casein, 0.1% Plurionic F-68 (ThermoFisher Scientific), 10 µM Taxol, and an oxygen-scavenging system (3 mg ml^{-1} glucose, 0.1 mg ml^{-1} glucose oxidase and 0.18 mg ml^{-1} catalase)] and incubated for 20 min RT. Flow cells were constructed from glass coverslips and treated with rigor-like kinesin to attach microtubules to the glass surface as previously described (Hilton et al.,

2018; Sladewski et al., 2018). The flow cells were then blocked with two passages of blocking buffer. The complex-microtubule mixture was passed over flow cells, and any complex-microtubule mixture not captured by the rigor-like kinesin was washed away with two passages of blocking buffer. Flow cells were imaged using epifluorescence as above. Figures are representative of three independent biological replicates using two separate PAVE complex preparations.

Total internal reflection fluorescence microscopy experiments. PEGylated flow cells were prepared to minimize background as previously described (Sladewski et al., 2018). Rigor-like kinesin was passed over the PEGylated flow cell, followed by two passages of blocking buffer. For the PAVE complex binding experiment, microtubules diluted in blocking buffer were allowed to attach to the rigor-like kinesin on the PEGylated surface, after which unbound microtubules were washed away with blocking buffer. 5 nM PAVE complex was added to the flow cell and immediately imaged using TIRF microscopy. For the PAVE complex patch stability experiment, PAVE complex patches were pre-seeded on microtubules in solution for 10 min RT and passed through the flow cell. Unbound material was removed with three washes of blocking buffer, after which the flow cell was imaged using TIRF microscopy. Figures and movies are representative of three independent biological replicates using two separate PAVE complex preparations.

Subtilisin-treated microtubule binding assay. The C-terminal tails of Taxol-stabilized Cy5 microtubules were cleaved using Subtilisin A (Sigma Aldrich) as previously described (Schmidt-Cernohorska et al., 2019). A 1:15 molar ratio of microtubules to subtilisin A were diluted into BRB80 blocking buffer [80 mM PIPES pH 6.8 with KOH, 1 mM $MgCl_2$, 1 mM EGTA, supplemented with 2 mg mL^{-1} κ-casein, 0.1% Plurionic F-68, 10

μM Taxol, and an oxygen-scavenging system as above] and incubated for 45 min at 30 ˚C. The cleaving reaction was stopped with the addition of 10 mM PMSF for 10 min at 30 ˚C. Samples of the microtubules were diluted into SDS-PAGE lysis buffer and incubated at 99 ˚C for 10 min for western blotting to confirm tail cleavage as above. Control or subtilisin-treated microtubules were incubated with 5 nM or 50 nM PAVE complex for 20 min RT and passed over prepared glass flow cells and imaged using epifluorescence as described above. Figures are representative of four independent biological replicates using one PAVE complex preparation.

ACKNOWLEDGEMENTS

The authors would like to thank Dr. Jeremy Balsbaugh (University of Connecticut Proteomics and Metabolomics Facility) for the mass spectrometry analysis. We would also like to thank Geoff Williams (Brown University Leduc Bioimaging Facility) for helpful advice on our TEM preparations. We thank Dr. Sebastian Lourido (Massachusetts Institute of Technology) for the Ty1 antibody and Dr. Jack Sunter (Oxford Brookes University) for the TAT1 antibody. We thank Dr. Alexandra Deaconescu (Brown University) for the pOKD5 plasmid. We would like to thank TrypTag, whose data helped us identify Tb927.9.10790 and Tb927.11.1840. TrypTag is a data resource generated through a Wellcome Trust biomedical resource grant [108445/Z/15/Z] that was awarded to Prof. Keith Gull (University of Oxford), Prof. Mark Carrington (University of Cambridge), Prof. Christiane Hertz-Fowler (Wellcome Trust), Dr. Richard Wheeler (University of Oxford), Dr. Jack Sunter (Oxford Brookes University), Dr. Samuel Dean (University of Warwick) and Prof. Sue Vaughan (Oxford Brookes University). Thermo Apreo VS SEM was purchased with a high-end instrumentation grant from the Office of the Director of the National Institutes of Health (S10OD023461). Work in CLdG.'s laboratory is supported by the National Institutes of Health (F31AI143163 to ANS and AI112953 to CLdG).

AUTHOR CONTRIBUTIONS

ANS, TES, JLZ, AER, and CLdG performed the conception and design of the study; ANS and CTH performed the experiments; ANS and CTH performed analysis or interpretation of the data; ANS and CLdG wrote the manuscript.

REFERENCES

Abeywickrema, M., Vachova, H., Farr, H., Mohr, T., Wheeler, R. J., Lai, D.H., Vaughan, S., Gull, K., Sunter, J. D. and Varga, V. (2019). Non-equivalence in old- and new-flagellum daughter cells of a proliferative division in Trypanosoma brucei. *Mol. Microbiol.* **112**, 1024–1040.

Angelopoulos, E. (1970). Pellicular Microtubules in the Family Trypanosomatidae. *The Journal of Protozoology* **17**, 39–51.

Aslett, M., Aurrecoechea, C., Berriman, M., Brestelli, J., Brunk, B. P., Carrington, M., Depledge, D. P., Fischer, S., Gajria, B., Gao, X., et al. (2010). TriTrypDB: a functional genomic resource for the Trypanosomatidae. *Nucleic Acids Res.* **38**, D457–62.

Baines, A. and Gull, K. (2008). WCB is a C2 domain protein defining the plasma membrane - sub-pellicular microtubule corset of kinetoplastid parasites. *Protist* **159**, 115–125.

Balaban, N., Waithaka, H. K., Njogu, A. R. and Goldman, R. (1989). Isolation of a subpellicular microtubule protein from Trypanosoma brucei that mediates crosslinking of microtubules. *Cell Motility and the Cytoskeleton* **14**, 393–400.

Bargul, J. L., Jung, J., McOdimba, F. A., Omogo, C. O., Adung'a, V. O., Krüger, T., Masiga, D. K. and Engstler, M. (2016). Species-Specific Adaptations of Trypanosome Morphology and Motility to the Mammalian Host. *PLoS Pathog.* **12**, e1005448.

Bayless, B. A., Galati, D. F., Junker, A. D., Backer, C. B., Gaertig, J. and Pearson, C. G. (2016). Asymmetrically localized proteins stabilize basal bodies against ciliary beating forces. *The Journal of Cell Biology* **215**, 457–466.

Bechstedt, S. and Brouhard, G. J. (2012). Doublecortin recognizes the 13-protofilament microtubule cooperatively and tracks microtubule ends. *Dev. Cell* **23**, 181–192.

Bechstedt, S., Lu, K. and Brouhard, G. J. (2014). Doublecortin Recognizes the Longitudinal Curvature of the Microtubule End and Lattice. *Current Biology* **24**, 2366–2375.

Bengueddach, H., Lemullois, M., Aubusson-Fleury, A. and Koll, F. (2017). Basal body positioning and anchoring in the multiciliated cell Paramecium tetraurelia: roles of OFD1 and VFL3. *Cilia* **6**, 6–16.

Bordier, C., Garavito, R. M. and Armbruster, B. (1982). Biochemical and Structural Analyses of Microtubules in the Pellicular Membrane of Leishmania tropica. *Journal of Protozoology* **29**, 560–565.

Bramblett, G. T., Chang, S. and Flavin, M. (1987). Periodic crosslinking of microtubules by cytoplasmic microtubule-associated and microtubule-corset proteins from a trypanosomatid. *PNAS* 3259–3263.

Brooker, B. E. (1971). Fine structure of Bodo saltans and Bodo caudatus (Zoomastigophora: Protozoa) and their affinities with the Trypanosomatidae. *Bull. Brit. Mus. Nat. Hist.* **22**, 89–102.

Buschmann, H., Chan, J., Sanchez-Pulido, L., Andrade-Navarro, M. A., Doonan, J. H. and Lloyd, C. W. (2006). Microtubule-associated AIR9 recognizes the cortical division site at preprophase and cell-plate insertion. *Current Biology* **16**, 1938–1943.

Buschmann, H., Sanchez-Pulido, L., Andrade-Navarro, M. A. and Lloyd, C. W. (2007). Homologues of Arabidopsis Microtubule-Associated AIR9 in Trypanosomatid Parasites: Hints on Evolution and Function. *Plant Signal Behav* **2**, 296–299.

Caljon, G., Van Reet, N., De Trez, C., Vermeersch, M., Perez-Morga, D. and Van Den Abbeele, J. (2016). The Dermis as a Delivery Site of Trypanosoma brucei for Tsetse Flies. *PLoS Pathog.* **12**, e1005744.

Capewell, P., Cren-Travaillé, C., Marchesi, F., Johnston, P., Clucas, C., Benson, R. A., Gorman, T.-A., Calvo-Alvarez, E., Crouzols, A., Jouvion, G., et al. (2016). The skin is a significant but overlooked anatomical reservoir for vector-borne African trypanosomes. *Elife* **5**, e17716.

Casanova, M., de Monbrison, F., van Dijk, J., Janke, C., Pagès, M. and Bastien, P. (2015). Characterisation of polyglutamylases in trypanosomatids. *International Journal for Parasitology* **45**, 121–132.

Cox, J. and Mann, M. (2008). MaxQuant enables high peptide identification rates, individualized p.p.b.-range mass accuracies and proteome-wide protein quantification. *Nat Biotechnol* **26**, 1367–1372.

de Graffenried, C. L., Anrather, D., Raußendorf, Von, F. and Warren, G. (2013). Polo-like kinase phosphorylation of bilobe-resident TbCentrin2 facilitates flagellar inheritance in Trypanosoma brucei. *Mol. Biol. Cell* **24**, 1947–1963.

Dean, S., Sunter, J. D. and Wheeler, R. J. (2017). TrypTag.org: A Trypanosome Genome-wide Protein Localisation Resource. *Trends Parasitol.* **33**, 80–82.

Dixit, R. and Cyr, R. (2004). The cortical microtubule array: from dynamics to organization. *Plant Cell* **16**, 2546–2552.

Dóró, É., Jacobs, S. H., Hammond, F. R., Schipper, H., Pieters, R. P., Carrington, M., Wiegertjes, G. F. and Forlenza, M. (2019). Visualizing trypanosomes in a vertebrate host reveals novel swimming behaviours, adaptations and attachment mechanisms. *Elife* **8**, 7140.

Fitzpatrick, C., Nwankwo, U., Lenk, E., de Vlas, S. J. and Bundy, D. A. P. (2017). *An Investment Case for Ending Neglected Tropical Diseases*. 3rd ed. (eds. Holmes, K. K., Bertozzi, S., Bloom, B. R., and Jha, P. International Bank for Reconstruction and Development.

Forth, S., Hsia, K.-C., Shimamoto, Y. and Kapoor, T. M. (2014). Asymmetric Friction of Nonmotor MAPs Can Lead to Their Directional Motion in Active Microtubule Networks. *Cell* **157**, 420–432.

Halliday, C., Billington, K., Wang, Z., Madden, R., Dean, S., Sunter, J. D. and Wheeler, R. J. (2019). Cellular landmarks of Trypanosoma brucei and Leishmania mexicana. *Molecular and Biochemical Parasitology* **230**, 24–36.

Heddergott, N., Krüger, T., Babu, S. B., Wei, A., Stellamanns, E., Uppaluri, S., Pfohl, T., Stark, H. and Engstler, M. (2012). Trypanosome motion represents an adaptation to the crowded environment of the vertebrate bloodstream. *PLoS Pathog.* **8**, e1003023.

Hemphill, A., Lawson, D. and Seebeck, T. (1991). The Cytoskeletal Architecture of Trypanosoma brucei. *The Journal of Parasitology* **77**, 603–612.

Hilton, N. A., Sladewski, T. E., Perry, J. A., Pataki, Z., Sinclair-Davis, A. N., Muniz, R. S., Tran, H. L., Wurster, J. I., Seo, J. and de Graffenried, C. L. (2018). Identification

of TOEFAZ1-interacting proteins reveals key regulators of Trypanosoma brucei cytokinesis. *Mol. Microbiol.* **109**, 306–326.

Janke, C. (2014). The tubulin code: molecular components, readout mechanisms, and functions. *The Journal of Cell Biology* **206**, 461–472.

Janke, C. and Bulinski, J. C. (2011). Post-translational regulation of the microtubule cytoskeleton: mechanisms and functions. *Nat. Rev. Mol. Cell Biol.* **12**, 773–786.

Jentzsch, J., Sabri, A., Speckner, K., Lallinger-Kube, G., Weiss, M. and Ersfeld, K. (2020). Microtubule polyglutamylation is important for regulating cytoskeletal architecture and motility in Trypanosoma brucei. *Journal of cell science* **133**, jcs248047.

Kilmartin, J. V. (1982). Rat monoclonal antitubulin antibodies derived by using a new nonsecreting rat cell line. *The Journal of Cell Biology* **93**, 576–582.

Kwan, A. C., Dombeck, D. A. and Webb, W. W. (2008). Polarized microtubule arrays in apical dendrites and axons. *Proc. Natl. Acad. Sci. U.S.A.* **105**, 11370–11375.

Lord, S. J., Velle, K. B., Mullins, R. D. and Fritz-Laylin, L. K. (2020). SuperPlots: Communicating reproducibility and variability in cell biology. *Journal of Cell Biology* **219**, 94.

Los, G. V., Encell, L. P., McDougall, M. G., Hartzell, D. D., Karassina, N., Zimprich, C., Wood, M. G., Learish, R., Ohana, R. F., Urh, M., et al. (2008). HaloTag: a novel protein labeling technology for cell imaging and protein analysis. *ACS Chem. Biol.* **3**, 373–382.

May, S. F., Peacock, L., Almeida Costa, C. I. C., Gibson, W. C., Tetley, L., Robinson, D. R. and Hammarton, T. C. (2012). The Trypanosoma brucei AIR9-like protein is

cytoskeleton-associated and is required for nucleus positioning and accurate cleavage furrow placement. *Mol. Microbiol.* **84**, 77–92.

McAllaster, M. R., Sinclair-Davis, A. N., Hilton, N. A. and de Graffenried, C. L. (2016). A unified approach towards Trypanosoma brucei functional genomics using Gibson assembly. *Molecular and Biochemical Parasitology* **210**, 13–21.

Mir, R., Morris, V. H., Buschmann, H. and Rasmussen, C. G. (2018). Division Plane Orientation Defects Revealed by a Synthetic Double Mutant Phenotype. *Plant Physiol* **176**, 418–431.

Mitchison, T. and Kirschner, M. (1984). Dynamic instability of microtubule growth. *Nature* **312**, 237–242.

Olego-Fernandez, S., Vaughan, S., Shaw, M. K., Gull, K. and Ginger, M. L. (2009). Cell morphogenesis of Trypanosoma brucei requires the paralogous, differentially expressed calpain-related proteins CAP5.5 and CAP5.5V. *Protist* **160**, 576–590.

Portman, N. and Gull, K. (2014). Identification of paralogous life-cycle stage specific cytoskeletal proteins in the parasite Trypanosoma brucei. *PLoS ONE* **9**, e106777.

Portran, D., Zoccoler, M., Gaillard, J., Stoppin-Mellet, V., Neumann, E., Arnal, I., Martiel, J. L. and Vantard, M. (2013). MAP65/Ase1 promote microtubule flexibility. *Mol. Biol. Cell* **24**, 1964–1973.

Redmond, S., Vadivelu, J. and Field, M. C. (2003). RNAit: an automated web-based tool for the selection of RNAi targets in Trypanosoma brucei. *Molecular and Biochemical Parasitology* **128**, 115–118.

Reid, T. A., Coombes, C., Mukherjee, S., Goldblum, R. R., White, K., Parmar, S., McClellan, M., Zanic, M., Courtemanche, N. and Gardner, M. K. (2019). Structural

state recognition facilitates tip tracking of EB1 at growing microtubule ends. *Elife* **8**, 6710.

Robinson, D. R., Sherwin, T., Ploubidou, A., Byard, E. H. and Gull, K. (1995). Microtubule polarity and dynamics in the control of organelle positioning, segregation, and cytokinesis in the trypanosome cell cycle. *The Journal of Cell Biology* **128**, 1163–1172.

Rodionov, V. I., Gyoeva, F. K., Kashina, A. S., Kuznetsov, S. A. and Gelfand, V. I. (1990). Microtubule-associated proteins and microtubule-based translocators have different binding sites on tubulin molecule. *J. Biol. Chem.* **265**, 5702–5707.

Rubinstein, B., Larripa, K., Sommi, P. and Mogilner, A. (2009). The elasticity of motor-microtubule bundles and shape of the mitotic spindle. *Phys Biol* **6**, 016005.

Ruiz, F., Garreau de Loubresse, N., Klotz, C., Beisson, J. and Koll, F. (2005). Centrin deficiency in Paramecium affects the geometry of basal-body duplication. *Current Biology* **15**, 2097–2106.

Sanchez, T., Welch, D., Nicastro, D. and Dogic, Z. (2011). Cilia-like beating of active microtubule bundles. *Science* **333**, 456–459.

Schmidt, T. G. M. and Skerra, A. (2007). The Strep-tag system for one-step purification and high-affinity detection or capturing of proteins. *Nature Protocols* **2**, 1528–1535.

Schmidt-Cernohorska, M., Zhernov, I., Steib, E., Le Guennec, M., Achek, R., Borgers, S., Demurtas, D., Mouawad, L., Lansky, Z., Hamel, V., et al. (2019). Flagellar microtubule doublet assembly in vitro reveals a regulatory role of tubulin C-terminal tails. *Science* **363**, 285–288.

Shaner, N. C., Lambert, G. G., Chammas, A., Ni, Y., Cranfill, P. J., Baird, M. A., Sell, B. R., Allen, J. R., Day, R. N., Israelsson, M., et al. (2013). A bright monomeric green fluorescent protein derived from Branchiostoma lanceolatum. *Nat. Methods* **10**, 407–409.

Sheriff, O., Lim, L.-F. and He, C. Y. (2014). Tracking the biogenesis and inheritance of subpellicular microtubule in Trypanosoma brucei with inducible YFP-α-tubulin. *Biomed Res Int* **2014**, 1–12.

Sherwin, T. and Gull, K. (1989a). Visualization of Detyrosination along Single Microtubules Reveals Novel Mechanisms of Assembly during Cytoskeletal Duplication in Trypanosomes. *Cell* **57**, 211–221.

Sherwin, T. and Gull, K. (1989b). The cell division cycle of Trypanosoma brucei brucei: timing of event markers and cytoskeletal modulations. *Philosophical Transactions of the Royal Society B: Biological Sciences* **323**, 573–588.

Sherwin, T. and Gull, K. (1989c). The cell division cycle of Trypanosoma brucei brucei: timing of event markers and cytoskeletal modulations. *Philosophical Transactions of the Royal Society B: Biological Sciences* **323**, 573–588.

Siahaan, V., Krattenmacher, J., Hyman, A. A., Diez, S., Hernández-Vega, A., Lansky, Z. and Braun, M. (2019). Kinetically distinct phases of tau on microtubules regulate kinesin motors and severing enzymes. *Nat. Cell Biol.* **21**, 1086–1092.

Sinclair, A. N. and de Graffenried, C. L. (2019). More than Microtubules: The Structure and Function of the Subpellicular Array in Trypanosomatids. *Trends Parasitol.* **35**, 760–777.

Sinclair-Davis, A. N., McAllaster, M. R. and de Graffenried, C. L. (2017). A functional analysis of TOEFAZ1 uncovers protein domains essential for cytokinesis in Trypanosoma brucei. *Journal of cell science* **130**, 3918–3932.

Sladewski, T. E., Billington, N., Ali, M. Y., Bookwalter, C. S., Lu, H., Krementsova, E. B., Schroer, T. A. and Trybus, K. M. (2018). Recruitment of two dyneins to an mRNA-dependent Bicaudal D transport complex. *Elife* **7**, 1169.

Song, Y. and Brady, S. T. (2015). Post-translational modifications of tubulin: pathways to functional diversity of microtubules. *Trends in Cell Biology* **25**, 125–136.

Souto-Padrón, T., de Souza, W. and Heuser, J. E. (1984). Quick-freeze, deep-etch rotary replication of *Trypanosoma cruzi* and *Herpetomonas megaseliae*. *Journal of cell science* **69**, 167–178.

Sun, S. Y., Kaelber, J. T., Chen, M., Dong, X., Nematbakhsh, Y., Shi, J., Dougherty, M., Lim, C. T., Schmid, M. F., Chiu, W., et al. (2018). Flagellum couples cell shape to motility in Trypanosoma brucei. *Proc. Natl. Acad. Sci. U.S.A.* **115**, E5916–E5925.

Sunter, J. D. and Gull, K. (2016). The Flagellum Attachment Zone: "The Cellular Ruler" of Trypanosome Morphology. *Trends Parasitol.* **32**, 309–324.

Tan, R., Lam, A. J., Tan, T., Han, J., Nowakowski, D. W., Vershinin, M., Simó, S., Ori-McKenney, K. M. and McKenney, R. J. (2019). Microtubules gate tau condensation to spatially regulate microtubule functions. *Nat. Cell Biol.* **21**, 1078–1085.

Trindade, S., Rijo-Ferreira, F., Carvalho, T., Pinto-Neves, D., Guegan, F., Aresta-Branco, F., Bento, F., Young, S. A., Pinto, A., Van Den Abbeele, J., et al. (2016). Trypanosoma brucei Parasites Occupy and Functionally Adapt to the Adipose Tissue in Mice. *Cell Host & Microbe* **19**, 837–848.

Vedrenne, C., Giroud, C., Robinson, D. R., Besteiro, S., Bosc, C., Bringaud, F. and Baltz, T. (2002). Two related subpellicular cytoskeleton-associated proteins in Trypanosoma brucei stabilize microtubules. *Mol. Biol. Cell* **13**, 1058–1070.

Vickerman, K. (1962). The mechanism of cyclical development in trypanosomes of the *Trypanosoma brucei* sub-group: an hypothesis based on ultrascructural observations. *Transactions of the Royal Society of Tropical Medicine and Hygiene* **56**, 487–495.

Wheeler, R. J., Gull, K. and Sunter, J. D. (2019). Coordination of the Cell Cycle in Trypanosomes. *Annu. Rev. Microbiol.* **73**, 133–154.

Wheeler, R. J., Scheumann, N., Wickstead, B., Gull, K. and Vaughan, S. (2013). Cytokinesis in Trypanosoma brucei differs between bloodstream and tsetse trypomastigote forms: implications for microtubule-based morphogenesis and mutant analysis. *Mol. Microbiol.* **90**, 1339–1355.

Wirtz, E. (1999). A tightly regulated inducible expression system for conditional gene knock-outs and dominant-negative genetics in Trypanosoma brucei. *Molecular and Biochemical Parasitology* 1–13.

Woods, A., Baines, A. J. and Gull, K. (1992). A high molecular mass phosphoprotein defined by a novel monoclonal antibody is closely associated with the intermicrotubule cross bridges in the Trypanosoma brucei cytoskeleton. *Journal of cell science* **103**, 665–675.

Chapter 4:

Discussion

The results of this thesis research lay the foundation for understanding the cytokinetic mechanism of *T. brucei*, which is inextricably linked to how the subpellicular microtubule array is built and regulated. The subpellicular array defines the shape of the cell, and thus defines the mechanism by which cytokinesis takes place in these divergent organisms. In Chapter 2, we determined that the first cytokinesis-specific protein identified in *T. brucei,* TOEFAZ1, is a modular protein that consists of three domains with separable functions. TOEFAZ1 acts as a scaffold to recruit regulatory proteins to the location of cleavage furrow ingression. This work provided the starting point to conduct proteomic screens to identify potential TOEFAZ1 binding partners that are involved in cytokinesis and subpellicular array remodeling. The proteomic screen led to the discoveries detailed in Chapter 3, in which we determined that the protein PAVE1 is a component of the inter-microtubule crosslinking fibrils of the array and discovered a mechanism by which array-associated proteins are organized and regulated across this extensive cytoskeletal structure. Below, we outline the potential implications and future directions of this work.

Chapter 2 — Discussion and Future Directions

In Chapter 2, we determined that TOEFAZ1 is a scaffolding protein that recruits cytokinesis regulators to the tip of the new FAZ. Scaffolding proteins contain several protein-protein interaction domains that bring together multiple binding partners to coordinate their interrelated functions (Garbett and Bretscher, 2014). Scaffolding proteins tend to have highly specific subcellular localizations in order to position their binding partners for local activation, such as the polarity-marking scaffold protein Bem1 (Irazoqui et al., 2003). Bem1 localizes the activity of the Rho-family GTPase Cdc42 and its upstream and downstream effectors to create a positive feedback loop to ensure the production of a single bud during cellular replication in budding yeast. Similarly, the local activation of the polo-like kinase PLK1 in metazoan cells is mediated by binding specific phosphorylated scaffolding proteins at distinct subcellular localizations at the mitotic spindle and midbody (Elia et al., 2003).

TOEFAZ1 localizes to a small anterior subdomain of the newly replicating FAZ in dividing cells. TOEFAZ1 consists of three modular domains, two of which are required for its function. The N-terminal α-helical domain has a coiled-coil motif that consists of six negatively-charged repeats (EEEDRKRKQR) that likely function in protein-protein interactions (Hu et al., 2017; Sinclair-Davis et al., 2017). Its C-terminal domain contains two zinc fingers (ZnF) that oligomerize the protein, which is required for its localization to the tip of the new FAZ (Sinclair-Davis et al., 2017). The ZnF domain also appears to mediate TOEFAZ1 interaction with CIF2, a recently-identified protein that also localizes to the new FAZ tip, and may also function in protein-protein interactions (Hu et al., 2017; Zhou et al., 2016b). The localization of TOEFAZ1 to the site of cytokinesis initiation, its essential role in this process, and its scaffold-like characteristics launched a rapid succession of protein-proximity interaction assays to identify the key regulators of cytokinesis that TOEFAZ1 likely recruits (Hilton et al., 2018; Zhou et al., 2016b; Zhou et al., 2018). These assays identified kinases, phosphatases, kinesins, microtubule modifying and severing enzymes, and secretory components that are under active investigation in the field. Many of these newly identified proteins localize to the new FAZ tip, suggesting that TOEFAZ1 may mediate their positioning at the initiation site of cytokinesis, thus creating a cytokinetic complex.

Several questions remain concerning TOEFAZ1 localization and function. Cytokinesis initiates from the anterior tip of the new FAZ, as this location demarcates the anterior tip of the cell body for the daughter cell that contains the newly synthesized flagellum (Abeywickrema et al., 2019; Robinson et al., 1995; Wheeler et al., 2013). It is unclear how TOEFAZ1 localizes exclusively to the anterior tip of the new FAZ and not the entire new FAZ length. This localization pattern suggests that there is a unique structure at the tip of the new FAZ that differentiates it from the rest of the FAZ. A likely candidate for this unique structure is the growing end of the new microtubule quartet (MtQ). The MtQ has an inverted polarity to the rest of the array microtubules, with its growing plus-ends facing the cell anterior (Lacomble et al., 2009; Robinson et al., 1995), and also appears to be decorated with unique post-translational modifications (Gallo and

Anderton, 1983). The new MtQ likely contacts the pre-existing MtQ (Ikeda and de Graffenried, 2012), creating a unique junction that may control the cytotactic replication of the FAZ structure (Beisson and Sonneborn, 1965). As the new MtQ grows, the polymerization of microtubules with opposing polarity within the array likely differentiates the anterior tip of the new FAZ from the rest of its length, as well as the pre-existing old FAZ. The EF-hand containing protein CIF2 and the kinetoplastid-specific phosphatase KPP1, both of which were discovered in TOEFAZ1 interaction screens, are required for TOEFAZ1 stability at the tip of the new FAZ and may specifically recognize the unique MtQ junction as the cytokinetic complex moves towards the cell anterior (Hilton et al., 2018; Zhou et al., 2016b).

After the initiation of cleavage furrow ingression at the new FAZ tip, the TOEFAZ1 cytokinetic complex moves back towards the cell posterior with the ingressing furrow (Sinclair-Davis et al., 2017; Zhou et al., 2016a). Strikingly, it does not move along the length of the new FAZ, but instead follows the cleavage furrow in close proximity to the old FAZ—more specifically, the old MtQ. If the TOEFAZ1 cytokinetic complex localizes to the junction between new and old MtQs, the old MtQ makes an ideal track to control the position of the ingressing cleavage furrow, as the old MtQ retains the opposing polarity and unique post-translational modifications that distinguish it from the other microtubules in the subpellicular array. The localization pattern of TOEFAZ1 suggests that the MtQs function as a set of outbound and inbound tracks to guide and position the cleavage furrow. Super-resolution microscopy of cells dual-labeled for TOEFAZ1 and the MtQ may help determine if TOEFAZ1 localizes to the MtQ junction. Alternatively, it may be possible to use transmission electron microscopy of immunogold-labeled and negatively stained cytoskeletons to distinguish TOEFAZ1 proximity to the MtQs.

As the TOEFAZ1 cytokinetic complex tracks toward the cell anterior with the growth of the new FAZ, extensive microtubule remodeling is taking place to accommodate the intercalation of the new MtQ into the subpellicular array (Wheeler et al., 2013). Additional microtubule polymerization and insertion is simultaneously taking place in the portion of the array between the

old and new flagellum to widen and replicate the array prior to cytokinesis. After the initiation of cleavage furrow ingression, microtubule remodeling and severing must take place in order to separate the subpellicular array into two distinct structures. This suggests that the cytokinetic complex may be composed of differing sets of proteins on its outbound track in comparison to its inbound track, making TOEFAZ1 a 'dynamic scaffold' (Garbett and Bretscher, 2014). TOEFAZ1 localizes to the tip of the new FAZ when it first forms (Sinclair-Davis et al., 2017; Zhou et al., 2016a), but it is unclear if this initial localization contains the entirety of TOEFAZ1 used in the cytokinetic process or if there is turnover of TOEFAZ1 to recruit new proteins as it tracks toward the cell anterior on the new FAZ. A dual-color HaloTag capping assay to determine if newly synthesized TOEFAZ1 is recruited to the new FAZ tip as it grows over time may shed light on TOEFAZ1 dynamics.

What factor or signal initiates cytokinesis and cleavage furrow ingression is still an open question in the field. There are morphological cues to cytokinesis initiation—the membrane inflection that demarcates the path of furrow ingression forms prior to initiation (Farr and Gull, 2012; Wheeler et al., 2013), and initiation typically takes place when the new to old flagellar length ratio reaches 0.8-0.9 (Sherwin and Gull, 1989b). However, there doesn't appear to be any 'licensing' of cytokinesis in connection to the successful completion of mitosis, like in yeast and metazoan systems. *T. brucei* cells in which mitosis is inhibited can still initiate and complete cytokinesis, resulting in daughter cells that contain no nuclei (0N1K, also called 'zoids') (Ploubidou et al., 1999). It is far more likely that the cue for initiation is regulated by the proper development of the new flagellum, as depletion of IFT components or disruption of flagellar attachment inhibits cytokinesis (Kohl et al., 2003; LaCount et al., 2002; Rotureau et al., 2014; Zhou et al., 2011). TOEFAZ1 contains over 30 phosphosites that could be part of a signaling cascade (McAllaster et al., 2015; Urbaniak et al., 2013). Both the morphogenic kinase TbPLK and the chromosomal passenger complex kinase Aurora B homolog TbAUK1 require the presence of TOEFAZ1 to localize to the new FAZ tip (McAllaster et al. 2015; Zhou et al. 2016a). Depletion of TbPLK but

not TbAUK1 blocks TOEFAZ1 recruitment to the new FAZ (Zhou et al., 2016a). However, the kinase activity of these proteins is not required late in the cell cycle for the initiation of cleavage furrow ingression (Li et al., 2009; Lozano-Núñez et al., 2013; Sinclair-Davis et al., 2017). Discovering the elusive cytokinesis initiation signal will be of upmost interest in understanding this unique process in *T. brucei,* and the answer may lie in some of the uncharacterized kinases and phosphatases that have been identified in TOEFAZ1 interaction screens.

After the initiation of cytokinesis, the cleavage furrow ingresses until the location of the old basal body, which is the nucleation site of the old MtQ and flagellum. At this point, a TOEFAZ1-independent process appears to take over (Hilton et al., 2018). Microtubules in the subpellicular array are gathered to form the new posterior end for the old flagellum-containing daughter cell, after which cells finally abscise and separate (Wheeler et al., 2013). This gathering and remodeling is dependent on a kinesin called KLIF, discovered in TOEFAZ1 interaction screens (Hilton et al., 2018; Zhou et al., 2018). Depletion of KLIF results in cells stalling at the point of posterior end formation, with cells eventually developing multiple ingressed furrows as they are unable to separate their arrays at the cell posterior. An alternative 'back-up' cytokinetic mechanism has been proposed to occur in the absence of TOEFAZ1, in which cleavage furrow ingression initiates at the cell posterior and moves toward the cell anterior (Zhou et al., 2016a). In our TOEFAZ1 depletion studies, we found no evidence of this phenomenon (Sinclair-Davis et al., 2017). The aberrant multi-nucleated and anucleated DNA states of TOEFAZ1-depleted cells calls into question whether the 'back-up' cytokinesis, if it takes place, can produce viable progeny. Live cell imaging of *T. brucei* cells lacking TOEFAZ1 will allow us to observe if 'back-up' cytokinesis occurs, and if the daughter cells produced by this process can continue to replicate. We have observed cells with multiple posterior ends without an ingressed cleavage furrow in TOEFAZ1 RNAi cells, but it has become clear with the discovery of KLIF that some posterior end remodeling can take place in the absence of TOEFAZ1. Our data suggests that cleavage furrow ingression and posterior end remodeling are two distinct phases of cytokinesis that can happen

independently of each other. How these phases are coordinated in wild-type conditions is not yet known.

A limiting factor in understanding the cytokinetic mechanism in *T. brucei* is a lack of detailed knowledge of array architecture. The microtubules of the subpellicular array are spaced 18-20 nm apart, which is the very edge of resolution currently attainable by established super-resolution methods such as STORM (Tam and Merino, 2015). Moreover, as the array encompasses the entirety of the cell, fluorescence signal from both the underside and surface of the array may complicate super-resolution techniques. An intriguing possibility to 'map' the subpellicular array microtubules would be to combine expansion microscopy (ExM) with structured illumination microscopy (SIM) (Halpern et al., 2017; Truckenbrodt et al., 2018). ExM would allow us to increase the overall distance between microtubules so that they might be compatible with super-resolution, and SIM would enable the use of conventional fluorophores with ExM to improve resolution both laterally and axially. Alternatively, it may be possible to use electron tomography or focused-ion beam scanning electron microscopy (FIB-SEM) to reconstruct the array, although these methods are much more labor-intensive. A detailed high-resolution map of the subpellicular array throughout the cell cycle would revolutionize the field and allow us to visualize the separation of one array into two distinct arrays for each daughter cell during cytokinesis, which would reveal how this remarkable microtubule remodeling takes place.

Finally, it is important to take these studies into the related kinetoplastid parasites *Trypanosoma cruzi* and *Leishmania*. Cytokinesis in these parasites is morphologically similar to *T. brucei*; cleavage furrow ingression initiates at the new FAZ tip at the cell anterior and progresses towards the cell posterior. (Elias et al., 2007; Wheeler et al., 2011). TOEFAZ1 and the majority of the proteins identified in the TOEFAZ1 screens—including CIF2, KPP1, and KLIF—are conserved in these species (Hilton et al., 2018; Zhou et al., 2016b; Zhou et al., 2018). This conservation suggests that the cytokinetic mechanism in trypanosomatids relies on the same core machinery. However, the shape of the subpellicular array and the extent of flagellar

attachment in the primary epimastigote and promastigote morphotypes of *T. cruzi* and *Leishmania* differs from *T. brucei* and argues that there are species-specific adaptations to the cytokinetic process (Rocha et al., 2006; Wheeler et al., 2016). Determining what is conserved and unique in these parasites will build the foundations of the general cytokinetic mechanism in this divergent branch on the tree of life.

Chapter 3—Discussion and Future Directions

In Chapter 3, we determined that PAVE1 was a component of the inter-microtubule crosslinking fibrils of the array, and also show that PAVE1, along with its binding partner PAVE2, is a true microtubule-associated protein (MAP) that binds microtubules in vitro. An intriguing discovery that developed from our PAVE1 work is the concept of subdomains in the subpellicular microtubule array, which are local areas of the array that are decorated with different array-associated proteins. The composition of these subdomains is controlled by TbAIR9, which localizes to the entirety of the array.

PAVE1 was discovered in the TOEFAZ1 protein-proximity biotinylation screen we conducted after identifying TOEFAZ1 as a scaffold for the cytokinetic complex (Hilton et al., 2018). PAVE1 was most likely biotinylated by TOEFAZ1 as the cytokinetic complex reached the apex of the cleavage furrow near the mid-zone of the cell (Chapter 3). PAVE1 does not appear to have a direct role in cytokinesis but is an essential component of the posterior subpellicular array and is required to form and maintain this subdomain of the array. This result shows the utility of protein-proximity screens, in that they can identify near neighbors that may not form a stable complex with the bait protein, but may briefly interact or come into close proximity with it to play an important and related role. The fact that TOEFAZ1 was not identified in the mNeonGreen-PAVE1 immunoprecipitations (Chapter 3) illustrates that the discovery of PAVE1 could only be accomplished by a more sensitive protein-proximity approach.

Prior to our study, the composition of the inter-microtubule crosslinks was entirely unknown. We demonstrated that PAVE1 localized to the inter-microtubule crosslinking fibrils of the posterior array using immunogold labeling on extracted cytoskeletons that were 'unroofed' to expose a single layer of the subpellicular array (Chapter 3). Our unroofing assay disrupts many of the inter-microtubule crosslinking fibrils, but as of yet, there is no other available technology to both label and visualize the crosslinks. However, when PAVE1 immunogold beads were not on an inter-microtubule crosslink due to its disruption, they localized to small protrusions along the ventral side of the microtubule (using flagellar placement to establish the dorsal-ventral axis) that had the same periodicity and spacing expected from an intact, non-disrupted crosslink (de Souza, 1999; Sherwin and Gull, 1989a). This is an important result, for two reasons: first, it suggests that PAVE1 is a component of the inter-microtubule crosslinking fibrils but it does not make up the entire crosslink. Other proteins must exist that are that span the inter-microtubule distance and contact the dorsal side of the neighboring microtubule. The crosslinking fibrils themselves are likely composed of multiple proteins that are asymmetrically distributed throughout the crosslink, and that there are proteins that primarily localize to the dorsal side of neighboring microtubules to complete the crosslink. Secondly, this result illustrates the geometric constraint placed upon these crosslinks, as the ventral localization of PAVE1 implies a tight spatial regulation of crosslink placement along a specific area long the outside wall of the microtubule. The microtubules of the array are crosslinked into a single layer, which is unlike the more canonical three dimensional bundles of microtubules found at the mitotic spindle, for example (Ogbadoyi et al., 2000). The positioning of the inter-microtubule crosslinking fibrils of the array must be under tight regulation in order to maintain this single microtubule layer. The proteins CAP51/51V and the kinesin TbKIN-D appear important in maintaining the spatial regulation of the crosslinking fibrils. Although their identity as components of inter-microtubule crosslinking fibrils has not been shown, depletion of CAP51/51V and the kinesin TbKIN-D results in multiple layers of array microtubules accumulating under the plasma membrane (Hu et al., 2012a; Portman and Gull, 2014). These depletion

phenotypes suggest that either the crosslinks themselves are disrupted without these proteins, or that the crosslinks are no longer confined geometrically to a specific area long the outside wall of the microtubules, resulting in a three-dimensional bundle instead of a single layer of microtubules. Thus, the localization of PAVE1 along the ventral side of array microtubules reflects the tight spatial regulation of the inter-microtubule crosslinks. The geometric constraint of crosslink placement is also exhibited by the array-associated protein WCB, which appears to have a role in linking the plasma membrane to the subpellicular array (Baines and Gull, 2008; Woods et al., 1992). In immunogold-labeled subpellicular array sheets, WCB is found exclusively on the plasma-membrane facing side of array microtubules. It would be informative to conjugate purified PAVE complex to gold beads and visualize its specific distribution on negatively stained microtubules in vitro using transmission electron microscopy. This might reveal if the polarized distribution of the PAVE complex along microtubules is due to the way that it interacts with microtubules, or if the polarization is enforced upon it in vivo by other array-associated factors.

Fewer than thirty proteins are known to localize to the subpellicular array (Sinclair and de Graffenried, 2019). It is not clear if these proteins are all MAPs or associate with the array indirectly through protein-protein interactions. And of those that are MAPs, it is not known if they are all components of the crosslinking fibrils. Array-associated proteins must work in concert to maintain the array as a single layer, retain the shape of the cell, and remodel the array during cell division and differentiation. It is likely that some proteins are components of the inter-microtubule crosslinking fibrils, which are 6 nm in diameter and 18-20 nm in width (de Souza and Attias, 2010). These fibrils are regularly spaced at 12-30 nm intervals (Bordier et al., 1982; Souto-Padrón et al., 1984), which indicates that perhaps other array-associated proteins bind directly to microtubules to occlude potential binding sites of the crosslinks to maintain their regimented spacing. Still other array-associated proteins must form the attachment between the subpellicular array and plasma membrane, which is required for cell shape and viability, and also consists of smaller, similarly spaced fibrils (Baines and Gull, 2008). There is likely a hierarchy to the order with which these

proteins bind to microtubules to build the elaborate organizational structure of the array. Identifying more array components, precisely localizing them to array structures, and determining when and where they bind to the array using HaloTag technology will begin to unravel how the array is constructed in *T. brucei.*

PAVE1 and PAVE2 stabilize the microtubules of the posterior subdomain of the array (Chapter 3). It is possible that the PAVE complex maintains the inter-microtubule crosslink on ventral side of array microtubules, which in turn stabilizes them against depolymerization. Interestingly, this function is in direct opposition to that of the kinesin TbKIN-C (Hu et al., 2012b). Depletion of TbKIN-C leads to the development of cells with elongated 'nozzle' posteriors, indicating that it may actively depolymerize microtubules at the posterior subpellicular array. The elongated 'nozzle' phenotype also develops when sphingolipid biosynthesis is impaired, demonstrating that there is cross-talk between the lipid composition of the plasma membrane and subpellicular array regulation (Pasternack et al., 2015). The opposing phenotypes of PAVE1 and PAVE2, TbKIN-C, and sphingolipid depletion suggests that there is a fine balance of microtubule polymerization, stabilization, and depolymerization from a variety of pathways that work in concert to maintain and create the rounded, tapered shape of the trypanosome posterior array. Dynamic microtubule assays with GTP-tubulin and purified PAVE complex would reveal if the complex is able to stabilize microtubules against catastrophe in vitro, or if it needs to interact with other proteins of the crosslinking fibrils for this purpose.

The PAVE complex binds in static patches to microtubules, with very little turnover of protein (Chapter 3). These patches are not mediated by a preference for post-translational modifications on the tubulin C-terminal tails; rather, it is likely the complex recognizes a specific structure of the microtubule lattice. Taxol-stabilized microtubules are not uniform, as Taxol binding introduces heterogeneity into the microtubule lattice (Díaz et al., 1998; Kellogg et al., 2017). Stabilized microtubules also accumulate damage over time (Reid et al., 2017). Interestingly, the plus-ends of growing microtubules have extremely heterogeneous architecture, characterized by

open two dimensional sheets and curved protofilaments (Chrétien et al., 1995). It is possible that the PAVE complex recognizes the more heterogeneous and open conformations of microtubules at their plus-ends, and statically binds to these locations. This binding behavior could explain its addition to the extreme posterior end of the subpellicular array, where there is a concentration of array microtubule plus-ends (Chapter 3). Conducting in vitro binding experiments with gold-conjugated PAVE complex using transmission electron microscopy, as mentioned above, will reveal if the PAVE complex has a preference for these open structures. Moreover, the dynamic microtubule assays suggested previously will show if the PAVE complex has any plus-end tip tracking behavior.

It is interesting that in vivo PAVE1 moves towards the cell anterior over time, especially given how statically it appears to bind to microtubules in vitro (Chapter 3). The PAVE complex binds to microtubules in patches even at high concentrations (500 nM), and there is no evidence of these patches diffusing or disappearing over time. In light of these in vitro results, the movement of PAVE1 in vivo may be due to tubulin turnover in the array. The concept of microtubule dynamics within the subpellicular array has not been pursued in the field, as the array microtubules appear unusually stable and do not undergo catastrophes (Sherwin and Gull, 1989a). However, microtubules appear to constantly polymerize at the cell posterior while the length of the cell body is cell cycle regulated (Sheriff et al., 2014; Wheeler et al., 2013), which suggests that tubulin subunits must be removed from the minus-ends of microtubules within the array in order to maintain cell shape and length. Tubulin turnover in the array has not been seriously considered before, but the inherently dynamic nature of microtubules suggests that it must exist in order to maintain the length and shape subpellicular array. It will be fascinating to discover how and where tubulin is added and removed within the highly organized context of the array, and if different domains of the array turnover tubulin at different rates. A dual-color HaloTag capping assay on tubulin would test if there is treadmilling or turnover of array microtubules. We could append a

HaloTag protein to α- or β-tubulin at their endogenous loci (which may result in tagging multiple tubulin loci, as they are arranged in tandem arrays), or overexpress the HaloTag-tubulin fusion.

Although PAVE1 moves toward the cell anterior over time, it does not spread over the entirety of the array. The stability with which it binds to microtubules in vitro suggests that it is removed from the anterior portion of the array, especially if the microtubules of the array treadmill. It is likely that TbAIR9 is involved in this process. When TbAIR9 is depleted, PAVE1 spreads over the entirety of the array, including the anterior portion (Chapter 3). In *Arabidopsis*, AtAIR9 binds to the cortical microtubule array via its microtubule binding domain at its N-terminus. At the end of cytokinesis, AtAIR9 localizes to the newly formed cross-wall between the daughter cells before the re-establishment of cortical microtubules, which is mediated by the A9 repeats at its C-terminus (Buschmann et al., 2006). The TbAIR9 protein does not contain the microtubule binding domain, which indicates that it interacts with the array indirectly, through association with array-associated proteins like PAVE1. TbAIR9 labeling intensity on the array is enriched at the cell anterior, where PAVE1 labeling intensity rapidly declines, which suggests that an antagonistic relationship could exist between PAVE1-microtubule binding and TbAIR9. In vitro protein interaction assays between the PAVE complex, TbAIR9, and microtubules will reveal how the PAVE complex interacts with TbAIR9, and whether TbAIR9 competes with microtubules to bind to the complex.

TbAIR9 is also involved in confining the proteins Tb927.9.10790 and Tb927.11.1840 to the middle and anterior portions of the array, respectively. In our analysis of potential array-associated proteins in the TrypTag database thus far, the array posterior, middle, and anterior comprise the most common localizations, suggesting that these regions are the primary subdomains of the array (Dean et al., 2017). Many proteins also localize to the entirety of the array, like TbAIR9. As TbAIR9 immunoprecipitated with mNeonGreen-PAVE1 (Chapter 3), it is likely that it associates with proteins on the inter-microtubule crosslinks. It is possible that the inter-microtubule crosslinks contain a core set of proteins that are consistent throughout the array,

like TbAIR9, and are tailored in specific subdomains by accessory proteins, like PAVE1/2, 10790, and 1840. Proximity-dependent biotin identification screens of PAVE1 and TbAIR9 are likely to identify new components of these crosslinks and provide insight in how they are built, maintained, and modified over the length of the array.

There is much to be discovered about the purpose of these subdomains. The primary subdomains each occur at unique places with respect to the flagellum in *T. brucei*. The posterior subdomain comprises an area without flagellar attachment, as the flagellum exits onto the cell surface ~4-5 μm from the posterior edge of the array. The middle subdomain covers the widest point of the cell body, directly after the flagellum exits the flagellar pocket and is attached to the cell surface. This includes the area where the flagellar pocket, kinetoplast, and nucleus are located. The flagellum is attached throughout the entirety of the anterior subdomain, where the array rapidly tapers to a narrow point. The flagellar beat in *T. brucei* can initiate from either its base or tip and creates asymmetric waveforms along the cell body (Engstler et al., 2007; Heddergott et al., 2012; Krüger et al., 2018). It is likely that each of these three subdomain regions experience different amounts of force during flagellar beating. The unique combination of array-associated proteins at each subdomain may be present to regulate the flexibility, stabilize, or repair microtubules in response to these differential forces. In addition to force response, subdomain proteins may also be present to create the curvature and helicity of array microtubules and retain cell shape throughout the cell cycle, like PAVE1 and PAVE2. Depleting newly identified subdomain proteins using RNAi will elucidate their specific functions in their respective subdomains, which will inform on the properties of each subdomain. As mentioned previously, a high-resolution map of the subpellicular array would be invaluable in the study of these subdomains and their associated proteins. Dual-color ExM followed by SIM, in which both tubulin and an array-associated protein are labeled, may help more easily determine if these proteins are on the inter-microtubule crosslinking fibrils in each subdomain (Halpern et al., 2017).

Finally, trypanosome tubulin itself may provide a mechanism of array regulation. The biophysical characteristics of trypanosome tubulin are not well characterized; although trypanosome tubulin has been successfully purified, it does not polymerize robustly. Rather, it assembles into sheets and ribbons (MacRae and Gull, 1990; Russell et al., 1984; Werbovetz et al., 1999). The reason for this is unknown, but it has been suggested that trypanosome tubulin has especially high nucleation efficiency (Werbovetz et al., 1999). In light of the heavily crosslinked environment in which trypanosome tubulin exists, it is also possible that it has different polymerization characteristics and requires tip-trackers or stabilizing proteins to form into complete filaments. We have been able to successfully purify tubulin from *Leishmania* species but have encountered the same polymerization characteristics as others in the field. The ability to work with native tubulin in our in vitro protein interaction experiments will be invaluable, as there could be yet-undiscovered functions of the PAVE complex or other array-associated proteins that are specific to the conformation or characteristics of trypanosome tubulin.

Concluding Remarks

The research presented in this thesis has established a foundation to understand the fundamental mechanism of cytokinesis in trypanosomatid parasites. Before the identification of TOEFAZ1 as a cytokinetic scaffold, there were only a handful of proteins implicated in cytokinesis; now, nearly five hundred new proteins have been identified that may have a role in this unique process, many of which are under active investigation (Hilton et al., 2018; Zhou et al., 2016b; Zhou et al., 2018). Moreover, this thesis has launched a new area of research in trypanosome cytoskeletal regulation. Prior to this work, it was unknown how the array developed and maintained its shape. We discovered that the subpellicular microtubule array is organized into subdomains, which control array shape and likely motility in response to flagellar force. We are now poised to uncover how these subdomains are formed and maintained, and how they regulate microtubule dynamics within the array.

TOEFAZ1 and PAVE1 may have different localizations and functions, but the work presented here illustrates how interconnected cytokinesis, the cytoskeleton, and cell shape are (Figure 1). We began with the discovery of TOEFAZ1, the first cytokinetic protein identified in *T. brucei*. We determined that TOEFAZ1 was a scaffolding protein that recruited cytokinetic regulators to a privileged area at the tip of the new FAZ from which cleavage furrow ingression initiates (Fig. 1A) (Hilton et al., 2018; Sinclair-Davis et al., 2017). The evolutionary need to maintain the array while dividing is reflected by cytokinesis taking place unidirectionally following the polarity of array microtubules while using unique microtubule-based machinery. The proteins that TOEFAZ1 recruits to the initiation site are tasked with the sequential breaking inter-microtubule crosslinks, followed by severing and sorting microtubules into two distinct arrays, and finally reestablishing the inter-microtubule crosslinks to create and cement the shape of the cell. PAVE1 is involved in this final stage. After the microtubules are gathered at the midzone of the dividing cell to form a new posterior end for the old flagellum-containing daughter cell, which is a process most likely mediated by the kinesin KLIF, PAVE1 is recruited to the inter-microtubule crosslinks of the newly formed posterior array to establish its shape and length.

The construction of these inter-microtubule crosslinks is unclear, but we are beginning to establish a model of their composition (Fig. 1B). They are made up of multiple proteins that are asymmetrically distributed throughout the crosslink, and the molecular components of each crosslink most likely differ depending on their subdomain localization in the array. At the posterior subdomain, PAVE1 and PAVE2 form the ventral side of the crosslink along array microtubules (using the flagellum to establish the dorsal-ventral axis) and there are likely proteins that attach to the dorsal side of the neighboring microtubule to complete the crosslink. TbAIR9 appears to maintain and confer crosslink ‘identity’ depending on the subdomain location, but it is unclear if TbAIR9 is on the inter-microtubule crosslinks.

These discoveries highlight the plasticity of the fundamental mechanisms of life. All cells must divide; all cells must regulate their size and shape. The work presented here demonstrates

the importance of researching diverse organisms—'non-model' model systems—to understand the wide range of ways in which these mechanisms can be accomplished.

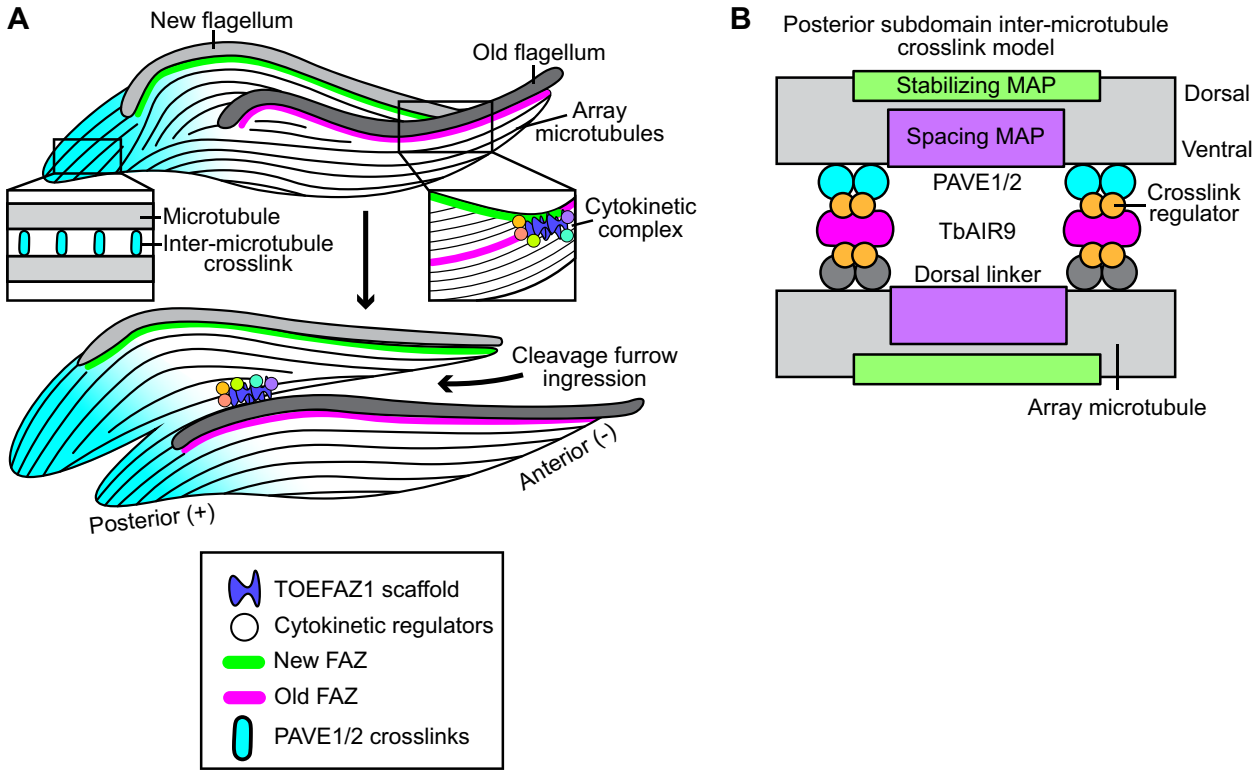

Figure 1. Summary and model of the work described in this dissertation. (A) The TOEFAZ1 scaffold (blue) accumulates at the tip of the new FAZ (green) and recruits cytokinetic regulators (circles) to the initiation site of cleavage furrow ingression. The cytokinetic complex tracks the cleavage furrow as it ingresses towards the growing (+)-ends of array microtubules, breaking inter-microtubule crosslinking fibrils to separate the array into two distinct structures. PAVE1/2 (cyan) 'cements' the formation of the new posterior end during cell division as an essential component of the inter-microtubule crosslinking fibrils of the posterior subdomain. **(B)** A model of array composition at the posterior subdomain. PAVE1/2 (cyan) contacts the crosslinks on the ventral side of array microtubules, using the flagellum placement as in (A) to establish the dorsal-ventral axis. TbAIR9 (magenta) retains PAVE1/2 at the posterior crosslinks, perhaps as a protein-protein interactor that does not directly bind to microtubules. Additional proteins, whose identity are not yet known (gray), complete the crosslink on the dorsal side of the neighboring microtubule. There are likely regulatory proteins (orange) that modify the biophysical properties of the crosslinks in each subdomain, rendering them more flexible or rigid. There are likely microtubule associated proteins (MAPs) that bind directly to the array microtubules to stabilize them (green), as well as MAPs that form 'spacers' (purple) that correctly positions each crosslink with regular periodicity.

REFERENCES

Abeywickrema, M., Vachova, H., Farr, H., Mohr, T., Wheeler, R. J., Lai, D.-H., Vaughan, S., Gull, K., Sunter, J. D. and Varga, V. (2019). Non-equivalence in old- and new-flagellum daughter cells of a proliferative division in Trypanosoma brucei. *Mol. Microbiol.* **112**, 1024–1040.

Baines, A. and Gull, K. (2008). WCB is a C2 domain protein defining the plasma membrane - sub-pellicular microtubule corset of kinetoplastid parasites. *Protist* **159**, 115–125.

Beisson, J. and Sonneborn, T. M. (1965). Cytoplasmic inheritance of the organization of the cell cortex in paramecium aurelia. *PNAS* **53**, 275–282.

Bordier, C., Garavito, R. M. and Armbruster, B. (1982). Biochemical and Structural Analyses of Microtubules in the Pellicular Membrane of Leishmania tropica. *Journal of Protozoology* **29**, 560–565.

Buschmann, H., Chan, J., Sanchez-Pulido, L., Andrade-Navarro, M. A., Doonan, J. H. and Lloyd, C. W. (2006). Microtubule-associated AIR9 recognizes the cortical division site at preprophase and cell-plate insertion. *Current Biology* **16**, 1938–1943.

Chrétien, D., Fuller, S. D. and Karsenti, E. (1995). Structure of growing microtubule ends: two-dimensional sheets close into tubes at variable rates. *Journal of Cell Biology* **129**, 1311–1328.

de Souza, W. (1999). A Short Review on the Morphology of *Trypanosoma cruzi*: from 1909 to 1999. *Mem Inst Oswaldo Cruz* **94**, 17–36.

de Souza, W. and Attias, M. (2010). Subpellicular Microtubules in Apicomplexa and Trypanosomatids. In *Structures and Organelles in Pathogenic Protists* (ed. de Souza, W., pp. 27–62. Berlin, Heidelberg: Springer Berlin Heidelberg.

Dean, S., Sunter, J. D. and Wheeler, R. J. (2017). TrypTag.org: A Trypanosome Genome-wide Protein Localisation Resource. *Trends Parasitol.* **33**, 80–82.

Díaz, J. F., Valpuesta, J. M., Chacón, P., Diakun, G. and Andreu, J. M. (1998). Changes in microtubule protofilament number induced by Taxol binding to an easily accessible site. Internal microtubule dynamics. *J. Biol. Chem.* **273**, 33803–33810.

Elias, M. C., da Cunha, J. P. C., de Faria, F. P., Mortara, R. A., Freymüller, E. and Schenkman, S. (2007). Morphological events during the Trypanosoma cruzi cell cycle. *Protist* **158**, 147–157.

Engstler, M., Pfohl, T., Herminghaus, S., Boshart, M., Wiegertjes, G., Heddergott, N. and Overath, P. (2007). Hydrodynamic flow-mediated protein sorting on the cell surface of trypanosomes. *Cell* **131**, 505–515.

Farr, H. and Gull, K. (2012). Cytokinesis in trypanosomes. *Cytoskeleton (Hoboken)* **69**, 931–941.

Gallo, J.-M. and Anderton, B. H. (1983). A subpopulation of trypanosome microtubules recognized by a monoclonal antibody to tubulin. *The EMBO Journal* **2**, 479–483.

Garbett, D. and Bretscher, A. (2014). The surprising dynamics of scaffolding proteins. *Mol. Biol. Cell* **25**, 2315–2319.

Halpern, A. R., Alas, G. C. M., Chozinski, T. J., Paredez, A. R. and Vaughan, J. C. (2017). Hybrid Structured Illumination Expansion Microscopy Reveals Microbial Cytoskeleton Organization. *ACS Nano* **11**, 12677–12686.

Heddergott, N., Krüger, T., Babu, S. B., Wei, A., Stellamanns, E., Uppaluri, S., Pfohl, T., Stark, H. and Engstler, M. (2012). Trypanosome motion represents an adaptation to the crowded environment of the vertebrate bloodstream. *PLoS Pathog.* **8**, e1003023.

Hilton, N. A., Sladewski, T. E., Perry, J. A., Pataki, Z., Sinclair-Davis, A. N., Muniz, R. S., Tran, H. L., Wurster, J. I., Seo, J. and de Graffenried, C. L. (2018). Identification of TOEFAZ1-interacting proteins reveals key regulators of Trypanosoma brucei cytokinesis. *Mol. Microbiol.* **109**, 306–326.

Hu, H., Hu, L., Yu, Z., Chasse, A. E., Chu, F. and Li, Z. (2012a). An orphan kinesin in trypanosomes cooperates with a kinetoplastid-specific kinesin to maintain cell morphology by regulating subpellicular microtubules. *Journal of cell science* **125**, 4126–4136.

Hu, H., Majneri, P., Li, D., Kurasawa, Y., An, T., Dong, G. and Li, Z. (2017). Functional analyses of the CIF1-CIF2 complex in trypanosomes identify the structural motifs required for cytokinesis. *Journal of cell science* **130**, 4108–4119.

Hu, L., Hu, H. and Li, Z. (2012b). A kinetoplastid-specific kinesin is required for cytokinesis and for maintenance of cell morphology in Trypanosoma brucei. *Mol. Microbiol.* **83**, 565–578.

Ikeda, K. N. and de Graffenried, C. L. (2012). Polo-like kinase is necessary for flagellum inheritance in Trypanosoma brucei. *Journal of cell science* **125**, 3173–3184.

Irazoqui, J. E., Gladfelter, A. S. and Lew, D. J. (2003). Scaffold-mediated symmetry breaking by Cdc42p. *Nat. Cell Biol.* **5**, 1062–1070.

Kellogg, E. H., Hejab, N. M. A., Howes, S., Northcote, P., Miller, J. H., Díaz, J. F., Downing, K. H. and Nogales, E. (2017). Insights into the Distinct Mechanisms of Action of Taxane and Non-Taxane Microtubule Stabilizers from Cryo-EM Structures. *journal of molecular biology* **429**, 633–646.

Kohl, L., Robinson, D. and Bastin, P. (2003). Novel roles for the flagellum in cell morphogenesis and cytokinesis of trypanosomes. *The EMBO Journal* **22**, 5336–5346.

Krüger, T., Schuster, S. and Engstler, M. (2018). Beyond Blood: African Trypanosomes on the Move. *Trends Parasitol.* **34**, 1056–1067.

Lacomble, S., Vaughan, S., Gadelha, C., Morphew, M. K., Shaw, M. K., McIntosh, J. R. and Gull, K. (2009). Three-dimensional cellular architecture of the flagellar pocket and associated cytoskeleton in trypanosomes revealed by electron microscope tomography. *Journal of cell science* **122**, 1081–1090.

LaCount, D. J., Barrett, B. and Donelson, J. E. (2002). Trypanosoma brucei FLA1 is required for flagellum attachment and cytokinesis. *J. Biol. Chem.* **277**, 17580–17588.

Li, Z., Umeyama, T. and Wang, C. C. (2009). The Aurora Kinase in Trypanosoma brucei plays distinctive roles in metaphase-anaphase transition and cytokinetic initiation. *PLoS Pathog.* **5**, e1000575.

Lozano-Núñez, A., Ikeda, K. N., Sauer, T. and de Graffenried, C. L. (2013). An analogue-sensitive approach identifies basal body rotation and flagellum attachment zone elongation as key functions of PLK in Trypanosoma brucei. *Mol. Biol. Cell* **24**, 1321–1333.

MacRae, T. H. and Gull, K. (1990). Purification and assembly in vitro of tubulin from Trypanosoma brucei brucei. *Biochem. J.* **265**, 87–93.

McAllaster, M. R., Ikeda, K. N., Lozano-Núñez, A., Anrather, D., Unterwurzacher, V., Gossenreiter, T., Perry, J. A., Crickley, R., Mercadante, C. J., Vaughan, S., et al. (2015). Proteomic identification of novel cytoskeletal proteins associated with TbPLK, an essential regulator of cell morphogenesis in Trypanosoma brucei. *Mol. Biol. Cell* **26**, 3013–3029.

Ogbadoyi, E., Ersfeld, K., Robinson, D., Sherwin, T. and Gull, K. (2000). Architecture of the Trypanosoma brucei nucleus during interphase and mitosis. *Chromosoma* **108**, 501–513.

Pasternack, D. A., Sharma, A. I., Olson, C. L., Epting, C. L. and Engman, D. M. (2015). Sphingosine Kinase Regulates Microtubule Dynamics and Organelle Positioning Necessary for Proper G1/S Cell Cycle Transition in Trypanosoma brucei. *MBio* **6**, e01291–15.

Ploubidou, A., Robinson, D. R., Docherty, R. C., Ogbadoyi, E. O. and Gull, K. (1999). Evidence for novel cell cycle checkpoints in trypanosomes: kinetoplast segregation and cytokinesis in the absence of mitosis. *Journal of cell science* **112**, 4641–4650.

Portman, N. and Gull, K. (2014). Identification of paralogous life-cycle stage specific cytoskeletal proteins in the parasite Trypanosoma brucei. *PLoS ONE* **9**, e106777.

Reid, T. A., Coombes, C. and Gardner, M. K. (2017). Manipulation and quantification of microtubule lattice integrity. *Biol Open* **6**, 1245–1256.

Robinson, D. R., Sherwin, T., Ploubidou, A., Byard, E. H. and Gull, K. (1995). Microtubule polarity and dynamics in the control of organelle positioning, segregation, and cytokinesis in the trypanosome cell cycle. *The Journal of Cell Biology* **128**, 1163–1172.

Rocha, G. M., Brandão, B. A., Mortara, R. A., Attias, M., de Souza, W. and Carvalho, T. M. U. (2006). The flagellar attachment zone of Trypanosoma cruzi epimastigote forms. *J. Struct. Biol.* **154**, 89–99.

Rotureau, B., Blisnick, T., Subota, I., Julkowska, D., Cayet, N., Perrot, S. and Bastin, P. (2014). Flagellar adhesion in Trypanosoma brucei relies on interactions between different skeletal structures in the flagellum and cell body. *Journal of cell science* **127**, 204–215.

Russell, D. G., Miller, D. and Gull, K. (1984). Tubulin heterogenicity in the trypanosome Crithidia fasciculata. *Mol. Cell. Biol.* **4**, 779–790.

Sheriff, O., Lim, L.-F. and He, C. Y. (2014). Tracking the biogenesis and inheritance of subpellicular microtubule in Trypanosoma brucei with inducible YFP-α-tubulin. *Biomed Res Int* **2014**, 1–12.

Sherwin, T. and Gull, K. (1989a). Visualization of Detyrosination along Single Microtubules Reveals Novel Mechanisms of Assembly during Cytoskeletal Duplication in Trypanosomes. *Cell* **57**, 211–221.

Sherwin, T. and Gull, K. (1989b). The cell division cycle of Trypanosoma brucei brucei: timing of event markers and cytoskeletal modulations. *Philosophical Transactions of the Royal Society B: Biological Sciences* **323**, 573–588.

Sinclair, A. N. and de Graffenried, C. L. (2019). More than Microtubules: The Structure and Function of the Subpellicular Array in Trypanosomatids. *Trends Parasitol.* **35**, 760–777.

Sinclair-Davis, A. N., McAllaster, M. R. and de Graffenried, C. L. (2017). A functional analysis of TOEFAZ1 uncovers protein domains essential for cytokinesis in Trypanosoma brucei. *Journal of cell science* **130**, 3918–3932.

Souto-Padrón, T., de Souza, W. and Heuser, J. E. (1984). Quick-freeze, deep-etch rotary replication of *Trypanosoma cruzi* and *Herpetomonas megaseliae*. *Journal of cell science* **69**, 167–178.

Tam, J. and Merino, D. (2015). Stochastic optical reconstruction microscopy (STORM) in comparison with stimulated emission depletion (STED) and other imaging methods. *J. Neurochem.* **135**, 643–658.

Truckenbrodt, S., Maidorn, M., Crzan, D., Wildhagen, H., Kabatas, S. and Rizzoli, S. O. (2018). X10 expansion microscopy enables 25-nm resolution on conventional microscopes. *EMBO Rep.* **19**, e45836.

Urbaniak, M. D., Martin, D. M. A. and Ferguson, M. A. J. (2013). Global Quantitative SILAC Phosphoproteomics Reveals Differential Phosphorylation Is Widespread between the Procyclic and Bloodstream Form Lifecycle Stages of Trypanosoma brucei. *J. Proteome Res.* **12**, 2233–2244.

Werbovetz, K. A., Brendle, J. J. and Sackett, D. L. (1999). Purification, characterization, and drug susceptibility of tubulin from Leishmania. *Molecular and Biochemical Parasitology* **98**, 53–65.

Wheeler, R. J., Gluenz, E. and Gull, K. (2011). The cell cycle of Leishmania: morphogenetic events and their implications for parasite biology. *Mol. Microbiol.* **79**, 647–662.

Wheeler, R. J., Scheumann, N., Wickstead, B., Gull, K. and Vaughan, S. (2013). Cytokinesis in Trypanosoma brucei differs between bloodstream and tsetse trypomastigote forms: implications for microtubule-based morphogenesis and mutant analysis. *Mol. Microbiol.* **90**, 1339–1355.

Wheeler, R. J., Sunter, J. D. and Gull, K. (2016). Flagellar pocket restructuring through the *Leishmania* life cycle involves a discrete flagellum attachment zone. *Journal of cell science* **129**, 854–867.

Woods, A., Baines, A. J. and Gull, K. (1992). A high molecular mass phosphoprotein defined by a novel monoclonal antibody is closely associated with the intermicrotubule cross bridges in the Trypanosoma brucei cytoskeleton. *Journal of cell science* **103**, 665–675.

Zhou, Q., An, T., Pham, K. T. M., Hu, H. and Li, Z. (2018). The CIF1 protein is a master orchestrator of trypanosome cytokinesis that recruits several cytokinesis regulators to the cytokinesis-initiation site. *J. Biol. Chem.* **293**, 16177–16192.

Zhou, Q., Gu, J., Lun, Z.-R., Ayala, F. J. and Li, Z. (2016a). Two distinct cytokinesis pathways drive trypanosome cell division initiation from opposite cell ends. *PNAS* 201601596–15.

Zhou, Q., Hu, H. and Li, Z. (2016b). An EF-hand-containing protein in Trypanosoma brucei regulates cytokinesis initiation by maintaining the stability of the cytokinesis initiation factor CIF1. *J. Biol. Chem.* **291**, jbc.M116.726133–14409.

Zhou, Q., Liu, B., Sun, Y. and He, C. Y. (2011). A coiled-coil- and C2-domain-containing protein is required for FAZ assembly and cell morphology in Trypanosoma brucei. *Journal of cell science* **124**, 3848–3858.